

Universidad de Oviedo

Departamento de Biología de Organismos y Sistemas

Programa de Doctorado: "Biogeociencias"

**CHARACTERIZATION OF THE MAIN HYDROGRAPHIC STRUCTURES OF
THE NORTHWEST AND NORTH IBERIAN PENINSULA: INFLUENCE ON THE
MESOZOOPLANKTON STRUCTURE**

CARACTERIZACIÓN DE LAS PRINCIPALES ESTRUCTURAS
HIDROGRÁFICAS DEL NOROESTE Y NORTE DE LA PENÍNSULA IBÉRICA:
INFLUENCIA SOBRE LA ESTRUCTURA DEL MESOZOOPLANCTON

TESIS DOCTORAL

Gonzalo González-Nuevo González

Oviedo, 2015



RESUMEN DEL CONTENIDO DE TESIS DOCTORAL

1.- Título de la Tesis	
Español/Otro Idioma: Caracterización de las principales estructuras hidrográficas del Noroeste y Norte de la Península Ibérica: Influencia sobre la estructura del mesozooplancton.	Inglés: Characterization of the main hydrographic structures of the NW and N Iberian Peninsula: Influence on mesozooplankton structure.
2.- Autor	
Nombre: Gonzalo González-Nuevo González	DNI/Pasaporte/NIE:
Programa de Doctorado: Biogeociencias	
Órgano responsable: Centro Internacional de Postgrado	

RESUMEN (en español)

Entre los años 1987 y 2008 se han llevado a cabo 20 campañas oceanográficas de primavera que tenían como objetivo la evaluación de recursos pesqueros. Al mismo tiempo se pusieron en marcha 5 programas de monitoreo de secciones oceanográficas localizados frente a Vigo, A Coruña, Cudillero, Gijón y Santander. En los dos casos se obtuvieron, de forma rutinaria, perfiles de temperatura y salinidad en la columna de agua, junto con otra serie de mediciones tanto de variables físicas como biológicas.

Estas dos grandes bases de datos se han utilizado inicialmente para caracterizar la variabilidad espacio-temporal de las condiciones termohalinas en el N y NW de la Península Ibérica. Con estos datos se ha elaborado un marco que sirve como punto de partida para entender la dinámica oceanográfica del área de estudio y que de alguna forma complementa los resultados obtenidos en los siguientes apartados.

Después de obtener esta visión general del sistema se estudio la dinámica de algunos de los principales procesos oceanográficos de la zona, la corriente ibérica hacia el polo (Iberian Poleward Current IPC), las plumas de ríos y el afloramiento. En los tres casos se siguió una estructura de trabajo similar, en la que inicialmente se desarrollaron métodos de detección que permitieron definir las distintas estructuras así como caracterizar la variabilidad tanto espacial como temporal de las mismas. Por último se estimaron las relaciones con los principales forzadores de cada proceso así como los momentos en los que estas relaciones eran más relevantes.

El estudio de la IPC permitió definir de forma cualitativa la estacionalidad de la influencia del agua cálida y salina advectada por esta corriente utilizando los datos de las 5 secciones. Los métodos desarrollados para la detección de la IPC se aplicaron a los datos obtenidos en las campañas de primavera. Con este análisis se obtuvo la variabilidad interanual de esta corriente en esta época del año. Los resultados obtenidos se relacionaron con los principales factores forzadores.

Para estudiar la variabilidad espacio temporal de las plumas de ríos en la zona se aplicó un esquema de trabajo similar. Se desarrollaron métodos de detección objetiva, basados en gradientes de salinidad que en este caso se estimaron tanto para las 5 secciones como para las campañas de primavera. La aplicación de esta metodología en el primer caso, permitió estimar la estacionalidad de la presencia ausencia de plumas. Los resultados



obtenidos con las campañas de primavera permitieron definir la variabilidad interanual de la influencia de las descargas de ríos, así como la situación media. Como en el caso de la IPC los resultados obtenidos para las plumas se utilizaron para definir las relación de estas estructuras oceanográficas con las precipitaciones y las descargas de los principales ríos en cada caso.

Los métodos utilizados para estimar la presencia y variabilidad del afloramiento en la zona de estudio se basaron en gradientes temperatura. Estos métodos se aplicaron también a las dos bases de datos principales caracterizándose, como en los casos anteriores, la variabilidad espacio temporal del afloramiento. En este caso se estimó la relación de la presencia ausencia de este proceso con la intensidad de los vientos obteniéndose los valores críticos a partir de los cuales se detectó afloramiento.

En el último capítulo de esta tesis, se utilizaron las herramientas desarrolladas, para estudiar la interacción de los procesos de mesoescala sobre la composición del mesozooplankton en una campaña de primavera llevada a cabo en el N y NO de la Península Ibérica en el 2004. Los resultados obtenidos mostraron la influencia directa de la zonación basada en los procesos oceanográficos, sobre la composición y distribución del mesozooplankton.

RESUMEN (en Inglés)

Twenty spring oceanographic cruises were carried out between 1987 and 2008, with the aim of assess pelagic fisheries resources of the N and NW Iberian Peninsula. At the same time 5 monitoring programs with monthly frequency located off Vigo, A Coruña, Cudillero, Gijón and Santander were developed. In the two cases temperature and salinity water column profiles were obtained routinely together with other measurements of physical and biological parameters.

These two huge data bases have been initially used to characterize the spatial and temporal variability of the thermohaline conditions in the N and NW Iberian Peninsula. In this sense, climatologies of temperature and salinity fields have been elaborated using the spring cruises database and also has been used to analyze their spatial variability. Moreover time series analysis methods have been applied to the 5 sections in order to understand the temporal variability of the temperature and salinity in the studied area. These two approximations allow to make a framework that serve as a starting point to understand the oceanographic dynamic of the studied area and somehow complements the results obtained in the following chapters.

After the elaboration of this general vision of the system, specific methodologies has been developed to characterize some of the main oceanographic processes of the zone, the Iberian Poleward Current (IPC), river plumes and de upwelling. In the three cases, similar work structure has been followed. Initially detection methods were developed to define objectively the oceanographic structures and to characterize both their temporal and spatial variability. With these results the relationships with the main forcing factors of each oceanographic process has been estimated together with the times when this relationships were more intense.

The study of the IPC using the 5 sections database has allowed to define the seasonality of the warm and salty water advected by this current. The method developed to detect



the IPC influence has been applied to the spring cruises data bases. With this analysis has been possible to define the interannual variability of this oceanographic process in this part of the year. These results were related with the main forcing factors of the current. Different lagged correlations were found for both factors, corroborating the common theories about the dynamic of this current.

In order to study the spatial and temporal variability of the river plumes in the studied area, the same working scheme has been applied. Objective detection methods, based on salinity gradients, were developed and later applied to the 5 sections and spring cruises databases. The use of this methodology with the first database allowed to estimate the seasonality of the presence/absence of plumes. The spring cruises database was used to define the interannual variability of this oceanographic process as well as the climatology. As in the case of the IPC the obtained results were used to define the relationship between the river plumes and the precipitations and river runoffs of the main rivers.

The methods used to estimate the presence and variability of the upwelling in the studied area were based on the temperature gradients. These methodologies were applied to the two databases, to characterize, as in the previous cases, the spatial and temporal variability. The relationship between upwelling and winds was also studied, which allowed obtaining the critical wind values from which the upwelling was detected.

The developed methods are useful to define objectively the influence of IPC, the river plumes and upwelling. In the last chapter of the thesis these analytic tools were used to study the mesozooplankton during a spring cruise carried out in the N and NW of the Iberian Peninsula in 2004. The results showed the direct influence of the hydrographic zonation based on the presence of oceanographic processes, on the composition and distribution of mesozooplankton.

Agradecimientos

El proceso de elaboración de esta tesis comienza en Agosto de 2005 cuando me conceden unas prácticas en Centro Gijón del Instituto Español de Oceanografía. Desde entonces ha pasado bastante tiempo, una beca predoctoral y varios contratos con cargo a distintos proyectos. Han sido muchas horas de trabajo en el centro, muchas campañas, muchos congresos, muchas reuniones... Teniendo en cuenta que además, parte de todo este tiempo he estado trabajando en el centro oceanográfico de Vigo, son demasiadas las personas con las que me he cruzado y a las que tengo que agradecer la presentación de esta tesis.

Como no quiero que esta sección sea la más amplia del documento y aprovechándome de que estamos en el siglo XXI, la era de internet y los contenidos interactivos, voy a copiar la tendencia que hay actualmente en la administración pública de externalizar. La lista de gente con la que he vivido todo este tiempo está en el siguiente enlace:



Independientemente que estés en la lista o no, si simplemente no tienes tiempo y estás muy liado para buscarte en ella, o te da pereza sacar el móvil, solo puede decirte que:

¡Muchas Gracias!

Muchas gracias por tu trabajo, por el tiempo compartido, por los buenos momentos y también por los malos. También tengo que darte las gracias por empezar a leer esta tesis y te invito a que continúes. Probablemente no descubras en ella el sentido de la vida, ni encuentres grandes leyes del saber universal pero sí que puedo decirte hay muchas horas de trabajo y dedicación dentro. Además tiene muchos gráficos de colores, que son muy llamativos en los documentos científicos y que a su vez gustan tanto a la gente.

Si que quiero que estén en estas páginas las personas más cercanas. Los primeros que tienen que aparecer aquí son mis padres, a los que les debo todo no solo por una obiedad biológica, sino por la educación que me han dado. Gracias a ellos he podido dedicarme durante toda mi vida a tiempo completo a estudiar y más tarde al mundo de la investigación (también a otras cosas menos eruditas pero que no creo que deban aparecer aquí). Son los que desde bien pequeño me han inyectado las ganas de conocer y de descubrir el mundo que me rodeaba. En mis primeros pasos, enseñándome a leer con los nombres de las estaciones de tren, mostrándome la naturaleza, la montaña y aprendiendo con ellos a conocer y disfrutar del mar.

Otra persona que tiene que estar aquí es Quincho, mi hermano. Al ser él el mayor y llevarme solo 2 años ha contribuido más de lo que piensa en mí desarrollo. Son muchas las horas que hemos perdido hablando de ciencia, discutiendo problemas concretos y problemas generales. Con él, he aprendido una de las cosas más importantes de todo este camino. La importancia y la necesidad de discutir con profesionales de otras disciplinas para obtener otros puntos de vista completamente distintos. Aprender cómo se responden preguntas comunes desde otras perspectivas y poder descubrir que, problemas ya resueltos en una disciplina, son nuevos y están si resolver para otra. Me parece algo muy importante teniendo en cuenta que aunque estamos en el 2014, todavía sigue habiendo demasiadas torres de marfil en ciencia, haciendo que los avances se produzcan mucho más despacio de lo que debería.

Por último y no menos importante tengo que agradecer a Sylvia que haya estado a mi lado todo este tiempo, aguantándome hasta la extenuación. Ha soportado horas y horas de brasas sobre el trabajo que estaba haciendo y sobre los avances y retrocesos que tenía. Si con Quincho (Astrofísico) he obtenido perspectivas distintas, con Sylvia (Restauradora de Libros y Editora de arte) la visión de los problemas desde una formación tan alejada pasa a un nivel superior. Siempre ha estado ahí para hacerme dar un paso atrás y obligarme a repensar las cosas desde otras posiciones.

Gracias a todos y espero que disfrutéis con el resto de las páginas.

Gonzalo González-Nuevo González

Índice

Agradecimientos.....	i
Índice.....	1
List of abbreviations	5
Hipótesis de trabajo y Objetivos	11
Hipótesis de trabajo	11
Objetivos.....	11
Resumen.....	13
Chapter 1: Introducción General	19
Chapter 2: Temporal and spatial variability of thermohaline properties in the North Iberian Shelf (NIS): 1987-2008.....	29
Introduction.....	31
Material and Methods	32
Results.....	36
Discussion	57
Chapter 3: Seasonal and interannual variation of the incursion of the Iberian Poleward Current (IPC) along the Northern Iberian Shelf derived from in situ thermohaline data.....	67
Introduction.....	69
Material and methods	72
Results.....	79
Discussion	89
Chapter 4: Temporal and spatial variability of river plumes in the NW and N Iberian Shelf (1987-2007).....	99
Introduction.....	101
Materials and methods	104
Results.....	110
Discussion	119
Chapter 5: Temporal and spatial variability of wind-driven coastal upwelling in the NW and N Iberian shelf from 1987 to 2008	127
Introduction.....	129
Material and Methods	131
Results.....	140
Discussion	149
Chapter 6: Mesozooplankton species distribution in the NW and N Iberian shelf during spring 2004: Relationship with frontal structures.....	157
Introduction.....	159

Materials and methods	160
Results	162
Discussion	171
Chapter 7: Conclusions	179
Chapter 8: Conclusiones (Castellano)	185
Chapter 9: Bibliography	191

List of abbreviations

Chapter 2: Temporal and spatial variability of thermohaline properties in the North Iberian Shelf: 1987-2008

α	Significant level
ε	White noise
θ_i	Phase of the i^{th} harmonic
ϕ_i	Auto-regressive parameter
A	Correlation factor
a	Intercept of the linear regression (trend analysis)
AC	Atlantic Coast
acf	Auto-correlation function
A_i	Amplitude of the i^{th} harmonic
b	Slope of the linear regression (trend analysis)
CC	Central Cantabrian Sea
CTD	Conductivity-temperature-depth sensor
EBUS	Eastern Boundary Upwelling System
EC	East Cantabrian Sea
ENACW _{sp}	Eastern North Atlantic Central Water, subpolar mode
ENACW _{st}	Eastern North Atlantic Central Water, subtropical mode
ENSO	El Niño southern Oscillation
F	Phase of the harmonic
IPC	Iberian Poleward Current
L	Spatial characteristic scale
LT	Linear trend component
MTG	Meridional Thermal Gradient
p	Order of the autorregressive model
pacf	Partial auto-correlation function
R	Correlation coefficient
S	Salinity
S ²	Variance
SC	Periodic trend component
SST	Sea Surface Temperature
STD	Standard deviation
T	Temperature
t	Time
T_i	Period of the i^{th} harmonic
UV	Ultra Violet radiation
WIBP	West Iberian Bouyant Plume

Chapter 3: Seasonal and interannual variation of the incursion of the Iberian Poleward Current (IPC) along the Northern Iberian Shelf derived from in situ thermohaline data

ε	White noise
γ	Spatial Correlation
θ_i	Phase of the i^{th} harmonic
ϕ_i	Auto-regressive parameter
AC	Atlantic Current
acf	Auto-correlation function
A_i	Harmonic amplitude
AVHRR	Advance very high resolution radiometer
CM	Current meters
CTD	Conductivity-temperature-depth sensor
CZCS	Coastal zone color scanner
EA	Eastern Atlantic atmospheric pattern
EBUS	Eastern Boundary Upwelling System
ENACW	Eastern North Atlantic Central Water
ENACW _{sp}	Eastern North Atlantic Central Water, subpolar mode
ENACW _{st}	Eastern North Atlantic Central Water, subtropical mode
EOF	Eigen Objective Function
EPC	Eastern Poleward Currents
IPC	Iberian Poleward Current
IPCF	Iberian Poleward Current Front
JEBAR	Join Effect of Baroclinicity and Relief
L	Spatial characteristic scale
l	Along-shelf location
l_{se}	Location of the end of the along-shelf IPC front
l_{si}	Location of the beginning of the along-shelf IPC front
LT	Long-term component
MTG	Meridional Thermal Gradient
NAC	North Atlantic Current
NAO	North Atlantic Oscillation
NIS	Northern Iberian Shelf
pacf	Partial auto-correlation function
PC	Portugal Current
PCCC	Portugal Coastal Counter Current
R	Correlation coefficient
R	Distance
r	Correlation Coeficient
s	Spiciness
s'	Spiciness observed values
S _{BoB}	Spiciness averaged values of the Bay of Biscay Area
SC	Seasonal component
S _{IPC}	Spiciness averaged values of the IPC area

s_i	Spiciness calculated values
SST	Sea Surface Temperature
T_i	Period of the i^{th} harmonic
u	East-West wind component
v	North-South wind component
V_n	Noise variance
V_s	Signal variance

Chapter 4: Temporal and spatial variability of river plumes in the NW and N Iberian Shelf (1987-2007)

ε	White noise
γ	Spatial Correlation
θ_i	Phase of the i^{th} harmonic
ϕ_i	Auto-regressive parameter
Δs	Salinity gradient
Δs_c	Salinity gradient criterion
A_i	Amplitude of the i^{th} harmonic
A_{Pz}	Area affected by plumes at a depth z .
CC	Central Cantabrian Sea
CTD	Conductivity-temperature-depth sensor
EC	East Cantabrian Sea
F	Phase of the harmonic
GWC	Galician and West Cantabrian Sea
IPC	Iberian Poleward Current
k	Lag
L	Spatial characteristic scale
LT	Long-term component
NIS	Northern Iberian Shelf
r^2	Square correlation coefficient
SC	Periodic trend component
T_i	Period of the i^{th} harmonic
V_n	Noise variance
V_p	Volume of the plume
V_s	Signal variance
Z_{maxP}	Maximum depth of the plume
Z_P	Mean depth of the plume

Chapter 5: Temporal and spatial variability of wind-driven coastal upwelling in the NW and N Iberian shelf from 1987 to 2008

ε	White noise
γ	Spatial Correlation
θ_i	Harmonic phase
ϕ_i	Auto-regressive parameter
acf	Auto-correlation function
A_i	Amplitude of the i^{th} harmonic
CTD	Conductivity-temperature-depth sensor
EBUS	Eastern Boundary Upwelling System
F	Phase of the i^{th} harmonic
l	Along-shelf location
L_b	Across-shelf location of the beginning of gradient area
L_e	Across-shelf location of the end of the gradient area
LT	Long-term component
$P_{70}(T)$	70 th Percentil of the temperature of the upwelled area
pacf	Partial auto-correlation function
S^2	Variance
SC	Periodic trend component
SST	Sea Surface Temperature
T	Calculated values of temperature
T	Period of the harmonic
T'	Observed values of temperature
T_c	Temperature of the coastal edge of the section
T_i	Period of the i^{th} harmonic
T_{nu}	Temperature of the non upwelled area
T_o	Temperature at the oceanic edge of the section
T_u	Temperature in the upwelled area
u	Zonal (East-West) wind component
U_a	Area influenced by upwelled waters
UFWC	Upwelling favorable wind component
U_p	Probability of upwelling occurrence
UTI	Upwelling thermal index
UTI_a	Averaged Temperature from 30 to 80m depth
UTI_c	Upwelling thermal index criterion
v	Meridional (North-South) wind component
W15	Mean value of UFWC obtained for 15 days before the date of hydrographic sampling

Chapter 6: Mesozooplankton species distribution in the NW and N Iberian shelf during spring 2004: Relationship with frontal structures

CC	Central Cantabrian Sea
CTDF	Conductivity–temperature– depth–fluorescence sensor
EC	Eastern Cantabrian sea
ENACW	Eastern North Atlantic Central Water
ENACW _{sp}	Eastern North Atlantic Central Water, subpolar mode
ENACW _{st}	Eastern North Atlantic Central Water, subtropical mode
IPC	Iberian Poleward Current
JEBAR	Join Effect of Baroclinicity and Relief
MLD	Mix Layer Depth
PCCC	Portugal Coastal Counter Current
WC	Western Cantabrian sea

Hipótesis de trabajo y Objetivos

Hipótesis de trabajo

Las hipótesis utilizadas para el desarrollo de esta tesis son:

- Las condiciones termohalinas permiten determinar de forma objetiva las características de las principales estructuras hidrográficas que tienen lugar en la zona de estudio: plumas asociadas a aportes continentales, filamentos asociados a procesos de afloramiento costero y la intrusión de la contra-corriente de talud hacia el polo ('Iberian Poleward Current', IPC).
- La variabilidad espacio-temporal de las principales estructuras hidrográficas asociadas a los aportes de agua dulce, afloramiento costero e IPC está directamente relacionada con la dinámica atmosférica.
- Las estructuras hidrográficas y los procesos oceanográficos que las generan condicionan la composición, distribución y estructura de la comunidad de mesozooplankton en el NO y N de la Península Ibérica.

Objetivos

Los objetivos principales de esta tesis son:

- Caracterizar la variabilidad espacio-temporal de las estructura hidrográficas asociadas a los procesos oceanográficos que tienen lugar en el Noroeste y Norte de la plataforma continental Ibérica (aportes de agua dulce, afloramiento e IPC).
- Evaluar la variabilidad espacio-temporal de dichas estructuras hidrográficas y su relación con sus principales factores forzadores.
- Determinar la influencia de este tipo de estructuras hidrográficas asociadas a los aportes continentales, afloramiento e IPC sobre la distribución y estructura del meso-plancton.

Resumen

Entre los años 1987 y 2008 se han llevado a cabo 20 campañas oceanográficas de primavera que tenían como objetivo la evaluación de recursos pesqueros. Al mismo tiempo se pusieron en marcha 5 programas de monitoreo de secciones oceanográficas localizados frente a Vigo, A Coruña, Cudillero, Gijón y Santander. En los dos casos se obtuvieron, de forma rutinaria, perfiles de temperatura y salinidad en la columna de agua, junto con otra serie de mediciones tanto de variables físicas como biológicas.

Estas dos grandes bases de datos se han utilizado inicialmente para caracterizar la variabilidad espacio-temporal de las condiciones termohalinas en el N y NW de la Península Ibérica. En este sentido se han elaborado climatologías de los campos de temperatura y salinidad utilizando las campañas de primavera. Por otro lado se ha analizado su variabilidad espacial utilizando métodos geostadísticos con los que se obtuvieron los principales parámetros de variación. Además, se aplicaron técnicas de análisis de series temporales a los datos de las secciones para definir y entender la variabilidad temporal de la temperatura y la salinidad en la zona. Estas dos aproximaciones permitieron elaborar un marco que sirve como punto de partida para entender la dinámica oceanográfica del área de estudio y que de alguna forma complementa los resultados obtenidos en los siguientes apartados.

Después de obtener esta visión general del sistema se estudio la dinámica de algunos de los principales procesos oceanográficos de la zona, la corriente ibérica hacia el polo (Iberian Poleward Current IPC), las plumas de ríos y el afloramiento. En los tres casos se siguió una estructura de trabajo similar, en la que inicialmente se desarrollaron métodos de detección que permitieron definir las distintas estructuras así como caracterizar la variabilidad tanto espacial como temporal de las mismas. Por último se estimaron las relaciones con los principales forzadores de cada proceso así como los momentos en los que estas relaciones eran más relevantes.

El estudio de la IPC permitió definir de forma cualitativa la estacionalidad de la influencia del agua cálida y salina advectada por esta corriente utilizando los datos de las 5 secciones. De octubre a diciembre las aguas centrales de origen subtropical ($ENACW_{st}$) advectadas por la IPC, estuvieron presentes en toda la plataforma norte de la Península Ibérica (fase de desarrollo de la IPC). De febrero a agosto, la IPC retrocede hacia el oeste provocando el desarrollo de un frente (IPCF) que separa los modos subtropicales y subpolares de las aguas centrales (fase de decaimiento). Entre

estas dos situaciones extremas en enero y septiembre se encontraron periodos de transición con condiciones hidrográficas intermedias.

Los métodos desarrollados para la detección de la IPC se aplicaron a los datos obtenidos en las campañas de primavera. Con este análisis se obtuvo la variabilidad interannual de esta corriente en esta época del año. En la primavera, al inicio de la fase de decaimiento, la posición de IPCF a lo largo de la plataforma varía anualmente entre los extremos de Rías Baixas (42.5°N 9.0°W) en 1990 y 1994 hasta el cañón de Cabo Breton (44.0°N 2.0°W) en 2006, encontrándose la situación promedio en la parte central del mar Cantábrico, en los alrededores de Cabo Peñas (44.0°N 6.5°W). La posición de la IPCF presentó un desplazamiento significativo de 6,5 mn por año ($r = 0.62$, $p = 0.003$, $n = 20$). Este parámetro, estuvo positivamente correlacionado con el gradiente de temperatura meridional (MTG) medido durante el verano anterior ($r = 0.67$, $p < 0.005$, lag = 8 –August) y con los vientos del norte y del este medidos durante el invierno previo (v-component, $r = -0.53$, $p < 0.05$, lag = 5 –November; u-component, $r = -0.85$, $p < 0.001$, lag = 4 –December). También se encontraron relaciones significativas con el índice climático del Atlántico Este (EA). Estas relaciones están de acuerdo con las teorías que proponen al MTG y a los vientos regionales, forzados por los patrones de circulación atmosférica de larga escala (EA), como moduladores de la incursión de la IPC en la plataforma norte de la Península Ibérica.

Para estudiar la variabilidad espacio temporal de las plumas de ríos en la zona se aplicó un esquema de trabajo similar. Se desarrollaron métodos de detección objetiva, basados en gradientes de salinidad que en este caso se estimaron tanto para las 5 secciones como para las campañas de primavera. La aplicación de esta metodología en el primer caso, permitió estimar la estacionalidad de la presencia ausencia de plumas. Este patrón de variación está principalmente relacionado con la estacionalidad del régimen de precipitación que varía a lo largo de la plataforma norte de la Península Ibérica. La mayor probabilidad de ocurrencia de plumas (>70%) tiene lugar entre Noviembre y Febrero en el Cantábrico Central, se extiende hasta marzo en la zona oeste y hasta mayo en las partes más al este de la zona de estudio.

Los resultados obtenidos con las campañas de primavera permitieron definir la variabilidad interannual de la influencia de las descargas de ríos, así como la situación media. Se definieron dos zonas de alta frecuencia, una en el área de influencia del río Miño y las Rías Baixas y otra en frente de la desembocadura del río Adour. También se encontró una zona de menor frecuencia e intensidad en el Cantábrico central, relacionada con el río Nalón y otros ríos de menor relevancia. Como en el caso de la

IPC los resultados obtenidos para las plumas se utilizaron para definir las relación de estas estructuras oceanográficas con las precipitaciones y las descargas de los principales ríos en cada caso.

Los métodos utilizados para estimar la presencia y variabilidad del afloramiento en la zona de estudio se basaron en gradientes temperatura. Se aplicaron a las dos bases de datos principales caracterizándose, como en los casos anteriores, la variabilidad espacio temporal del afloramiento. Los resultados obtenidos utilizando las series temporales de las radiales permitieron definir la estacionalidad de este proceso, que fue claramente distinta, en las secciones de la plataforma oeste (Vigo y A Coruña) respecto a las secciones del norte (Cudillero, Gijón y Santander). El comportamiento de este proceso en la costa oeste presentó una estacionalidad muy marcada, con un periodo de afloramiento que fue de Abril a Octubre y que se caracterizó por probabilidades de presencia superiores al 70% que se contraponen con el periodo de Octubre a Marzo en las que la probabilidad cae al 20%. En la costa norte, las probabilidades más altas de afloramiento tuvieron lugar en verano (50%) mientras que en el resto del año fueron bajas, sin llegar a alcanzar el 20%. Se utilizo un método de regresión logística para caracterizar la relación entre la intensidad los vientos favorables al afloramiento promediados los 15 días previos a cada muestreo (W_{15}) y la presencia/ausencia del mismo [$U_p = e^{-0.206 \cdot w_{15} - 0.379} / (1 + e^{-0.206 \cdot w_{15} - 0.379})$]; $n = 549$, $r = 0.32$, $p < 0.001$]. Utilizando esta relación se determinó que valores de W_{15} menores de -2 ms^{-1} determinan probabilidades de presencia de afloramiento superiores al 50%.

El análisis de los datos obtenidos en las campañas de primavera permitió definir dos áreas de alta probabilidad de ocurrencia de afloramiento, una localizada a lo largo de la costa de Galicia, desde las Rías Bajas ($42.1^\circ \text{ N } 9.0^\circ \text{ W}$) hasta el cabo Finisterre ($42.9^\circ \text{ N } 9.3^\circ \text{ W}$), con una probabilidad superior al 50%. La segunda zona estaba localizada en los alrededores del cabo Peñas ($43.6^\circ \text{ N } 5.8^\circ \text{ W}$) con una probabilidad del 20%. La relación entre W_{15} y la presencia de este proceso en ésta época del año fue [$U_p = e^{-0.899 \cdot w_{15} - 1.761} / (1 + e^{-0.899 \cdot w_{15} - 1.761})$]; $n = 32$, $r = 0.72$, $p < 0.001$]. Valores de W_{15} menores de -2 ms^{-1} se correspondieron con probabilidades de presencia de afloramiento superiores al 50%. En este caso se encontró una relación significativa entre el W_{15} y el área influenciada por el afloramiento que fue [$U_a = -1941 w_{15} + 4012$; $n=14$, $r = -0.74$, $p < 0.005$].

En el último capítulo de esta tesis, se utilizaron las herramientas desarrolladas, para estudiar la interacción de los procesos de mesoescala sobre la composición del mesozooplankton en una campaña de primavera llevada a cavo en el N y NO de la Península Ibérica en el 2004. La determinación de la IPCF y la influencia de las

plumas de ríos permitió dividir el área de estudio en tres regiones, la región oeste (WC) definida por agua calidad y salina relacionada con la presencia de la IPC, la región este caracterizada por agua más fría y dulce en relación a la influencia de la pluma del río Adour de la costa francesa. Por último la región central que se caracterizó por condiciones termohalinas intermedias respecto a las otras dos divisiones.

La profundidad de la capa de mezcla en estas tres regiones fue distinta: WC se caracterizó por una columna de agua completamente mezclada mientras que en EC, las descargas de los ríos produjeron la estratificación de los metros superficiales (<10m). En CC se encontraron dos regímenes distintos que separaban las estaciones más costeras (estratificación) de las de la plataforma (columna de agua mezclada)

Se encontró una clara relación entre la zonación basada en la presencia de los distintos procesos oceanográficos y la distribución de los grupos de mesozooplancton basados en su composición específica. Los resultados del test de Mantel mostraron una relación entre la distribución espacial de las condiciones físicas y los grupos de mesozooplancton ($n = 63$, $r = 0.70$, $p < 0.001$). En WC la comunidad se encontró dominada por *Paracalanus parvus*, *Oithona helgolandica*, *Acartia clausi* y *Clausocalanus pergens*, mientras que en EC las principales especies fueron *Noctiluca scintillans*, *Oncaea media* y *Temora longicornis*. La región CC mostró una composición similar de copépodos que WC pero en este caso los larvaceos (*Oikopleura spp* y *Fritillaria spp.*) fueron más abundantes. Dentro de cada una de las zonas las abundancias relativas de las especies dominantes variaron entre las estaciones de la costa y la plataforma.

Chapter 1: Introducción General

En 1892 Havelok Ellis definió la Ecología como el estudio científico de las interacciones entre los organismos y su ambiente. Esta definición fue ampliada años más tarde por Krebs (1972) al considerar también el estudio de la distribución de los organismos siendo capaz de definir en qué lugares se encuentran, en qué cantidades aparecen y cuáles son los procesos que dan lugar a la distribución y abundancia de los organismos.

La ecología es una ciencia que se aproxima a estos problemas considerando distintos niveles de organización de los organismos, a nivel de individuo (determinando como le afecta el ambiente), de población (definiendo la presencia ausencia, etc) y de comunidad (estudiando la composición y organización). Los ecólogos también estudian estos problemas con una perspectiva más amplia considerando el sistema como conjunto de flujos de materia y energía entre los componentes vivos de cada uno de los niveles organizativos en los que se dividen. El proceso de entendimiento de los distintos niveles de organización de una disciplina tan compleja como esta, implica una aproximación desde el método científico en el que el primer paso nos obliga a entender y explicar los principales procesos que median en los sistemas que observamos. La primera aproximación en este nivel cognitivo es la descripción de los procesos tanto físicos como biológicos siendo necesario centrarse en problemas o elementos concretos del sistema (Begon *et al.*, 2006).

Los ecólogos intentan predecir cómo se comporta una especie o una población, y también una comunidad o ecosistema bajo condiciones controladas. En muchas de estas situaciones las relaciones o las explicaciones que se dan se hacen sin entender las interacciones y procesos que median y producen los cambios que observamos. La única vía para obtener predicciones robustas en el estudio de los distintos niveles y partes de un ecosistema, incluso cuando las circunstancias se apartan de las condiciones normales, es cuando entendemos que procesos están operando en el cambio.

El desarrollo de los modelos matemáticos juega un papel muy importante en la evolución de la ecología. Tiene mucha importancia en sus habilidades para predecir procesos futuros pero en última instancia, en el mundo real, este tipo de herramientas son muy útiles para obtener información de los sistemas naturales y estudiar su funcionamiento.

Tabla 1: Artículos que tienen como objetivo el estudio del plancton en el Norte y Noroeste de la Península Ibérica publicados entre 1990 y 2014

Periodo	Aproximación	Artículos
1990-1995	Descripción	Delbee and Castel (1991), Villate (1991b), Villate (1991a), Acuna and Anadon (1992), Bode and Fernandez (1992), Fernandez <i>et al.</i> (1993) y Fernandez <i>et al.</i> (1995)
1996-2000	Descripción	Villate (1997), Villate <i>et al.</i> (1997), Barquero <i>et al.</i> (1998b), Ruiz <i>et al.</i> (1998) y Serret <i>et al.</i> (1999)
	Descripción y Relaciones	Valdes and Moral (1998), Beaugrand <i>et al.</i> (2000), y Quevedo and Anadon (2000)
2001-2005	Descripción	Bode <i>et al.</i> (2002a), Gil <i>et al.</i> (2002), Rodriguez <i>et al.</i> (2003), Fernandez <i>et al.</i> (2004), Isla <i>et al.</i> (2004) y Uriarte and Villate (2004)
	Descripción y Relaciones	Fernandez and Acuna (2003) y Calvo-Diaz <i>et al.</i> (2004)
2006-2010	Modelado	Albaina and Irigoien (2004)
	Descripción	Huskin <i>et al.</i> (2006), Albaina and Irigoien (2007b), Lopez <i>et al.</i> (2007), Valdés <i>et al.</i> (2007), d'Elbee <i>et al.</i> (2009), Rodríguez <i>et al.</i> (2009) y Zarauz <i>et al.</i> (2009)
	Descripción y Relaciones	Uriarte and Villate (2006), Ceballos <i>et al.</i> (2006), Villate <i>et al.</i> (2008), Bode <i>et al.</i> (2009) e Irigoien <i>et al.</i> (2009)
2011-2014	Modelado	Stenseth <i>et al.</i> (2006), Albaina and Irigoien (2007a), Zarauz <i>et al.</i> (2007), Zarauz <i>et al.</i> (2008) y Albaina <i>et al.</i> (2009)
	Descripción	Lezama-Ochoa <i>et al.</i> (2011), Pascual <i>et al.</i> (2011) y Bode <i>et al.</i> (2012)
	Descripción y Relaciones	Tortajada <i>et al.</i> (2012), Intxausti <i>et al.</i> (2012) y Lezama-Ochoa <i>et al.</i> (2014)
	Modelado	Irigoien <i>et al.</i> (2011) y Chust <i>et al.</i> (2014)

Si ya de por si el estudio de los sistemas ecológicos es un problema complejo que implica una inversión en tiempo, capital humano y dinero excepcional, cuando hablamos de ecología marina estas inversiones aumentan de forma considerable. Las infraestructuras necesarias y los altísimos costes que implican el muestreo en el mar hace que los avances estén muy limitados y que el conocimiento del sistema se encuentre en las primeras niveles del proceso cognitivo. En este momento la ecología marina está en una fase observación y descripción de los principales procesos que rigen el funcionamiento de los ecosistemas marinos. Aunque en la actualidad se están dando pasos para desarrollar modelos que nos permitan entender y predecir distintos aspectos de estos sistemas, todavía queda mucho camino para obtener resultados robustos.

A modo de ejemplo, se ha hecho una revisión bibliográfica, no exhaustiva, sobre los artículos que estudian el plancton en el Norte y Noroeste de la Península Ibérica (Figura 1 y Tabla 1) desde 1990 hasta la actualidad. De los 51 artículos revisados en este periodo, únicamente 7 (14%) tienen como resultado final modelos con mayor o menor capacidad de predicción. Los artículos que se han denominado como

“Descripción y relaciones” hacen referencia a trabajos en los que se obtienen algún tipo de relación entre algún aspecto del plancton y alguna variable física. En la figura 1 se puede observar que la proporción de estos dos tipos de trabajos aumenta en los últimos años como tendencia general.

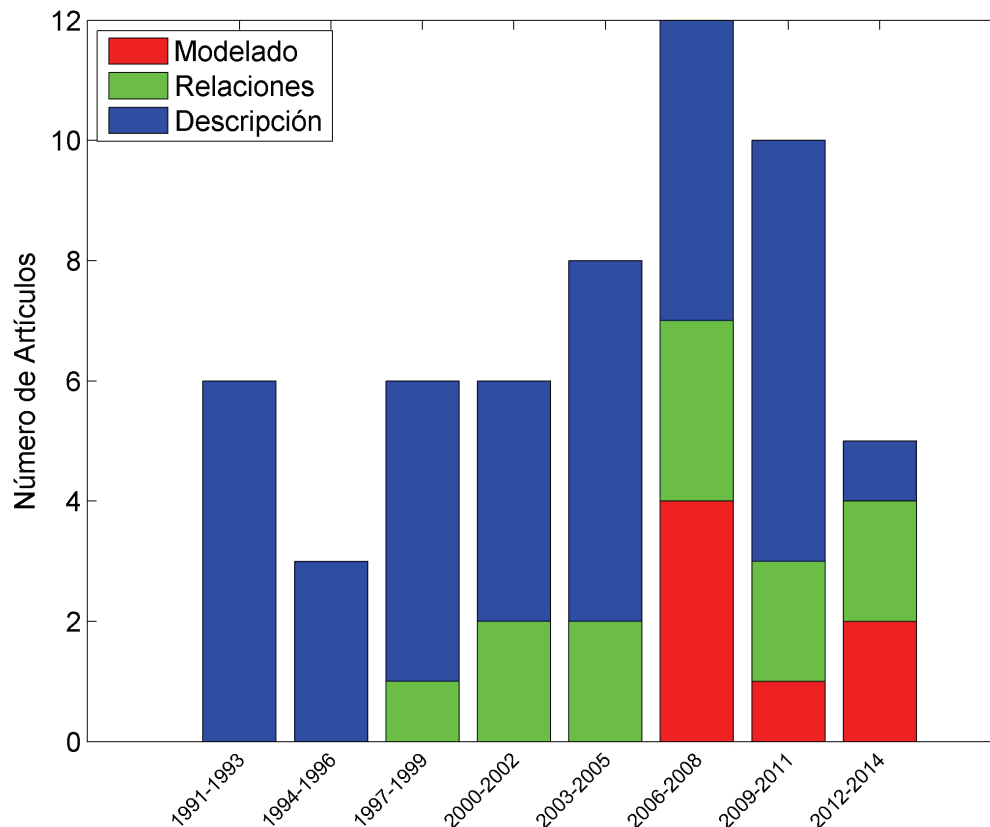


Figure 1: Evolución temporal de el número de artículos que tienen como temática la descripción (azul) la obtención de relaciones (verde) y el modelado (rojo) de distintos aspectos del plancton en el Norte y Noroeste de la Península Ibérica.

Los avances en nuevas tecnologías, como el desarrollo de sistemas de observación ambiental instalados en satélites, la aparición de programas internacionales como Argos (www.argo.ucsd.edu) o, en los últimos años, el desarrollo de sistemas de muestreo autónomo (e. g. Gliders), hace que en la actualidad haya aumentado considerablemente la información disponible sobre condiciones ambientales. Aunque se ha avanzado mucho en la obtención automática de información sobre variables químicas y biológicas, la disponibilidad de estos datos es mucho menor. En este sentido el desarrollo de sensores que nos permiten obtener este tipo de información ha sido considerable, pero el uso de estas tecnologías implica una inversión en mantenimiento ingente lo que hace que se limite mucho su utilización y en cierta

medida la calidad de los datos que obtienen. En este contexto se pone de manifiesto lo imprescindible del muestreo in situ mediante campañas oceanográficas, además de la importancia de programas de monitoreo continuo que permitan recabar información directa y cuasi sinóptica tanto del ambiente físico como de los distintos aspectos de los componentes del ecosistema.

Los ecólogos marinos, cuando se plantean estudiar y modelar un proceso concreto, a escala de organismo, población, comunidad etc., independientemente del nivel en el que se encuentre, la información ambiental de la que se dispone, en muchos de los casos son las variables oceanográficas básicas como temperatura, salinidad, presión y en el mejor de los casos nutrientes y fluorescencia/clorofila. Es muy difícil dar un paso más allá y pasar de la descripción a la cuantificación y modelado de los procesos sin disponer de datos adecuados, series temporales suficientemente largas, distribuciones espaciales con resoluciones altas, etc. Sin esta información es complicado entender e intentar interpretar y predecir los procesos a los que nos enfrentamos. Un camino muy extendido en la comunidad científica que trabaja en ecología marina es intentar explicar todo, modelos de hábitats, dinámicas poblacionales, interacciones entre especies etc. en función de estas variables básicas. Este tipo de aproximación es muy habitual simplemente porque no se dispone de más información. En el océano este tipo de forzador, la influencia directa (fisiológica) de la temperatura o la salinidad, puede actuar como limitante de la distribución de especies de su actividad y de sus interacciones pero como factor de variación, a nivel regional, no es de gran relevancia. La dinámica de una especie está modulada por muchos procesos. La disponibilidad de recursos, la competencia, depredación, parasitismo, etc. Las condiciones ambientales actúan sobre todos ellos a distintos niveles y con distintas intensidades. La incapacidad de poder manejar todas estas interacciones, debido a que no se dispone de información y datos suficientes, hace que intentemos simplificar al máximo las relaciones y modelos que elaboramos.

Si queremos estudiar y modelar la dinámica del fitoplancton en las costas Gallegas, una zona de afloramiento estacional, es fácil que consigamos obtener modelos o relaciones entre la cantidad de fitoplancton en la zona y la temperatura o incluso con la salinidad. En este caso estas variables nos sirven como aproximaciones o estimadores de la intensidad del afloramiento. La presencia de este proceso oceanográfico implica entrada de agua fría, más salina y con mayor concentración de nutrientes. Estas condiciones unidas a que en esta zona el afloramiento se produce en un periodo en el que la radiación no es limitante hace que sean posibles concentraciones altas de fitoplancton. La utilidad de este modelo es muy baja en tanto en cuanto se utiliza la

temperatura como un estimador de la intensidad de afloramiento y por tanto como estimador de la concentración de nutrientes. Teniendo en cuenta que la temperatura del agua puede ser modificada por muchos procesos (plumas, corrientes, giros, radiación, etc.) hace que cambios sobre ella que no estén producidos por afloramiento no impliquen aumento de nutrientes y por tanto no permitan niveles altos de fitoplancton. En la misma línea si intentamos aplicar la relación o el modelo obtenido en otra zona como el mar Cantábrico, en la que el afloramiento tiene una dinámica estacional distinta, y en el que la dinámica de variación de la temperatura es completamente diferente, los resultados obtenidos serán de muy baja calidad. En la mayoría de los casos en este tipo de relaciones y modelos las variables que se utilizan actúan como proxies de los procesos que realmente modifican la distribución, dinámica e interacciones de las especies. El problema que tiene utilizar este tipo de aproximación es que estas variables no solo son modificadas por los procesos que queremos monitorizar.

En este contexto es en el que se enmarca el desarrollo de esta tesis. Ante la imposibilidad de tener las bases de datos adecuadas con las variables necesarias para afrontar el estudio de la dinámica del mesozooplancton, se consideró que era necesario previamente, el afrontar este problema desde el punto de vista de la caracterización y cuantificación de los procesos oceanográficos que más influyen sobre la dinámica de las condiciones ambientales en la zona en el que se desarrolla esta tesis.

Inicialmente, en el capítulo 2, se estudió la variabilidad espacio temporal de la temperatura y la salinidad en el Norte y Noroeste de la península Ibérica y se relacionan los patrones de cambio encontrados con los principales procesos oceanográficos que los generan. Esta aproximación inicial busca elaborar un marco básico que permita entender los principales factores de variación del sistema desde un punto de vista deductivo. De esta manera aunque se parametrize la dinámica de estas dos variables se interpretará de forma cualitativa su relación con los principales procesos que fuerzan los distintos cambios.

En los siguientes apartados el estudio se afrontará desde una perspectiva completamente opuesta. Se seleccionaron, la Corriente Ibérica hacia el polo (Iberian Poleward Current, IPC), las plumas de ríos y el afloramiento, como algunos de los principales procesos oceanográficos de la zona, con mayor influencia en la variabilidad ambiental del sistema. El estudio de la dinámica de las condiciones físicas se hará partiendo de estos procesos oceanográficos y definiéndolos en función de los cambios que provocan sobre las variables básicas oceanográficas.

En el capítulo 3 se muestran los métodos desarrollados para la determinación objetiva de la influencia de agua cálida y salina advectada por la Corriente Ibérica hacia el polo. Estos métodos se aplican sobre las bases de datos disponibles para obtener la variabilidad espacio temporal del proceso así como su relación con sus principales forzadores.

Siguiendo la misma estructura de trabajo, en el capítulo 4, se describen los métodos que se elaboraron para la detección y caracterización de plumas de ríos. Utilizando estas herramientas se caracterizó la variabilidad espacio temporal de este proceso así como su relación con las precipitaciones y las descargas de ríos, considerados como principales forzadores.

En el capítulo 5 el proceso que se estudia es el afloramiento. Se muestran los métodos utilizados para su detección, basados en la temperatura, así como la variabilidad espacio temporal del proceso y su relación con el viento.

Por último en el capítulo 6 se utilizan los métodos desarrollados en los apartados anteriores para determinar la influencia de estos procesos oceanográficos sobre la composición y distribución de las especies de mesozooplancton.

Chapter 2: Temporal and spatial variability of thermohaline properties in the North Iberian Shelf (NIS): 1987-2008

Introduction

The North Iberian Shelf (NIS) is located in the inter-gyre zone of the North-East Atlantic that separates the subpolar and subtropical gyres (Pollard *et al.*, 1996). This implies that the area is characterized by two modes of Eastern North Atlantic Central Water (ENACW): the subpolar (ENACW_{sp}) and subtropical (ENACW_{st}). The ENACW_{st} ranges from 12.2 to 18.5 °C and from 35.66 to 36.75 psu (Ríos *et al.*, 1992) and its origin is located in a frontal area near the Azores islands. The subpolar mode (ENACW_{sp}) is formed around 46 °N and corresponds to waters between 4 and 12 °C and between 34.96 and 35.66 psu (Harvey, 1982). At the easternmost part of the Cantabrian Sea we can find other water mass named Bay of Biscay Central Water (Fraga *et al.*, 1982; Botas *et al.*, 1989), which is characterized by lower values of temperature (11.0 to 11.8 °C) and salinity (35.53 to 35.58).

The variability of the meteorological, and hence hydrographic, scenario over the NIS is determined to large extent by the dipole originated by the interaction of the Azores High and the Iceland Low pressure systems, which varies its intensity and position seasonally, generating different hydrographic processes along the year. During winter, the intensity of the Azores High is relatively low, which favours the intrusion of cold atmospheric fronts giving rise to the predominance of southerly and westerly winds and moderate-to-high precipitations. The importance of river discharges promotes the development of river plumes along the NIS, such as the so called West Iberian Buoyant Plume (WIBP) associated with discharges from river Miño and from the short-course rivers located along the Galician Rias Baixas and Rías Altas (Peliz *et al.*, 2005; Otero *et al.*, 2008b; Otero *et al.*, 2009b; González-Nuevo & Nogueira, 2014b) and the plume from Adour River located in the easternmost part of the Cantabrian Sea (Puillat *et al.*, 2004; González-Nuevo & Nogueira, 2014b). Also during this season, the Iberian Poleward Current (IPC), a compensatory current mainly forced by the Meridional Thermal Gradient (MTG) and modulated by wind patterns (Peliz *et al.*, 2005), flows along the Galician coast and Cantabrian Sea conveying warm and salty waters of subtropical origin (ENACW_{st}). (Peliz *et al.*, 2005). During spring, the strengthening of the Azores High pressure cell promotes the predominance of northerly and easterly winds which cause coastal upwelling along the western Iberian shelf (Alvarez *et al.*, 2008). River plumes are still important in the central and eastern parts of the Cantabrian Sea because of snow melting in the Cantabrian Sea Range and the Pyrenees respectively, but are in general terms less intense along the NIS as a consequence of the reduction of the influence of cold fronts and precipitations (González-Nuevo & Nogueira, 2014b). The IPC reduce also its strength, entering in the decaying phase of its seasonal cycle (Peliz *et al.*, 2005).

The summer is characterized by the atmospheric stability associated to the intensification and northward displacement of the Azores High pressure cell. The intensity of northerly and easterly winds generate frequent coastal upwelling events along the western part of the NIS (Fraga, 1981; Fiúza *et al.*, 1982). The occurrence, strength and duration of upwelling events along the Cantabrian coast are different because upwelling favourable winds (easterlies) are less constant and intense (Botas *et al.*, 1990; Fontán *et al.*, 2008). The influence of the IPC along the NIS diminish also during this part of the year (Peliz *et al.*, 2005). During autumn, the Azores high weakens and displaces southwards, which allows the entrance of cold fronts and hence the increment of the frequency and intensity of precipitations. The influence of river plumes gains importance along the whole NIS, especially in the proximities of Miño and Adour rivers. The intensification of southerly and westerly winds promotes the occurrence of coastal downwelling events (Fiúza *et al.*, 1982; Álvarez-Salgado *et al.*, 2003). The influence of the IPC increase in this season as a consequence of the intensification of the MTG (Peliz *et al.*, 2005).

Although the atmospheric configuration determines to large extent the seasonality of oceanographic processes along the NIS, the interannual variability of the intensity and duration of the mesoscale processes generate deviations of temperature and salinity fields from its seasonal cycles. In the current context of climate change and for a complex oceanographic domain such as the NIS, it is relevant to define the baseline conditions in order to be able to disentangle the natural variability of the system and the changes generated by human activities. The objective of this work is to describe and parameterize the spatial and temporal variability of temperature and salinity in the western (Galician) and northern (Cantabrian Sea) parts of the NIS.

Material and Methods

Database

Sea Surface Temperature (SST)

In order to evaluate the long term variability of sea surface temperature (SST) in the western and northern parts of the NIS, time series of SST at 42.5° N 11° W and 44 ° N 6° W (Figure 1) were extracted from the NOAA extended reconstructed SST version 3 (NOAA_ERSST_V3) data base, provided by the NOAA/OAR/ESRL PSD, Boulder, Colorado, USA, from their Web site at <http://www.esrl.noaa.gov/psd/>. The time series data extends from 1850 to 2009 and the sampling frequency was monthly.

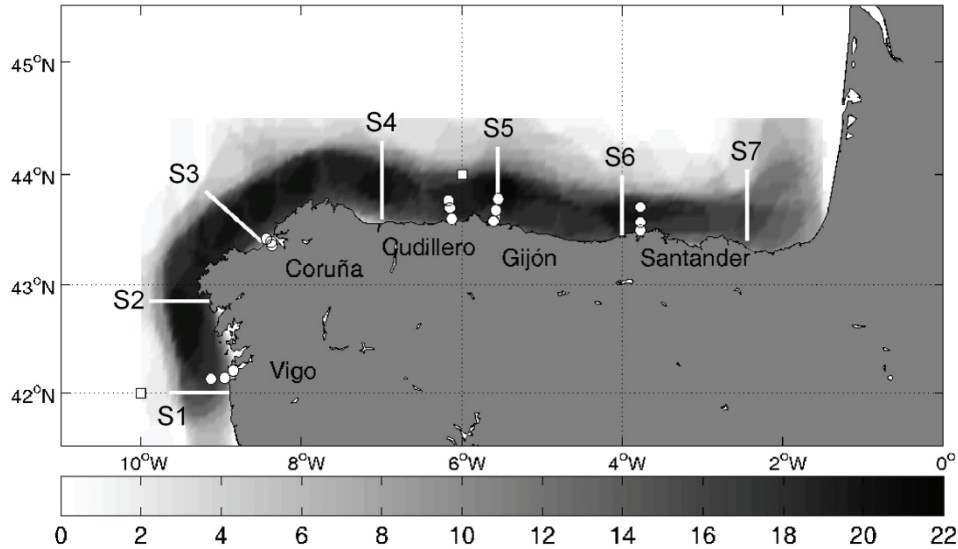


Figure 1: Map of the study area with the sampling density of the spring surveys. White dots represent the stations of the sections of Vigo, Coruña, Cudillero, Gijón and Santander. The white squares are the locations of the SST time series obtained from NOAA/OAR/ESRL PSD, Boulder, Colorado, USA. The climatic sections of the spring cruises are represented as white lines.

Across-shelf variability of temperature and salinity along the NIS

To characterize the temporal variability of thermohaline water column conditions along the NIS we used temperature and salinity data from Vigo, A Coruña, Cudillero, Gijón and Santander across-shelf sections supported by the RADIALES project of the Instituto Español de Oceanografía (Figure 1). These series have been sampled from 1994 to 2005 with monthly frequency, with the exception of the Gijón section that started in 2001. Sampling was carried out using different models of CTD to obtain temperature and salinity profiles from the surface down to the bottom of each hydrographic station of the across-shelf sections.

Temperature and salinity fields along the NIS during spring

The database of spring surveys is integrated by temperature and salinity CTD profiles obtained in the NIS during spring (March-April) between the years 1987 and 2008 (Table 1) in hydrographic stations distributed over the shelf and arranged in transects perpendicular to the coast. Some areas were visited up to 20 times during the analyzed 21-year period. The profiles extend from the surface (5m depth) down to 5 m above the bottom or to a maximum 500 m depth in deeper stations.

Time series analysis

The time series of temperature and salinity of each station were modeled following a time series additive model (Equation 1 and Figure 2) to make them stationary and correct the overestimation of the correlations due to the possible autocorrelation of the time series (Wei, 1989)

$$Y_t = \bar{y} + LT[y_t] + SC[y_t] + R[y_t] + \varepsilon_t \quad (1)$$

where, subscripts t is the index for time, \bar{y} is the average value of time series, LT and SC represent the linear and periodic trend components respectively, R the autocorrelation and ε_t the white noise. LT and SC were treated as deterministic components (Chatfield, 1996)

The first component (LT) is calculated using a classical least-square regression method applying a linear model (Equation 2)

$$LT = bt + a \quad (2)$$

where LT is the value of the series added by the linear trend at time t , b is the slope and a the intercept. With this approximation we will select the model for which the sum of squared residuals (difference between an observed value and the value given by the model) has its least value.

The periodic component (SC) was fitted using a sum of periodic functions (harmonics) that follow the model (Equation 3),

$$SC[y_t] = \sum_{i=1}^{\frac{n}{2}} A_{T_i} \cos\left(\frac{2\pi}{T_i} t + \theta_{T_i}\right) \quad (3)$$

where, A_i is the amplitude T_i the period and θ_i the phase in radians of the harmonic i . Using this approximation we can characterize both long-term variation like, interannual or decadal oscillations, and seasonal cycle. The parameters of this model were extracted by means of Fourier analysis (Poularikas & Seely, 1991) and were used to reconstruct the periodogram that is a graphical representation of the variance explained by each harmonic in function of the period. The determination of significant harmonics is carried out using Fisher test or G statistic (Davis, 1986) (Equation 4). This method is based in the relationship between the variance of one harmonic (s_{\max}^2) and the total variance (s^2) of the series.

$$G = \frac{s_{\max}^2}{s^2} \quad (4)$$

One harmonic is significant if G is higher than one critic value G_c (Equation 5) calculated following

$$G_c = 1 - e^{-\frac{\left(\ln(\alpha) - \ln\left(\frac{n}{2}\right)\right)}{\frac{n}{2}-1}} \quad (5)$$

where p is the significance level and n the number of data of the time series. This statistics is valid only for time series with more than 30 observations.

Table 1: Name of the project, vessel used, and period (start and end date) of the spring surveys.

Campaign	Vessel	Start	End
SARPAREA	Lura	13/04/87	24/04/87
MPHSARACUS	Cornide Saavedra	01/04/88	04/05/88
MPH	Investigador	18/04/90	09/05/90
ECOSARP	Cornide Saavedra	17/04/91	09/05/91
ITIONORTE	Investigador	22/04/92	09/05/92
PELACUS	Cornide Saavedra	14/04/93	03/05/93
SEFOS	Cornide Saavedra	15/03/94	13/04/94
MPH	Cornide Saavedra	26/03/95	14/04/95
SEFOS	Cornide Saavedra	11/03/96	31/03/96
PELACUS	Thalassa	08/03/97	31/03/97
PELACUS	Thalassa	17/03/98	08/04/98
PELACUS	Thalassa	03/03/99	29/03/99
PELACUS	Thalassa	27/03/00	12/04/00
PELACUS	Thalassa	30/03/01	22/04/01
PELACUS	Thalassa	09/03/02	04/04/02
PELACUS	Thalassa	19/03/03	12/04/03
PELACUS	Thalassa	30/03/04	22/04/04
PELACUS	Thalassa	05/04/05	29/04/05
PELACUS	Thalassa	01/04/06	28/04/06
PELACUS	Thalassa	27/03/07	23/04/07
PELACUS	Thalassa	28/03/08	20/04/08

The autocorrelation was modeled by means of the Box-Jenkins approach (Box & Jenkins, 1976). The stochastic component (Equation 6), the de-trended and de-seasonalized residuals, was parameterized by means of an autoregressive model, which involves the description of the time series in terms of a weighted sum of its own past values,

$$R[y_t] = \sum_{i=1}^{i=p} \phi_i (R[y_{t-i}]) \quad (6)$$

where, p is the order of the auto-regressive model and ϕ_i are the auto-regressive parameters. The order of the autoregressive process is defined by the inspection of the auto-correlation (acf) and partial auto-correlation functions (pacf), and the auto-regressive parameters were estimated using the Yule-Walker equations (Wei, 1989).

The last component is the white noise (ε), a random signal with a flat power spectral density. In other words, the signal contains equal power within a fixed bandwidth at any center frequency.

Geostatistic analysis

The spatial variation of temperature and salinity along the NIS was parameterized calculating the empirical correlograms (Legendre & Legendre, 1998) of the horizontal fields of these variables, from 5 to 100 m depth at each 5 m depth interval, for each survey. The empirical functions were fitted using a Gaussian model [Equation 8] where R , A , L and d are, respectively, the correlation, correlation factor, characteristic length scale and distance:

$$R(d) = A \cdot e^{\frac{-d^2}{2 \cdot L^2}} \quad (8)$$

An example of the results obtained with this approach for the salinity field at 10 m depth during the Pelacus 2002 cruise is shown in Figure 3.

We interpolated the temperature field using values of $A = 0.57$ and $L = 27.8$, and of $A = 0.61$ and $L = 46.1$ for the salinity field. These parameters were obtained using data for all the cruises and for the horizontal fields between 5 to 100 m depth and at depth intervals of 1 meter depth. The mean and standard deviation (STD) fields of temperature and salinity at 10 30 50 75 and 100 m depth were derived from the interpolated values. The same methodology was applied to obtain seven climatic across-shelf sections selected to cover all the NIS (Figure 1).

Results

Long-term variation of sea surface temperature

A deterministic time series analysis was carried out on the SST time series for the Galician and Cantabrian parts of the NIS. In general terms, the results were similar at both locations. The differences in the components of variation were probably produced as a consequence of different influence of mesoscale processes in the two areas.

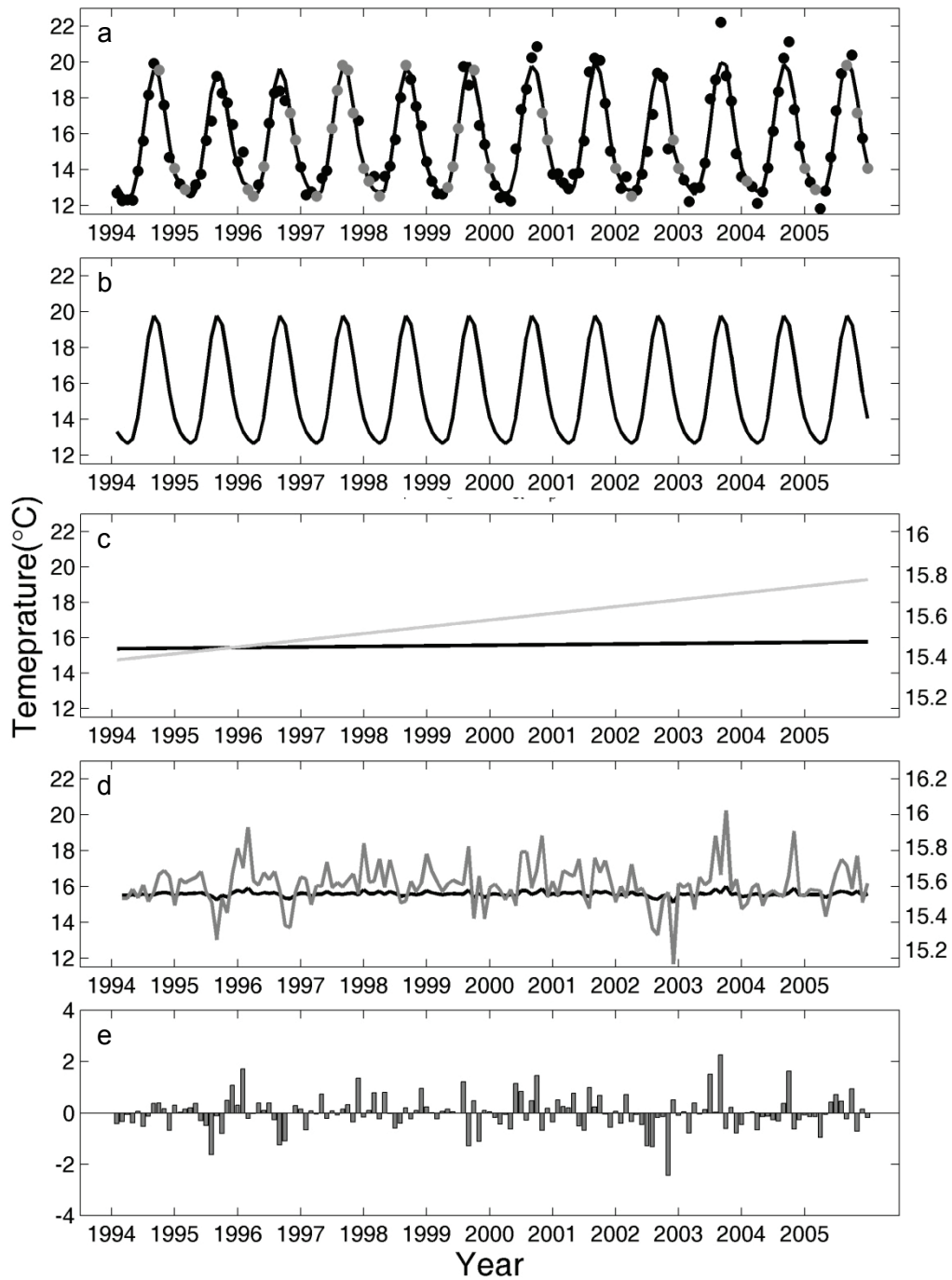


Figure 2: Example of the time series analysis applied to temperature at 10m depth of the coastal station of the section of Cudillero. The different panels show (a) raw (black dots) and interpolated data (gray dots), (b) seasonal cycle, (c) linear trend, (d) autocorrelation component and (e) white noise error. All components are represented with black lines with the same scale (left axis) and with gray line with an adjusted scale (right axis).

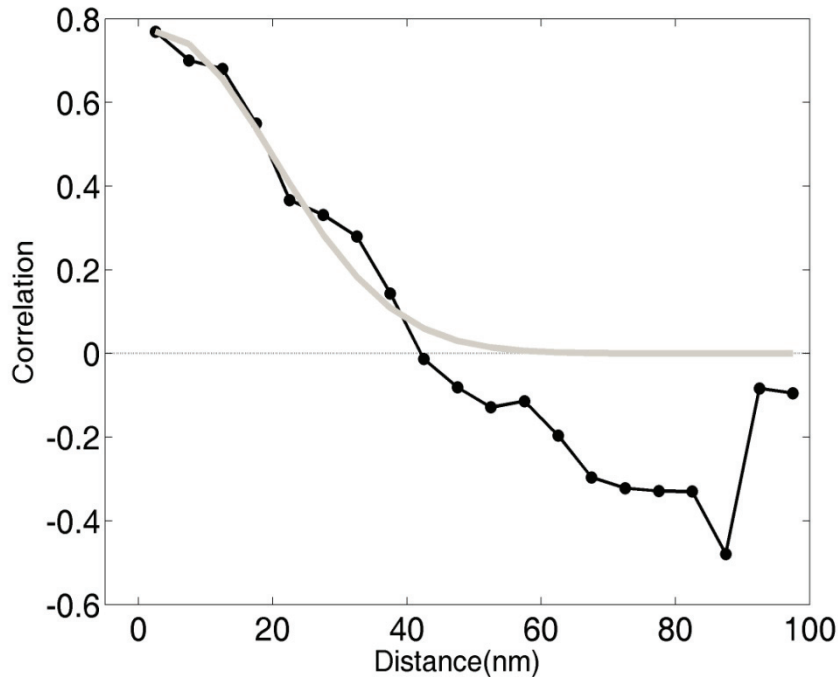


Figure 3: Example of correlogram fitted to the salinity field at 75 m depth during the spring survey of 1999 (Pelacus1999). Field data are represented with black line and the Gaussian fitted function with a gray line.

The general mean values were 15.20 and 15.6 °C for the Galician and Cantabrian series respectively. In both locations, the extracted seasonal cycle (Figure 4) follow the expected pattern of variation, characterized by minima values in winter and maxima in summer. The amplitude of the seasonal cycle was, however, higher in the Cantabrian than in the Galician time series, 4.2 °C (95% of explained variance) and 3.3 °C (93%) respectively (Table 2).

Before the extraction of other components of temporal variation, we analyzed different periods of the resultant de-seasonalised residuals (Figure 4). We defined four periods attending to the characteristics of their linear trends. We distinguish two decreasing periods between 1870 and 1910 ($n = 492$, $b = -0.0148$ °C y^{-1} ; $r = -0.29$; $p < 0.001$) and between 1945 and 1975 ($n = 372$, $b = -0.0024$ °C y^{-1} ; $r = -0.37$; $p < 0.001$), and two increasing periods between 1910 and 1945 ($n = 456$, $b = 0.0164$ °C y^{-1} ; $r = -0.33$; $p < 0.001$) and between 1975 and 2009 ($n = 408$, $b = 0.027$ °C y^{-1} ; $r = 0.49$; $p < 0.001$).

It is remarkable that increasing/decreasing parts of the first cycle (1870-1945) had similar length (492 and 456 months) and slope (-0.0148 and 0.0164), so the resultant trend for whole cycle was not significant different from 0. The decreasing part of the second cycle (1996-2009) was shorter (372 respect 408 months) and had lower slope than the

increasing part (-0.002 and 0.027), making that the second cycle presents an upward temperature trend of $0.0074 \text{ }^{\circ}\text{C y}^{-1}$ ($n = 768$; $r = 0.25$; $p < 0.001$).

These alternating ascending/descending together with other oscillations with different frequency were detected and parameterized using harmonic analysis (Tables 3). The harmonics that explained more variance were 1860 months (155 years), 620 months (51 years) and 930 months (77.5 years), which together explained 14% and 16 % of the total variance for the Galician and Cantabrian de-seasonalized time series respectively.

Table 2: Parameters of the harmonic of the seasonal cycle obtained from the sea surface temperature time series.

Series	T	A	F	Tmax	%var
Galician	12	2.92	1.92	8.33	91.17
	6	0.42	4.10	2.08	1.92
Cantabrian	12	3.61	1.95	8.26	92.60
	6	0.62	4.19	1.99	2.78

After the extraction of the different statistically significant harmonic components, we did not find significant linear trends. The autocorrelation component of order 1 was significant in both series. The fitted autoregressive parameters were $\phi = 0.58$ for the Atlantic and $\phi = 0.60$ for the Cantabrian sites, explaining, respectively, 25 and 27 % of the variance of the de-seasonalized time series.

Across-shelf variation along the NIS

Temperature

Vigo

The analysis of the mean profiles of temperature derived from the time series analysis of the Vigo section showed a clear descent of temperature with depth and an increasing coastal-offshore pattern (Figure 5a). Average values at the surface layer (5 m depth) were 14.8, 14.9 and 15.2 $^{\circ}\text{C}$ for coastal, mid-shelf and outer-shelf locations respectively.

The structure of the average temperature profile of the oceanic station was slightly stratified, showing two distinct layers, one from 0 to 30 m depth with values higher than 14 $^{\circ}\text{C}$ and the other from 35 m down to the bottom with values between 13 and 14 $^{\circ}\text{C}$. The pattern of temperature decrease with depth was less intense in the mid-shelf and coastal stations of the section.

The seasonal cycle was calculated as a composition of the first and second harmonics of the annual period (i.e. $T=12$ and $T=6$ months respectively) (figure 6 a-c). The fitted

parameters of the significant harmonics for 10, 50 and 100 m depth were showed in table 4. The seasonality was more intense at the surface than in deeper layers for the three stations of the section, with amplitudes of, respectively, 0.95, 1.11 and 1.42 °C, which explained 30, 42 and 53% of total variance for coastal, mid-shelf and outer-shelf locations respectively.

The shape of the seasonal cycle was clearly unimodal and the maximum values occurred during summer (Tmax 8.64, 8.56 and 8.09 months –i.e. around August, for coastal, mid-shelf and outer-shelf locations. Figure 6a-c). The importance of this component diminishes with depth and its shape moves gradually from an unimodal to a bimodal cycle with a primary maximum in winter and the secondary in spring (figure 6 a-c).

The autocorrelation was significant at different depths (table 4) but explained a marginally significant amount of total variance. We did not find significant linear or cyclical long-term components of temporal variation.

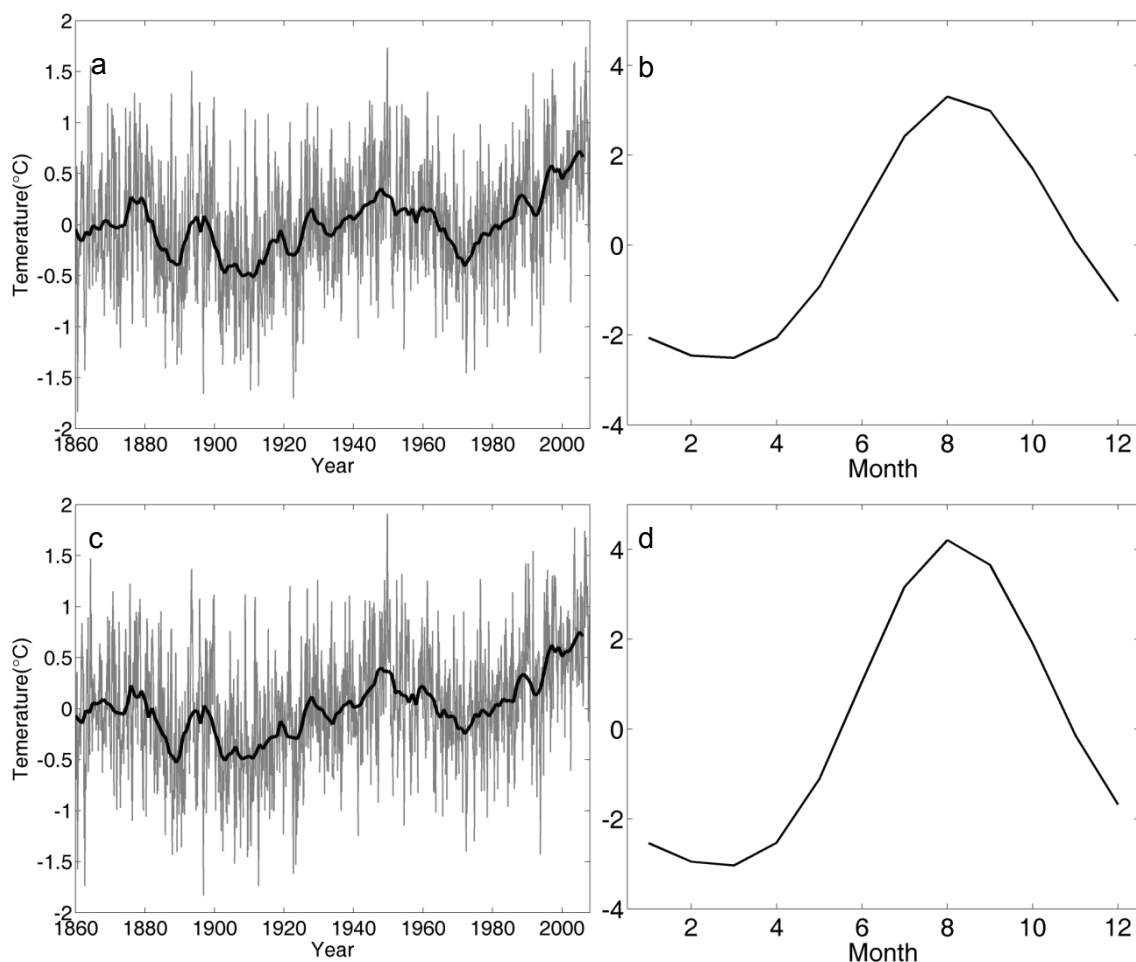


Figure 4: De-seasonalized time series and seasonal cycle (SC) of Sea Surface Temperature (SST); (a, b) for the Atlantic coast; and (c, d) for the Cantabrian Coast. The data were provided NOAA/OAR/ESRL PSD, Boulder, Colorado, USA. See figure 1 for more details.

Table 3. Parameters of the significant supra annual harmonics obtained from the SST time series. The T, A, F, Tmax and %var are respectively the period, amplitude, phase in radians; month when the maximum of a given cycle occurs and percentage explained variance by the cycle.

Station	T month (year)	A	F	Tmax	%var
Galicia	1860 (155)	0.19	0.81	1621.37	5.7
	620 (51.6)	0.17	1.46	475.75	4.3
	930 (77.5)	0.16	5.80	71.97	3.9
	69 (5,7)	0.12	1.22	55.50	2.0
Cantabrian Sea	1860 (155)	0.24	0.90	1593.27	8.9
	620 (51.6)	0.15	1.43	478.81	3.4
	930 (71.5)	0.15	5.84	66.26	3.4
	310 (25.8)	0.12	1.51	235.47	2.1

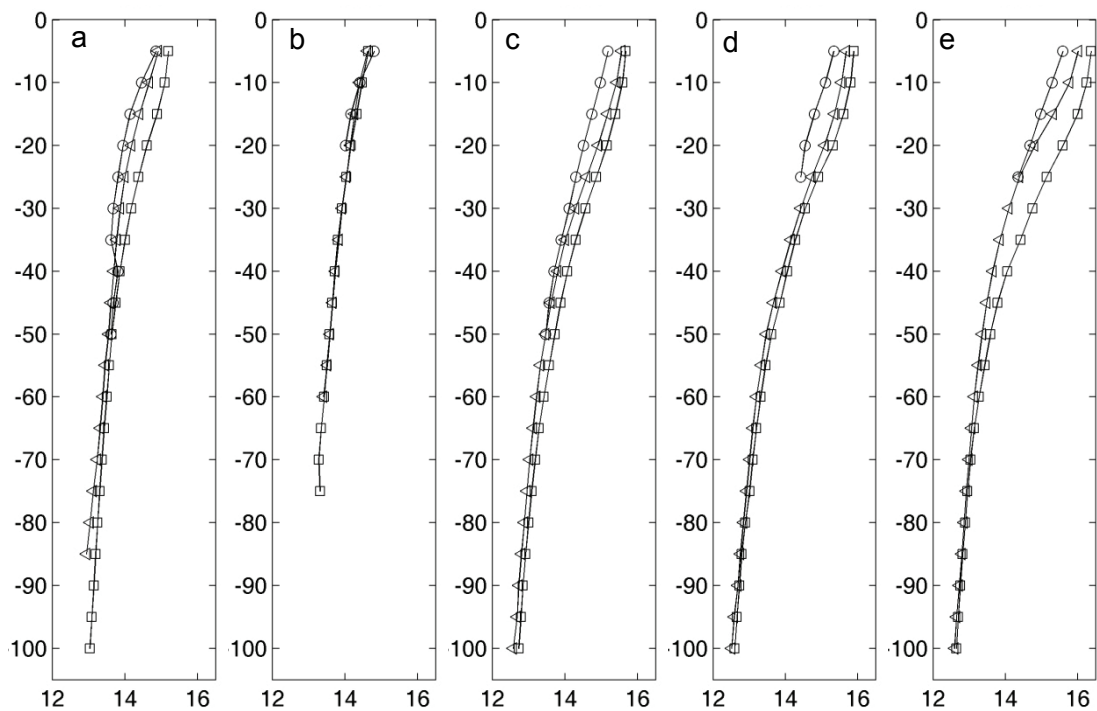


Figure 5: Mean profile of temperature at coastal (circle), mid-shelf (triangle) and outer-shelf (square) hydrographic stations of the across-shelf sections of (a) Vigo, (b) A Coruña, (c) Cudillero, (d) Gijón and (e) Santander sections.

A Coruña

The section off A Coruña was characterized by the proximity between the stations and their relative short distance from the coast (Figure 1). The mean temperature profiles were similar for the three stations, with higher values at the surface (14.8, 14.6, and 14.6 °C for coastal, intermediate and oceanic stations respectively). These values decreased slightly with depth (Figure 5b).

The shapes of the seasonal cycles were similar to those found in the section off Vigo (Figure 6 d-f and Table 4). The surface cycle was unimodal, with maximum values in summer and minimum in winter. The maximum amplitudes of the seasonal cycle were of 1.39, 1.33 and 1.38 °C for coastal, mid-shelf and outer-shelf locations respectively, slightly higher than those measured off Vigo, and this component of temporal variation explained more than 50 % of the total variance in all the stations. The seasonality at depths higher than 20 m was bimodal, with maximum values in summer and a secondary maximum in spring, although the second harmonics of the annual period was marginally significant. Autocorrelation was significant at all depths but explained less than 7 % of variance. No statistically significant linear or cyclical long-term trends were detected in the series.

Cudillero

The Cudillero section showed clear differences between the mean temperature values of the surface layers and deeper layers (Figure 5c). The values at the surface were 14.97, 15.41 and 15.58 °C whereas the average temperature at 100 m depth only reach 12.57 and 12.72 °C at the mid-shelf and outer-shelf locations respectively. Moreover, temperature diminishes towards the coastal end of the section at all depths.

The seasonal component was more marked than in the Atlantic sections, with amplitudes of the first harmonic of the annual cycle at 10 m depth of 2.82, 3.20 and 3.51°C, which explained 80, 86 and 89% of the total temporal variance of the series in coastal, mid-shelf and outer-shelf locations respectively. The maximum values of temperature were measured in summer, while minima were recorded during winter. In the same way than for the Atlantic sections, the seasonal cycle at sub-surface layers was bimodal, with the maximum temperature in winter and a secondary maximum in spring (Figure 6 g-i).

The oceanic station presented significant linear trends of 0.03 ° C yr⁻¹ at 5 and 10 m depth (table 4). The mid-shelf station also showed significant linear trend but of opposite sign (-0.03 ° C yr⁻¹). The autocorrelation was significant at different depths but did not explain more than 5 % of the total variance.

Gijón

The mean values of temperature presented similar patterns than in the section off Cudillero, but with slightly higher temperatures at the surface layers (15.10, 15.4 and 15.8 °C from coastal to the outer shelf) that decreased with depth, reaching around 12.59 °C at 100 m depth. The temperature values diminished toward coast for whole water column.

The seasonal cycle was notorious at the surface layers, with amplitudes of the first harmonic of the annual period of 3.2, 3.6 and 4.0 ° C for coastal, mid-shelf and outer-shelf stations respectively, explaining more than the 80 % of the total variance in all sampled locations. The maximum occurred in summer and the minimum in winter. The seasonality changed progressively with depth, becoming bimodal below 45 m depth, with maximum values in winter and a secondary maximum in spring. The seasonal cycle did not explain more than 50% of the variance below 50 m. Neither the long-term, nor the autocorrelation components were statistically significant at any depth or location.

Santander

The Santander section showed similar patterns than the other two westernmost Cantabrian sections, but with more marked differences among stations in temperature profiles, gradients and amplitude and contribution to total variability of the seasonal cycle.

The temperature increased from the coast to the outer shelf at all depths, with average surface values of 15.28, 15.72 and 16.24 °C for coastal, mid-shelf and outer-shelf locations respectively. Average values at 100 m depth were of 12.59 and 13.58 °C for the mid-shelf and outer-shelf stations respectively. This section had the higher average values of temperature of all the analyzed sections.

Seasonality was intense at the surface layers with amplitudes of the first harmonic of the annual period of 3.25, 3.77 and 4.35 °C which explained 74, 86 and 90% of the total variance of the coastal, mid-shelf and outer-shelf time series. The shape of the seasonal cycle at different depths was similar than in the other Cantabrian sections. The maximum values were measured in winter and a secondary maximum was observed in spring below 50 m depth. The variance explained below 50 m depth was lower than 50 %.

We did not measured significant trends at any depth for the three stations. The autocorrelation was significant at different depths but explained less than 7 % of the total variance.

Salinity

Vigo

The mean salinity profiles of the three stations of the section of Vigo showed a marked coastal-offshore gradient. Average salinity at 10 m depth was 34.90, 35.32 and 35.56 psu for coastal, mid-shelf and outer-shelf locations respectively (Figure 7a). The intensity of this coastal-offshore gradient diminished with depth.

The seasonality of this variable is less marked than that of temperature. The oscillations of salinity were higher towards the coast (Figure 8a-c). The amplitudes of the first harmonic of the annual period at the surface (10 m) were 0.6 and 0.37 psu for the coastal and mid-shelf locations respectively, explaining 24% and 33% of the total variance. In contrast, this harmonic was not significant for the outer-shelf station (amplitude of 0.03 psu and 1.5 % of explained variance). The minimum and maximum values of the seasonal cycle occurred in winter and summer respectively. The magnitude of the seasonal signal decrease sharply with depth.

Salinity exhibited long-term periodic trends of period $T = 48$ (4 years) at 50 m depth in the mid-shelf location, which explained 11% of the total variance of the time series at this depth. Periodic components with frequencies lower than 12 months were significant in the oceanic station at different depths (Table 5). The mid-shelf and outer-shelf locations presented significant decreasing linear trends between 30 and 100 m depth, with a slope of $-0.01 \text{ psu}\cdot\text{year}^{-1}$ that explained 6% of the variance. The autocorrelation component was only significant in the mid-shelf station at 50 m depth, explaining 8 % of the variance.

A Coruña

The proximity to the coast of the stations of the section of A Coruña explains the similarity of the average salinity profile among the stations of the section. Mean salinity values at 5 m depth were 35.26, 35.39 and 35.35 psu from the coastal to offshore edges of the section, with a value of 35.4 psu at 10 m depth for all the stations (Figure 7b).

The three stations of the section have also similar seasonal patterns. The winter was characterized by low values of salinity and the rest of the year the salinity values varied between 35.5 and 35.6 psu (Figure 8d-f). The amplitudes of the first harmonic of the annual period were 0.21, 0.19 and 0.17 psu along the coastal-offshore section, explained 17, 13 and 10% of the total variance, although the seasonal cycle at the offshore edge of the section was not statistically significant. This section did not present linear or long-term periodic trends. The autocorrelation was important at all the depths and the variance explained by the autoregressive component, reached 45% in some cases.

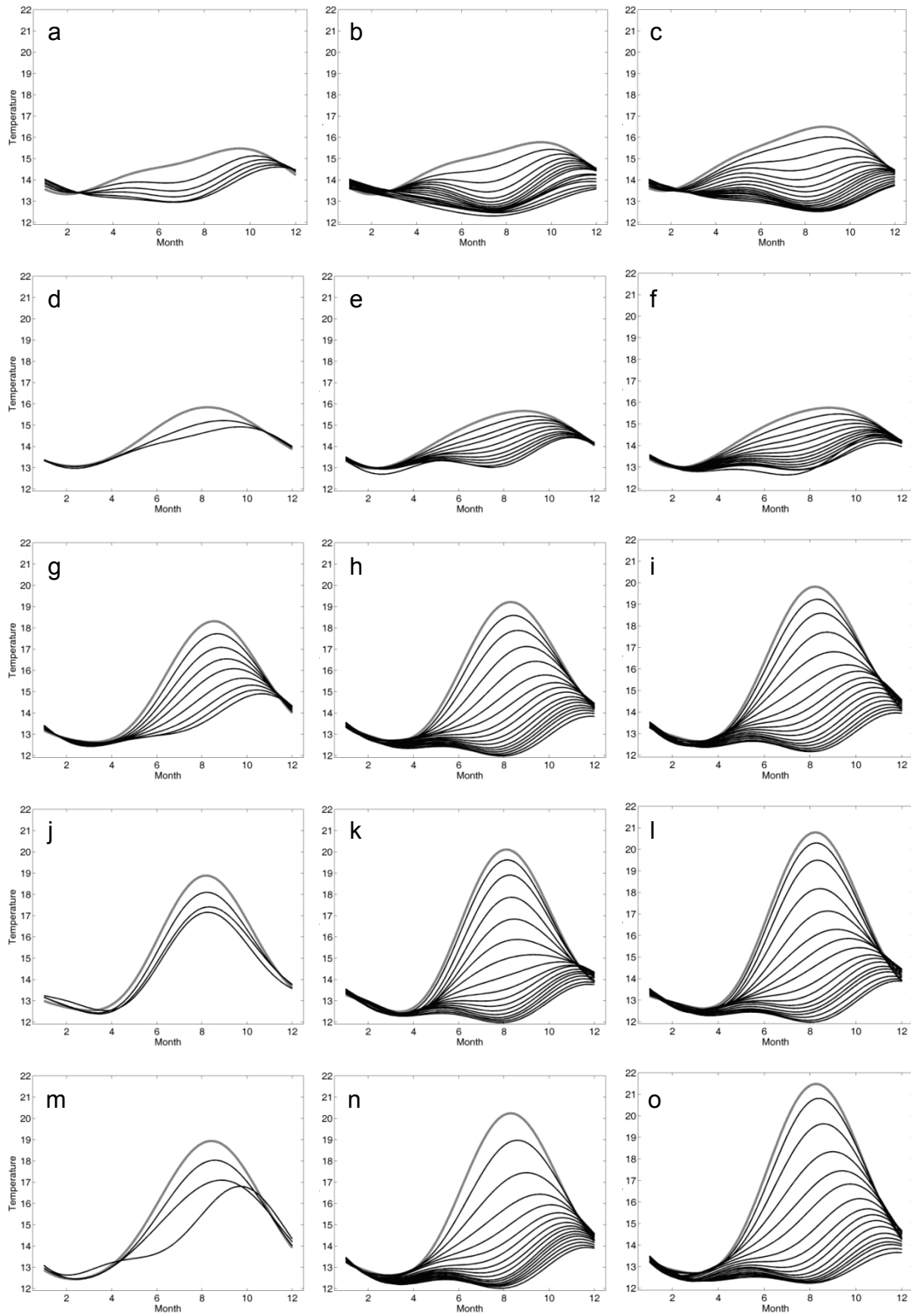


Figure 6: Seasonal cycles of temperature at the coastal, mid-shelf and outer-shelf hydrographic stations, obtained from the time series analysis of the sections of (a-c) Vigo, (d-f) A Coruña, (g-i) Cudillero, (j-l) Gijón and (m-o) Santander. The gray line represents 5 m depth SC and there is one line for each 5 m depth.

Table 4: Parameters of the time series analysis applied on temperature of the 5 sections distributed along shelf. Only depths with significant components are showed. The T, A, F and Tmax are respectively the period of the harmonic, amplitude, phase (in radians) and month when the maximum of a given harmonic occurs respectively. ϕ is the autocorrelation parameter and finally %var is the percentage of explained variance by the respective component.

Section	Station	z	Mean	Linear trend			Cyclical components					Autoregressive		
				b	p	%var	T	A	F	Tmax	%var	ϕ	%var	
Vigo	Coastal	10	14.4	0.00	0.92	0.0	12	1.0	1.8	8.6	29.5	0.21	0.03	
		50	13.6	-0.02	0.56	0.2	12	0.8	0.3	11.5	25.8			
	Mid-Shelf	10	14.6	0.02	0.53	0.3	12	1.1	1.8	8.6	42.4	0.29	0.05	
		50	13.5	-0.02	0.45	0.4	12	0.7	6.2	0.2	28.9			
	Outer-Shelf	10	15.0	-0.01	0.87	0.0	12	1.4	2.1	8.1	53.9			
		50	13.6	-0.01	0.61	0.2	12	0.4	6.1	0.4	21.8			
							6	0.4	0.6	5.5	16.7			
A Coruña	5	100	13.0	-0.02	0.26	0.9	12	0.6	5.5	1.5	47.8			
	Coastal	10	14.4	0.01	0.83	0.0	12	1.4	1.9	8.3	56.3	0.19	0.02	
		50	13.5	-0.02	0.46	0.4	12	0.6	0.8	10.6	21.4	0.28	0.06	
Cudillero	Coastal	10	14.9	0.05	0.40	0.5	12	2.8	1.8	8.6	80.9	0.18	0.00	
		50	13.4	-0.01	0.74	0.9	12	1.1	0.9	10.3	42.9			
	Mid-Shelf	10	15.4	0.05	0.40	0.5	12	3.2	1.8	8.5	86.9			
		50	13.4	-0.01	0.80	0.1	12	1.1	0.8	10.6	44.1			0.23
			100	12.5	-0.03	0.03*	1.2	12	0.7	6.9	0.4	43.3	0.19	0.02
								6	0.4	0.1	6.0	13.8		
	Outer-Shelf	10	15.5	0.03	0.04*	0.8	12	3.5	1.9	8.4	89.4	0.19	0.00	
Gijón	Coastal	50	13.7	0.00	0.88	0.0	12	1.2	1.0	10.0	55.9	0.22	0.02	
		100	12.7	-0.01	0.71	0.1	12	0.6	6.2	0.2	48.3			
		100					6	0.4	0.2	5.8	20.3			
	Mid-Shelf	10	15.1	0.21	0.33	1.6	12	3.1	1.9	8.3	86.3			
		50	13.4	0.00	0.96	0.00	12	1.0	0.9	10.2	39.1			
	Outer-Shelf	100	12.5	-0.03	0.71	0.2	12	0.7	6.2	0.1	42.5	0.30	0.01	
		10	15.8	0.22	0.42	1.1	12	4.0	1.9	8.4	86.8			
			50	13.6	-0.04	0.76	0.2	12	1.2	1.0	10.1	38.9		
			100	12.5	-0.04	0.60	0.5	12	0.7	6.1	0.4	45.1		
	Santander	Coastal	10	15.2	0.00	0.99	0.0	12	3.3	1.9	8.4	79.8		
50			13.3	-0.03	0.40	0.5	12	1.1	0.7	10.7	38.1			
Mid-Shelf		100	12.5	-0.01	0.49	0.3	12	0.7	6.3	0.0	43.3			
		100					6	0.4	0.3	5.7	13.6			
Outer-Shelf		10	16.2	0.05	0.53	0.3	12	4.4	1.9	8.4	90.5	0.32	0.01	
		50	13.5	0.00	1.00	0.0	12	1.2	0.9	10.4	50.1	0.26	0.03	
			50				6	0.6	1.1	4.9	13.1			
			100	12.6	-0.03	0.05	2.7	12	0.5	6.2	0.2	45.0	0.38	0.07
			100				6	0.3	0.1	6.0	13.7			

Cudillero

Mean salinity profiles did not present major differences between surface and bottom layers, and among the three stations of the section (Figure 7c). The seasonal component was less important than in the Galician sections. The first harmonic of the annual period was only significant in the outer-shelf location at 100 depth, with an amplitude of 0.03 psu and a percentage of explained total variance of 14%. In the coastal station, the lowest values of salinity occurred during winter and the maximum during summer. The other two stations did not show this pattern; for instance, the outer-shelf location showed an inverse pattern, with lower salinity values during summer-autumn and higher values during winter (Figure 8g-i).

In this section we found significant long-term periodic trends with periods of 24, 36, 72 and 144 months at different depths, and significant long-term linear trends between 50 and 100 m depth in the outer-shelf station (see Table 5). The autocorrelation was significant in the three stations at all depths, explained a maximum of 48 % of total variance.

Gijón

The mean salinity profiles did not present differences between the surface and bottom layers similar to what occurred at the section off Cudillero. Neither seasonal nor long-term periodic trends were statistically significant probably as a consequence of the relatively short extent of the time series (Figure 7d). The seasonal cycle was not clear. The mid-shelf and outer-shelf locations had the lowest values of salinity in spring and autumn and the highest in winter (Figure 8j-l). We obtained marginally significant increasing linear trend at all depths with a slope of 0.05 at the surface, diminishing its intensity with depth. Autocorrelation was significant at several depths, reaching a maximum of 25 % of explained variance (Table 5).

Santander

The Santander section presented a coastal–offshore salinity gradient similar, although less intense, than that found in the section off Vigo. At the surface, salinity values were 35.19, 35.34 and 35.39 psu for coastal, mid-shelf and outer-shelf locations respectively. The differences among stations diminished with depth (Figure 7e).

The seasonal cycle was significant at the surface, with amplitudes of the first harmonic of the annual period of 0.14 and 0.19 psu, which explained 18 and 23% of the total variance, for the mid-shelf and outer-shelf stations respectively. These results contrast with those obtained in the coastal station, where the first harmonic was not significant and presented amplitude of 0.08 psu and explained 3.9% of the total variance.

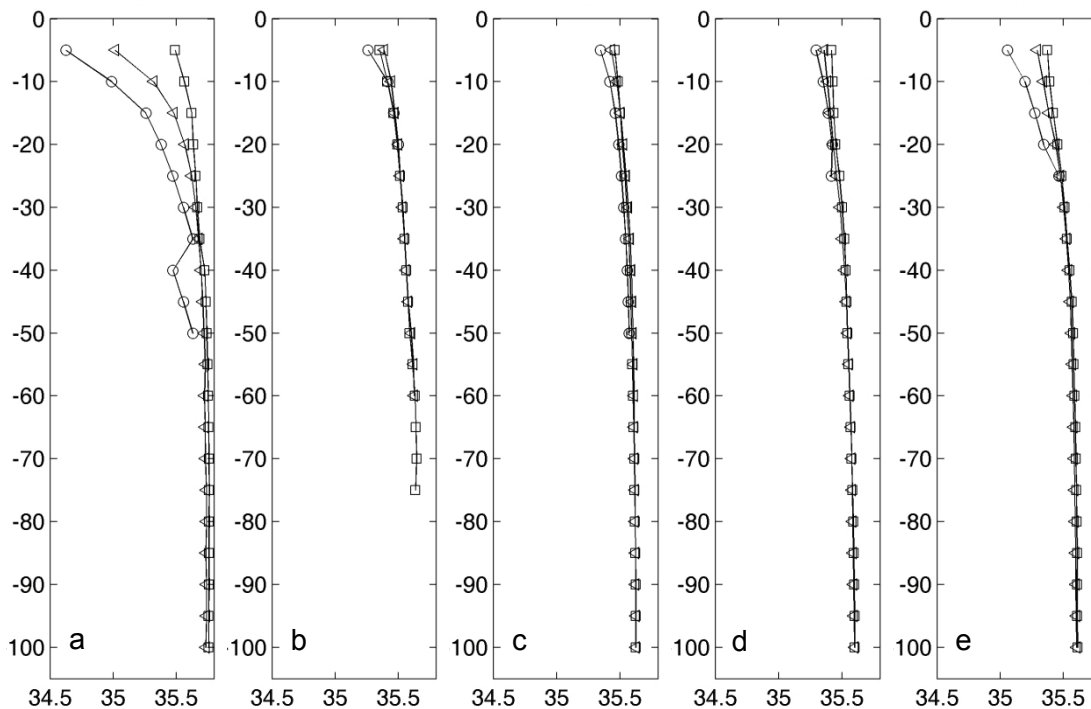


Figure 7: Mean vertical profiles salinity at coastal (circle), mid-shelf (triangle) and outer-shelf (square) locations of (a) Vigo, (b) A Coruña, (c) Cudillero, (d) Gijón and (e) Santander.

Thermohaline fields during spring

Geostatistic analysis

The mean profiles of the correlation factor (A , dimensionless) and the characteristic scale (L , nautical miles) calculated from the correlograms of temperature at different depths are showed in figure 9a-b. The correlation factor values (A) were higher at the surface layers (0.7), diminishing slightly with depth. Between 20 and 50 m depth we measured minimum values around 0.48. From 60 to 100 m depth, A was stable, with values oscillating around 0.6. The characteristic scale (L) presented a different pattern, defined by three peaks: one at the surface (40 nm), other between 30 and 40 m depth (38 nm) and the last one at 90 m depth (30 nm). The minimum values were measured between 20 and 30 m (28 nm) and between 50 and 70 (22 nm).

The profiles of A and L calculated from the correlograms derived from the salinity fields showed similar patterns of variation than those for temperature (Figure 9 c-d). The values of A were higher at the surface (0.58) and increased progressively with depth, reaching 0.68 at the bottom layers. L showed the same pattern of variation, with low values at the surface (23 nm) and an increasing trend towards bottom layers, with values of 60 nm at 100 m depth.

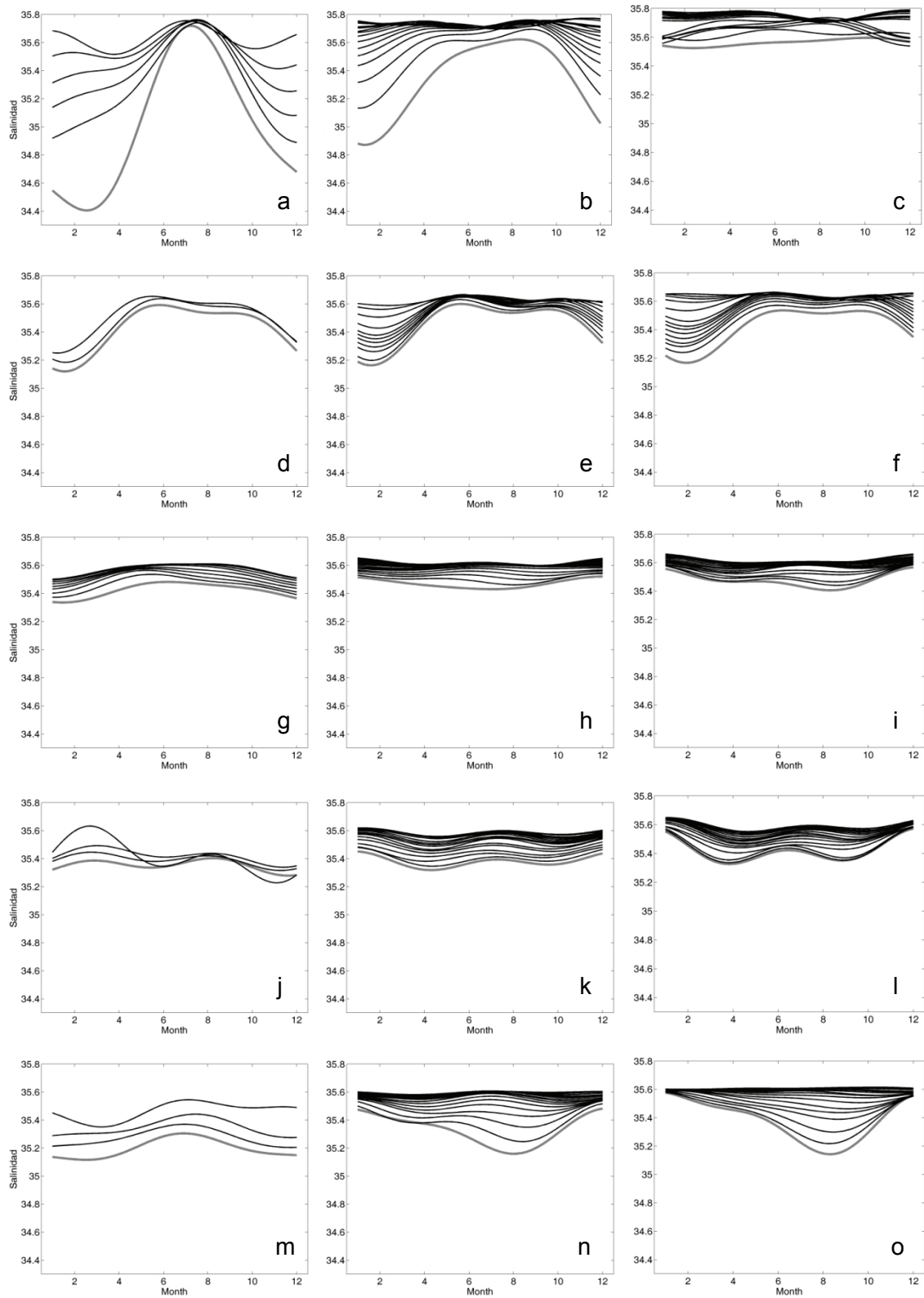


Figure 8: Seasonal cycles of temperature at the coastal, mid-shelf and outer-shelf hydrographic stations, obtained from the time series analysis of the sections of (a-c) Vigo, (d-f) A Coruña, (g-i) Cudillero, (j-l) Gijón and (m-o) Santander. The gray line represents 5 m depth SC and there is one line for each 5 m depth..

Table 5: Parameters of the time series analysis applied on salinity of the 5 sections distributed along shelf. Only depths with significant components are showed. The T, A, F and Tmax are respectively the harmonic period, amplitude, phase in radians and month when the maximum of a given cycle occurs respectively. ϕ is the autocorrelation parameter and finally %var is the percentage of explained variance by the respective component.

Section	Station	z	Mean	Linear trend			Cyclical components					Autoregressive	
				b	p	%var	T	A	F	Tmax	%var	ϕ	%var
Vigo	Coastal	10	34.99	0.02	0.26	0.9	12	0.62	2.3	7.6	23.7		
		50	35.63	-0.01	0.15	1.4	6	0.09	5.3	1.0	13.0		
	Mid-Shelf	10	35.32	0.00	0.79	0.1	12	0.37	2.4	7.5	33.1		
		50	35.72	-0.01	0.00	6.1	48	0.04	2.0	32.6	11.7	0.31	0.1
		100	35.73	0.00	0.52	0.3	12	0.03	6.3	0.1	13.1		
	Outer-Shelf	10	35.56	-0.01	0.11	1.8	2.4	0.08	0.4	2.3	11.3		
							4	0.08	0.5	3.7	10.9		
50		35.74	-0.01	0.00	6.3	3	0.04	0.0	3.0	11.2			
	100	35.75	-0.01	0.00	6.6	12	0.05	5.4	1.8	25.7	0.17	0.1	
A Coruña	Coastal	10	35.41	0.01	0.41	0.5	12	0.21	2.4	7.3	17.8	0.27	0.1
	Mid-Shelf	10	35.44	0.01	0.54	0.3	12	0.19	2.4	7.5	13.3	0.28	0.1
	Outer-Shelf	10	35.41	0.01	0.53	0.3						0.48	0.2
		50	35.59	0.00	0.98	0.0						0.35	0.1
Cudillero	Coastal	10	35.42	0.01	0.24	1.0						0.37	0.1
		50	35.57	0.00	0.39	0.5						0.51	0.3
	Mid-Shelf	10	35.47	0.00	0.44	0.4	72	0.09	1.4	55.8	11.9	0.44	0.2
		50	35.60	0.00	0.20	1.2	72	0.05	1.2	58.0	15.3	0.69	0.5
		100	35.62	0.00	0.38	0.5	24	0.03	5.5	2.8	12.4	0.38	0.1
	Outer-Shelf	10	35.48	0.00	0.66	0.1	36	0.08	0.5	33.0	10.3	0.46	0.2
		50	35.59	0.00	0.06	2.4	144	0.04	4.7	37.5	12.3	0.53	0.3
							72	0.04	1.2	58.4	11.5		
	100	35.62	0.00	0.03	3.3	12	0.03	6.1	0.4	13.7	0.45	0.2	
						72	0.03	1.3	57.0	12.9			
Gijón	Coastal	10	35.35	0.05	0.00	13.0						0.29	0.1
	Mid-Shelf	10	35.38	0.06	0.00	15.9						0.48	0.2
		50	35.54	0.03	0.00	16.2						0.33	0.1
		100	35.60	0.01	0.19	3.0						0.44	0.2
	Outer-Shelf	10	35.42	0.06	0.01	11.4							
		50	35.54	0.03	0.00	12.9						0.33	0.1
100		35.60	0.01	0.16	3.3						0.56	0.3	
Santander	Coastal	10	35.19	0.01	0.37	0.6							
	Mid-Shelf	10	35.34	0.00	0.75	0.1	72	0.15	1.6	54.1	18.4	0.60	0.3
							12	0.14	5.5	1.5	17.7		
		50	35.56	0.00	0.25	1.0	72	0.05	1.4	56.4	18.7	0.41	0.2
						144	0.04	4.4	42.8	12.0			
	100	35.60	0.00	0.05	2.7	72	0.02	1.3	57.6	11.7	0.19	0.1	
						144	0.02	3.9	55.7	10.3			
	Outer-Shelf	10	35.39	0.00	0.63	0.2	12	0.19	5.3	1.8	23.4	0.66	0.3
						72	0.17	1.6	53.6	18.4			
50		35.58	0.00	0.04	2.9	72	0.08	1.6	53.6	33.7	0.62	0.4	
	100	35.61	0.00	0.00	7.3	72	0.04	1.5	54.6	33.9	0.63	0.4	
						144	0.03	4.2	47.0	16.3			

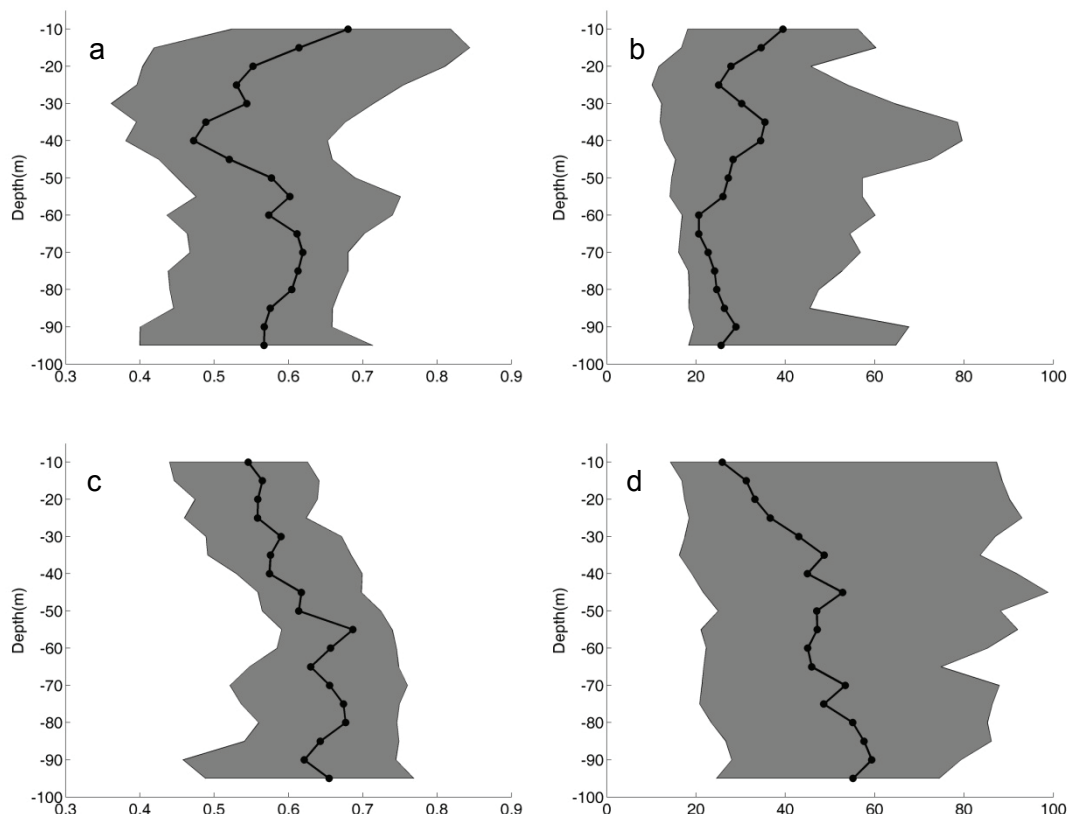


Figure 9: Vertical profiles of A and L parameters obtained by fitting a gaussian function to (a, b) temperature and (c, d) salinity horizontal fields. The black line represents mean value and the gray envelope defines the standard deviation of the parameter.

Horizontal thermohaline fields in spring

Temperature

The mean horizontal temperatures fields at 10, 30, 50, 75 and 100 m depth are showed in figure 10a-e. As a general rule, we measured the highest values of temperature, between 13.2 and 14 °C, along the Galician coast. These values decreased along-shelf, reaching temperatures below 12.2°C in the easternmost part of the Cantabrian Sea. At the surface layer this regional along-shelf pattern was blurred because surface temperature values between 5° W and 2° W were higher than 13 °C.

The area with the highest variability of temperature was located in the proximity of the Rías Baixas at all depths probably as a combined effect of the influenced of river discharges and coastal upwelling-downwelling events. In the easternmost part of the Cantabrian Sea we found another area with high temperature variability due to the

influence of discharges from the Adour River. At deeper layers, the values of temperature were more stable all along the NIS.

Linear trends of temperature for each 5 m depth between 5 and 100 m depth were calculated by averaging the values of the spring cruises for the areas located in the Galician Coast (AC, 10°-7° W), Central Cantabrian (CC, 7°-4° W) and East Cantabrian Sea (EC, 4°-1° W). These values are showed in figure 11a.

The values slopes in the Galician Coast were higher than $0.02 \text{ } ^\circ\text{C y}^{-1}$ for the whole water column. In the Central Cantabrian Sea the slope increase towards the bottom reaching $0.015 \text{ } ^\circ\text{C y}^{-1}$. EC showed negative trends at all depth but were more intense at the surface ($-0.015 \text{ } ^\circ\text{C y}^{-1}$). We only found significant trends in the Atlantic coast at depths below 75 m, with values around $0.025 \text{ } ^\circ\text{C yr}^{-1}$. For the Cantabrian areas (CC and EC) the slopes of the linear trends were not statistically significant.

Since the shape of spring temperature time series was clearly not linear, we calculated de difference between the averages of temperature of the second decade (1997-2008) of the sampling period and the first one (1987-1997). The values were plotted in figure 11b. The structure was similar to the slope of the linear trends with a clear along-shelf gradient, with values $0.37 \text{ } ^\circ\text{C dec}^{-1}$, $0.18 \text{ } ^\circ\text{C dec}^{-1}$ and $-0.05 \text{ } ^\circ\text{C dec}^{-1}$ for AC, CC and EC respectively.

Salinity

Salinity fields showed two clear spatial patterns (Figure 12). The first one was a characteristic along-shelf decreasing trend with relatively high salinity values in the AC area (higher than 35.65 psu) that decreased gradually eastward, reaching stable values in CC and EC areas varying between 35.55 and 35.65 psu. This general pattern is less clear at the surface than at the sub-surface layers as a consequence of the low salinities located in the proximities of the river mouths of Miño and Adour Rivers, in the westernmost and easternmost locations of the NIS, and in the small Cantabrian Rivers. The reduction of salinity at sub-surface layers (more than 75 m depth) was only apparent close to the Adour River mouth. The zones with higher variability of the salinity field were associated with the area of influence of Adour River and Rías Baixas systems.

Using the same approach than that followed for temperature fields we have evaluated the interannual variability of salinity in spring. Figure 13a shows the linear trend obtained for the three areas (AC, CC and EC) for the first 100 m of the water column. We did not found significant trends in any case. The pattern of the slope this parameter in the water column was similar for the three areas with low values at the surface layers that increased with depth, been positive in AC (0.001), neutral in CC and negative in EC (-0.004).

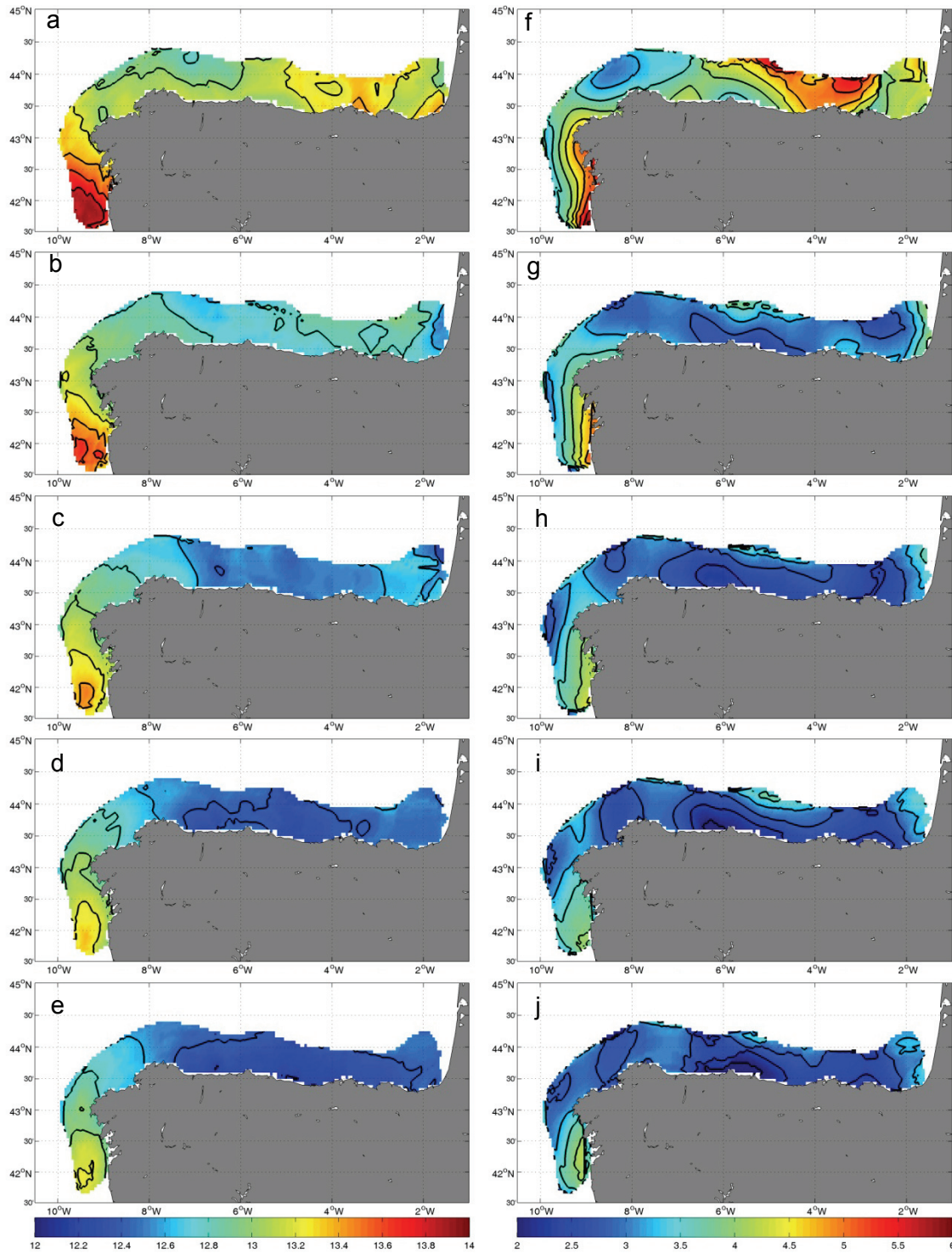


Figure 10: Mean and standard deviation of the horizontal fields of temperature at (a, b) 10 m, (c, d) 30 m, (e, f) 50 m, (g, h) 75 m and (i, j), 100 m.

Comparing the mean values of the salinity between the two decades we have found a general decreasing pattern of salinity in the whole studied area, which was more intense at the surface layers (Figure 13b). This descent of salinity varied along-shelf, being more intense in the western zone (AC area). The values at deep layers were -0.05, -0.01 and 0 psu for EC, CC and AC respectively.

Climatic across-shelf sections in spring

Temperature

Average temperature in the across-shelf sections showed a clear along-shelf decreasing pattern similar to that found for the horizontal fields (Figure 14). Average surface temperature in the sections located in the AC area was higher (around 14 °C) than in the sections located in the Cantabrian Sea (CC and EC areas). In the proximity of the coast, the values of temperature are about 1 °C lower than in the offshore edge of the section and the isotherms tend to be vertical. This structure was evident in the first three sections (S1, S2 and S3) but with relatively lower coastal-offshore gradient in S2 and S3. In the Galician sections (S1 to S3) the higher of variability of temperature was located at the surface layers, between 10 and 30 m depth, with variability values higher than 0.5 °C. The variability of temperature diminished from coast to offshore and from surface to bottom. The southern sections were more variable than the northern ones.

The four Cantabrian sections (S4 to S7) had similar temperature structure. We measured the highest values of temperature at the surface (around 13 °C) that did not descend below 12 °C with depth. The stratification was clear in the first 30-40 m of the water column. The difference among the sections was the distribution of temperature variability. Whereas the first Cantabrian section (S4) replicates the distribution of the Atlantic sections (S1 to S3), with the variance associated mainly to the coastal edge of the section in the surface layers, the section S5 exhibited a contrasting pattern regard to temperature variability, with higher variability at the offshore edge. In the last two sections (S6 and S7), the higher values of variability were measured at the surface and decreased quickly with depth, reaching values close to 0 below 30 m depth.

Salinity

The general patterns observed for the across-shelf sections of salinity were similar to those reported for the horizontal fields. We measured higher values of salinity in the sections belonging to the AC area (S1, S2 and S3), that decreased eastward. On the other hand, the section located close to the Rías Baixas (S1) and the Adour River (S7) presented notorious decrease in surface salinity which intensity decreased with depth.

The higher values of salinity were measured at the sub-surface, being around 36 psu in S1 and around 35.65 psu in S3. Surface values in those sections were lower than 35.5 psu, contrasting with values higher than 35.6 psu below the surface layer (20 m) in all the Galician sections. The higher variability of salinity was observed in the surface layer in the coastal edge of the section, diminishing with depth and towards the offshore edge of the section. This pattern was similar in the first three sections located in the AC area, with the difference that the absolute salinity values decreased northwards from S1 to S3.

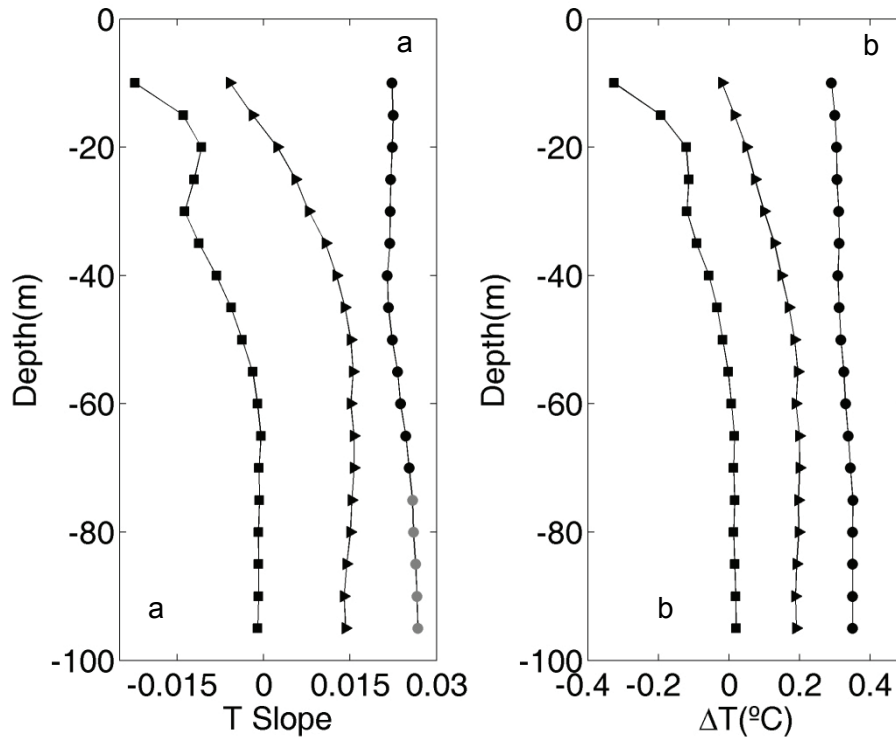


Figure 11: Vertical profiles of the linear trend (a) and decadal increment (b) of Temperature of the Galician (circles), West Cantabrian Sea (triangles) and East Cantabrian Sea (squares). Significant trends ($p < 0.05$) are represented with gray markers.

The salinity distribution in the Cantabrian across-shelf sections S4, S5 and S6 was similar, with lower values at the surface that decrease with depth to reach maximum values around 35.6 psu. The lower values of salinity measured at the surface layer influence the whole section, that presented values below 35.3 psu in the surface layer all across section 6. The distribution of variance was similar to that obtained for temperature: it was higher in the surface layers and in the coastal edge of the sections, except in section S5 where the lower values were measured offshore.

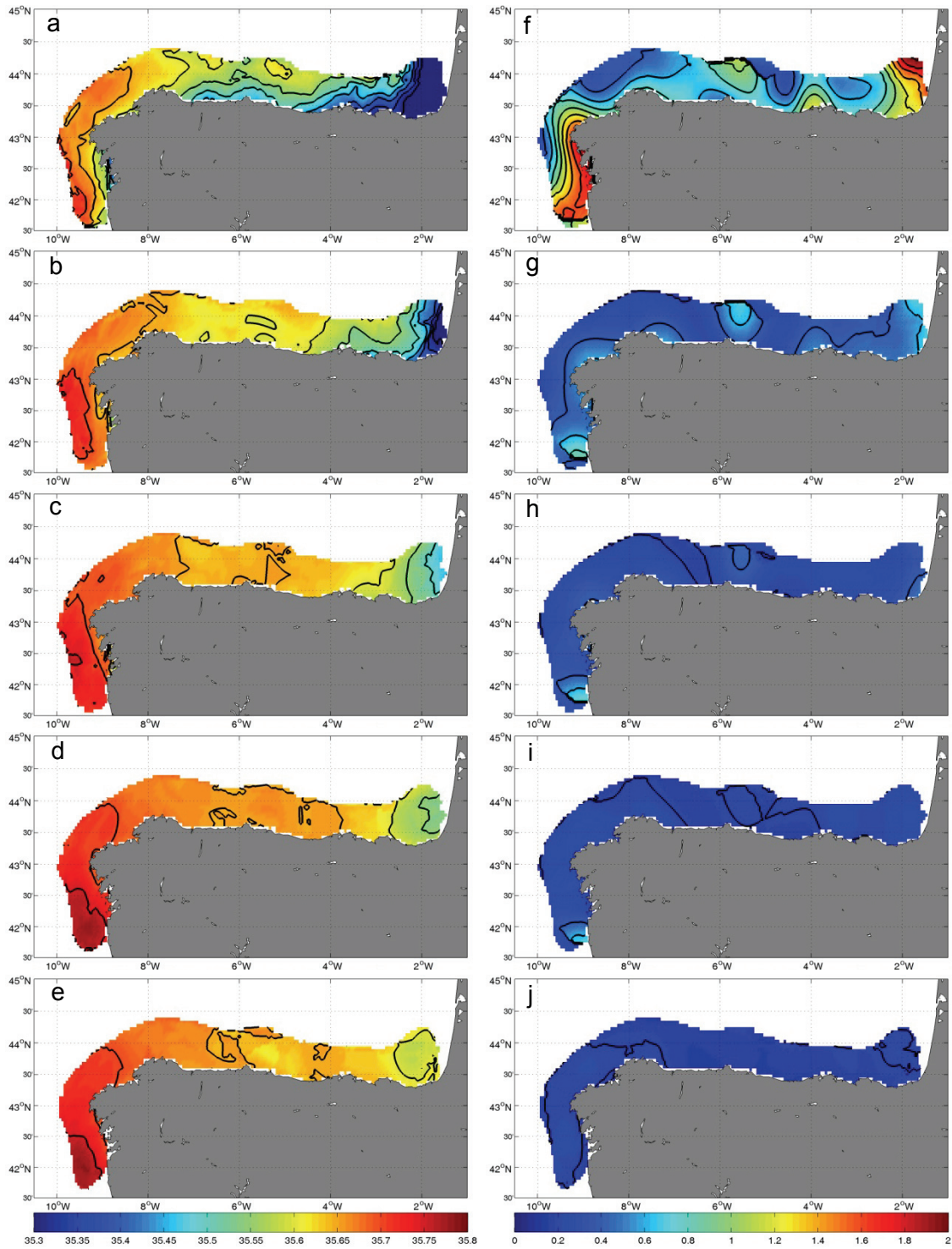


Figure 12: Mean and standard deviation fields of salinity at (a, b) 10 m, (c, d) 30 m, (e, f) 50 m, (g, h) 75 m and (i, j) 100 m.

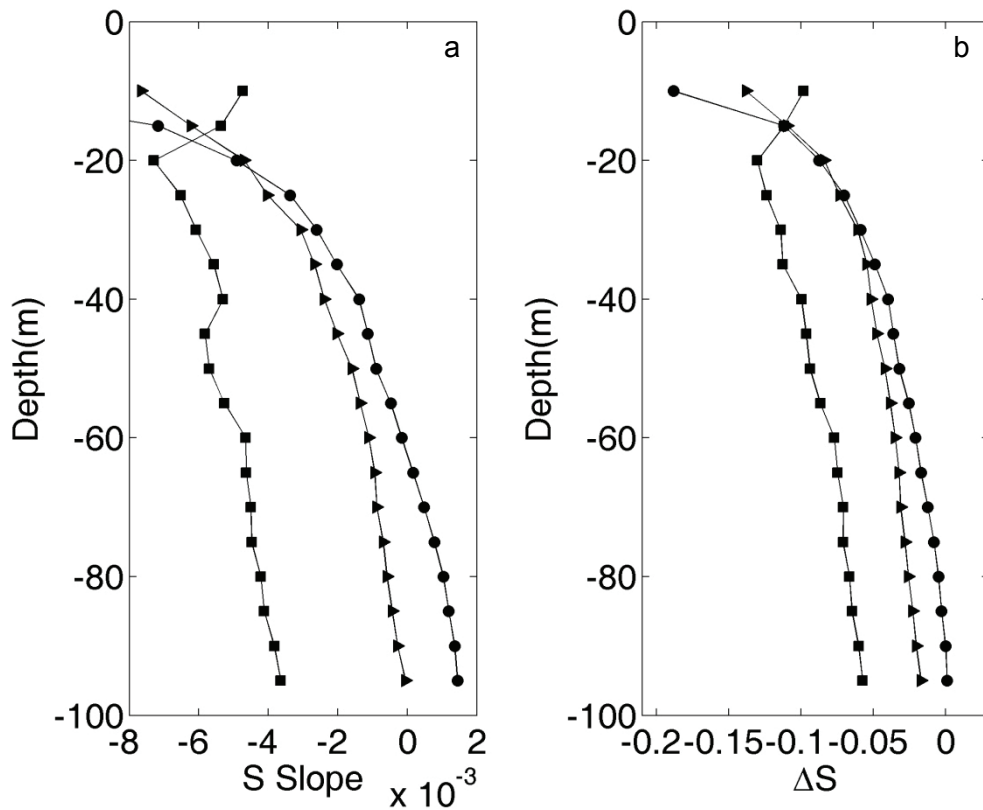


Figure 13: Vertical profiles of the (a) slope of the linear trend and (b) decadal increment of salinity of the Galician (circles), West Cantabrian Sea (triangles) and East Cantabrian (squares). Significant trends ($p < 0.05$) are represented with gray markers.

Discussion

SST long term linear trends

Seasonality was the most important component of temporal variation of the SST time series explaining more than 90 % of the total variance. The strength of the seasonal component of SST is a consequence of the latitudinal location of the study area on the temperate zone, which is subjected to high solar irradiances during spring-summer that contrast with the low irradiance during winter (Foltz *et al.*, 2003).

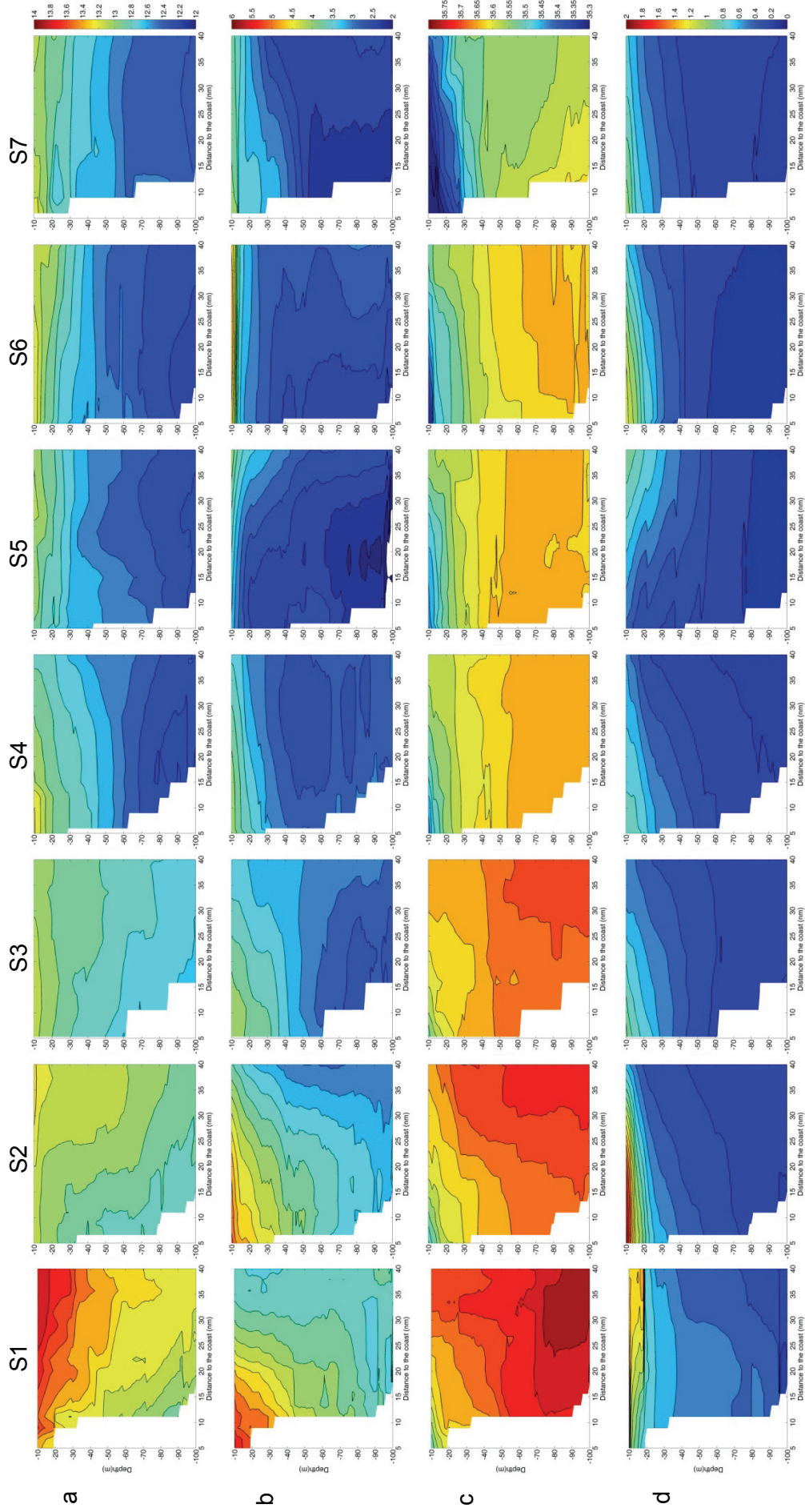


Figure 14: Climatic sections of (a) mean and (b) standard deviation of Temperature and (c) mean and (d) standard deviation of Salinity. See locations in figure 1.

After removing the seasonal component, other periodic trends with lower frequencies were also significant. It is very complicated to determine the factors that generate these long-term cyclical variations. Solar activity cycles are forcing mechanisms that could generate changes on SST at this temporal scale. In table 6 are showed different solar cycles and their periods that were coherent with the low frequency cycles measured on the SST time series. There exists, however, large controversy concerning the relationship between this low-frequency cycles of solar activity and earth temperature, and there is not a validated theory of the mechanism that mediated this plausible coupling. For instances, it is worth noting that the oscillations of radiation between maximum and minimum situations of the solar cycles is about $0.2 \text{ W}\cdot\text{m}^{-2}$ whereas the radiation necessary to increase SST in $0.1 \text{ }^\circ\text{C}$ is of the order of $0.5 \text{ W}\cdot\text{m}^{-2}$ (Meehl *et al.*, 2009). Accordingly, without any corroborated mechanism, all correlations between solar activity and temperature were considerate spurious or at least indirect relationships. Recent studies (Meehl *et al.*, 2009) suggested an amplification mechanism that may allow higher changes in temperature. According to that proposed mechanisms, the oscillations in the incident solar radiation could change the atmospheric circulation, cloud formation and UV radiation intensity that, by mean of the albedo intensity, could amplify temperature changes.

Table 6: Main solar activity periodic oscillations.

Cycle	Type	Period (year)
Schwabe	Sunspot	11
Hale	Sunspot	22
Buckner	Sunspot	33
Gleisberg	Secular	60-120
King Hale	Motion	178

Once removed the long term periodic trends, we did not found significant linear trends neither for the whole period, neither for partial periods. A bibliography revision was carried out in order to obtain values of SST trends in the study area (Table 7). Using the raw SST series, analyzed in this work, we estimated the linear trends for the periods studied in the different articles. The parameters obtained using the raw SST time series were very similar to the obtained by the different authors (Table 7). Uniquely clear differences were found with the estimations by Koutsikopoulos *et al.* (1998) and Lavín *et al.* (1998). In first case, the slope was 3 times lower than the slope measured in the bibliography and in the second case 1 order of magnitude lower. We think that this comparison is relevant because some studies have reported linear trends for different periods of the past century.

The implications which can be derived from the consideration of long-term changes in SST as periodic cycles or as linear trends is important since the obtained results are completely different. Primarily, because the mechanisms that generate these two kinds of responses are different and secondly because the projections from the two approximations can provide divergent long-term forecast.

Table 7: North Atlantic SST linear trends based on bibliography (T_p) and NOAA extended reconstructed SST time series used in this paper (T_e).

Author	T_p ($^{\circ}\text{C}\cdot\text{yr}^{-1}$)	Period	T_e ($^{\circ}\text{C}\cdot\text{yr}^{-1}$)
Koutsikopoulos <i>et al.</i> (1998)	0.064	1972-1993	0.026
Lavin <i>et al.</i> (1998)	0.42	1991-1995	0.04
Planque <i>et al.</i> (2003)	0.060	1990-1999	0.060
Rayner <i>et al.</i> (2003)	0.0033	1861-2000	0.0034
Gonzalez-Pola <i>et al.</i> (2005)	0.032	1992-2003	0.045
Rayner <i>et al.</i> (2006)	0.0042	1850-2005	0.0033
Llope <i>et al.</i> (2006)	0.050	1993-2003	0.034
Gómez-Gesteira <i>et al.</i> (2008)	0.015 to 0.035	1985-2006	0.027
deCastro <i>et al.</i> (2009)	0.033	1985-2006	0.027
Goikoetxea <i>et al.</i> (2009)	0.026	1977-2007	0.030
Michel <i>et al.</i> (2009)	0.022 to 0.031	1985-2003	0.025
Hermant <i>et al.</i> (2010)	0.035	1987-2005	0.025

Monthly across-shelf variation along the NIS

The dynamics of the distribution of thermohaline properties along the North Iberian Shelf (NIS) is strongly conditioned by the geographical location (both latitude and longitude) of the sampled sections. The NIS is exposed to strong seasonal oscillations of different atmospheric drivers such as solar radiation, air temperature, wind patterns, precipitations, etc. The winter season is characterized by the predominance of southerly and westerly winds, the periodic influence of atmospheric low pressure systems, high precipitations and relatively low solar irradiance. These conditions favor water column mixing with low values of temperature. Solar radiation increases, together with SST, during spring, promoting the beginning of water column stratification. The precipitations are less intense and the winds change to a predominance of northerlies and easterlies. SST and radiation get its maximum values in summer, when the influence of the passage of low atmospheric pressure systems is also reduced. Under these conditions, the water column is strongly stratified. Winds patterns change again to southerlies and westerlies during the autumn, when the influence of low atmospheric pressure systems is more frequent and the radiation decreases. The difference of temperature between the surface and sub-surface and bottom layers diminished and the stratification was broken up by physical disturbances produced by storms and progressive cooling of the surface layers.

This general seasonal cycle of the atmospheric drivers affect in a similar way all the North Iberian Shelf region. Over this general pattern, processes at finer scales produced changes that generate heterogeneity among the across-shelf sections distributed along the NIS. The Iberian Poleward Current (IPC) is one of the processes that modify the regional general pattern along the NIS. This current conveys warm and salty waters poleward following the shelf-break (Peliz *et al.*, 2005). It is a thermohaline compensatory current mainly modulated by the meridional gradient of temperature and locally by winds (Huthnance, 1984; Torres & Barton, 2006). The behaviour of this current exhibits also a notorious seasonality. It had its maximum intensity during autumn and winter, reducing its influence in spring and summer (Peliz *et al.*, 2003) (See Chapter 3). This process actuates changing the distribution of thermohaline properties from the sub-surface layers (depth of the core of the current around 70-100 m upwards to the surface and from southern to northern locations following the slope and inner parts of the shelf. Accordingly to the dynamics of this slope current we found the highest values of temperature and salinity at deeper layers in winter contrasting with the relatively lower values of these variables measured at the surface layers as a consequence of the seasonality of the atmospheric drivers. On other hand, the IPC generates a geographic along-shelf gradient with high values of temperature and salinity in the Galician sections that decrease eastward along the Cantabria Sea (Cudillero, Gijón and Santander sections).

Coastal upwelling is another mesoscale process that generates heterogeneity along the NIS. It is forced by winds and produces the ascension of sub-surface cold and salty waters (Bakun, 1990). Due to the different orientation of the Galician and Cantabrian coast, the upwelling favorable winds are different: northerlies in the first of this sub-regions and easterlies in the second one. In both cases, however, upwelling favorable winds have its higher intensity during summer. The major difference between both sub-regions is that the northerly winds are more intense and had lower interannual variability in comparison with easterly winds, which are less intense and predictable. The distinct pattern of upwelling favorable winds generates that the Galician sections (Vigo and A Coruña) had patterns of thermohaline variation clearly different to the Cantabrian sections. In hydrographic terms, upwelling actuates reducing the expected summer increase of surface temperature and, as a consequence, the stratification promoted by solar radiation. This reduction of temperature is observed from the sub-surface intermediate layers up to the surface layers. Besides, mid-shelf and coastal stations are more influenced by upwelling than the outer-shelf stations. The section off Cudillero showed a similar pattern of variation than that observed in the Galician sections, although much less intense. This similarity is probably due to the intensification of upwelling westward of Cape Peñas and

to other hydrodynamic processes linked to the physiographic features imposed by the Aviles canyon system (Sánchez *et al.*, 2014).

Another feature that influences the distribution of temperature is the surface warming in the south-east part of the Bay of Biscay (Lavín *et al.*, 1998; OSPAR, 2000), which is more intense at the surface layers and diminishes its influence westward. Its signal cannot be measured in the section of A Coruña. This phenomenon reinforces the seasonality of the surface layers increasing the stratification of the water column during summer, and is due to a continental weather effect affecting the cul-de-sac of the Bay of Biscay.

The aforesaid features are more perceptible by means of the analysis of the distribution of temperature. In the case of salinity, the process that generates more intense changes is the occurrence of buoyancy driven river plumes. The descents of salinity are more intense at the surface layer and in coastal edge of the sections, diminishing with depth and towards the offshore edge. Precipitations are more relevant in winter and spring mediated by the seasonality of the meteorological conditions, related to the west-to-east passage of low atmospheric pressure systems, which promote increased river discharges and continental runoff and the concomitant decrease of salinity during this part of the year. The sections that are close to river mouths, like Vigo, A Coruña and Cudillero, suffered important decreases of salinity at the surface layers in the coastal and mid-shelf parts of the across-shelf sections. The seasonal variation of salinity in those locations that are not influenced by rivers is much lower. The case of the Santander section is slightly different to the rest because the minimum values of salinity were measured during summer probably due to the influence of the discharges from the Adour, which are more important during this part of the year (González-Nuevo & Nogueira, 2014b). Besides, the reduction of the intensity of the IPC during spring, and the presence of northeasterly winds, make that this fresh water mass, enhanced by the discharges of the short Cantabrian rivers, extends its influence westward. A coast offshore salinity gradient was not measured in this section. The intermediate and ocean station were the most influenced by low salinity waters.

The long-term cyclical components of temporal variation found in the salinity time series off Vigo, Cudillero and Santander sections at different depths had periods of 12, 6, 4, 3 and 2 years. These kinds of oscillation are probably related with the interannual variations of the precipitations regimen. Lechuga (1973) analyzed the series of annual precipitations of the Iberian Peninsula between 1947 and 1976 and found that oscillations with periods of 46-72, 30-46 and 144 months that explain 37, 35 and 10% of the total variance of the precipitation time series. This author suggests that the oscillation of 144 months is related with the sun spots cycle. Other study carried out between 1919-1992 found oscillations of

2.7, 7 and 16 years (García *et al.*, 2002). These authors related the shorter cycles with the Niño southern Oscillation (ENSO). Other papers found periods of 13.7, 8.5, 5.5, 3.6 and 2.7 years relating the most frequent variations with ENSO (Gámiz-Fortis *et al.*, 2004).

Spring Cruises

Geostatistic analysis

The distribution of the geostatistical parameters with depth was the result of the interaction between regional and short-term scale processes. High values of the correlation factor (A), both for temperature and salinity, imply that the values for these variables between neighbour stations are similar in the whole studied area. This behavior reflects the constancy of the variable or the constancy of the variation rate, that is, the homogeneity of the processes in the whole area. The opposite situation, low values of A , represents high spatial variation rates and, consequently, denotes the heterogeneity of the processes across the covered area. High values of the length scale parameter (L) showed the prevalence of large-scale processes in contrast to low values of L which indicates the dominance of short-term scale processes. Taking into account the meaning of these geostatistical parameters, we can explain the water column distribution of A and L as a function of the predominant processes. In spite of the fact that the surface layer is influenced by more spatially heterogeneous and highly temporal variable processes, such as river plumes or coastal upwelling, the combination of the along-shelf temperature and salinity gradients generated by the IPC and the higher intensity of the stratification in the easternmost part of the Cantabrian Sea make that the differences of temperature at the surface layers were reduced and that the relationships between the values of neighbour stations were similar, obtaining relatively high values of both A and L . Between 20 and 50 m depth, however, the most important processes are the upwelling and the stratification-mixing cycles. These type of processes generate short-term spatial heterogeneity that is translated into relatively low values of A . Large scale processes such as the IPC gain importance with depth and local noise produced by lower scale processes diminish, making A and L increase their values simultaneously.

In the case of salinity, we measured an increase of A and L with depth. The main processes that modify the distribution of salinity are buoyancy river plumes and runoff, which act at the surface layers, and the progress of the IPC, which modify the distribution of this conservative property at surface and sub-surface layers. Accordingly, we have found low values of A and L at the surface due to salinity gradients generated by river plumes and runoff. The diminished influence of river plumes with depth and the salinity

distribution forced by the IPC makes that higher values of A and L were found at sub-surface layers.

Climatic fields and across-shelf sections

The results obtained using the hydrographic information acquired during the stock assessment spring surveys reflected similar temperature patterns than those obtained with the time-series monthly monitoring programme for this period of the year. The cruises were carried out during the winter-spring transition, where the system progress from winter meteo-hydrographic conditions to a characteristic early-summer situation characterised in hydrographic terms by the development of water column thermal stratified conditions.

The increase of incident solar radiation promotes water column stratification in the whole NIS area. This feature has more relevance in the easternmost part of the Cantabrian Sea. The differences of temperature between 10 and 50 m are of 0.4 and 0.8 °C for the Atlantic Coast and East Cantabrian Sea (AC and EC areas) respectively. In this part of the year takes place also the beginning of the decaying phase of the IPC development, which diminishes its influence all along the Bay of Biscay. The along-shelf thermohaline gradient was observed both in the horizontal fields and in the across-shelf sections. The signal of this gradient due to the combined effect of the aforesaid regional-scale processes is more evident in the deeper than in the surface layers, where other mesoscale processes, such as continental runoff and coastal upwelling, introduce considerable thermohaline variability. For instances, this general regional pattern along the NIS was modified by local salinity decrease associated with runoff in the Rias Baixas and Rias Altas and the buoyancy driven plume of the Adour River. The Miño and Adour are rivers with 17667 km² and 16880 km² catchment area respectively that generate noticeable plumes which influence the distribution of salinity down to 30 m depth (González-Nuevo & Nogueira, 2014b).

The Central Cantabrian Sea is less influenced by river plumes than the rest of the study area. Feeble salinity descents measured close to de coast did not extend its influence down to 5 m depth. The influence of the Adour River on the Eastern Cantabrian Sea was reinforced by the discharges of the Cantabrian Shorts Rivers. The presence of fresh waters in this zone favours the intensification of the stratification process.

In the Atlantic coast, coastal upwelling is detectable by means of relative cold waters at the coastal and mid-shelf. Although the structure is visible in horizontal temperature fields, it is clearer in the temperature climatic sections S1 and S2. The upwelling signal was not

much intense probably as consequence of the spring surveys were carried out in a transition season, making that the occurrence upwelling was not observed all years.

Chapter 3: Seasonal and interannual variation of the incursion of the Iberian Poleward Current (IPC) along the Northern Iberian Shelf derived from in situ thermohaline data

Introduction

All five mid-latitude eastern ocean boundaries (Northwest Africa / Iberian Peninsula, Southwest Africa, South and North America and west Australian coast) exhibit poleward flowing undercurrents along their continental margins (Smith *et al.*, 1989). Eastern Poleward Currents (EPC) flow counter to the dominant regional surface circulation, and are driven primarily by the interaction between large-scale meridional geopotential gradients, mainly of thermal origin, and topography (Huthnance, 1984), but are also forced and modified in different ways in response to local wind patterns (Neshyba *et al.*, 1989). The EPCs affect the distribution of heat, salt, chemical properties and biological components, and consequently are an important regulator of the structure and functioning of eastern boundary upwelling ecosystems (EBUEs, Fréon *et al.*, 2009 and articles therein)

In the North Atlantic, the pattern of surface currents is dominated by two major oceanic gyres: the subpolar, extending approximately between 45°-65°N and driven by the Icelandic low pressure system, and the subtropical, between 10°-40°N and forced by the anticyclonic atmospheric circulation around the Azores high atmospheric pressure cell (Tomczak & Godfrey, 1994). Within these regions, distinct types of Eastern North Atlantic Central Water (ENACW) are formed: the subpolar mode (ENACW_{sp}), which originates in the eastern North Atlantic north of 46°N by winter cooling and deep convection, and the subtropical mode (ENACW_{st}), produced along the Azores Front at about 35°N by strong evaporation and winter cooling (Fiuza, 1984). These water masses present contrasting θ -S characteristics, being the subtropical mode warmer (13.15-18.50 °C) and saltier (35.70-35.75 pss), thus spicier (Flament, 2002) (spiciness, s; 2.32-3.50 kg m⁻³—calculated for the extreme θ -S values of the range), than the subpolar mode, with θ -S characteristics in the range 10-12.2 °C, 35.40-35.66 pss (Harvey, 1982; Ríos *et al.*, 1992) (s; 1.44-2.03 kg m⁻³).

The North Iberian shelf (between 42-45°N, 9-1°W) lies in the inter-gyre region that separates the subpolar and subtropical oceanic gyres, bounded to the north by the southeastern branch of the North Atlantic Current (NAC) and to the south by the Azores Current (AC) (Maillard, 1986). Surface currents across this region are weak and run southwestward (Krauss, 1986; Pollard *et al.*, 1996) seeding the equatorward Portugal Current (PC) (Maillard, 1986). Fraga *et al.* (1982), using data collected between June and October, described the existence of a subsurface front between the subpolar and subtropical modes of ENACW off Cape Finisterre (43°N, 9°W), and were the first authors who suggested a poleward advection of the subtropical mode water along the Iberian margin. Since the nineties, the Iberian Poleward Current (IPC), named also 'Navidad'

(Christmas) Current (Pingree & Le Cann, 1992a) or Portugal Coastal Counter Current (PCCC) (Fiuza, 1984; Álvarez-Salgado *et al.*, 2003), has been confirmed using *in situ* hydrographic data, sea surface temperature (SST) from advance very high resolution radiometer (AVHRR), satellite images, surface drifting buoys, current meter records, satellite images from the coastal zone color scanner (CZCS) or biogeochemical data (Table 1).

The IPC was originally described as a narrow (25-40 km wide), weak (5-30 cm·s⁻¹) subsurface (core about 200 m deep) current bounded to the shelf-break zone off the Western Iberian margin (Frouin *et al.*, 1990; Haynes & Barton, 1990). Pingree and Le Cann (1990) described the poleward flowing slope currents along the shelf and slope of the Western Iberian Peninsula and the Bay of Biscay as an interconnected circulation process (Pingree & Le Cann, 1990; Pingree & Le Cann, 1992b; Pingree & Le Cann, 1992a; Pingree, 1993). Recent observational and modeling studies (Table 1) have confirmed previous interpretations of the IPC, but stressed its permanent, seasonally varying character, the role of large-scale meridional thermal gradient as primary driving mechanism, the influence of local-to-regional wind patterns as modulators of its intensity, position relative to shelf break and depth, and the strong eddy shedding activity associated with the current (reviewed by Peliz *et al.*, 2005). Observations have been also accumulated on the possible effect of the IPC on the distribution of different ecosystem components, from plankton (Fernández *et al.*, 1991; Calvo-Díaz *et al.*, 2004; Bode *et al.*, 2005; Cabal *et al.*, 2008) to fish larvae (Santos *et al.*, 2006; Rodríguez *et al.*, 2008), and processes such as primary production (Álvarez-Salgado *et al.*, 2003), bacterial production (Moran *et al.*, 2007) or fish recruitment (Sanchez & Gil, 2000).

However, despite the relatively large number of observations of the IPC, most of them spanned for relatively short time intervals, focused at the time when the poleward flow is considered to be more intense (autumn-winter), and were carried out preferentially in the West and/or Northwest Iberian waters (Table 1). Therefore, there are some open questions regarding seasonal and interannual variability of the incursion of the IPC along the Northern Iberian shelf (NIS), from Galicia to the eastern part of the Southern Bay of Biscay. The aim of this work is to clarify these questions by analyzing *in situ* temperature and salinity data from CTD casts recorded in the NIS in an ongoing monthly time series monitoring program started in the nineties and a set of oceanographic surveys carried out during early-spring (March-April) between 1987 and 2008.

Table 1: List of papers published dealing with different aspects of the Iberian Poleward Current (IPC), specifying the methodological approach applied and the location (North, North-West or West parts of the North Iberian shelf -NIS) and period of time (season and year) covered by the specific study. Methodology: CM, current meters; SST, sea surface temperature from advanced very high resolution radiometer (AVHRR); DB, drifting buoys; BGC, biogeochemical approach; H; hydrographic studies; CZCS, satellite images from coastal zone color scanner. Site: W, off Portugal (37-42°N); NW, off Galicia (42-44°N); N, Cantabrian Sea (44°N, 7-1°W). Season: wi, winter; sp, spring; su, summer; au, autumn.

Reference	Method	Site	Season				Year
			wi	sp	su	au	
Swallow <i>et al.</i> (1977)	CM						
Ambar <i>et al.</i> (1986)	CM	W	■				83
Barton (1989)	DB	NW			■	■	86
Pingree and Le Cann (1990)	SST/CM			■	■		88-89 (CM) 83, 89, 90 (SST)
Frouin <i>et al.</i> (1990)	SST/H	W	■				83-84
Haynes and Barton (1990)	DB/SST/C M/H	W				■	86
Bode <i>et al.</i> (1990)	BGC	N		■			87
Haynes and Barton (1991)	H/DB	W	■			■	86-87
Pingree and Le Cann (1992a)	H/SST	N	■				89-90
Pingree and Le Cann (1992b)	DB/SST	N	■	■	■		91-92
Perez <i>et al.</i> (1993)	BGC	W-NW					
Pingree (1993)	H/DB	W					
Pingree (1994)	DB	N		■			92
Garcia-Soto and Pingree (2009)	H	NW		■			89
Castro <i>et al.</i> (1997)	BGC	NW				■	86
Fiúza <i>et al.</i> (1998)	H	W-NW		■			93
Peliz and Fiúza (1999)	CZCS	W	■	■	■	■	79-85
Perez <i>et al.</i> (2001)	BGC	W-NW		■	■	■	83, 89, 93
van Aken (2002)	DB	N		■	■		95-99
Bode <i>et al.</i> (2002b)	H, BGC	NW-N		■			91-92
Garcia-Soto <i>et al.</i> (2002)	SST	NW-N	■				79-00
Gil (2003)	H	N				■	95
Álvarez-Salgado <i>et al.</i> (2003)	SST/H/B GC	NW	■				87-99 (SST)
Cabanas <i>et al.</i> (2003)	H	NW-N	■	■	■	■	92-02
Ruiz-Villarreal <i>et al.</i> (2004)	CM	N	■	■	■	■	95
Peliz <i>et al.</i> (2005)	SST/H/C M	W	■	■	■	■	85-01 (ΔT zonal)
González-Nuevo and Nogueira (2005)	H	NW-N		■			87-05
Gonzalez-Pola <i>et al.</i> (2005)	H	NW-N		■			00
Llope <i>et al.</i> (2006)	H	N	■	■	■	■	92-03
Torres and Barton (2006)	H,CM,SS T		■	■	■		99
Ruiz-Villarreal <i>et al.</i> (2006)	H, CM	NW-N		■		■	02-03
Gil and Gomis (2008)	H	N		■			05
Herrera <i>et al.</i> (2008)	H	NW	■	■	■	■	01-02
Le Cann and Serpette (2009)	H,DB,SST	NW-N		■		■	06-07
Alvarez <i>et al.</i> (2010)	H	N		■			08
deCastro <i>et al.</i> (2011)	SST	W-NW					96-06
Esnaola <i>et al.</i> (2012)	SST	NW-N	■			■	81-10

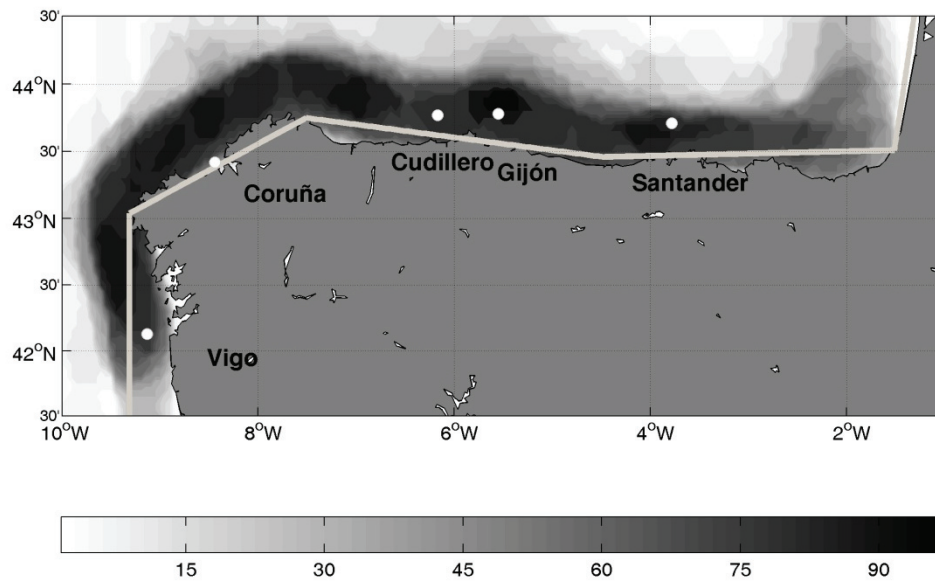


Figure 1: Map of the study area, the North Iberian shelf (NIS), including: frequency of sampling during the spring surveys (Table 1); positions of the mid-shelf hydrographic stations of the five across-shelf 'RADIALES' sections; reference along-shelf line (nautical miles) for the calculation of the position of the Iberian Poleward Current Front (IPCF).

Material and methods

Hydrographic database

The hydrographic database is integrated by temperature and salinity (θ -S) data from two different sources (Figure 1 and Table 2): a time series monitoring program and a set of oceanographic surveys carried out in early-spring. Within the frame of the long-term time-series monitoring program 'RADIALES' (www.seriestemporales-ieo.com), five sections are sampled monthly by the Instituto Español de Oceanografía (IEO) in the Northwest and North Iberian shelf. Four of them, located off Vigo (RA-Vi: 42.2°N, 8.2°W –position of the coastal station of the across-shelf section), A Coruña (RA-Co: 43.4°N, 8.4°W), Cudillero (RA-Cu: 43.6°N, 6.1°W), and Santander (RA-St: 43.5°N, 3.8°W), have been visited continuously at least since 1994, while the section off Gijón (RA-Gi: 43.6°N, 5.6°W) started in 2001. The set of surveys were carried out between 1987 and 2008 (except for the year 1989, $n = 21$) in March-April for stock assessment of small pelagic fishes (PELASSES-PELACUS, www.ieo.es). The grid of oceanographic stations in these surveys extends from the coast (around 30 m depth) up to the slope (≥ 200 m) along the Northern Iberian shelf (NIS; 41.5°-44.5°N, 10°-1°W). Maximum depth of sampling was always greater than 400 m, except for those surveys conducted between 1998 and 2005 for which maximum sampling depth was around 200 m. The density of sampling in the

whole area is represented in Figure 1; those stations located along the mid-shelf were always visited.

Hydrographic data were obtained with different conductivity-temperature-depth (CTD) *SeaBird* instruments calibrated using the standard protocols established by the manufacturer. The profiles extended from the surface (around 3 m depth) down to 5 m above the bottom in the casts conducted over the shelf. The database of CTD profiles was subject to a quality control, which included the removal of spurious data by visual inspection and low-pass filtering with a moving-median filter. Pressure reversals were also excluded. From the purged hydrographic data, salinity (UNESCO, 1983) and derived variables (potential temperature and spiciness) were calculated after vertical averaging in pressure intervals of 1 dbar when possible, or at least for each 2 or 5 dbar in those stations (at the beginning of the series) that were sampled at an acquisition rate of 0.5 or 0.2 Hz respectively.

Table 2: Details of the spring cruises (acronym of the cruise, research vessel and start and end date of the survey) carried out in the studied area to obtain in situ thermohaline data.

Campaign	Research Vessel	Start	End
SARPAREA	Lura	13/04/87	24/04/87
MPHSARACUS	Cornide Saavedra	01/04/88	04/05/88
MPH	Investigador	18/04/90	09/05/90
ECOSARP	Cornide Saavedra	17/04/91	09/05/91
ICTIONORTE	Investigador	22/04/92	09/05/92
PELACUS	Cornide Saavedra	14/04/93	03/05/93
SEFOS	Cornide Saavedra	15/03/94	13/04/94
MPH	Cornide Saavedra	26/03/95	14/04/95
SEFOS	Cornide Saavedra	11/03/96	31/03/96
PELACUS	Thalassa	08/03/97	31/03/97
PELACUS	Thalassa	17/03/98	08/04/98
PELACUS	Thalassa	03/03/99	29/03/99
PELACUS	Thalassa	27/03/00	12/04/00
PELACUS	Thalassa	30/03/01	22/04/01
PELACUS	Thalassa	09/03/02	04/04/02
PELACUS	Thalassa	19/03/03	12/04/03
PELACUS	Thalassa	30/03/04	22/04/04
PELACUS	Thalassa	05/04/05	29/04/05
PELACUS	Thalassa	01/04/06	28/04/06
PELACUS	Thalassa	27/03/07	23/04/07
PELACUS	Thalassa	28/03/08	20/04/08

In order to characterize the incursion of the IPC onto the Northern Iberian shelf we analyzed the temporal and spatial changes of spiciness (s , $\text{kg}\cdot\text{m}^{-3}$), a state variable derived from potential temperature and practical salinity ($\theta-S$) data (Flament, 1986; Flament, 2002) which is sensitive to isopycnal thermohaline variations. Analysis based on this variable has been applied to typify saline intrusions and water masses in the California eastern boundary upwelling system (Jackett & McDougall, 1985; Lynn & Simpson, 1990). In our case, spiciness was used to discriminate between the warmer and saltier (thus spicier) waters of ENACW_{st} conveyed by the IPC, from the colder and fresher waters of ENACW_{sp} characteristic of the southern and south-eastern parts of the Bay of Biscay.

Remote and local forcing

We have analyzed the relationship between the interannual variability of the incursion of the IPC along the shelf and potential large-scale and local drivers. The Meridional Thermal Gradient (MTG) was defined as the slope ($^{\circ}\text{C}\cdot^{\circ}\text{latitude}^{-1}$) of the linear regression of monthly sea surface temperature (SST) estimated between 40°N and 50°N along 13°W . Monthly time series of the zonal (u) and meridional (v) components of the wind estimated at 42°N , 10°W were used to analyze the effect of wind patterns. Both SST and wind data were extracted from the NOAA Earth System Research Laboratory (www.esrl.noaa.gov) database. The monthly time series of the North Atlantic Oscillation (NAO) and Eastern Atlantic (EA) climatic indices were obtained from the Climate Prediction Centre of the NOAA (www.cpc.ncep.noaa.gov).

Time series analysis

The time series of spiciness from the long-term monitoring program were subjected to spectral analysis in order to recognize the main modes of temporal variability (Platt & Denman, 1975). Afterwards, the time series were modeled by means of the Box-Jenkins approach (Box & Jenkins, 1976), assuming that the time series follow an additive model,

$$s_{t,z} = \bar{s}_z + LT[s_{t,z}] + SC[s_{t,z}] + R[s_{t,z}] \quad (1)$$

where, subscripts t and z are the index for time and depth respectively, \bar{s} is the average value of spiciness, LT and SC represent the long-term and seasonal components respectively and R accounts for the remaining fluctuations of the time series. LT and SC were treated as 'deterministic' components (Chatfield, 1996).

The seasonal component was defined by the combination of the first and second harmonics of the annual period,

$$SQ[s_t] = A_{12} \cos\left(\frac{2\pi}{12}t + \theta_{12}\right) + A_6 \cos\left(\frac{2\pi}{6}t + \theta_6\right) \quad (2)$$

where, A_{12} and A_6 are the amplitudes of the first (period, $T = 12$ months) and second ($T = 6$ months) harmonics of the annual period respectively, and θ_{12} and θ_6 are their phases in radians. These parameters were extracted by Fourier analysis (Poularikas & Seely, 1991). The long-term variation was parameterized by the slope of the linear trend and/or the amplitude, phase and period of long-term cycles ($T > 12$ months). Those cycles that accounted for more than 10% of the variance of the time series are significant at $p < 0.05$ according to Anderson criterion (Legendre & Legendre, 1998):

$$A_c = -(2/n) \log_e(1 - \sqrt[m]{1 - \alpha}) \quad (3)$$

where, n is the number of observations in the series, m is the largest computed harmonic period, and α is the probability level.

The 'stochastic' component, the de-trended and de-seasonalized residuals, was parameterized by means of an autoregressive model, which involves the description of the time series in terms of a weighted sum of its own past values,

$$R[s_{t,z}] = \phi_i (R[s_{t-i,z}]) + a_t \quad (4)$$

where, ϕ_i are the auto-regressive parameters, and a_t represents the pre-whitened residuals, a time series of independent, identical and normally distributed random shocks (or white noise) with zero mean and constant variance (σ_a^2). The order of the autoregressive process is defined by the inspection of the auto-correlation (acf) and partial auto-correlation functions (pacf), and the auto-regressive parameters were estimated using the Yule-Walker equations (Wei, 1989).

Interpolation of the spiciness field

The average spatial distribution of spiciness in early-spring was obtained by averaging the data of all the spring surveys (1987-2008, $n = 21$) for a given depth. Prior to averaging, the actual data for each survey were interpolated on a regular grid of $0.1^\circ \times 0.1^\circ$ decimal degrees using an objective interpolation method (Haagenson, 1982). The data were interpolated using an isotropic correlogram Gaussian model (equation 5):

$$\gamma(R) = \frac{V_s}{V_s + V_n} \cdot e^{\frac{-R^2}{2 \cdot L^2}} \quad (5)$$

where, $\gamma(R)$ is the correlation for a distance R (in decimal degrees), V_s is the signal variance, V_n is the noise variance, and L is the characteristic length-scale. The values

used for interpolation were $V_s = 0.6$, $V_n = 0.4$ and $L = 0.6^\circ$, which corresponded to the average values derived from the analysis of the correlograms from each of the surveys (Chapter 2).

Detection of the Iberian Poleward Current Front (IPCF)

In order to infer the interannual variation of the incursion of the IPC along the Northern Iberian shelf during spring surveys (i.e. March-April) we developed an *ad hoc* method to localize the position of the frontal area that separates the different modes of ENACW. The method consists on an iterative algorithm that operates on the spiciness field data of each survey, searching for a theoretical across-shelf frontal structure (IPCF) in the along-shelf direction. The process is schematized in Figure 2a. The basis for this procedure is that the distribution of spiciness along the shelf defines three spatial domains: an IPC area, characterized by high and relatively constant values of spiciness distinctive of ENACW_{st}; the Bay of Biscay area, identified by low and relatively constant values of spiciness typical of ENACW_{sp}; and a zone in between which is characterized by a decreasing gradient of spiciness (gradient area). Hence, the structure of the front could be defined by two along-shelf locations (l), one at the beginning (l_{si}) and the other at the end (l_{se}) of the gradient area. This conceptual model was formalized according to the following discontinuous function (equation 6a-c):

$$s_l = \frac{\sum_{l_1}^{l_n} s_l'}{n}, \text{ for those } n \text{ along-shelf locations where } l \leq l_{si} \quad (6a)$$

$$s_l = \frac{s_{BoB} - s_{IPC}}{l_{se} - l_{si}} l + \frac{s_{IPC} l_{se} - s_{BoB} l_{si}}{l_{se} - l_{si}}, \text{ for those locations where } l_{si} < l < l_{se} \quad (6b)$$

$$s_l = \frac{\sum_{l_1}^{l_n} s_l'}{n}, \text{ for those } n \text{ along-shelf locations where } l \geq l_{se} \quad (6c)$$

where, s_l are the calculated values of the spiciness in each along-shelf location (l) belonging to the IPC ($l \leq l_{si}$), gradient ($l_{si} < l < l_{se}$) and Bay of Biscay areas ($l \geq l_{se}$) respectively, s_l' are the observed values of spiciness in each along-shelf location, and s_{IPC} and s_{BoB} are the average values of spiciness in the IPC and Bay of Biscay areas. The best fit to the discontinuous function was obtained minimizing equation 7 by iterating l_{si} and l_{se} :

$$r = \sum_{l_1}^{l_n} |s_l' - s_l|, \text{ for all along-shelf locations } l \quad (7)$$

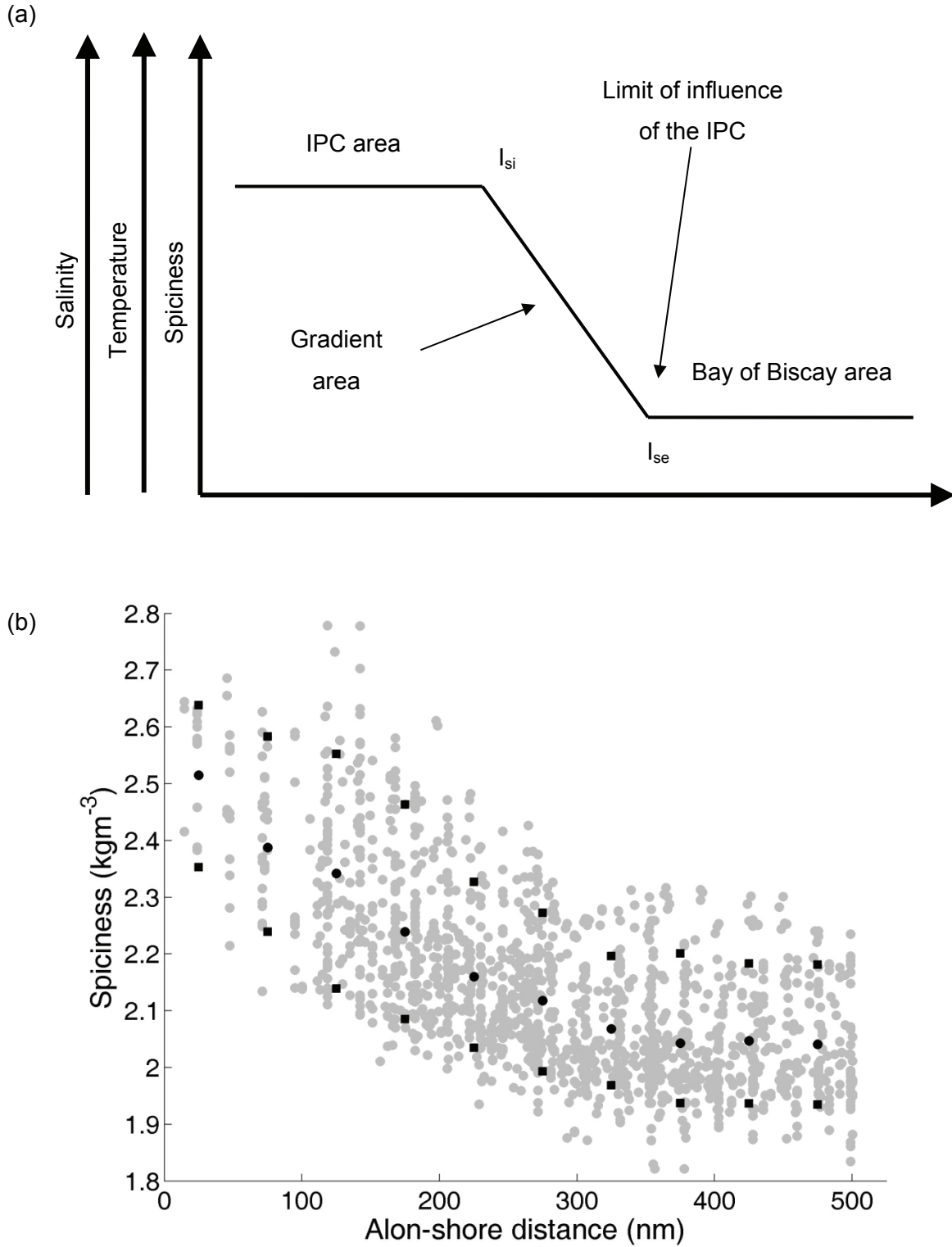


Figure 2: (a) Scheme of the conceptual model in which is based the detection algorithm (equation 5) of the IPCF, the proposed index of the intensity of the IPC. (b) Example of the along-shelf distribution of spiciness at 70 dbar from data of all the spring surveys (gray dots), mean values (black dots) and percentile 90th and 10th (black squares).

This method was applied to the spiciness field of each survey, for every 10 dbar between 10 and 140 dbar. We have considered that the location of I_{se} defines the limit of influence of ENACW_{sp} conveyed by the IPC, and that this along-shelf location labels the position of the front of the poleward current (IPCF) in a given year at a defined depth. Figure 2b illustrates the along-shelf distribution of spiciness at 70 dbar with data from all surveys.

The interannual variability of the along-shelf location of the IPCF ($= I_{se}$) was analyzed for each 10 dbar. Linear trends of the position of the IPCF were characterized by the slope of the linear regression (nautical miles per year, nm·yr⁻¹). We applied cross-correlation analysis to infer the relationships between the position of the IPCF and the main modes of climatic variability in the North Atlantic (NAO and EA), the meridional thermal gradient (MTG) and the wind regime (zonal and meridional wind components). Prior to the application of cross-correlation analysis, the time series analyzed were pre-whitened to make them stationary and to correct the overestimation of correlation values due to serial dependence (autocorrelation) (Wei, 1989).

Comparison with other indices of IPC strength

We assumed that the along-shelf position of the across-shelf frontal area that separates the subtropical and subpolar modes of ENACW in spring (the IPCF) is an indicator of the intensity of the incursion of the IPC along the northern Iberian shelf. To ascertain the validity of this assumption we have compared the IPCF with other indices suggested by several authors to assess the strength of the IPC: Four of them are based on satellite derived SST gradients, calculated on the basis of coastal-offshore (Álvarez-Salgado *et al.*, 2003; Peliz *et al.*, 2005) or along-shelf differences (García-Soto *et al.*, 2002; deCastro *et al.*, 2011). The index proposed by Esnaola *et al.* (2013) is based on Eigen Objective Functions (EOF) analysis of satellite derived SST fields. The aforesaid indices are quantitative, while the one proposed by Llope *et al.* (2006) evaluated the presence/absence of the IPC in the Central Cantabrian Sea using in situ $\theta-S$ characteristics. All these indices have been standardized to facilitate their inter-comparison.

The IPC index proposed by Peliz *et al.* (2005) was obtained by calculating the differences of the averaged satellite derived SST between two boxes located at 40° N 14° W and 40° N 10° W respectively (Figure 3). Álvarez-Salgado *et al.* (2003) used also satellite derived SST, but at two northernmost locations, one covering the shelf (40° N 9.5° W) and the other oceanic waters (40° N 14° W), to describe the dynamics of the IPC. We re-analyzed these data to derive an index (Figure 3) similar to that of Peliz *et al.* (2005), which associated the across-shelf SST gradient with IPC intensity. In contrast with these two

indices, deCastro *et al.* (2011) and Garcia-Soto *et al.* (2002) based their estimations of the IPC intensity on along-shelf SST gradients. The former authors calculated the difference of the SST between two domains over the shelf, in the Northwest Iberian and West Cantabrian Sea (Figure 3). Garcia-Soto *et al.* (2002) index was estimated as the SST difference between two locations, at 44° N 8° W and 44°N 6° W (Figure 3). The index proposed by Esnaola *et al.* (2013) is the result of applying EOF analysis on SST satellite derived data. These authors use the winter values of the time series of the first component as an indicator of the strength of IPC. Finally, Llope *et al.* (2006) proposed a qualitative IPC presence-absence index based on temperature and salinity pairs (θ -S diagram) measured in one station located in 43° 46' N 06° 09' W (Figure 3).

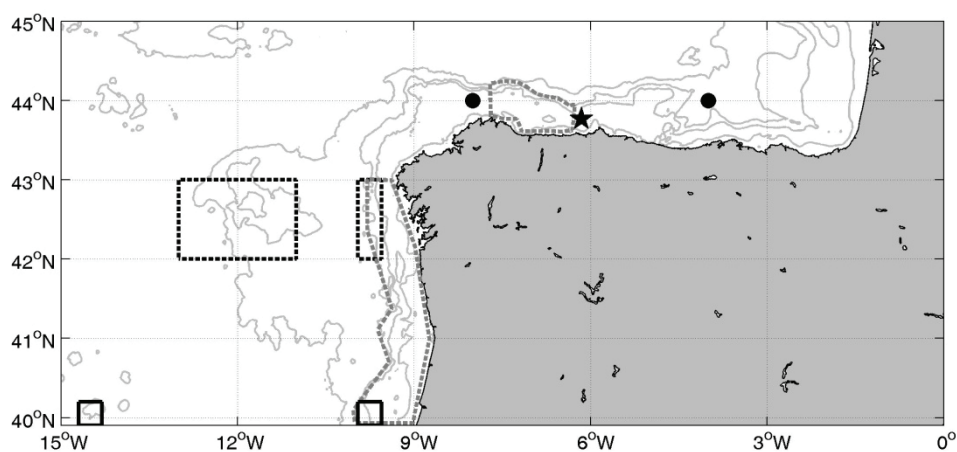


Figure 3: Locations of the data used from different authors to derive indices of the intensity of the IPC: García-Soto *et al.* 2002 (dots), Alvarez-Salgado *et al.* 2003 (dashed lined boxes), Peliz *et al.* 2005 (solid lined boxes), deCastro *et al.* (2011) (grey dashed lined boxes), and Llope *et al.* 2006 (asterisk) used to calculate different indices to account for IPC strength.

Results

Temporal variation of spiciness along the North Iberian shelf

To illustrate the pattern of temporal variation of spiciness along the NIS we focused on the time series of this variable at 70 dbar, at the core of the slope current according to recent model estimations (Pascual *et al.*, 2011), in the outer oceanographic station of each of the five across-shelf sections of the time series program 'RADIALES' (Figure 4).

The average value of the time series of spiciness showed an eastward decreasing trend, from 2.35 kg·m⁻³ off Vigo to 2.16 kg·m⁻³ off Santander (Table 3). Harmonic analysis of the time series highlighted two main periodic modes of variation (Table 3): long-term and

seasonal. The long-term component retains a significant percentage of total variability in all the time series (except in the shortest –Gijón), which ranged from 10.5% (Santander) to 3.3% (Cudillero). The period of these long-term oscillations was 12 years (the length of the time series) and the phase captured the relatively high values of spiciness recorded around 1997-1998. This long-term pattern was more marked in the easternmost section between 1998 and 2000 (Figure 4e).

The seasonal component of spiciness ($SC[s_i]$), defined as the combination of the first and second harmonics of the annual period, explained around 40-50% of the variability of the time series, except for A Coruña series, where the $SC[s_i]$ retained only around 20% (Table 3). This lower percentage of variance could be attributed to the location of the outer station of this section, at ca. 4 nautical miles apart from the coast, where the influence of other coastal processes such as runoff inputs could be noticeable.

The phase of the first harmonic of the annual period pointed out that the seasonal maximum occurs in December-January in the westernmost section (Vigo) and in November in the remainder sections (Table 3). The phase of the second harmonic indicated that secondary maxima occur in May and November. The secondary maximum in November captured the enlargement of the stage of relatively high seasonal values of spiciness in the westernmost section and the enhancement of the primary maximum in all the other sections. From the different seasonal cycles, we can infer that the seasonality of the along-shelf distribution of spiciness presents three different stages (Figure 5). From October to December, high and relatively constant values of spiciness ($2.4-2.5 \text{ Kg}\cdot\text{m}^{-3}$, corresponding to average $\theta-S$ values around 14° and 35.8) were observed all along the shelf. The exception to this pattern occur in October off Vigo and A Coruña sections, where the average values of spiciness were slightly lower (around 2.3 and $2.4 \text{ Kg}\cdot\text{m}^{-3}$ respectively). From February to August, a steep eastward decreasing trend of spiciness developed. During this stage, the values in the easternmost sections (Cudillero, Gijón and Santander) ranged between $2.1 \text{ kg}\cdot\text{m}^{-3}$ ($\theta-S$: 13°C , 35.60) and $2.0 \text{ kg}\cdot\text{m}^{-3}$ ($\theta-S$: 12.2°C , 35.55), while in the westernmost section (Vigo), the average values of spiciness evolve from 2.4 to $2.2 \text{ kg}\cdot\text{m}^{-3}$. In between these two major stages of the seasonal cycle, transitional periods were observed in January and September. From the described along-shelf progress of the seasonal cycle of spiciness we can infer that the seasonal incursion of the IPC exhibits a development phase around winter, when $ENACW_{sp}$ conveyed by the IPC is present all along the NIS, and a decaying phase the rest of the year, when the IPC shrunk westward. Short transitional periods occur between this two phases.

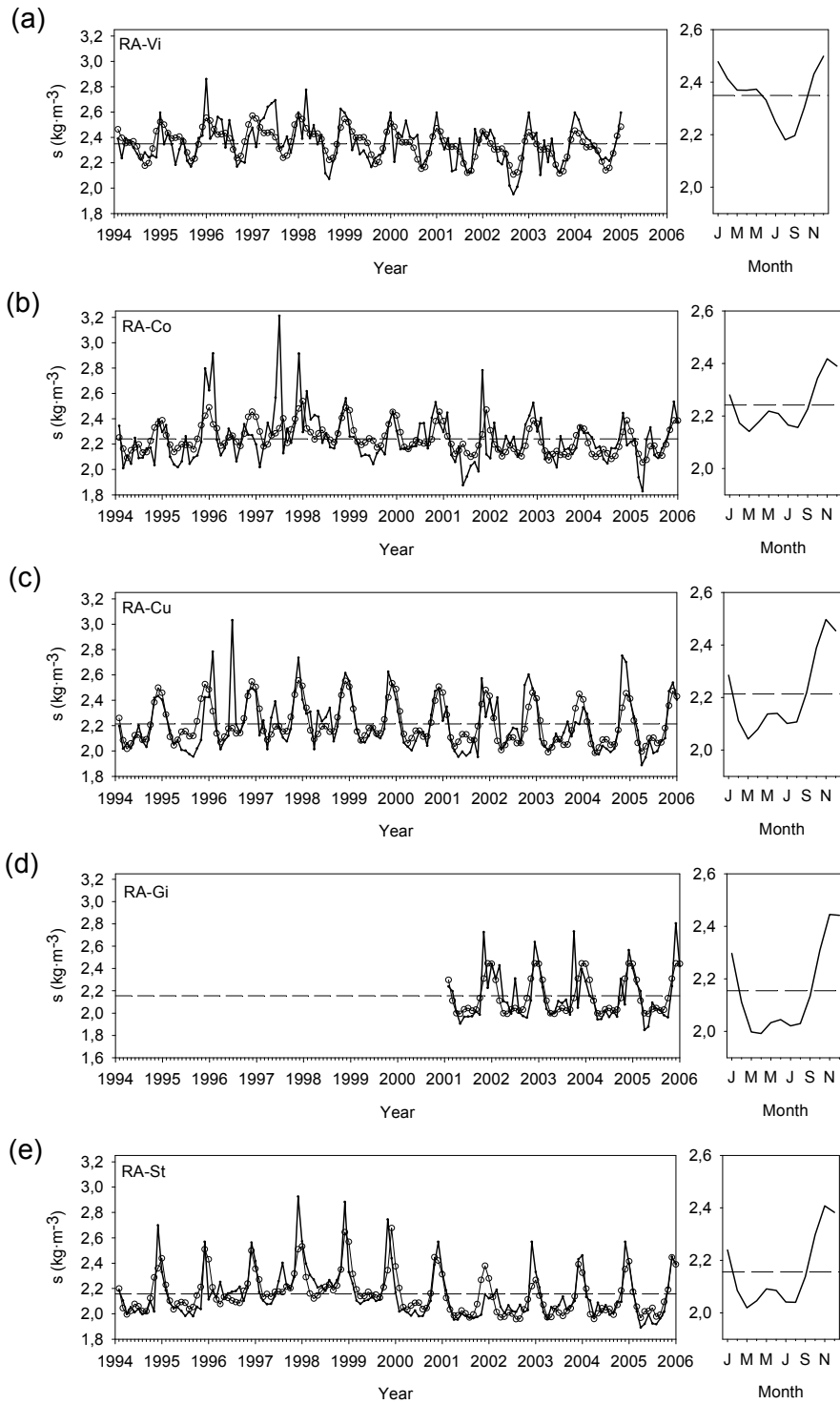


Figure 4: Time series of spiciness at 70 dbar in the outer hydrographic station of each of the 'RADIALES' sections: (left column) sampled data (circles) and additive time series model (solid line); (right column) seasonal cycle (first and second harmonics of the annual period). From top to bottom, 'RADIALES' sections off: (a) Vigo, (b) A Coruña, (c) Cudillero, (d) Gijón and (e) Santander.

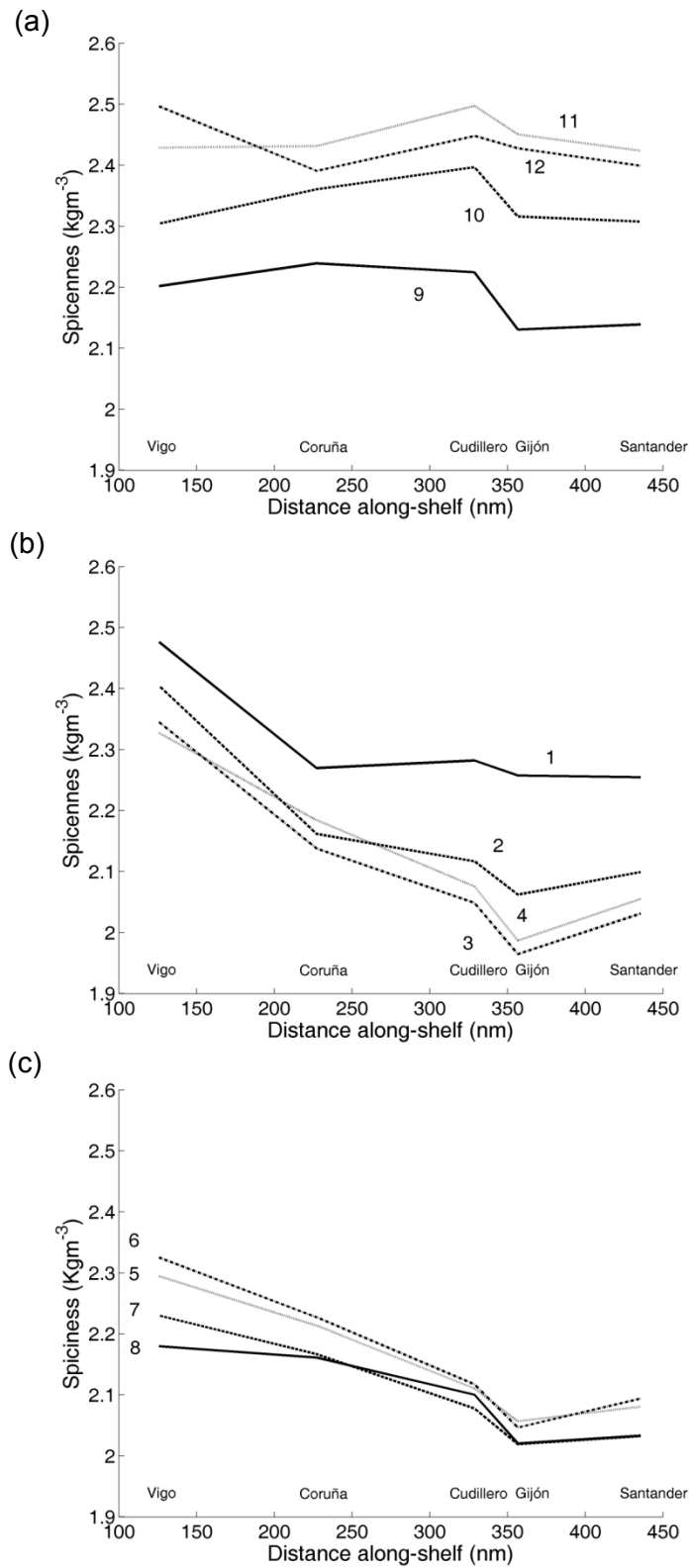


Figure 5: Seasonal variation of the along-shelf distribution of spiciness at 70 dbar in the mid-shelf station of the different 'RADIALES' sections: (a) from September to December; (b) from January to March; (c) from May to August. Numbers indicate month of the year.

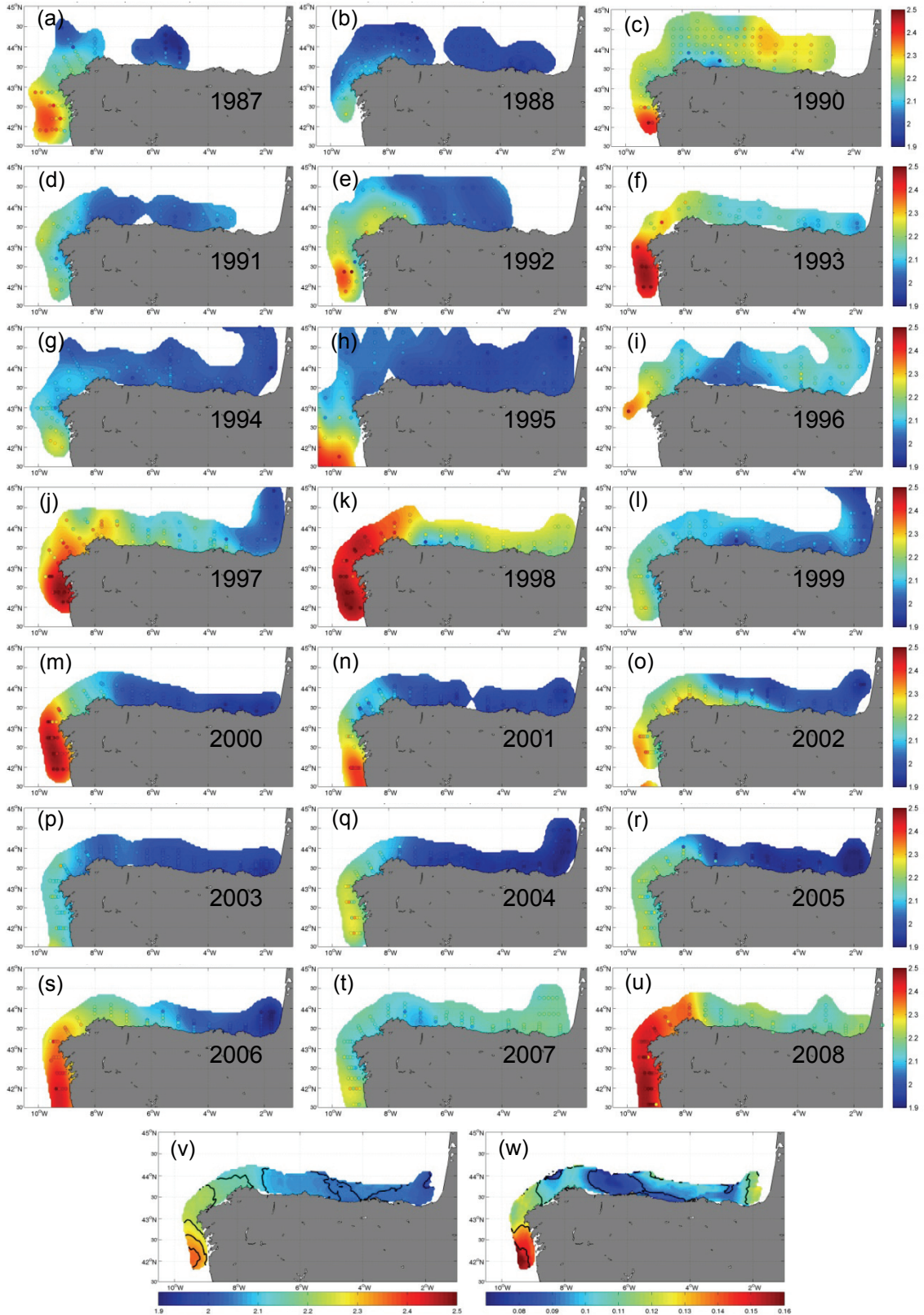


Figure 6: Interannual variation of the spiciness field at 70 dbar: (a-u) for the different spring surveys carried out between 1987 and 2008 (except for the year 1989); (v) mean and (w) standard deviation fields.

Table 3: Parameters of the univariate time series models for spiciness at 70 dbar in the sections off Vigo (Vi), A Coruña (Co), Cudillero (Cu), Gijón (Gi) and Santander (St). LT, SC and AR are the long-term, seasonal and autoregressive components of the time series respectively; \bar{x} , average value of spiciness; T , period; A , amplitude; θ , phase in radians; T_{mT} , month when the maximum of a given cycle occurs; r^2 , percentage of explained variance by the cycle; ϕ , parameters of the AR component; r^2 , total variance explained by the additive time series model.

Section	Period	\bar{s}	Cyclical components				Autoregressive			r^2 (total)	
			T	A_T	θ_T	T_{mT}	r^2	k	ϕ_k	r^2	r^2
RA-Vi	1994-04	2.35	12	0.48	5.48	1.5	0.30	-	-	-	0.50
			6	0.07	0.33	5.7	0.11	-	-	-	-
			132	0.07	4.37	40.1	0.09	-	-	-	-
RA-Co	1994-05	2.24	12	0.10	0.44	11.2	0.14	1	0.18	0.02	0.30
			6	0.08	0.76	5.3	0.08	-	-	-	-
			144	0.07	4.19	47.9	0.06	-	-	-	-
RA-Cu	1994-05	2.21	12	0.18	0.51	11.0	0.38	-	-	-	0.53
			6	0.11	0.71	5.3	0.15	-	-	-	-
			144*	0.05	4.16	48.7	0.03	-	-	-	-
RA-Gi	2001-05	2.15	12	0.21	0.33	11.4	0.43	-	-	-	0.53
			6	0.10	0.48	5.5	0.10	-	-	-	-
RA-St	1994-05	2.16	12	0.16	0.38	11.3	0.34	1	0.24	0.03	0.66
			6	0.10	0.68	5.4	0.15	12	0.42	0.03	-
			144	0.09	4.21	47.5	0.11	-	-	-	-

Once the ‘deterministic’ components of the time series have been removed, the remaining irregular fluctuations in the sections of Vigo, Cudillero and Gijón behave as a white noise process. In the case of A Coruña section, a first order, marginally significant (p -value = 0.03) autoregressive component accounted for the short-term dependence between consecutive values of spiciness. For the Santander section, the irregular fluctuation retained a short-term and a seasonal component that can be parameterized respectively by a first order and a seasonal autoregressive parameter which are both highly significant (p -value < 0.001) (Table 3). The pre-whitened residuals from the different time series exhibited significant correlations at zero-lag. These correlations followed an eastward decreasing pattern: Vigo versus Coruña ($r = 0.26$, p -value < 0.01); Coruña versus Cudillero ($r = 0.34$, p -value < 0.001) and Coruña versus Santander ($r = 0.19$, p -value < 0.05); Cudillero versus Santander ($r = 0.21$, p -value < 0.05) (Gijón section was excluded from this analysis because of the short length of the series).

Interannual variation of spiciness fields and location of the IPC front (IPCF) in early spring

The occurrence of poleward currents along eastern oceanic boundaries is usually concomitant with the transport of warm and salty (spicy) waters (Mooers 1989). Thus, inspection of the horizontal distribution of spiciness provides information relative to the extent and variability of the poleward transport. We selected the spiciness field at 70 dbar to illustrate the degree of interannual variability of the IPC during spring (Figure 6 a-u). The average spiciness field (Figure 6v) showed an along-shelf eastward pattern ranging from 2.4 to 1.9 $\text{kg}\cdot\text{m}^{-3}$. Isolines were slightly tilted on the west part of the NIS and run almost perpendicular to the coastline in the northern part. The variability was relatively low (Figure 6w), with the highest values (standard deviation of 0.15 $\text{kg}\cdot\text{m}^{-3}$) in the southwestern and north-eastern parts.

The annual fields of spiciness showed the development of distinct along- and across-shelf frontal structures over the NIS in spring. Most years, a strip of low spiciness water bordering the coast was separated by a neat front from the spicier waters located over the outer-shelf and slope. This front runs parallel to the coast and is more marked in the west and northwestern parts of the NIS, where relatively low salinity and cool waters are discharged from the adjacent ría-type estuaries. That situation was observed neatly in 1987, 1991, 1992, 1999, 2002, 2004, 2005 and 2007. Other years, this along-shelf front off the northwest coast was absent, as occurred in 1997, 1998, 2000 and 2006. Only in 1990 and 1998 the along-shelf front was more marked in the northern part of the NIS (at 6-7°W).

The across-shelf frontal structure that separates the distinct Central Water mass modes present in the studied area, $ENACW_{st}$ conveyed by the IPC and $ENACW_{sp}$ characteristic of the Bay of Biscay, was observed in all the spring surveys (Figures 6a-u). The depth-averaged (from 10 to 140 m) position of this front (IPCF), varied from year-to-year between Cape Finisterre ($43.2^{\circ} N$ $8.9^{\circ} W$) and Cape Ajo ($43.5^{\circ} N$ $4.0^{\circ} W$), with a mean position around Cape Peñas ($43.5^{\circ} N$ $7.0^{\circ} W$). The position of the IPCF is independent of the starting date of the cruise, which varied between early March (e.g. in 1999) and mid April (e.g. in 1992) (Table 2), as indicate the non-significant correlation between these two variables ($n = 20$ $r = 0.30$, p -value = 0.18).

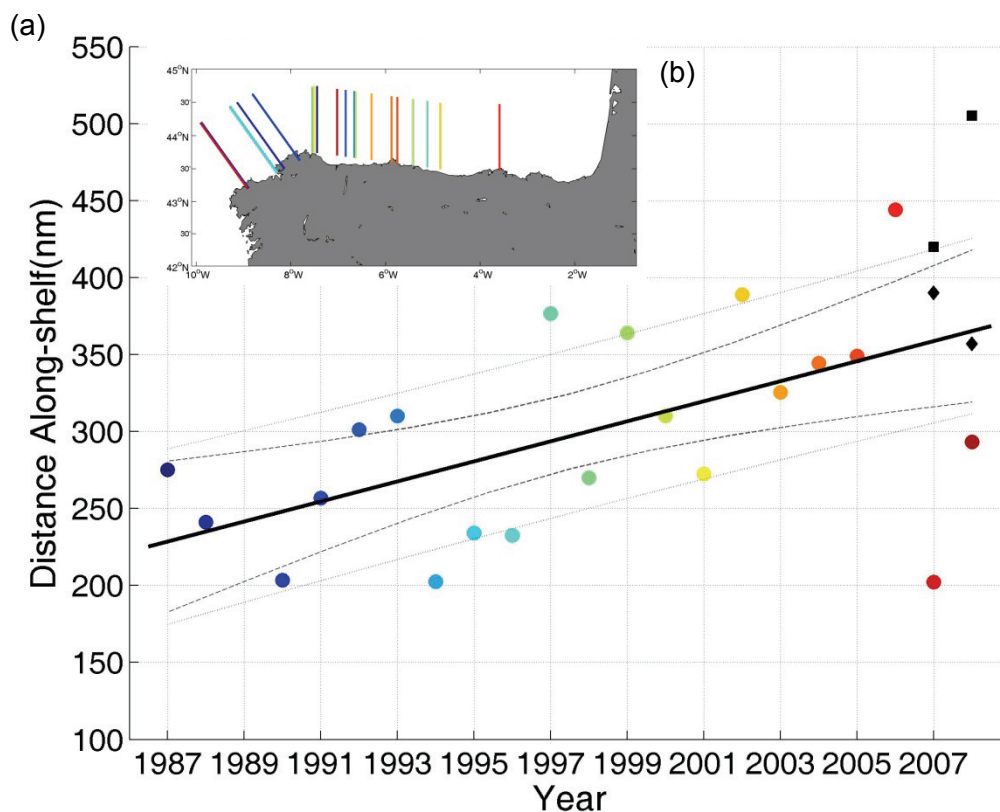


Figure 7: Time series of the location of the depth-averaged IPCF in spring: (a) time series (the year 2007 is excluded for the estimation of the linear trend, $n = 20$) and (b) along-shelf location of the IPCF. The year 2008 was included to test the long-term linear trend and the model of the location of the IPCF in spring driven by physical (black diamonds) or climatic (black squares) factors.

The time series of the depth-averaged position of the IPCF along the NIS showed a significant eastward trend of 6.5 nm year^{-1} ($n = 20$, $r = 0.62$, $p = 0.003$) (Figure 7). The interannual trends varied, however, with depth (Table 4). The eastward interannual displacement of the IPCF in spring was significant at all depths (except for the surface layers, 10 and 20 dbar), but was more acute in the upper, around 9 nm-yr^{-1} between 30

and 60 dbar, than in the lower layers, around $6 \text{ nm}\cdot\text{yr}^{-1}$ between 70 and 140 dbar. For the calculation of the interannual trends we have not considered the estimated position of the IPCF in 2007 because the occurrence of upwelling during this survey masked the detection of a neat along-shelf gradient (see the paragraph about the methodology of the IPCF detection in the Discussion section and chapter 5 for more details).

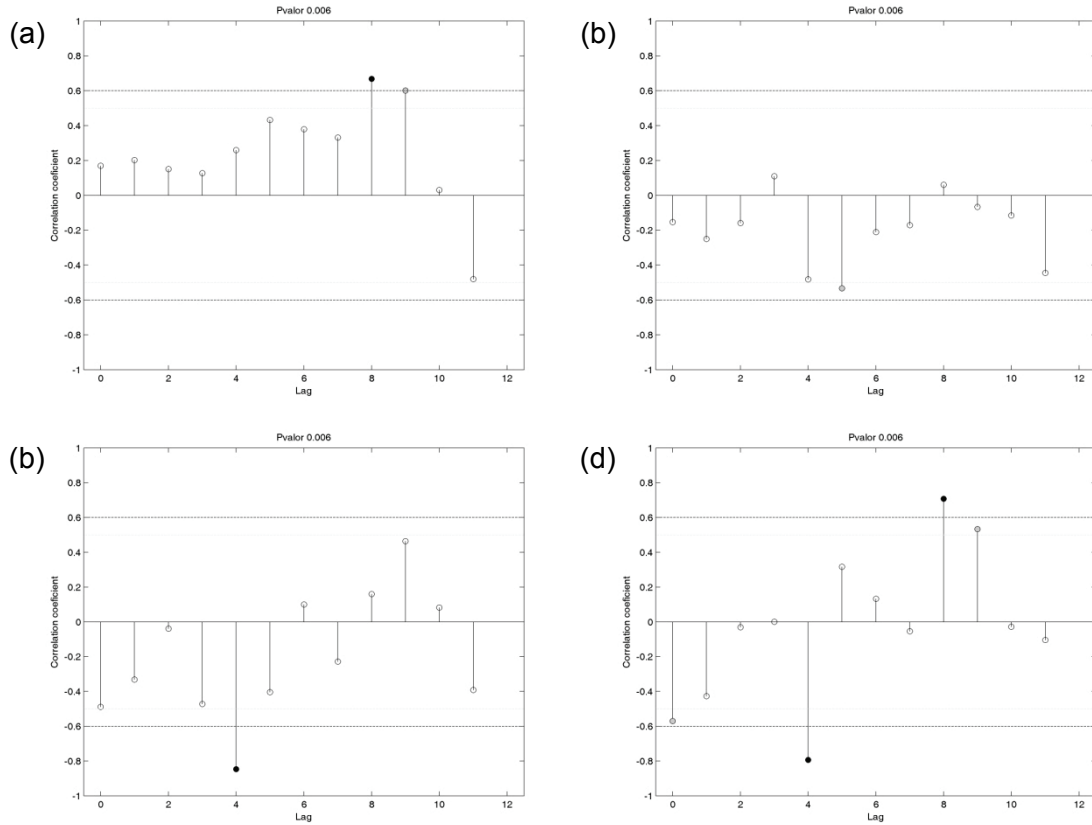


Figure 8: Cross-correlation between the position of the IPCF and: a) Meridional Thermal Gradient (MTG, $^{\circ}\text{C}\cdot\text{lat}^{-1}$), b-c) meridional and zonal components of the wind (u and v , $\text{m}\cdot\text{s}^{-1}$ negative values correspond to upwelling favorable winds – northerlies and easterlies respectively); d) Eastern Atlantic (EA) pattern. Dashed black and grey horizontal lines mark the $p < 0.01$ and $p < 0.05$ significance level respectively.

Relationships between the location of the IPCF and the meridional thermal gradient, wind pattern and climatic indices

The time series of the depth-averaged position of the IPCF in spring was positively correlated with the meridional thermal gradient (MTG) measured in summer of the previous year. The correlations were $r = 0.66$ ($p\text{-value} < 0.005$) and $r = 0.60$ ($p\text{-value} < 0.05$) for July and August (8 and 9-months lag) respectively (Figure 8a). It was also negatively correlated with the meridional and zonal components of the wind of the previous winter (November-December), indicating a positive relationship with northerlies (v -component: $r = -0.53$, $p\text{-value} < 0.05$, 5-months lag) (Figure 8b) and easterlies (u -

component: $r = -0.85$, p -value < 0.001 , 4-month lag) (Figure 8c). Finally we also found significant correlations with the Eastern Atlantic (EA) pattern at several lags ($r = -0.57$, $p < 0.05$, lag = 0 –April; $r = -0.79$, p -value < 0.001 , lag = 4 –December; $r = 0.70$, p -value < 0.005 , lag = 8 –August) (Figure 8d), but did not with the NAO index.

Table 4: Parameters of the long-term linear trend of the IPCF time series at different depths.

Depth	Slope	Intercept	R	p-value
10	1.6	-2919	0.08	0.742
20	2.8	-5211	0.16	0.506
30	8.6	-16799	0.48	0.033
40	8.7	-17138	0.50	0.024
50	9.2	-18001	0.53	0.016
60	9.3	-18182	0.58	0.008
70	5.1	-9857	0.43	0.056
80	5.4	-10588	0.47	0.035
90	6.1	-11860	0.50	0.025
100	6.7	-13095	0.56	0.011
110	6.9	-13526	0.59	0.006
120	6.9	-13510	0.64	0.002
130	7.3	-14320	0.65	0.002
140	6.5	-12761	0.61	0.004

On the basis of cross-correlation analysis we obtained two dynamic (lagged) regression models to account for the incursion of the IPC along the NIS, taking into account, in one case, the direct effect of physical drivers, the meridional thermal gradient (MTG) and wind patterns (u- and v-components of the wind), and the climatic scenario defined by the EA pattern on the other. In the first model, the MTG of the previous summer (MTG8, $p < 0.05$) and the meridional component of the wind of the previous winter (Uwind4, $p < 0.001$) were significant. The model based on direct drivers, $IPCF_i = 258.7 \cdot \Delta MTG8 - 13.6 \cdot \Delta Uwind4 + IPCF_{i-1}$, explained 75% of the variance of the position of the IPCF in spring ($n = 17$, $r^2_{adj} = 0.75$, $p < 0.001$). The model based on the climatic scenario, EA pattern of the previous winter and summer (EA4 and EA8 respectively, $p < 0.001$ in both cases; $IPCF_i = 22.9 \cdot \Delta EA8 - 42.4 \cdot \Delta EA4 + IPCF_{i-1}$), explained a higher percentage ($n = 17$, $r^2_{adj} = 0.85$, $p < 0.001$). According to the Akaike Information Criterion (AIC, Akaike, 1974), the models with two parameters were preferably than the models with only one parameter (AIC of 29.9 and 147.7 for models based, respectively, on 1 or 2 physical parameters; AIC of 28.5 and 149.4 for the models based on 1 or 2 climatic variables).

Relationship among indices of IPC strength

The time series of the different indices that have been proposed to assess the annual intensity of the IPC are shown in Figure 9. The mean squared error (MSE) has been calculated for each pair of IPC indices to obtain an estimation of the similitude among them (Table 5). Attending to this criterion, two groups of indices were found. The first group was composed by the IPCF and the index proposed by Garcia-Soto *et al.* (2002), with an MCE value of 0.9 between them and higher than 2 with the rest of the indices. Although the similarity between the IPCF and García-Soto indices was high, there were years with clear discrepancies (for instances 1994, 1999 and 2000).

Table 5: Mean Squared Error (MSE) between pairs of different indices of IPC strength.

	IPCF	García-Soto	Esnaola	deCastro	Peliz	Álvarez-Salgado
IPCF	0.0	0.9	2.0	2.8	2.4	2.1
García-Soto	0.9	0.0	3.1	2.7	2.5	2.2
Esnaola	2.0	3.1	0.0	1.1	1.4	1.7
deCastro	2.8	2.7	1.1	0.0	0.5	0.8
Peliz	2.4	2.5	1.4	0.5	0.0	0.7
Álvarez-Salgado	2.1	2.2	1.7	0.8	0.7	0.0

The other group is composed by the rest of the indices. The four indices belonging to this group showed a similar pattern of variation, characterized by two periods with high IPC intensity, centred around 1990 and 1997, and other period with low IPC intensity centred around 1993. In the case of the deCastro *et al.* (2011) index, the second period of high values was not as marked than it was by the rest of the indices. The general temporal pattern depicted by this group of indices differed from that described by the IPCF and Garcia-Soto *et al.* (2002), markedly for the period centred in 1993 for which both groups of indices showed opposite signs.

The increasing linear trend measured by the IPCF index was not found in any of the other indices, even in the Garcia-Soto *et al.* (2002). The indices by deCastro *et al.* (2011), Peliz *et al.* (2005) and Álvarez-Salgado *et al.* (2003) have the higher similarity, with values of MSE among them lower than 0.8. The qualitative (presence/absence) index proposed by Llope *et al.* (2006), although difficult to compare with the others indices, seems to have no similarity with any of them.

Discussion

Methodological considerations

We propose a simple and flexible method to characterize the extent of the intrusion of the IPC along the NIS based on the characterization of the spiciness field from in situ θ -S

data. Provided the accessibility to in situ θ -S data, the application of the proposed theoretical model allowed us to obtain consistent and robust results concerning the spread of the IPC over the shelf and the location of the frontal area (IPCF) separating the subtropical mode of ENACW conveyed by the IPC from other water masses also present in the study area. Besides, the method is relatively insensitive to changes in θ -S characteristics associated to hydrodynamic processes, such as coastal upwelling or river plumes, of moderate intensity and occurring at local-to-medium scales. Nevertheless, under strong mesoscale activity, the IPC could be displaced off shelf (Santos *et al.*, 2004; Serrano *et al.*, 2011), and therefore could not be detected if, as it is the case in the present study, the hydrographic sampling grid is restricted to shelf waters. This happened in the spring 2007 (Pelacus 2007 survey) when strong and persistent upwelling occurred all along the northwest shelf and in the Central Cantabrian Sea (see Chapter 5).

Indices of the IPC strength

We have assumed that the location of the IPCF in the spring of a given year is consequence of the intensity of the current in the previous autumn-winter, during the peak of the development phase of the seasonal IPC cycle. In an attempt to corroborate this assumption, we have compared the IPCF with other indices that have been proposed to assess IPC strength. The comparison is, however, not straightforward because the various indices proposed have been calculated using different input variables (satellite-derived SST or in situ θ -S data) and methodologies (across- or along-shelf gradients, EOFs or θ -S diagrams) and were applied to diverse temporal periods (winter or spring).

Most of the indices proposed to assess the intensity of the IPC in a given year are based on winter, during the seasonal development peak, satellite-derived SST values. SST is, however, strongly influenced by the occurrence of other process apart from the IPC strength, such as, river runoff, coastal upwelling-downwelling, eddying activity, development of the seasonal thermocline or atmosphere-ocean interactions, characterized by their frequency of occurrence, persistence and intensity. Using in situ θ -S values or a derived variable such as spiciness to infer an index of the IPC intensity is thus more appropriate since the influence of the hydrodynamic processes which modulate the thermohaline characteristics of water masses could be identified more precisely, furthermore if the data refer to the whole water column and not only to the surface layer. The IPCF index agreed reasonably well with the one proposed by Garcia-Soto *et al.* (2002). The coherence between the time-series of both indices is probably due to the fact that the method applied to calculate them is similar, based on along-shelf gradients.

Following this reasoning, we would have expected also a good agreement between the IPCF and the index proposed by deCastro *et al.* (2011).

We suggest that the observed lack of agreement could be due to the election by deCastro and colleagues of the southernmost area used to estimate the along-shelf SST gradient. This area is located along the western Iberian coast, where the Iberian buoyant plume (Otero *et al.*, 2008b; Otero *et al.*, 2009b) could strongly modify SST values in the area and thus bias the calculation of the along-shelf gradient. A similar argument applies to the estimation of IPC intensity on the basis of the across-shelf satellite-derived SST gradients (Álvarez-Salgado *et al.*, 2003; Peliz *et al.*, 2005) since they are also subjected to the occurrence of local-to-mesoscale hydrodynamic processes at the coastal side. The influence of continental runoff or river plumes that could modulate SST values at the coast is even more acute in autumn-winter, when these indices are calculated.

Eснаоla *et al.* (2013) use empirical orthogonal functions (EOFs) to extract the main modes of the spatial variability of SST. Although the methodological approach was different, the results were similar to those provided by the other indices that used SST (except Garcia-Soto *et al.* index), and is subject to the same bias caused by the assumption that the variability of SST is only related to the variability of IPC intensity.

There is not a clear relationship between the IPCF and the index proposed by Llope *et al.* (2006) to characterize the intensity of the IPC. This method has an important bias detecting the IPC because it is not taking into account which part of the thermohaline variability is consequence of interannual or mesoscale processes that are not directly related with the dynamics of the IPC. The only remarkable feature is that the two years for which the Llope's index detected low IPC intensity (1994 and 1999) are the same for which clear discrepancies were detected between the IPCF and the García-Soto indices. This result reflects that these two years were probably anomalous in terms of temperature and salinity signatures, making that the García-Soto index attributed these anomalies to the IPC dynamics whereas the IPCF index is less affected by this kind of changes because it is calculated on the basis of large scale fields of temperature and salinity and integrate the whole the water column.

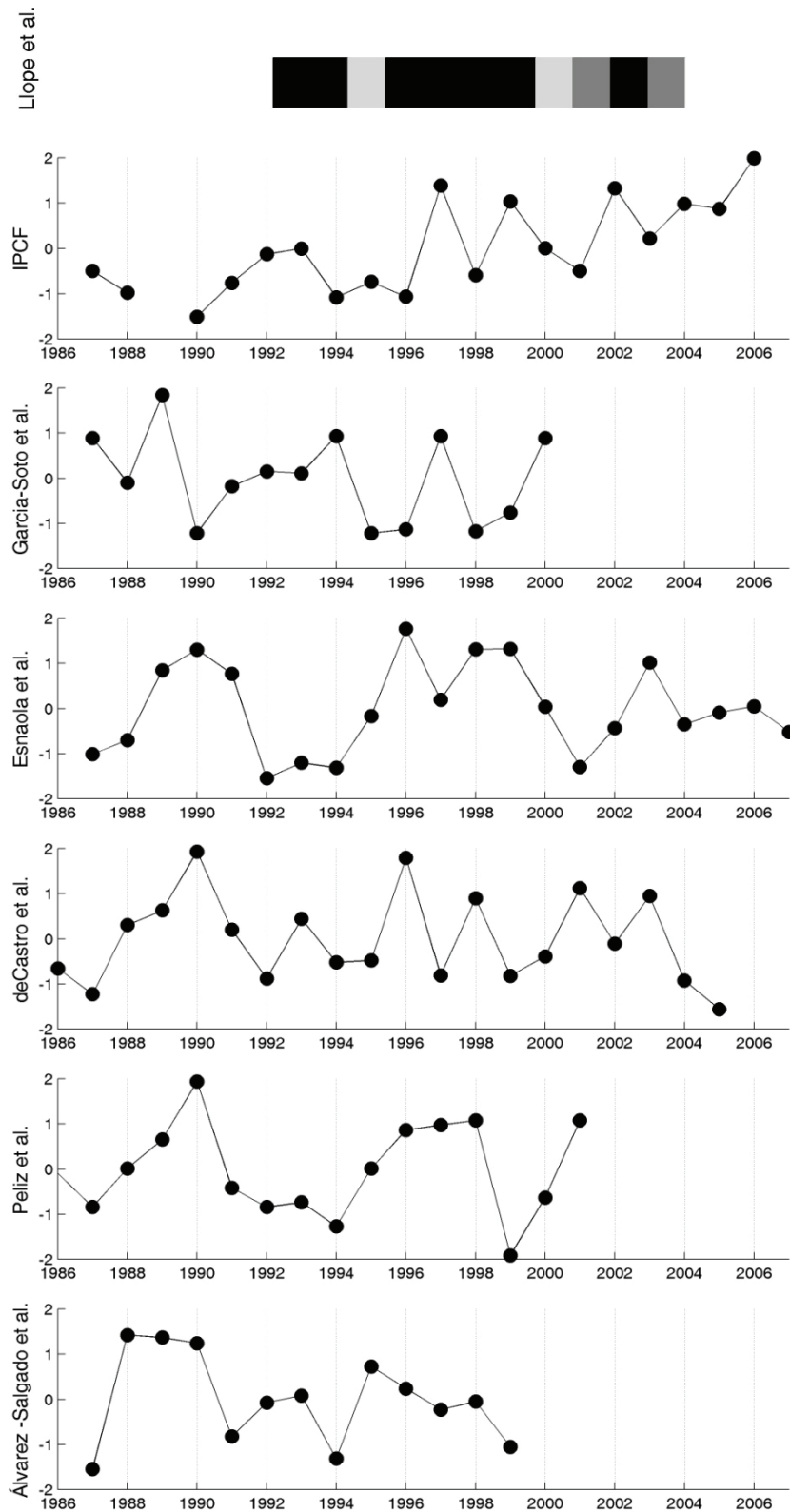


Figure 9: Comparison among different indices of the strength of the IPC (from top to bottom): Llope et al. (2006), IPCF, García-Soto et al., (2002), Esnaola et al. (2013), deCastro et al. (2011), Péliz et al. (2005) and Álvarez-Salgado et al. (2003). All the indices are standardized except the Llope index that only have three values, strong (black), weak (soft gray), and not clear (medium gray).

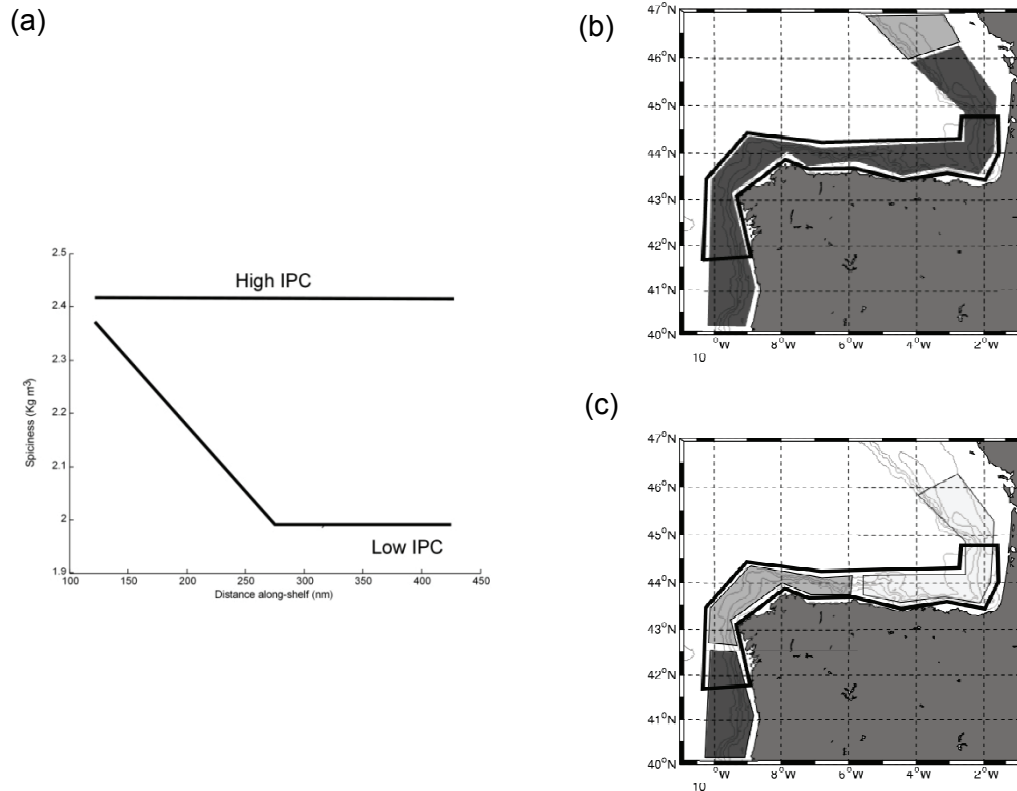


Figure 10: Conceptual scheme of the seasonal phases of the IPC to illustrate the along-shelf variation of spiciness at 70 dbar (a), and the spiciness field at 70 dbar during the development and decaying phases (b).

Seasonality of the IPC

In order to infer the seasonal dynamics of the IPC, we applied a semi-quantitative approach. We assumed that the IPC has a perceptible seasonality forced by the seasonally varying character of the main meteo-hydrographic drivers in the studied area (Peliz *et al.*, 2005). In the analysis of the temporal variability of ‘in situ’ spiciness in the across-shelf sections distributed along the NIS, we have taking into account, by means of the inspection of the thermohaline variability in the these sections (qualitative criteria), other mesoscale process that may affect thermohaline characteristics (spiciness) at meso-to-local scales. Accordingly, we deduced that the average distribution of spiciness is coherent with a poleward advection of ENACWst along the NIS. The results from the seasonal analysis agreed with the hypothesis of the evolution and seasonality of the IPC proposed by (Peliz *et al.*, 2005), who divided the seasonal cycle of the IPC in two main phases related with the dynamic of its main forcing factor, the meridional thermal gradient. The development phase occurred during fall and winter and was characterized by an intensification of the MTG (Figure 10a), which produces the strengthening of the IPC and the increased influence of warm and salty waters (spicy waters) northward. During this

development phase, we found that the whole NIS is characterized by the highest values of spiciness of the year (Figure 10b). In contrast, during the decaying phase, the meridional density gradient diminished (Figure 10a) reducing the intensity of the IPC and the influence of the spicy waters conveyed by the poleward current. In this situation, the along-shelf distribution of spiciness decreased and the influence of spicy waters was reduced only to the western part of the NIS, the Galician sections off Vigo and A Coruña (Figure 10c). The transition from the decaying phase to the development phase occurred during summer. This season was characterized by northerly and northeasterly winds that force the development of upwelling off Vigo and A Coruña sections. The cold and low salinity waters upwelled (low spiciness values) contrast with the increasing of spiciness in the whole area during this part of the year. These two features, the increasing of the latitudinal density gradient and the development of upwelling processes along the NW of the Iberian Peninsula generate intermediate spiciness values along-shelf, which correspond with a relative decrease of the spiciness in the two Galician sections between the development and the decaying phases of the seasonal cycle.

Interannual variability of the IPC

The main hypothesis to explain the dynamic of poleward flows along eastern ocean boundaries is based on the JEBAR (Join Effect of Baroclinicity and Relief) (Huthnance, 1984) mechanism, which assumes that the main forcing of the current is the interaction between topography and meridional geopotential gradients, primarily of thermal origin. The intensity and direction of this current can be modified by wind patterns (Coelho *et al.*, 1999; Peliz *et al.*, 2002). There is controversy about the relative importance of each forcing factor, which could be partly due to the limited spatial and temporal coverage of the observational (Garcia-Soto *et al.*, 2002; deCastro *et al.*, 2011) and modeling (Peliz *et al.*, 2003) studies dealing with the investigation on drivers of the IPC (or other poleward currents in EBUEs). Besides, there is a lack of long-term time series records from current-meters able to provide direct accounts of the variability of the IPC at an ample range of temporal scales. Relevant knowledge on the dynamics of eastern boundary poleward slope currents have been obtained in recent years using modeling approaches (Coelho *et al.*, 1999; Coelho *et al.*, 2002; Peliz *et al.*, 2003; Ruiz-Villarreal *et al.*, 2006).

Using in situ thermohaline data we have found that the influence of the IPC on the Cantabrian Sea during spring months is correlated with the MTG in the North Atlantic measured in July and August of the year before. This result is coherent with the JEBAR mechanism which assumes that MTG is one of the main forcing factors of the IPC. The seasonal evolution of the MTG is showed in Figure 11. It is worth noting that the maximum cross-correlation between the IPCF (measured in spring) and the MTG is lagged 8

months, thus occurring around the seasonal maximum of the MTG. It is plausible that the variation of the seasonal maximum of the MTG affects the seasonal evolution of the development phase of the IPC (autumn-winter) and the dynamics of the current for the rest of the year.

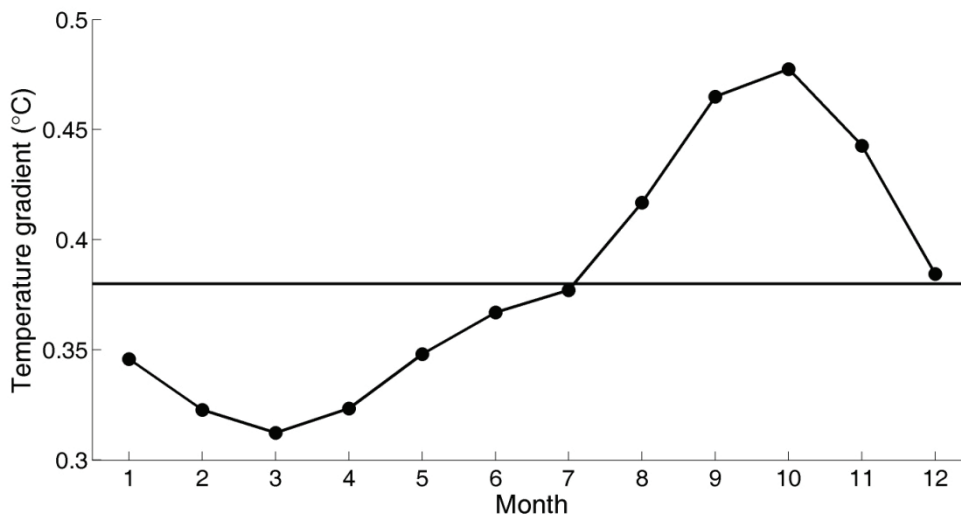


Figure 11: Seasonal cycle of the Meridional Thermal Gradient (MTG, °C·°latitude⁻¹) estimated between 40°N and 50°N along 13° W meridian.

On the other hand, we have also found significant correlations between northerly and easterly winds during winter and the IPC strength (i.e. position of the IPCF during spring). Our results, however, disagreed with those found by other authors who relate the increasing intensity and surfacing of the IPC in winter with the occurrence of southerly-westerly winds (Garcia-Soto *et al.*, 2002; Álvarez-Salgado *et al.*, 2003). Northerly and easterly winds promote, respectively, upwelling along the western and northern parts of the NIS, a relatively uncommon process during winter (see Chapter 5). Hurlburt and Thompson (1973) and Kindle and O'Brien (1974) studied the dynamics of upwelling in eastern boundaries of the oceans using physical models and found that upwelling favorable winds generate a poleward subsurface current. Zarauz *et al.* (2009) obtained similar results. In their model, northerly winds produce initially an equatorward acceleration of the coastal jet, and Ekman transport is supported by the occurrence of upwelling. This coastal jet stops when the latitudinal pressure gradient counteracts the effect of the wind. In this moment, a subsurface poleward current appears and the divergence of the coastal current supports the Ekman transport. The oceanic readjust is produced several months later. All these results support the plausible role of upwelling favorable winds (northerly and easterly along the western and northern parts of the NIS

respectively) during winter on the degree of incursion of the IPC onto the Cantabrian Sea in spring.

Chapter 4: Temporal and spatial variability of river plumes in the NW and N Iberian Shelf (1987-2007)

Introduction

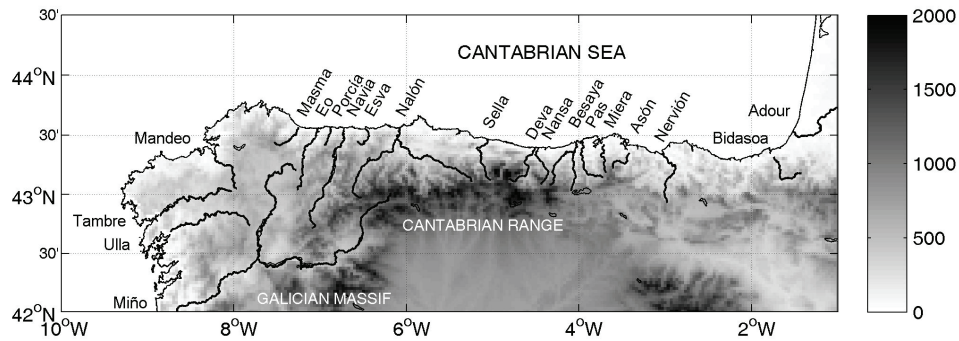


Figure 1: Map with the main orography features of the Northern Iberian Shelf (NIS). The rivers are represented by back lines and the gray scale represents the altitud.

The occurrence of river plumes is a relevant process in the Northern Iberian Shelf (NIS) (Figure 1). As a source of nutrients to the area, continental runoff help to sustain relatively high levels of standing stock phytoplankton biomass and primary production, which promote a cascading effect that affects bottom-up other ecosystem components (Le Fèvre & Frontier, 1988). Besides that, river plumes could be important in the spatial structuring of the life cycle of fish and shellfish species, acting as dispersion or retention zones for their planktonic life stages (Grimes & Kingsford, 1996) that could control the strength of recruitment of these organisms (Grimes & Finucane, 1991). The relative importance of nutrient enrichment associated to continental runoff in the NIS is, however, lower in Galicia than in the Cantabrian Sea due to the relevance of upwelling in the former of these areas (Irigoien *et al.*, 2007; Alvarez *et al.*, 2011).

The spatial and temporal variability of river plumes is tightly linked to atmospheric dynamics at regional and local scales due to the relationship between runoff and precipitation. The seasonal variation of the influence of the Azores high over the NIS and its relationship with the position of the Polar Front generates clear seasonal differences in wind and precipitation regimens. In autumn and winter, the diminished intensity and relatively southward position of the Azores high produces the southward displacement of the storm paths enabling the pass of fronts and depressions. This atmospheric configuration, with the predominance of south-westerly and westerly oceanic wet winds, promotes the occurrence of precipitations, which are reinforced by means of the orographic lift due to the location of mountain ranges running parallel to the coast, especially in the northern part of the Iberian Peninsula. Mountain ranges with a maximum

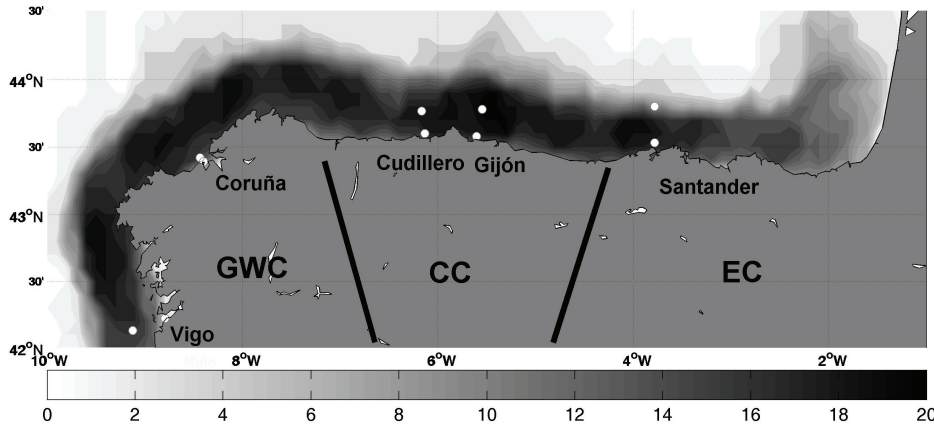


Figure 2: Spatial distribution of the number of spring cruises carried out (gray scale) in the Northern Iberian Shelf (NIS) region during the spring cruises and position of the inner and outer hydrographic stations (white dots) in the across-shelf sections of Vigo (42.22° N 8.79° W, inner and 42.13° N 9.12° W outer station), A Coruña (43.36° N 8.37° W, inner and 43.42° N 8.43° W outer station), Cudillero (43.6° N 6.13° W, inner and 43.76° N 9.17° W outer station), Gijón (43.58° N 6.60° W, inner and 43.77° N 5.55° W outer station) and Santander (43.5° N 3.78° W, inner and 43.71° N 3.78° W outer station) sampled monthly in the frame of the time series monitoring programme RADIALES. The NIS region was divided in three zones attending to the frequency of occurrence of low-density buoyant structures: Galician and West Cantabrian (GWC from 10.0° W to 7.5° W), Central Cantabrian (CC from 7.5° W to 4.0° W) and East Cantabrian (EC from 4.0° W to 1.0° W) zones.

height of 2400 m allow the existence of precipitations in form of snow. These situations favour the presence of plumes all along the NIS. In spring, the precipitation regimen and the snow melting induced by increased temperatures support the relatively high values of probability of plume occurrence. During the summer, the northward displacement of the Azores high and its intensification, induce the northward displacement of the Polar Front, generating relative atmospheric stability that diminishes precipitations to its annual minimum values. The probability of occurrence of river plumes reaches annual minimum values because they are generated by sporadic summer storms.

This general spatial and temporal pattern of occurrence of river plumes is modulated by mesoscale oceanographic processes that take place along the NIS. During autumn and winter, the Iberian Poleward Current (IPC) flows northward along the Iberian shelf transporting relatively warm and salty waters from sub-tropical origin (Peliz *et al.*, 2005). In this period, the increment of precipitations and consequently of river runoffs produces the development of the Western Iberian Buoyant Plume in the NW of the Iberian Peninsula (Peliz *et al.*, 2005; Otero *et al.*, 2008b; Otero *et al.*, 2009b). This marine structure is mainly promoted by the Miño River and reinforced by the Duero fresh waters advected from the south and by the discharges of short rivers of the Rías Baixas and Rías Altas Systems. The relatively high amount of fresh water discharged is, however, confined close to the coast by the IPC and by the predominant south-westerly and southerly winds, thus limiting

coastal-ocean exchange processes (Santos *et al.*, 2004; Otero *et al.*, 2013). In the Cantabrian Sea, the influence of river plumes is reduced and limited to coastal locations due to the relatively low freshwater discharge rates associated with the small drainage basins of the rivers located in this zone. Only in the easternmost part of the Cantabrian Sea a persistent plume associated with the river discharge of the Adour River occur. In spring and summer, the IPC is less intense, which diminish the influence of warm and salty waters in the NIS. The predominant northerly winds during this season generate a persistent upwelling structure in the Galician coast (Wooster *et al.*, 1976). The influence of upwelling is less important in the Cantabrian Sea, and is associated with easterly winds (Wooster *et al.*, 1976; Botas *et al.*, 1990). During this seasons, the precipitations are reduced and the presence of intense plumes are associated with storm events (Serrano *et al.*, 1999).

Table 1: Characteristics (acronym, vessel and dates) of the surveys carried out in spring in the North Iberian Shelf (NIS) area used in the present study.

Survey	Vessel	Start	End
SARPAREA87	Lura	13/04/87	24/04/87
MPHSARACUS88	Cornide de Saavedra	01/04/88	04/05/88
MPH90	Investigador	18/04/90	09/05/90
ECOSARP91	Cornide de Saavedra	17/04/91	09/05/91
ICTIONORTE92	Investigador	22/04/92	09/05/92
PELACUS93	Cornide de Saavedra	14/04/93	03/05/93
SEFOS94	Cornide de Saavedra	15/03/94	13/04/94
MPH95	Cornide de Saavedra	26/03/95	14/04/95
SEFOS96	Cornide de Saavedra	11/03/96	31/03/96
PELACUS97	Thalassa	08/03/97	31/03/97
PELACUS98	Thalassa	17/03/98	08/04/98
PELACUS99	Thalassa	03/03/99	29/03/99
PELACUS00	Thalassa	27/03/00	12/04/00
PELACUS01	Thalassa	30/03/01	22/04/01
PELACUS02	Thalassa	09/03/02	04/04/02
PELACUS03	Thalassa	19/03/03	12/04/03
PELACUS04	Thalassa	30/03/04	22/04/04
PELACUS05	Thalassa	05/04/05	29/04/05
PELACUS06	Thalassa	01/04/06	28/04/06
PELACUS07	Thalassa	27/03/07	23/04/07

The bibliography on plume detection methods is very prolific. The applied methods can be divided in three types depending on the source of the data used for the characterisation of river plumes: field data, (Ostrander *et al.*, 2008; Piola *et al.*, 2008), model outputs (Otero

et al., 2008a; Ferrer *et al.*, 2009; Gan *et al.*, 2009; Lazure *et al.*, 2009; Ou *et al.*, 2009; Hickey *et al.*, 2010; Schiller & Kourafalou, 2010; Woillez *et al.*, 2010; Pimenta *et al.*, 2011) and optical methods (Banas *et al.*, 2009; Jiang *et al.*, 2009; Teodoro *et al.*, 2009; Chassot *et al.*, 2011). In contrast, the studies that have performed a quantitative analysis of river plumes into the NIS are reduced and limited to local and intermediate spatial and temporal scales (Otero *et al.*, 2008b; Ferrer *et al.*, 2009; Otero *et al.*, 2009b; Teodoro *et al.*, 2009; Otero *et al.*, 2013)

A quantitative approximation to study the interactions between river plumes and the distribution, composition and dynamics of the different ecosystem components of the pelagic is necessary in order to improve ecosystem assessment and management. Accordingly, the objectives of this work are: 1) to develop methods to characterize river plumes (i.e. occurrence, extension, mean depth...); 2) to analyze the spatial and temporal patterns of river plumes in the NIS area; and 3) to investigate the observed characteristics of river plumes with the main forcing factors that influence its development (i.e. rainfall and river discharge).

Materials and methods

Salinity Data

Salinity data used to characterize river plumes in the North Iberian Shelf (NIS) (i.e. Galicia and the Cantabrian Sea) were obtained from CTD (conductivity-temperature-depth) casts performed during a set of oceanographic cruises and a time series monitoring program conducted in the studied area (Table 1 and Figure 2). The oceanographic cruises were carried out between 1987 and 2007 (except for 1989) around March-April (Table 1). The grid of oceanographic stations in these cruises extended from the coast (ca. 30 m depth isobath) to the slope (≥ 200 m) along the NIS. The number of cruises carried out in the area is represented in Figure 1.

Monthly time series of salinity were obtained from five sections sampled by the Instituto Español de Oceanografía (IEO) along the NIS within the frame of the long-term time-series monitoring program 'Radiales' (<http://www.seriestemporales-ieo.com>). Four of them, those located off Vigo (Vi: 42.2 ° N, 8.2 ° W), A Coruña (Co: 43.4 ° N, 8.4 ° W), Cudillero (Cu: 43.6 ° N, 6.1 ° W), and Santander (St: 43.5 ° N, 3.8 ° W), have been visited at least since 1994, while the section off Gijón (43.6 ° N, 5.6 ° W) started in 2001.

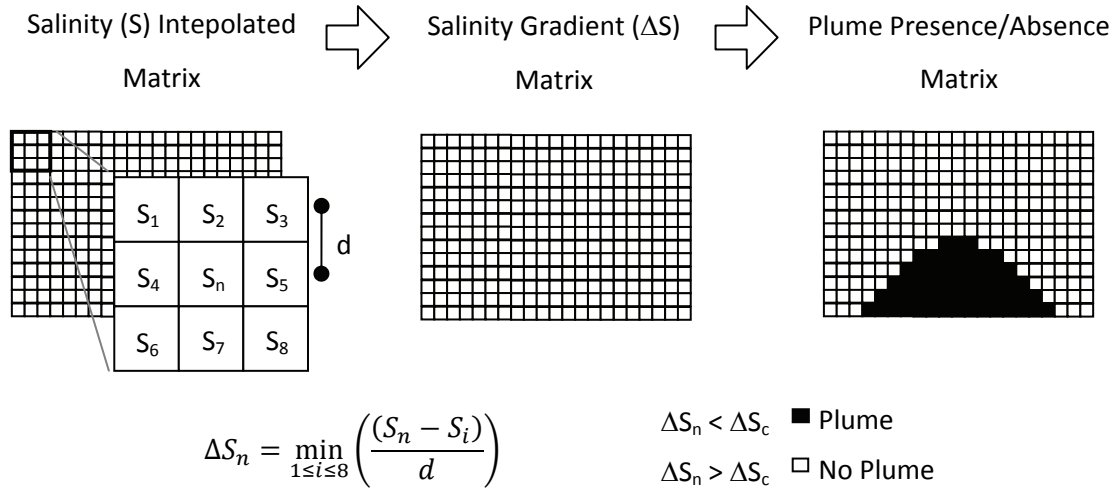


Figure 3: Scheme of the plume detection method. For each element of the salinity interpolated matrix (S_n) was calculated the salinity gradient (ΔS) using the equation 2 and obtaining the salinity gradient matrix. This matrix is transformed in the plume presence/absence matrix using the salinity gradient criterion ($\Delta S_c = -0,008$). The values of $\Delta S < \Delta S_c$ was considered as plume presence and $\Delta S > \Delta S_c$ as plume absence.

The CTD profiles were done with different CTD SeaBird instruments calibrated using the standard protocols established by the manufacturer. These profiles extended from the surface (around 2 m depth) down to 5 m above the bottom in those casts conducted over the shelf. The database of CTD profiles was subject to a quality control, which included the removal of spurious data by visual inspection and low-pass filtering with a moving-median filter. Pressure reversals were also excluded. From the purged hydrographic data, salinity was calculated (UNESCO, 1983) and averaged in pressure intervals of 1 m depth. Some CTD casts of different cruises (1995, 1996, 1997 and 1998 Table 1) were sampled at a lower acquisition rate and thus were averaged at depth intervals of 2 m depth. These casts were interpolated to 1 m depth intervals by a local linear interpolation.

Method of plume detection and characterisation

The spatial characterization of river plumes was based on the salinity fields obtained by interpolation of the salinity profiles of each cruise on a regular grid of $0.05^\circ \times 0.05^\circ$ in the horizontal for each 1 m depth of the water column. Data were interpolated using an objective interpolation method (Haagenson, 1982) based on an isotropic correlogram Gaussian model (equation 1):

$$\gamma(R) = \frac{V_s}{V_s + V_n} \cdot e^{\frac{-R^2}{2 \cdot L^2}} \quad (1)$$

where, $\gamma(R)$ is the correlation for a distance R (in decimal degrees), V_s is the signal variance, V_n is the noise variance, and L is the characteristic length-scale. The empirical

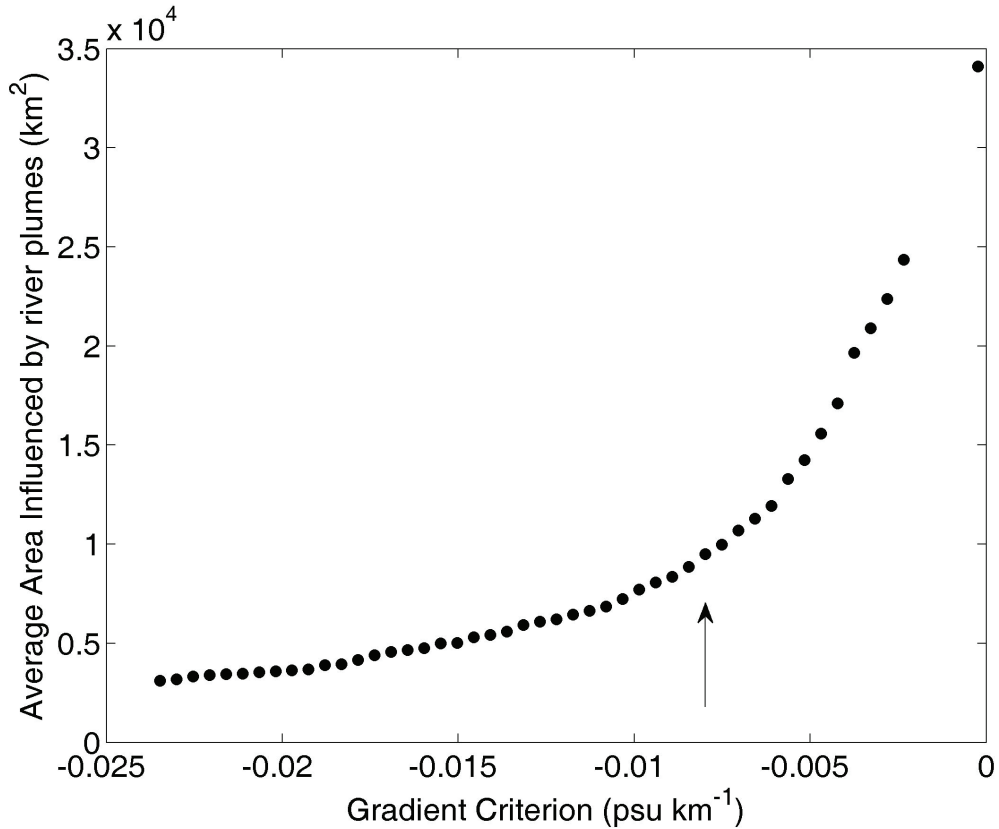


Figure 4: Relationship between the salinity gradient criterion (psu km⁻¹) and the averaged area at 10 m of the low-density buoyant structure calculated using all the spring cruises. The value at the inflexion point of this empirical relation was - 0.008 psu km⁻¹.

salinity correlograms, that are functions that represents the relationship between the spatial autocorrelation and distance (Legendre & Legendre, 1998), were calculated for each spring cruise at different depths and fitted to the equation 1 obtaining the values of V_s , V_n and L for each case. The averaged values of the previous analysis were used for the salinity interpolation ($V_s = 0.6$, $V_n = 0.4$ and $L = 0.6^\circ$).

The contrasting salinity between those locations of the spatial domain influenced by continental runoff or river discharges and proper seawater generates a traceable salinity gradient (Δs). The value of Δs is negative for those locations influenced by a river plume (i.e. values of salinity within the plume are lower than those in the surrounding waters outside the plume). The salinity gradient matrix was calculated following the equation 2:

$$\Delta S_n = \min_{1 \leq i \leq 8} \left(\frac{(S_n - S_i)}{d} \right) \quad (2)$$

where n is the index of the salinity interpolated matrix, s_n is the salinity at location n , s_i the salinity of the 8 contiguous locations around the position n , and d the distance between them (Figure 3).

One location of the salinity gradient matrix was considered under the influence of continental runoff or river discharges when the Δs_n was lower than a critical salinity gradient value (termed salinity gradient criterion) Δs_c .

This approximation, however, cannot detect salinity contrast among locations within the plume, which are characterised by reduced gradients but with low salinity values. In order to overcome this constraint of the method we calculated the median of the salinity values for those locations where $\Delta s < \Delta s_c$. Those positions located less than 150 km from these positive cases and with lower values than the median were considered as influenced by river / runoff plumes too.

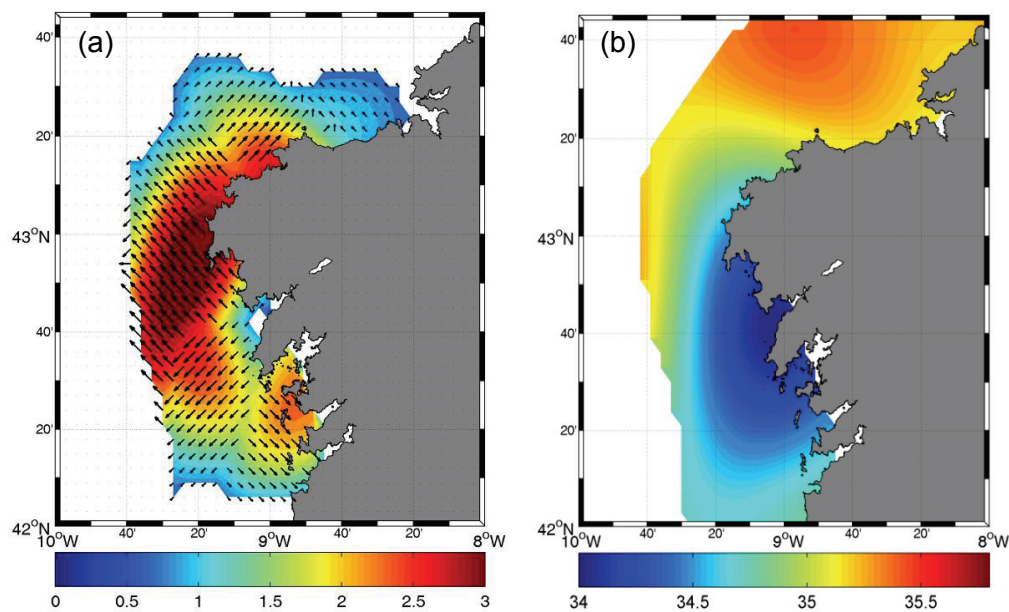


Figure 5: Example of (a) the intensity ($-\Delta s$, colour scale and lengths of the arrows) and direction (orientation of the arrows) of the salinity gradient in the Galician shelf during the cruise carried out in spring 2003 and (b) corresponding salinity field. Only those locations with values of the salinity gradient (Δs) lower than the salinity gradient criterion ($\Delta s_c = -0.008$) are represented in (a).

We chose a gradient criterion of $-0.008 \text{ psu km}^{-1}$. This election was a compromise between detect river plumes properly and consider locations not influenced by freshwaters as positive cases. The area influenced by river plumes was calculated using different values of Δs_c . In figure 4 are showed the averaged (among spring cruises) area influenced by river plumes in relationship with Δs_c values. The election of higher values of Δs_c implies the relaxation of the criterion and thus the determination of areas as plumes not influenced by freshwater inputs, whereas with lower values of this parameter, the low intensity river plumes would not be detected.

The plume detection algorithm was applied to the salinity field at every 1-m depth layer for each of the cruises. We estimated the maximum depth of the plume (z_p) in each location as the deeper water layer influenced by the plume. The algorithm of plume detection estimates also the direction and the intensity of the gradients (Figure 5). These descriptors can be useful to elaborate more exhaustive characterization of the plumes and to determine its origin and direction as a function of the orientation of the gradient. By integrating the results for the whole water column it is possible to reconstruct the 3-D structure of the plume.

Table 2.: Characteristics of the main rivers in the North Iberian Shelf (NIS) area (i.e. Galicia and Cantabrian Sea).

River	Zone	Mouth Latitude	Mouth Longitude	Length (km)	Catchment Area (km ²)
Miño	GWC	41,86	-8,87	308	17667
Ulla	GWC	42,50	-8,98	132	2761
Tambre	GWC	42,72	-9,05	134	1531
Mandeo	GWC	43,42	-8,32	56	370
Masma	GWC	43,57	-7,24	46	290
EO	CC	43,55	-7,04	92	819
Porcía	CC	43,56	-6,88	17	143
Navia	CC	43,56	-6,73	99	300
Esva	CC	43,55	-6,47	35	450
Nalón	CC	43,57	-6,08	153	3692
Sella	CC	43,47	-5,07	56	1195
Deva	CC	43,39	-4,51	64	1195
Nansa	CC	43,39	-4,47	46	418
Besaya	CC	43,44	-4,03	58	465
Pas	CC	43,44	-3,98	57	649
Miera	CC	43,44	-3,77	41	295
Asón	CC	43,40	-3,47	39	551
Nervión	EC	43,35	-3,04	72	1900
Bidasoa	EC	43,38	-1,79	69	710
Adour	EC	43,53	-1,52	335	16880

This approach was adapted for its application to the time series of salinity in the across-shelf sections distributed along the NIS area (off Vigo, A Coruña, Cudillero, Gijón and Santander). We estimated the across-shelf salinity gradient using the salinity measured at the coastal (s_n) and oceanic (s_o) ends of each section which are distant d nautical miles apart (equation 2). Then, we applied the salinity gradient criterion ($\Delta s_c = -0.008 \text{ psu}\cdot\text{km}^{-1}$) derived from the analysis of the salinity gradient field in the cruises carried out in the NIS in spring in order to estimate the probability of occurrence of river plumes at these locations.

Analysis of forcing factors

The NIS was divided in three zones: Galicia and West Cantabrian Sea (GWC), Central Cantabrian Sea (CC) and East Cantabrian Sea (EC) (Figure 1). For each of these zones we have calculated the time series of a set of river plume descriptors: area covered by the plume at a given depth of the water column (A_{Pz} , km²), averaged or maximum depth of the plume (z_P or z_{maxP} m), and its volume (area covered at 5 m depth multiplied by the averaged depth; $V_P = A_{P5} \times z_P$, km³).

We used the precipitation rate (kg·m⁻²·s⁻¹) and river runoff (hm³ month⁻¹) as the main forcing factors that explain the characteristics of river plumes in the winter-spring transition. The precipitation rate was obtained from the NOAA Earth System Research Laboratory (<http://www.esrl.noaa.gov>) and the NCEP/NCAR Reanalysis 1, Surface Flux daily database. The temporal coverage goes for 1948/01/01 to present and de spatial grid a T62 Gaussian with 192x94 points (88.542N-88.542S, 0E -358.125 E)

We calculated the daily average of precipitation rate for the areas delimited between: 42.5° and 44.5° N and 9° and 5° W for the GWC zone; 42.5° and 44.5° N and 7.5° and 3.5° W for the CC zone; and 42.5° and 44.5° N and 2° W and 2° E for the EC zone (Figure 1). The monthly time series of river runoff (hm³ month⁻¹) were obtained from the Confederación Hidrográfica del Norte (<http://www.chn.es>) and Eaufrance (<http://www.eaufrance.fr>). We used the main rivers discharging in each of the zones: Miño river (GWC zone, Frieira gauge station, 42.1° N, 8.2° W, 15153 Km² of basin area), Nalón river (CC zone, Rioseco gauge station 43.1° N 5.9° W, 147 Km² of basin area) and Adour river (EC zone, San Vincent Paul gauge station, 43.7° N, 1.0° W, 7830 Km² of basin area) (Figure 1, Table 2).

Prior to the application of cross-correlation analysis between river plume descriptors and the forcing factors, each time series was modelled following a univariate additive decomposition model (Equation 3):

$$y_t = \bar{y} + LT[y_t] + SC[y_t] + R[y_t] + \varepsilon[y_t] \quad (3)$$

where, subscripts t is the index for time, \bar{y} is the climatological average of the time series, LT and SC represent the long-term and periodic components respectively, R the autocorrelation and ε represents the pre-whitened residuals, a time series of independent, identical and normally distributed random shocks (or white noise). LT and SC were treated as deterministic components (Chatfield, 1996). The LT component was estimated using least-square regression. The periodic component (SC) was fitted using a sum of periodic functions (harmonics) that follow the model (Equation 3),

$$SC[y_t] = \sum_{i=1}^n A_{T_i} \cos\left(\frac{2\pi}{T_i} t + \theta_{T_i}\right) \quad (4)$$

where, A_i is the amplitude T_i the period and θ_i the phase in radians of the i -th harmonic. The parameters were extracted by Fourier analysis (Poularikas & Seely, 1991). The significance of each harmonic was determined using G-statistic (Davis, 1986). The autocorrelation was modelled by means of an autoregressive process which parameters were estimated using the Yule-Walker equations (Wei, 1989).

Using the time series of the pre-whitened residuals of the analyzed time series ($\varepsilon[y_t]$), we calculated the cross-correlation between the spring time series of plume descriptors (area covered at a given depth, average depth, and volume: A_{Pz} , Z_P and V_P respectively) and the time series of the forcing factors (daily precipitation rate and monthly river runoff). The time series of the forcing factors were lagged relative to the spring series of river plume descriptors, and for each lag (k) the parameters of the linear regression (i.e. p-value, correlation coefficient, slope and intercept of the fitted line) were calculated.

Results

Time series of precipitation rate and river runoff

The results of the time series analysis of the monthly values of precipitation rate and river runoff for the studied period (1987-2007) were showed in the table 3. The time series of precipitation rate have similar climatological averages in the three zones of the NIS area ($2.1 \cdot 10^{-5}$, $2.6 \cdot 10^{-5}$ and $2.5 \cdot 10^{-5}$ kg m² s⁻¹ for GWC, CC and EC respectively). Significant decreasing trends were found in the Cantabrian Sea, both in CC and EC ($p < 0.05$), explaining 2 % and 3 % of the total variance respectively. In the three zones, the first harmonic of the annual period ($T = 12$ months) is the unique significant component of the seasonal cycle. However, while in the GWC and CC zones the maximum value of the harmonic occurs in winter ($T_{\max} = 1.1$, January and $T_{\max} = 1.7$, February respectively) explaining 25 and 14% of the variance, in the EC zone it takes place in spring ($T_{\max} = 5.5$, May) and explains 23% of the variance. The autocorrelation with lag of 1 month (i.e. serial dependence between contiguous observations) was significant in the three locations, although the amount of variance explained by this component is marginally significant in all cases ($p \sim 0.05$).

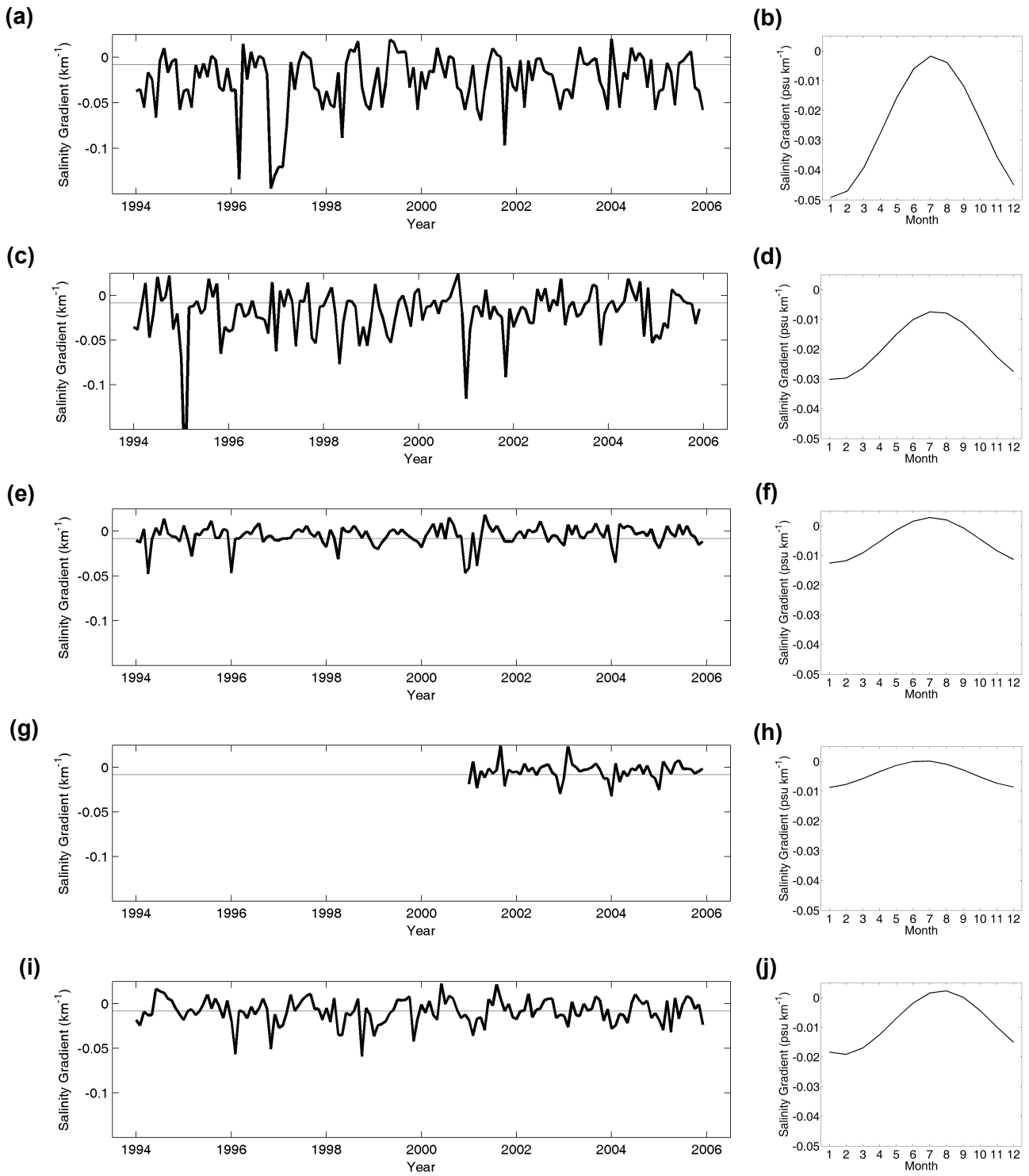


Figure 6: Time series and seasonal cycle (as the first harmonic of the annual period, $T = 12$ months) of the salinity gradient in the cross-shelf sections of (a-b) Vigo, (c-d) A Coruña, (e-f) Cudillero, (g-h) Gijón and (i-j) Santander.

Table 3. Results of the univariate additive decomposition model applied to the monthly time series of precipitation rate ($\text{Kg m}^{-2} \text{s}^{-1}$) and river runoff ($\text{Hm}^3 \text{ month}^{-1}$) in the different zones (GWC, CC and EC) of the NIS region. *b*, *a* and EV_{LT} are respectively the slope (year^{-1}), ordinate at the origin and explained variance of the linear trend (LT) component; *T*, *A*, *F*, T_{max} and EV_{SC} are respectively the period, amplitude, phase in radians, phase as the month when the maximum of the cycle takes place and the explained variance of the seasonal component (only first harmonic); ϕ_1 and EV_{AR} are respectively the coefficient of the autoregressive parameter at lag $k = 1$ month (dimensionless) and the amount of variance explained by the autoregressive component (AR).

Variable	Zone	Period	Mean	Linear trend (LT)			Seasonal cycle (SC)				Autoregressive (AR)		
				<i>b</i>	<i>a</i>	% EV_{LT}	<i>T</i>	<i>A</i>	<i>F</i>	T_{max}	% EV_{SC}	ϕ_1	% EV_{AR}
Precipitation rate	GWC	1950-2007	$2.1 \cdot 10^{-5}$	-	-	-	12	$1.8 \cdot 10^{-5}$	5.7	1.1	25	0.14	2
	CC	1950-2007	$2.6 \cdot 10^{-5}$	$-1.18 \cdot 10^{-7}$	$2.3 \cdot 10^{-4}$	2	12	$7.4 \cdot 10^{-6}$	5.4	1.7	14	0.19	3
	EC	1950-2007	$2.5 \cdot 10^{-5}$	$-1.41 \cdot 10^{-7}$	$2.8 \cdot 10^{-4}$	3	12	$6.0 \cdot 10^{-6}$	3.4	5.5	23	0.23	4
River runoffs	Miño	1971-2005	710	-	-	-	12	485	5.3	1.7	28	0.62	28
	Nalon	1971-2005	32	-0.37	751	2	12	20	5.1	2.2	27	0.29	6
	Adour	1986-2007	213	-2.88	5789	2	12	140	5.1	2.3	31	0.40	11

Table 4. Parameters of the first harmonic of the annual period ($T = 12$ months) extracted from the time series of the salinity gradient (psu km^{-1}) in the across-shelf sections distributed along the NIS area. A, amplitude (psu-nm^{-1}); F, phase (radians), Tmin month in which the minimum of the harmonic take place (month), Tmax, month in which the maximum of the harmonic take place (month); %EV, percentage of the variance of the time series explained by the first harmonic of the annual period. Significant harmonic (pvalue > 0.05) are marked by asterisk (*).

Section	Mean	Periodic Trends				
		A	F	Tmin	Tmax	%EV
Vigo	-0.025	0.023	2.53	1.241	7.165	30.5*
Coruña	-0.018	0.011	2.29	1.362	7.627	8.1*
Cudillero	-0.005	0.008	2.64	1.105	6.955	23.7*
Gijón	-0.004	0.005	2.81	0.620	6.620	10.0
Santander	-0.008	0.010	2.34	1.744	7.533	29.2*

The monthly time series of river runoff from the main rivers that discharge in the NIS area, Miño (GWC), Nalón (CC) and Adour (EC), exhibit some contrasting patterns regard to those found for the precipitation rate. A decreasing linear trend was detected in the CC y EC zones, which is coherent with the decreasing trend in precipitation rate estimated in these zones. The first harmonic of the annual period ($T = 12$) was significant for the three rivers, and the amount of variance explaining was 28, 27 and 31% for Miño, Nalón and Adour respectively, but the maximum seasonal values of runoff occur in January and February in the three rivers. The autocorrelation values at one-month lag were also higher than those for the precipitation rate values. These higher autocorrelation values reflect the higher inertia of runoff regard to precipitation rate due to the continuous, cumulative process of river discharge.

Salinity gradient in the across-shelf sections

The time series of the salinity gradient estimated for each of the five across-shelf sections distributed along the NIS area are showed in figure 6. The mean value of the gradient was higher in the Galician ($-0.025 \text{ psu km}^{-1}$ and $-0.018 \text{ psu km}^{-1}$ for Vigo and A Coruña respectively) than in the Cantabrian sections ($-0.005 \text{ psu km}^{-1}$, $-0.004 \text{ psu km}^{-1}$ and $-0.008 \text{ psu km}^{-1}$ for Cudillero, Gijón and Santander respectively) (Table 4). The first harmonic of the seasonal cycle ($T = 12$ months) was the only statistically significant component of temporal variation for the sections off Vigo, Cudillero and Santander, explaining 30.5 % 23.7 % and 29.2 % of the total variance respectively. In A Coruña and Gijón, the first harmonic explains only 8.1 % and 10.0 % of the total variance of the time series and was not statistically significant according to the G-statistics. In all the cases, the minimum value of the seasonal cycle occurred in winter, between January and February. The time

series of the salinity gradient, did not present statistically significant linear trends, neither autocorrelation between contiguous observations in any of the sections.

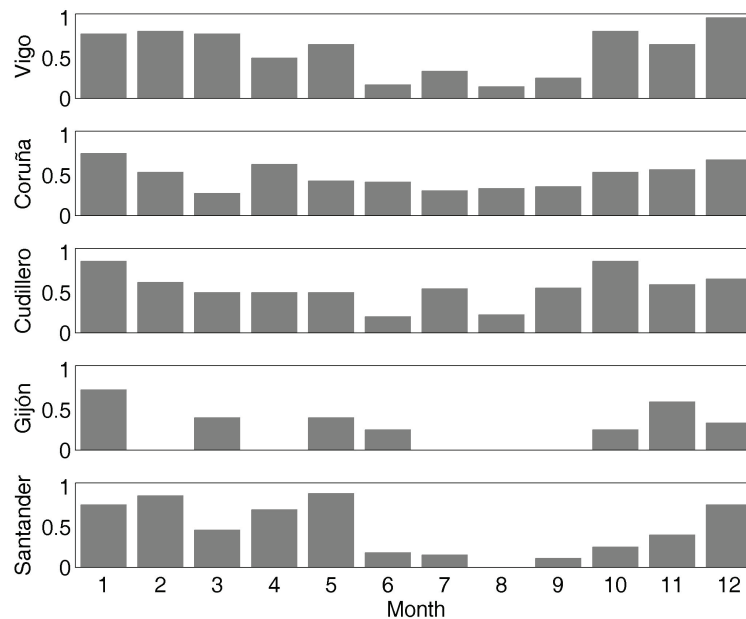


Figure 7: Seasonal cycle of the probability of the occurrence of low-density buoyant structures derived from the analysis of the salinity gradient in the across-shelf sections distributed along the NIS area.

The application of the salinity gradient criterion ($\Delta s_c = -0.008 \text{ psu km}^{-1}$, Figure 3) to the time series of the salinity gradient in the across-shelf sections allowed us to estimate the probability of occurrence of river plumes for the different locations along the NIS area. The averaged probability of occurrence of river plumes (i.e. percentage of observations of the salinity gradient below the gradient criterion) was around 50% for all the sections (Vigo; 54%; A Coruña, 50%; Cudillero 55% and Santander 44% Cudillero 55%) except in the case of Gijón, which presented a significant lower value (25%) probably due to reduced length of the time series. The probability of occurrence of river plumes exhibited marked seasonality (Figure 7). Its values are higher in autumn and winter (70-100%) than in summer (0-40%). During the spring and autumn, all sections except Cudillero showed intermediate to high probability of occurrence of plumes (50-90%). This seasonal pattern agreed, in general terms, with the seasonality of precipitations (Figure 8). The maximum values occurred in autumn and winter and the minimum during summer in the GWC and CC zones. The spring precipitations become more important towards the eastern part of the Cantabrian Sea (EC zone) and the probability of occurrence of river plumes in the Santander section showed a similar pattern, with relatively high occurrence of plumes extending up to late spring (May; Figure 7).

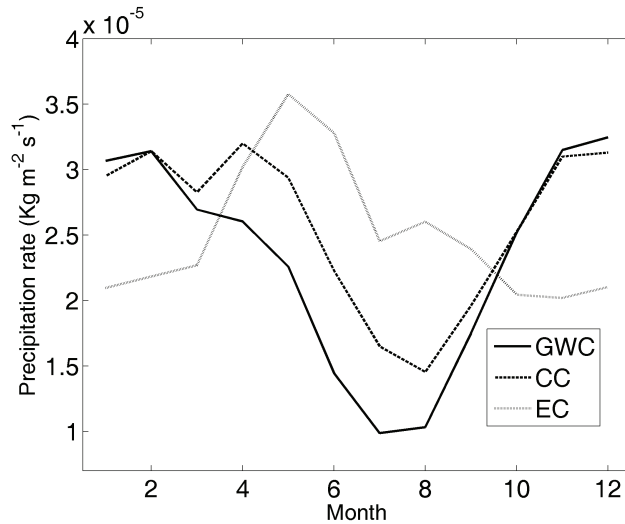


Figure 8: Seasonal cycles of monthly precipitation rate in the three zones within the NIS area: Galician and West Cantabrian (GWC), Central Cantabrian (CC) and East Cantabrian (EC) zones. See text for the position of the boxes used to average the precipitation rate for each zone.

The seasonality of runoff of those rivers located close to each section (Miño, Mandeo, Nalón and Besaya rivers for Vigo, Coruña, Cudillero-Gijón and Santander across-shelf sections respectively; Figure 2 and 9), were similar to the seasonality of the probability of occurrence of plumes. Maximum values of runoff occurred in autumn and winter, while the opposite situation was measured in summer, when the minimum values of the year were detected. We can divide the rivers in two groups attending to the characteristics of the runoff seasonal cycle. In spring, the rivers flowing into the Cantabrian shelf presented higher discharges than the Galician rivers. These differences between the two types of runoff patterns were, however, not reflected in the seasonality of the probability of occurrence of river plumes derived from the analysis of the salinity gradient in the across-shelf sections.

Table 5. Mean and standard error of the time series of the descriptors of the low-density buoyant structures in the different zones (GWC, CC and EC) of the NIS region in spring. A_{P5} and A_{P10} , area occupied by the buoyant structure (Km^2); z_P , mean depth of the structure (m); V_P , volume of the structure (Km^3)

Zone	$A_{P5} (\text{Km}^2)$	$A_{P10} (\text{Km}^2)$	z_P	$V_P (\text{Km}^3)$
GWC	$4.22 \cdot 10^3 \pm 1.20 \cdot 10^3$	$3.42 \cdot 10^3 \pm 1.16 \cdot 10^3$	8.37 ± 1.86	73 ± 26
CC	$4.47 \cdot 10^3 \pm 0.91 \cdot 10^3$	$2.10 \cdot 10^3 \pm 0.73 \cdot 10^3$	8.36 ± 1.60	60 ± 18
EC	$6.08 \cdot 10^3 \pm 0.83 \cdot 10^3$	$5.25 \cdot 10^3 \pm 0.84 \cdot 10^3$	17.2 ± 1.74	120 ± 20

Interannual variability of river plumes in the winter-spring transition

The distribution of river plumes in the North Iberian Shelf in spring between 1987 and 2007, estimated from the salinity field measured at 10 m depth (A_{P10}), is shown in figure 10. The interannual variability of the occurrence of river plumes in this part of the year is noticeable, both in terms of their spatial distribution and intensity (which can be inferred from the area occupied by the plume and its mean depth). For instance, in the spring of 1992 and 1996 river plumes were not detected in the whole NIS, while in 2001 freshwater influenced all the studied area. Between these two extreme situations, there were years where the occurrence of river plumes was detected only in the Galician shelf (e.g. 1987), in the easternmost part of the Cantabrian Sea (e.g. 1995) or in some locations in the three zones of the NIS (e.g. 1999). Although the spatial variability of the presence of river plumes is high, we can find groups of years with similar spatial distribution: such as 1997, 2003 and 2006, when river plumes were detected in Galicia and in the East Cantabrian Sea; 1993 and 2000, when small and well-defined plumes were detected all over the area; and 1994, 1995 and 2004, when the plumes were only detected in the inner part of the Bay of Biscay.

The probability of the presence of river plumes at a given depth in spring in the NIS can be derived from the analysis of the combination of the set of cruises (Figure 11). Considering three river plume descriptors, the area occupied by river plumes at 5 and 10 m and their maximum depth (A_{P5} , A_{P10} and Z_{maxP}), we can define three zones in the NIS. In Galicia, off the Rías Baixas and in the surroundings of Cape Finisterre, the probability of occurrence of plumes is high (> 75 %), with a maximum depth ranging between 25 and 30 m. The probability of river plume occurrence was lower (<40 %) in the Western and Central Cantabrian shelf, with increased probability in the proximity of the Nalón and Pas-Besaya river mouths (60 %).

In these zones, the plumes were significantly shallower than in the westernmost part of the studied area, with maximum depths that did not exceed 10 m and which were on average of about 5 m. The highest probability of river plume occurrence was found in the Eastern Cantabrian Sea (90 %). This zone was characterized by persistent and relatively deep plumes (mean depth about 30 m). Although plume depths in Galicia and Eastern Cantabrian zones were similar, the area affected by river plumes is smaller in the former than in the latter of these zones.

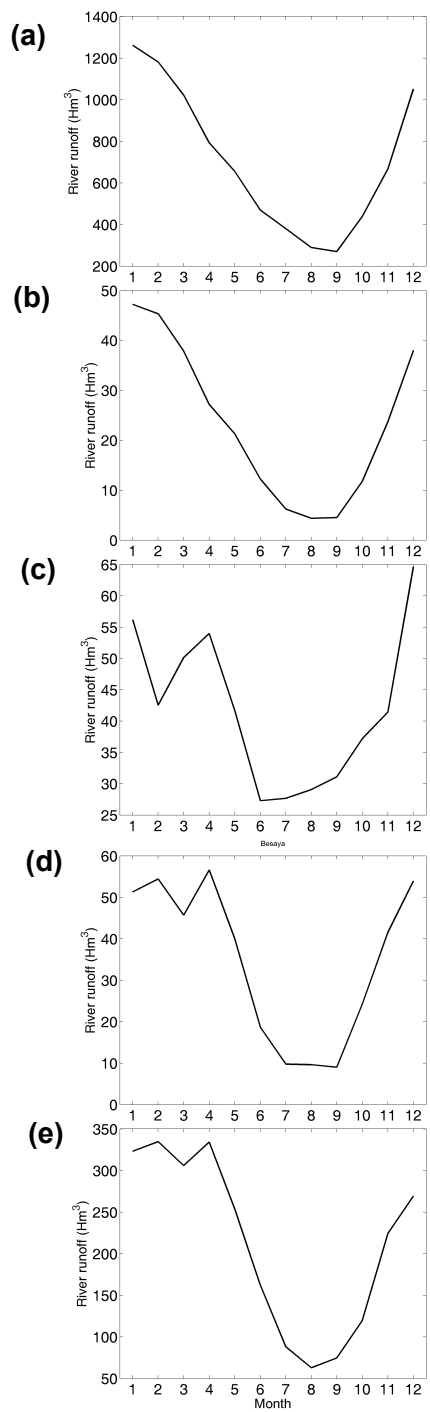


Figure 9: Seasonal cycles of monthly river runoff (Hm³) for those rivers which outflow closest to the hydrographic across-shelf sections sampled within the frame of the time series monitoring programme RADIALES: (a) Miño (for the section off Vigo), (b) Mandeo (A Coruña), (c) Nalón (Cudillero and Gijón); (d) Besaya (Santander) and (e) Adour (Santander). Note the different scales of river runoff.

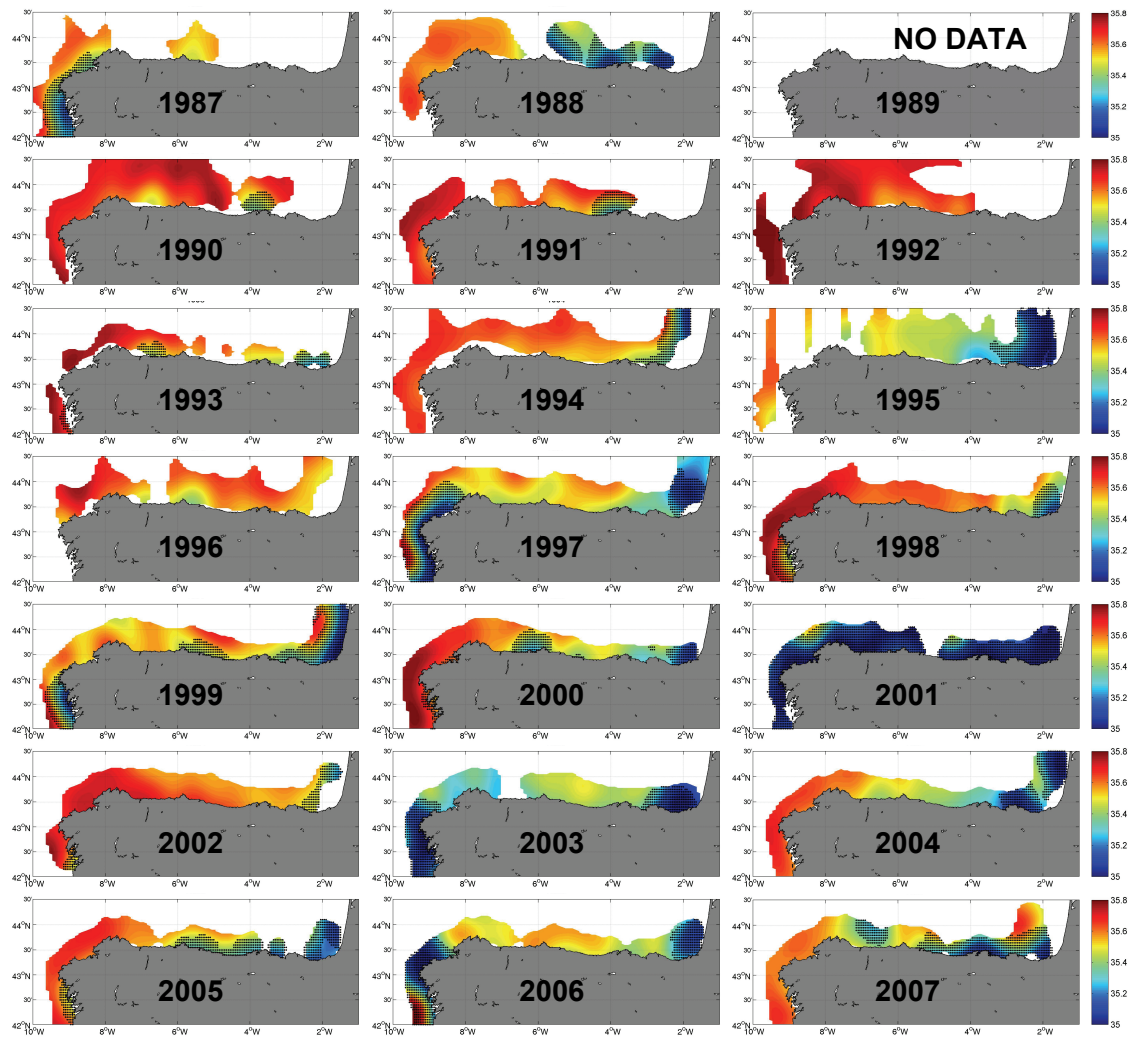


Figure 10: Interannual variability of the area occupied by low-density buoyant structures at 10 m depth (A_{P10}) in spring. The locations influenced by the river plume are represented by black dots.

Time series of plume descriptors were generated for each of these zones (GWC, CC and EC respectively) (Figure 12). The time series analysis applied to these series did not show any significant component of temporal variation (Table 5). Nevertheless, in the GWC zone we found two marked periods, between 1988 and 1995, characterized by a diminished occurrence of river plumes in spring, and between 1996 and 2006, characterized by the occurrence of river plumes in the spring of all years (except in 2004), with values of the area affected by river plumes ranging between 5000 and 15000 km², with an averaged depth around 15 m, reaching 30 m in 2001.

In the CC zone, river plumes have lower extension and depth, with average plume depth values that did not reach 10 m, except in 2001 where the averaged depth was of 30 m. The EC zone was characterized by the presence of plumes in all the cruises except 1987 and 1992 (this zone were not sampled during these cruises). The area influenced varies

from 1000 Km² in 2002 to approximately 13000 km² in 1995 and 1999. The averaged plume depth was higher than in the rest of the zones, with a mean value of 17 m. In contrast with other zones, 2001 was not a special year in terms of the area influenced by plumes although it was the year with the higher values of averaged plume depth (30 m). Whole period from 1987 to 2007 was characterised by a persistently moderate area ($A_{P5} = 7000 \text{ km}^2$) covered by relatively deep ($z_P = 20 \text{ m}$) plumes.

The determination coefficients (r^2) of the lagged cross-correlations between river plume descriptors and forcing factors are given in Table 6. The time series of the plume descriptors in the GWC zone were correlated with the precipitation rate of the month previous to the cruise (lag of 1 month; March) and with the precipitations occurred in the previous autumn (lags 4 and 5 months; December and November respectively). The results of the cross-correlation analysis calculated using discharges from river Miño were similar to that obtained with precipitation rates: significant correlations were observed at lags 1 and 4. In the CC zone, the relationship between the area influenced by river plumes at 5 m depth (A_{P5}) and the precipitation rate was not statistically significant at any lag. The other river plume descriptors considered (A_{P10} and z_P), however, were correlated with the precipitation rate in the month previous to the cruise (lag = 1 month). The correlation analysis of the discharges of the Nalón river reflect a relationship with the river plume area at 5 m depth, the mean depth and volume of the plume at a 2-months lag (i.e. February). The correlation patterns were different in the EC zone. Precipitation rate in this area was correlated with river plume descriptors with a 3-months lag (i.e. January) for A_{P5} and A_{P10} and with a 6-months lag (October) for z_P and volume of the plume. On the other hand, the influence of river runoff on river plume descriptors was detected with a 1-month lag. In the case of the plume area at 10 m depth (A_{P10}) the correlation was also significant at lag of 3 months (i.e. January).

Discussion

The method proposed here for the detection of zones of the shelf affected by continental waters is based on the calculation of the salinity gradient from in situ salinity data interpolated through a given spatial domain. The rationale of the method is that a traceable salinity gradient is established on the shelf due to the interaction between continental and ocean waters. Since the method is based on the gradient instead on absolute values of salinity, it is appropriate to define the locations influenced by continental inputs independently of the intensity of those inputs, the thermohaline characteristics of the marine end-member and the intensity of mixing and current circulation patterns. These factors vary at different temporal and spatial scales depending on the domain under study. Besides, from the application of the method it is possible to

obtain a series of descriptors related to the topology of the plume, such as the area affected at different depths (A_{Pz} , km^2), total volume (V_P , km^3), average or maximum depth (z_P and $z_{\text{max}P}$, m) and intensity of the gradient (ΔS_P). These descriptors are useful to compare plumes among them or with those simulated by numerical models (Otero & Ruiz-Villarreal, 2008; Otero *et al.*, 2009b), to account for their temporal and spatial variation and to analyse the relationships of plume occurrence and topology with forcing factors such as river runoff or precipitation. Besides, the application of the method to estimate the areas influenced by plumes, in combination with other methods to estimate the area affected by other physical processes such as coastal upwelling (González-Nuevo & Nogueira, 2014c) or the intrusion of the Iberian Poleward Current (IPC) along the NIS (González-Nuevo & Nogueira, 2005; González-Nuevo & Nogueira, 2014a), can be used to define different pelagic habitats which modulates the species distribution of different ecosystem components, such as mesozooplankton (Cabal *et al.*, 2008) and ichthyoplankton (Rodríguez *et al.*, 2009) in the NIS.

This kind of information is very relevant to model marine species. Nowadays the approximations to model habitats and dynamic of the different ecological components of the ocean are carried out using basic descriptive variables as temperature, salinity, etc. The results obtained with this kind of data are poor because the species can respond to the variation of this factors directly (physiological response), but their population dynamic mainly responds to the influence of the different effects of the process (e. g. plume) that promote the change of the basic variable (e.g. salinity)

In the case of river plumes this problem is more important because the use of the salinity as a direct proxy of river plumes is a complicated issue due to the values of salinity of the plumes varies among different locations and in the same location varies in time too. In this manner the use of the methodology explained in this paper could improve the models and in consequence our understanding on the habitats and dynamic of the marine species.

Along the North Iberian Shelf (NIS), the upper layers (i.e. those affected by winter mixing and overlain by the seasonally varying surface mixed layer) present contrasting salinity characteristics due to the differential occurrence of distinct water masses and several oceanographic processes. Most of the water on the NIS corresponds to the sub-tropical and sub-polar branches of Eastern North Atlantic Central Water (ENACW_{st} and ENACW_{sp} respectively). These water masses present contrasting thermohaline characteristics (12.2-13 °C, >35.75 psu; and 11-12.2°C and 35.55-35.70 psu respectively) and converge off the northwest corner of the NIS (Fraga *et al.*, 1982; Ríos *et al.*, 1992).

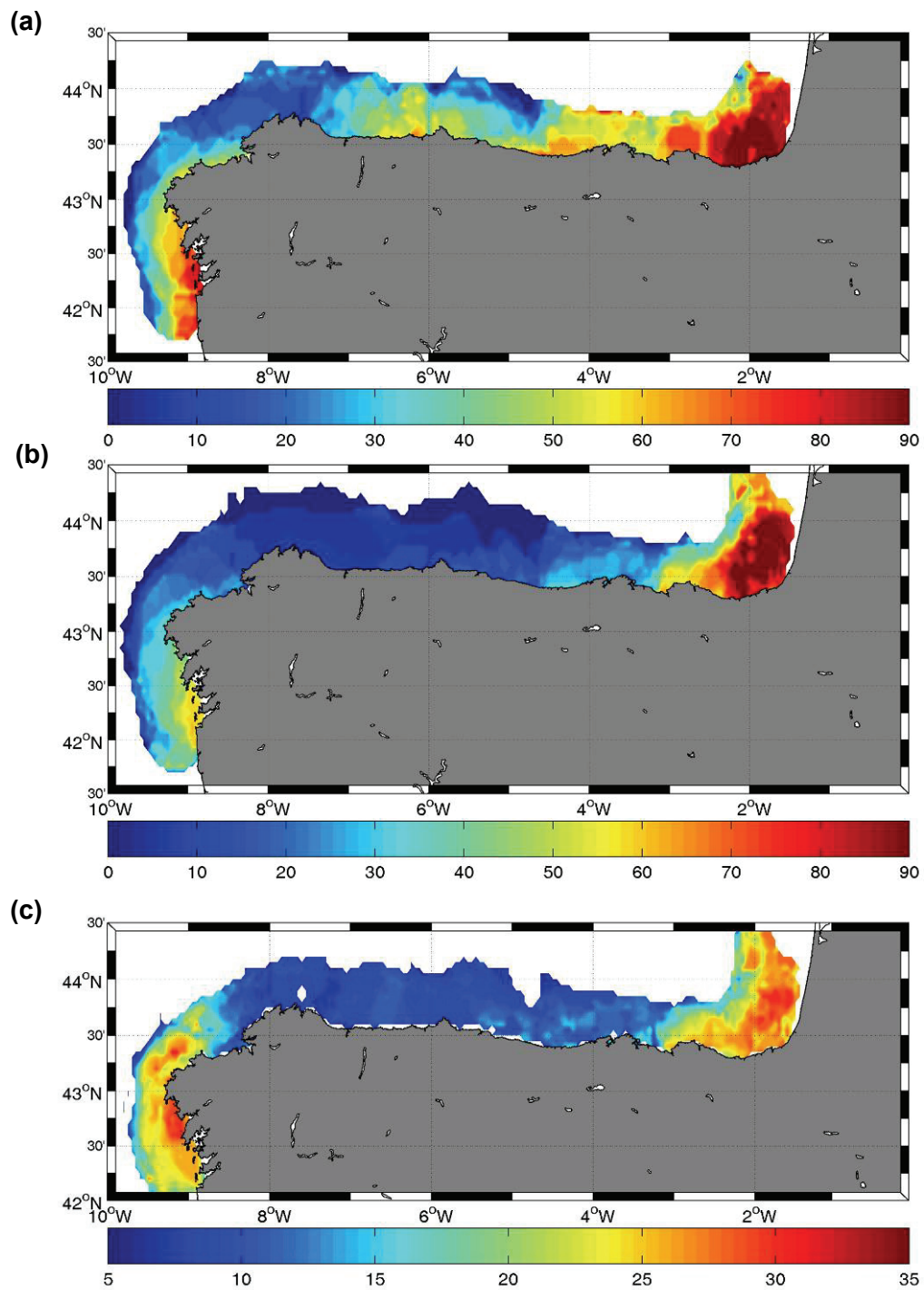


Figure 11: Spatial distribution of the probability of presence of river plumes at (a) 5 m and (b) 10 m depth (A_{P5} and A_{P10} respectively). In (c) is depicted the average depth of the buoyant structures along the NIS area.

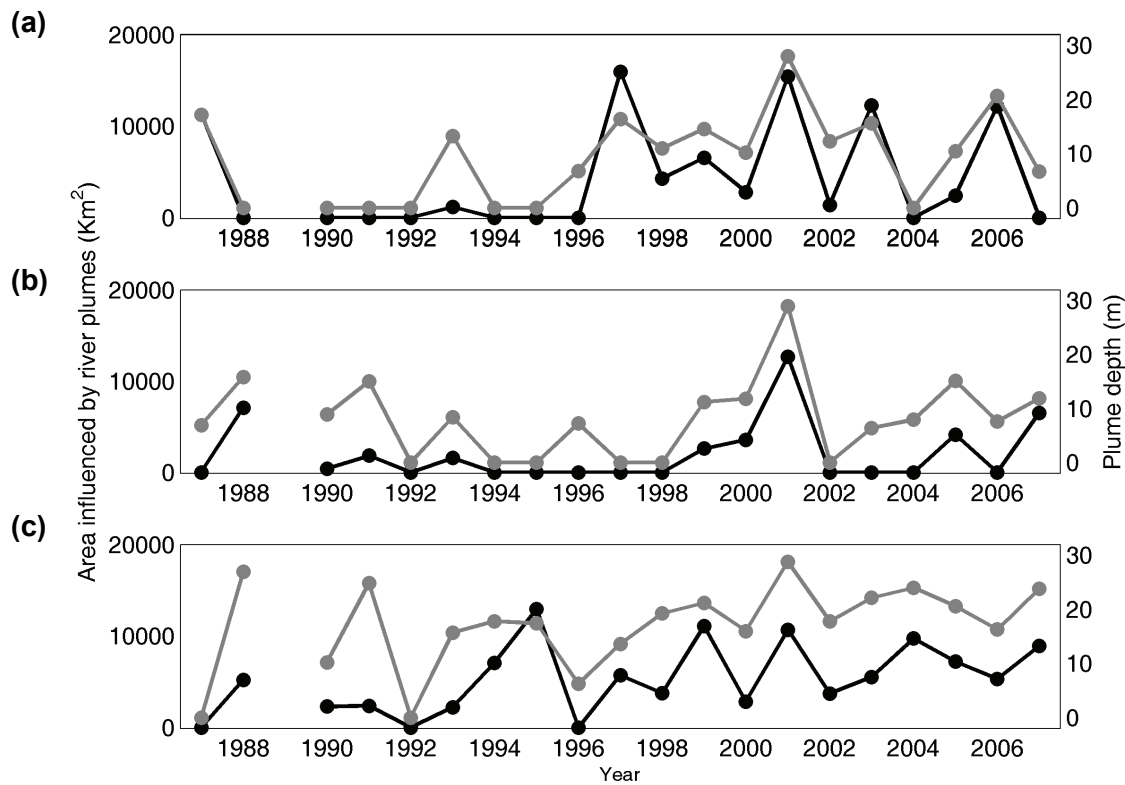


Figure 12: Time series of descriptors of the low-density buoyant structures: area at 5 m depth (A_{P5} , Km^2) (black line) and average depth (Z_P , m) (grey line) in: (a) Galician and West Cantabrian (GWC), (b) Central Cantabrian (CC) and (c) East Cantabrian (EC) zones.

Besides, a particular type of mode water formed by winter convection within the Bay of Biscay (Bay of Biscay Central Water, BBCW (11.0 -11.8°C and 35.55-35.60 psu) is present in the Cantabrian Sea (Botas *et al.*, 1989).

On the other hand, processes such as coastal upwelling and the influence of the Iberian Poleward Current (IPC), that showed their maximum expression in spring-summer and autumn-winter respectively (Peliz *et al.*, 2002; Álvarez-Salgado *et al.*, 2003; Peliz *et al.*, 2005), are stronger in the western than in the eastern parts of the NIS, promoting higher salinity in that area. The influx of relatively low salinity water from the central part of the Bay of Biscay onto the Cantabrian shelf in summer tend to enhanced even more the contrasting surface salinity along the NIS (Lavin *et al.*, 1998; Lazure *et al.*, 2009).

The seasonality of occurrence of river plumes, showed some distinct features along the NIS due to local differences in the precipitation regime and river runoff. The section off Vigo is located in the vicinity of the Rías Baixas system, where relatively large rivers (Miño, Tambre and Ulla) with a large catchment area ($\sim 20000 \text{ Km}^2$) and flow control

through a series of dams along their courses exists. These characteristics cause relatively high probability of plume occurrence in spring. The discharges close to the section off A Coruña are considerably lower (~500 Km² of catchment area), but relatively high probabilities are obtained all the year round. This pattern is due to the short distance between the outer and inner stations of the hydrographic section that precludes a robust estimation of the across-shelf salinity gradient. The sections in the Central Cantabrian Sea, off Cudillero and Gijón, are close together; the first at 5 km to the west and the second at 40 km to the east of the mouth of the Nalón river (3000 Km² of catchment area), showing a similar pattern of probability of occurrence of plumes. The Santander section is located off to the Santander Bay, where the Miera, Mina and Cubas flow into it (catchment area < 500 Km²). The section is influenced also by discharges from Pas and Besaya river mouths (~1000 Km² of catchment area) and also from the Adour in the inner part of the Bay of Biscay. The seasonal pattern of probability of plume occurrence differs from the other sections. This seasonal pattern resembles that of the precipitation rate in the EC zone.

The analysis of the influence of plumes in the spring season showed clear differences along the NIS. The GWC zone is influenced by Miño, Tambre and Ulla rivers that rise in the Galician Massive. In the north of Galicia, the rivers are shorter and the amount of water discharged into the Rías Altas is lower. The occurrences of the IPC and coastal downwelling processes during the period where precipitation and runoff reach maximum seasonal values tend to confine the Galician plumes in the inner part of the shelf, limiting the coastal-ocean exchange and acting as a retention area during this season. This structure is called the Western Iberian Buoyant Plume (Peliz *et al.*, 2005; Otero *et al.*, 2008b). The interannual variability of the area and mean depth of the plumes in GWC zone during spring was generated by contrasting precipitations rates and rivers runoff during these periods.

In the EC zone, the main river that promotes the generation of low-density buoyant structures is the Adour River that rises in the Pyrenees and the central zone of France. The existence of small rivers like Bidasoa and Nervion increases the intensity of the plumes in this zone but their reduced catchment areas limit their influence. The high levels of precipitations and the effect of the snow melting are responsible of the high values of probability of occurrence of plumes in late spring, with a large area affected, mean depth and volume.

Table 6. Results of the cross correlation analysis between the descriptors of the buoyant structures (area at 5 m depth area at 10 m depth, average depth and volume: A_{P5} , A_{P10} , Z_P and V_P respectively) and precipitation rate and river runoff, for the different zones (GWC, CC and EC zones) within the NIS region. The rivers used were Miño, Nalón and Adour for GWC, CC and EC respectively.

Forcing Factor	Zone	Descriptor	Lag	p-value	r^2	Slope	Intercept	
Precipitation	GWC	A_{P5}	1	< 0,01	0,37	1,80E+08	958,22	
			4	< 0,05	0,20	1,57E+08	388,12	
		A_{P10}	1	< 0,01	0,40	1,81E+08	965,67	
			5	< 0,05	0,19	1,12E+08	-440,06	
		Z_P	1	< 0,05	0,26	2,14E+05	1,14	
		V_P	1	< 0,001	0,56	4,94E+06	26,31	
			4	< 0,05	0,26	4,08E+06	10,09	
			5	< 0,05	0,23	2,79E+06	-11,02	
		CC	A_{P5}	-	-	-	-	-
			A_{P10}	1	< 0,05	0,35	1,45E+08	909,78
				6	< 0,05	0,20	1,07E+08	-634,96
			Z_P	1	< 0,01	0,34	3,12E+05	1,95
			V_P	1	< 0,01	0,33	3,61E+06	22,58
		EC	A_{P5}	3	< 0,05	0,26	2,04E+08	-62,44
			A_{P10}	3	< 0,01	0,33	2,32E+08	-71,01
	Z_P		6	< 0,05	0,39	5,05E+05	-1,62	
	V_P		3	< 0,01	0,30	5,31E+06	-1,62	
	6		< 0,05	0,26	4,24E+06	-13,59		
	Runoff	GWC	A_{P5}	1	< 0,05	0,28	3,97	-74,19
				4	< 0,01	0,26	3,46	-835,42
			A_{P10}	1	< 0,01	0,36	4,23	0,01
4				< 0,05	0,34	3,73	-817,26	
Z_P			1	< 0,05	0,26	0,01	0,38	
			4	< 0,05	0,26	0,005	-0,70	
V_P			1	< 0,05	0,57	0,13	1,70	
			4	< 0,001	0,47	0,10	-21,59	
CC			A_{P5}	2	< 0,01	0,32	136,51	1457,67
			A_{P10}	-	-	-	-	-
			Z_P	2	< 0,05	0,37	0,27	2,56
			V_P	2	< 0,05	0,27	2,63	31,54
		EC	A_{P5}	1	< 0,01	0,27	9,14	250,67
			A_{P10}	1	< 0,05	0,39	10,83	296,92
3		< 0,05		0,30	10,60	107,63		
Z_P		1	< 0,05	0,21	0,019	0,52		
V_P		1	< 0,01	0,43	0,28	7,60		

The CC zone presented clear differences with the other two zones, which are consequence of local characteristics mainly related to the continental relief. The Cantabrian Range is oriented parallel to the coast, limiting the catchment areas and the course length of the Cantabrian Rivers. In spring, the rainfall added to snow melting produce moderate values of the probability of presence of buoyant structures, which were shallower and with lesser extension than in the other zones. This zone is the unique where the correlation between the plume descriptors and the runoffs occurred at a lag higher than 1-month. The existence of this lagged correlation is probably a consequence of the high regulation of river Nalón: runoffs were obtained from a station located in its upper course, and between this point and the mouth of the river exist three dams (El Furacón 43.36°N 5.96° W, Valduno 43.38° N 6.00° W and Puerma 43.39° N 6.02° W) that could delay the flow of the waters into the sea.

Chapter 5: Temporal and spatial variability of wind-driven coastal upwelling in the NW and N Iberian shelf from 1987 to 2008

Introduction

Wind driven coastal upwelling has been largely studied along eastern boundary systems worldwide (deCastro *et al.*, 2006). The major eastern boundary upwelling systems (EBUS) in terms of biologic production are the Canary Current System (Pelegrí *et al.*, 2005), the California Current System (Di Lorenzo, 2003), the Benguela Current (Fennel, 1999; Monteiro & Largier, 1999) and the Peru-Humboldt Current (Nixon & Thomas, 2001; Mesias *et al.*, 2003). The NW and N Iberian shelf lies in the northern limit of the Canary Current System that extends along the eastern boundary of the North Atlantic Ocean from 10° to 44° N (Wooster *et al.*, 1976; Fiúza *et al.*, 1982; Herrera *et al.*, 2008). Coastal upwelling in this area shows a well defined seasonality (Wooster *et al.*, 1976; Fraga, 1981; Fiúza, 1983), characterized by an upwelling-favorable season during spring–summer due to the predominance of northerly and northeasterly winds (Fraga, 1981; Fiúza *et al.*, 1982), and a downwelling-favorable season during autumn–winter due to the predominance of southerly and northwesterly winds (Fiúza *et al.*, 1982; Álvarez-Salgado *et al.*, 2003). Seasonal variation is determined by the relative strength and position of the Azores High pressure cell (Fiúza *et al.*, 1982; Álvarez-Salgado *et al.*, 2003). Upwelling (downwelling) events occur also during autumn-winter (spring-summer) both in the northwest (Santos *et al.*, 2001; Álvarez-Salgado *et al.*, 2003; deCastro *et al.*, 2006; Prego *et al.*, 2007) and north Iberian shelves (Alvarez *et al.*, 2009). Notwithstanding, coastal upwelling is less intense in the Cantabrian than in the Galician coast due to the different orientation of the coast (zonal versus meridional) and the reduced extent of the seasonal period of upwelling favorable winds (easterlies versus northerlies) (Botas *et al.*, 1990; Alvarez *et al.*, 2008; Fontán *et al.*, 2008; Alvarez *et al.*, 2009). Despite this, coastal upwelling in the Cantabrian is also an important process in this area affecting the dynamics of different components of the pelagic ecosystem (Fernández & Bode, 1991; Hickey & Banas, 2003; Varela *et al.*, 2003; Llope *et al.*, 2006).

The main effect of upwelling is the fertilization of surface layers of the water column through the input of inorganic nutrients, consequently enhancing the productivity of coastal areas (Fernández & Bode, 1991; Hickey & Banas, 2003; Varela *et al.*, 2003; Llope *et al.*, 2006). It also exerts a direct effect on the structure and dynamics of pelagic and benthic domains, affecting many aspects of the ecosystem, from biogeochemical processes linked to the carbonate system (Borges & Frankignoulle, 2002; Gago *et al.*, 2003), or dissolved organic matter (Doval *et al.*, 1997; Álvarez-Salgado *et al.*, 1999) to those linked to the functioning and dynamics of ecosystem components, such as picoplankton (Barbosa *et al.*, 2001; Calvo-Díaz *et al.*, 2008), pelagic microplankton (Botas *et al.*, 1990; Varela *et al.*, 2003), benthic microplankton (Diz *et al.*, 2006), harmful algal bloom species (Figueiras *et*

al., 1994; Crespo *et al.*, 2008), meroplankton (Valdes *et al.*, 1990; Bode *et al.*, 2009) and zooplankton (Marta-Almeida *et al.*, 2006).

The high production levels of upwelling areas support important commercial fisheries and aquaculture production. For instances, the effect of upwelling on the Galician rías located in the Atlantic coast make this area one of the most important sources of mussel production in the world (Blanton *et al.*, 1987; Figueiras *et al.*, 2002). Besides it has been described in the bibliography the influence of upwelling on the stocks of other commercial species like octopus (Otero *et al.*, 2009a), pelagic fish species, such as sardine and horse mackerel (Santos *et al.*, 2001; Santos *et al.*, 2004), anchovy (Allain *et al.*, 2001), or albacore (Lavin *et al.*, 2007),

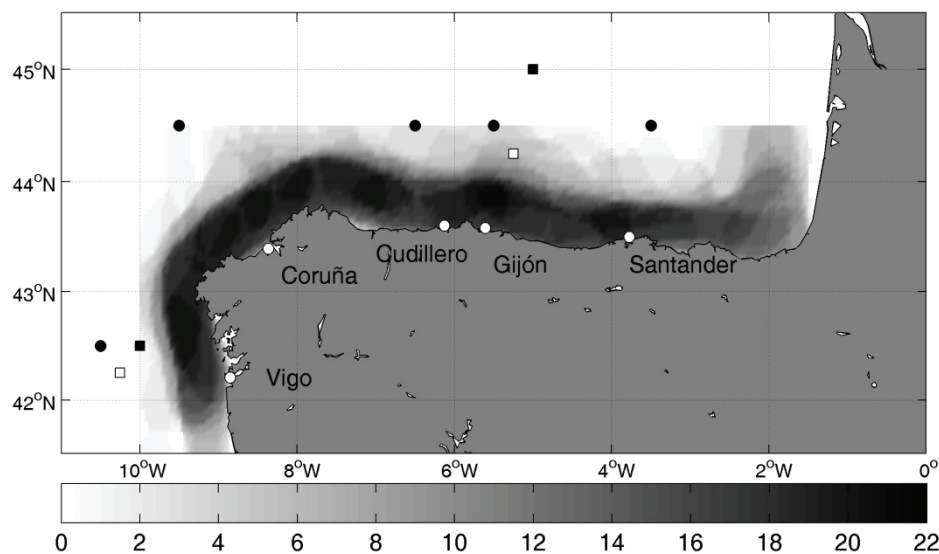


Figure 1: Study area (Northwest and North Iberian shelf waters) showing the spatial distribution of sampling intensity during the spring surveys. White dots represent the most coastal stations of the across-shelf sections sampled off Vigo, A Coruña, Cudillero, Gijón and Santander within the frame of the time-series monitoring programme RADIALES (<http://www.seriestemporales-ieo.com>). The location of ICOADS temperature data (<http://www.cdc.noaa.gov>) are represented by black dots. The locations where wind data were extracted are represented by the squares, black for NCEP data (<http://www.cdc.noaa.gov>) and white for Quicsckatt data (<http://cersat.ifremer.fr>).

Despite its relevance there is, however, a lack of numerical tools to objectively assess the characteristics of the process, such as temporal occurrence and persistence and/or the spatial distribution and extent of the water bodies affected by upwelling. Many of the published works describe these aspects in a somewhat subjective way (i. e. Botas *et al.*, 1990; Prego & Bao, 1997; Gil *et al.*, 2002) or indirectly through the description of the main forcing factor, the wind (Gomez-Gesteira *et al.*, 2006; Alvarez *et al.*, 2008; Alvarez *et al.*, 2009) consequently limiting the capabilities of understanding the interactions and

influence of the upwelling process. For instances, the proposed methodologies to characterize the upwelling process are based on thermal indices (Oliveira *et al.*, 2009), climatologies (Cheng *et al.*, 2009), front detection algorithms (Chaudhuri *et al.*, 2004; Marcello *et al.*, 2005) or thermal balance models (Ruiz & Navarro, 2006). The main problem of these methodologies is that they use as input variables surface values, generally of temperature (SST), and are thus only suited to detect intense upwelling able to induce the outcrop of sub-surface waters. The numerical approaches can be simple, such as those based on the calculation of thermal indices (Tapia *et al.*, 2009) or more complex, like Empirical Orthogonal Functions (Herrera *et al.*, 2008).

In this chapter we present an objective methodology to detect and characterize upwelling events, both in space and time, using temperature fields from *in situ* data. We have applied the proposed methodology to describe the spatial and temporal variability of coastal upwelling in the western and northern parts of the North Iberian shelf (NIS), Galician and Cantabrian Sea waters respectively, and explored the relationships of the upwelling characteristics with the wind patterns in the studied area.

Material and Methods

Temporal characterization of upwelling

Databases of temperature

The temporal characterisation of upwelling was based on the analysis of five coastal sections sampled monthly between 1994 and 2006 within the frame of the time-series monitoring programme RADIALES conducted by the Spanish Institute of Oceanography (IEO) (<http://www.seriestemporales-ieo.com>). These sections are located along the northwest and northern parts of the Iberian shelf, off Vigo (42.2° N, 8.8° W), A Coruña (43.3° N, 8.3° W), Cudillero (43.6° N, 6.1° W), Gijon (43.5° N, 5.6° W) and Santander (43.5° N, 3.6 W) (Figure 1). To complement this data base we have also used the time series of ICOADS sea surface temperature (SST) obtained from the NOAA/OAR/ESRL PSD, Boulder, Colorado, USA (<http://www.cdc.noaa.gov>). With combined these two datasets we to obtain a time series of an upwelling thermal index (UTI), defined as the difference between the oceanic temperature (T_o , from ICOADS) and the in situ temperature at the coastal edge of each section (T_c , from the time-series programme), corrected by the oceanic temperature value (Equation 1):

$$UTI = \frac{T_o - T_c}{T_o} \quad (1)$$

Wind data

In order to determine the relationship between the upwelling thermal index (UTI) and wind patterns, we analyzed the time series of wind velocities obtained from NCEP Reanalysis data provided by the NOAA/OAR/ESRL (<http://www.cdc.noaa.gov/>). We have selected the times series of the upwelling favorable wind component (UFWC), that is, the meridional component for the Galician coast (v -component at 42.0° N, 10.0° W) and the zonal component for the Cantabrian coast (u -component at 45.0° N, 5.5° W) (Figure 1). These two time series were modeled using the same time series analysis methods applied to the UTI database (see below).

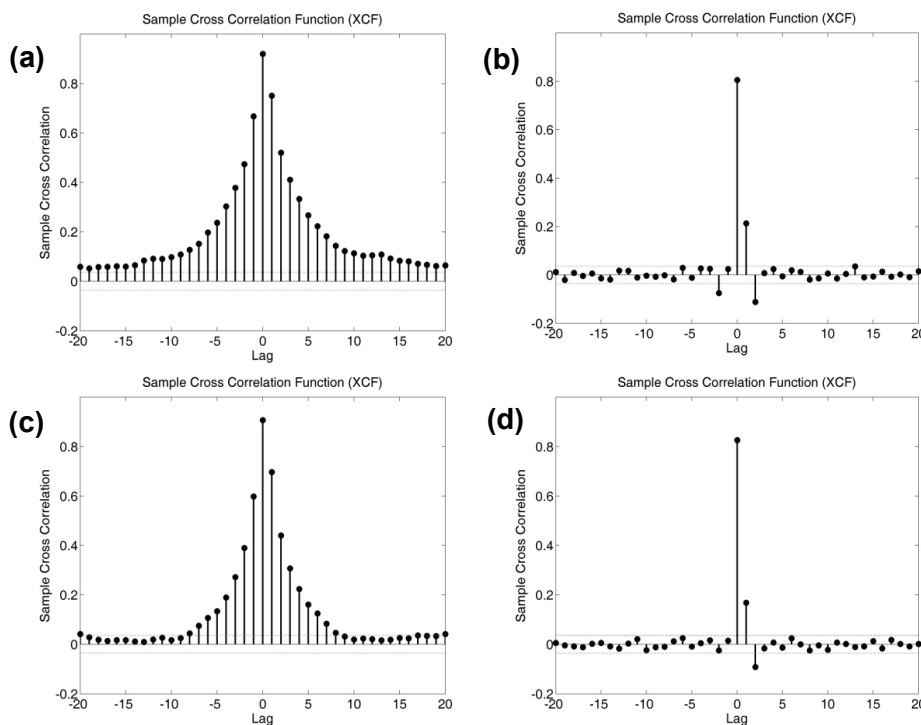


Figure 2: Cross-correlation function between daily zonal component of the wind from the NCEP and QuickStat datasets for the Atlantic coast (v -component) for (a) raw data and (b) pre-whitened residuals and for the Cantabrian Sea (u -component) for (c) raw data and (d) pre-whitened residuals.

The NCEP data are measured far away from the coast, so we considered also more coastal wind series from the Quikscatt satellite-derived data obtained from *CERSAT* (<http://cersat.ifremer.fr>). Aiming to test the comparability between both wind time series, we estimated the cross-correlation between NCEP and QuickScatt for the Galician coast (v -component at 42.25° N 10.25° W) and for the Cantabrian coast (u -component at 44.25° N 5.25° W) (Figure 1). Figure 2 shows the cross-correlation function between these series, both for raw data and pre-whitened residuals. In the two cases, the time series were

strongly correlated both for the Galician and Cantabrian coasts. Taking into account this result, we selected the NCEP winds as the forcing variable of coastal upwelling.

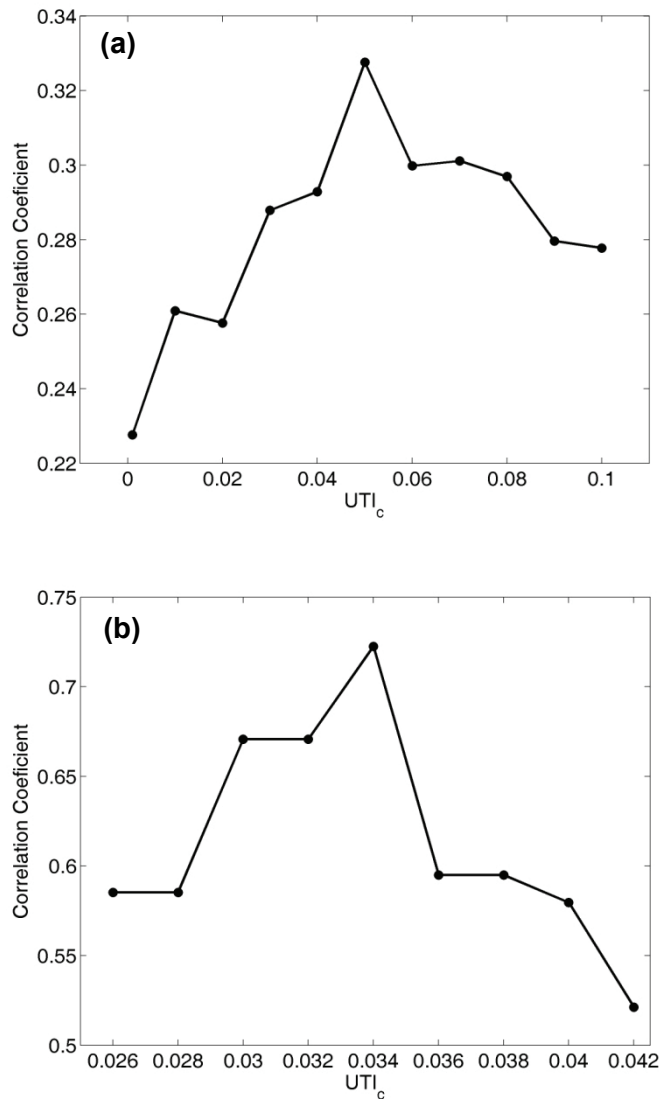


Figure 3: Relationship between the upwelling thermal index criterion (UTI_c) and the correlation coefficient obtained between upwelling wind favorable component averaged for the 15 days before the sampling (W15) and upwelling presence/absence calculated for data from (a) cross-shelf sections (RADIALES) and (b) spring surveys (Table 1).

To determine the presence or absence of upwelling in each of the across-shelf sections we established a threshold value to the UTI time series: values of UTI higher than that threshold (UTI_c) were considered to determine the occurrence of upwelling, while values of UTI lower than UTI_c were considered as indicate absence of the process. We set the UTI_c as the UTI for which we obtained the best logistic regression fit between the UTI time series and the averaged wind velocity series (mean value of upwelling favorable wind

velocity obtained for 15 days before the date of hydrographic sampling, W15). The UTI_c value was calculated iterating UTI_c from 0.001 to 0.1, using data from the five sections. Figure 3a shows the changes in the correlation coefficient of the logistic regression between UTI and W15 time series for different threshold values (UTI_c). The best fit was obtained with $UTI_c = 0.05$.

Time series analysis

Time series of the UTI in each section were modeled following a time series additive model (Equation 2):

$$Y_t = \bar{y} + LT[y_t] + SC[y_t] + R[y_t] + \varepsilon_t \quad (2)$$

where, subscript t is the index for time, \bar{y} is the average value of time series, LT and SC represent the long-term linear component and all periodic components (seasonal and long-term cycles) respectively, R the autocorrelation and ε_t the white noise. LT and SC were treated as deterministic components (Chatfield, 1996).

The first component (LT) is calculated using a classical least-square regression method applying a linear model (Equation 3):

$$LT = bt + a \quad (3)$$

where, LT is the value of the series added by the linear trend at time t , in which the parameters b and a represent, respectively, the slope and intercept of the linear model. We selected the model that minimized the sum of squared residuals (difference between observed and modeled values).

The periodic component (SC) was fitted using a sum of periodic functions (harmonics) (Equation 4):

$$SC[y_t] = \sum_{i=1}^n A_{T_i} \cos\left(\frac{2\pi}{T_i} t + \theta_{T_i}\right) \quad (4)$$

where, A_i is the amplitude T_i the period and θ_i the phase in radians of the i -th harmonic. The parameters of this model were extracted by means of Fourier analysis (Poularikas & Seely, 1991). The determination of the significance level of the extracted harmonics was carried out using G statistic (Davis, 1986), Equation 5), which is based on the relationship between the variance of the i -th harmonic ($s_{i-\max}^2$) and the total variance (s^2) of the time series.

$$G = \frac{s_{i-\max}^2}{s^2} \quad (5)$$

The i -th harmonic is significant if G is higher than one critic value G_c calculated following (Equation 6):

$$G_c = 1 - e^{-\frac{\left(\ln(\alpha) - \ln\left(\frac{n}{2}\right)\right)}{\frac{n-1}{2}}} \quad (6)$$

where α is significance level and n the number of data of the time series. This statistic is valid only for time series with more than 30 data.

The autocorrelation was modeled by means of the Box-Jenkins approach (Box & Jenkins, 1976). The time-series of the de-trended and de-seasonalized residuals (Equation 7), were parameterized by means of an autoregressive model, which involves the description of the time series in terms of a weighted sum of its own past values,

$$R[y_t] = \sum_{i=1}^{i=p} \phi_i (R[y_{t-i}]) \quad (7)$$

where, p is the order of the autoregressive model and ϕ_i are the set of autoregressive parameters. The order of the autoregressive process is defined by the inspection of the auto-correlation (acf) and partial auto-correlation functions (pacf), and the auto-regressive parameters were estimated using the Yule-Walker equations (Wei, 1989).

The remaining component of the series is the white noise or pre-whitened residuals (ε), that is, a random signal with a flat power spectral density.

Spatial characterization of upwelling

Database

The database of spring surveys is integrated by temperature data from CTD casts carried out in the NW and N Iberian shelf during spring (March-April) between the years 1987 and 2008 (Figure 1 and Table 1). The profiles were obtained in hydrographic stations distributed over the shelf and arranged in transects perpendicular to the coast. Some areas were visited up to 20 times during the analyzed 21-year period. The profiles extend from the surface (5m depth) down to 5 m above the bottom or to a maximum 200 m depth in deeper stations.

Upwelling detection method

The temperature field of each survey was estimated prior to the application of the method for upwelling detection. The fields were obtained by interpolating temperature data on a

regular grid of $0.05^\circ \times 0.05^\circ$, using an objective interpolation method based on an isotropic semi-variogram Gaussian model (Haagenson, 1982). (Equation 8):

$$\gamma(R) = \frac{V_s}{V_s + V_n} \cdot e^{-\frac{R^2}{2L^2}} \quad (8)$$

Where, $\gamma(R)$ is the correlation for a distance (spatial scale expressed in decimal degrees), V_s is the signal variance, V_n is the noise variance, and L is the characteristic length-scale (decimal degrees). The values of the parameters used for interpolation were $V_c = 0.6$, $V_e = 0.4$ and $L = 0.6^\circ$, which corresponded to the average values derived from the analysis of the correlogram of each cruise (see Chapter 2).

Table 1: Relation of the spring surveys used to analyze the characteristics of upwelling along the NW and N Iberian shelf, indicating the cruise's acronym, name of research vessel and the start and end dates of sampling at sea.

Cruise	Research vessel	Start date	End Date
SARPAREA	Lura	13/04/87	24/04/87
MPHSARACUS	Cornide Saavedra	01/04/88	04/05/88
MPH	Investigador	18/04/90	09/05/90
ECOSARP	Cornide Saavedra	17/04/91	09/05/91
ITIONORTE	Investigador	22/04/92	09/05/92
PELACUS	Cornide Saavedra	14/04/93	03/05/93
SEFOS	Cornide Saavedra	15/03/94	13/04/94
MPH	Cornide Saavedra	26/03/95	14/04/95
SEFOS	Cornide Saavedra	11/03/96	31/03/96
PELACUS	Thalassa	08/03/97	31/03/97
PELACUS	Thalassa	17/03/98	08/04/98
PELACUS	Thalassa	03/03/99	29/03/99
PELACUS	Thalassa	27/03/00	12/04/00
PELACUS	Thalassa	30/03/01	22/04/01
PELACUS	Thalassa	09/03/02	04/04/02
PELACUS	Thalassa	19/03/03	12/04/03
PELACUS	Thalassa	30/03/04	22/04/04
PELACUS	Thalassa	05/04/05	29/04/05
PELACUS	Thalassa	01/04/06	28/04/06
PELACUS	Thalassa	27/03/07	23/04/07

The upwelling detection method consists on an iterative algorithm that operates on the temperature field, searching for a theoretical along-shelf frontal structure in the across-shelf direction (Figure 4).

The basis for this procedure is that the across-shelf distribution of temperature during an upwelling event defines three spatial domains: an upwelling area, characterized by low and relatively constant values of temperature at the coastal side of the section, an area non affected by upwelled water in the outer edge of the section, identified by high and relatively constant values of temperature, and a zone in between which is characterized by a increasing coast-to-ocean temperature gradient, and which could be defined by two across-shelf locations (l), one at the beginning (l_b) and the other at the end (l_e) of the gradient area. This conceptual model was formalized according to the following discontinuous function (Equations 9a-c):

$$T_l = \frac{\sum_{l_1}^{l_n} T_l'}{n} \quad , \text{ for those } n \text{ across-shelf locations where } l \leq l_b \quad (9a)$$

$$T_l = \frac{T_{nu} - T_u}{l_e - l_b} l + \frac{T_u l_e - T_{nu} l_b}{l_e - l_b} \quad , \text{ for those locations where } l_b < l < l_e \quad (9b)$$

$$T_l = \frac{\sum_{l_1}^{l_n} T_l'}{n} \quad , \text{ for those } n \text{ across-shelf locations where } l \geq l_e \quad (9c)$$

Where, T_l are the calculated values of the temperature in each across-shelf location (l) belonging to the upwelling ($l \leq l_b$), gradient ($l_b < l < l_e$) and non upwelled areas ($l \geq l_e$), T' are the observed values of temperature in each across-shelf location, and T_u and T_{nu} are the average values of temperature in the upwelling and non-upwelling areas respectively. The best fit to the discontinuous function was obtained minimizing equation 10 by iterating l_b and l_e :

$$r = \sum_{l_1}^{l_n} |T_l' - T_l| \quad , \text{ for all across-shelf locations } l \quad (10)$$

The methodology applied to determine the presence/absence of upwelling and its influence on the area, is described in figure 5. Temperature sections perpendicular to de coast were obtained each along-shelf mile using the interpolated fields. The conceptual model (Equation 9a-c) was applied for each meter of the water column from 30 down to 80 m depth, and the parameters derived from the discontinuous function were used to calculate the UTI. This index was averaged in depth, obtaining UTI_a for each along-shelf location.

Similarly to what we have done for the across-shelf sections, we established empirically a threshold value of the upwelling thermal index (UTI_c) as indicative of upwelling

occurrence. The Atlantic and Cantabrian coast were treated independently and the time series of upwelling presence/absence and wind patterns treated separately. The time series of W15 (v-component for the Atlantic coast and u-component for Cantabrian coast) were calculated for each coast. The UTI_c was estimated as the value of UTI that generates the series of upwelling presence/absence with the higher correlation (logistic regression) with the 15-days averaged favorable upwelling wind velocities. Figure 3b shows the variability of the correlation coefficient between upwelling and wind in relation with UTI_c . The best fit was obtained with $UTI_c = 0.034$.

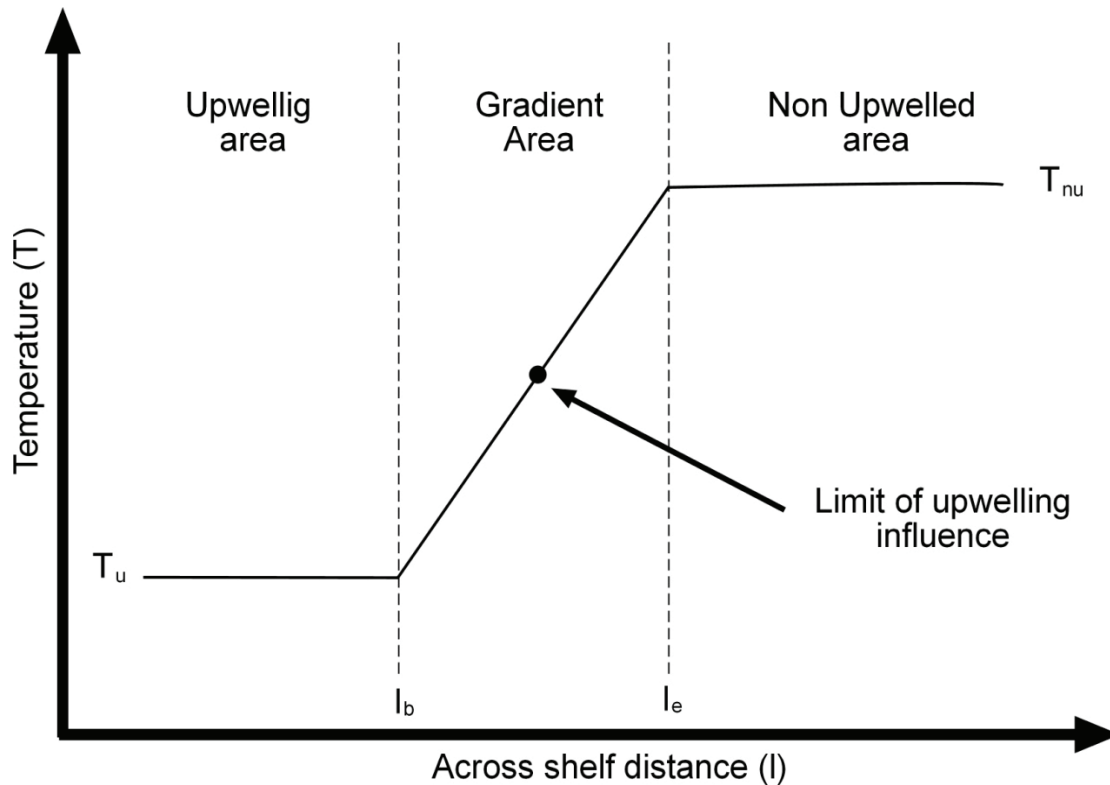


Figure 4: Representation of the conceptual model of the across-shelf distribution of temperature under upwelling conditions. l_b and l_e represent the across-shelf locations at, respectively, the beginning and the end of the gradient area; T_u and T_{nu} are the average temperatures in, respectively, the zones affected and non-affected by upwelling. The limit of influence of upwelling waters was set as the midpoint between l_b and l_e .

We determined the along-shelf locations influenced by upwelling applying this criterion ($UTI_a > 0.034$). At these locations, the intermediate point of the gradient area of the upwelling model was calculated (Figure 4). All points situated in between this location and the coast, were considered influenced by upwelling. In order to refine the upwelling detection, we calculated the percentile 70 ($P_{70}(T)$) of the temperature data measured at 50 m depth in each detected upwelling area. All the locations around the detected upwelling area with temperatures lower than ($P_{70}(T)$) were also considered influenced by upwelling.

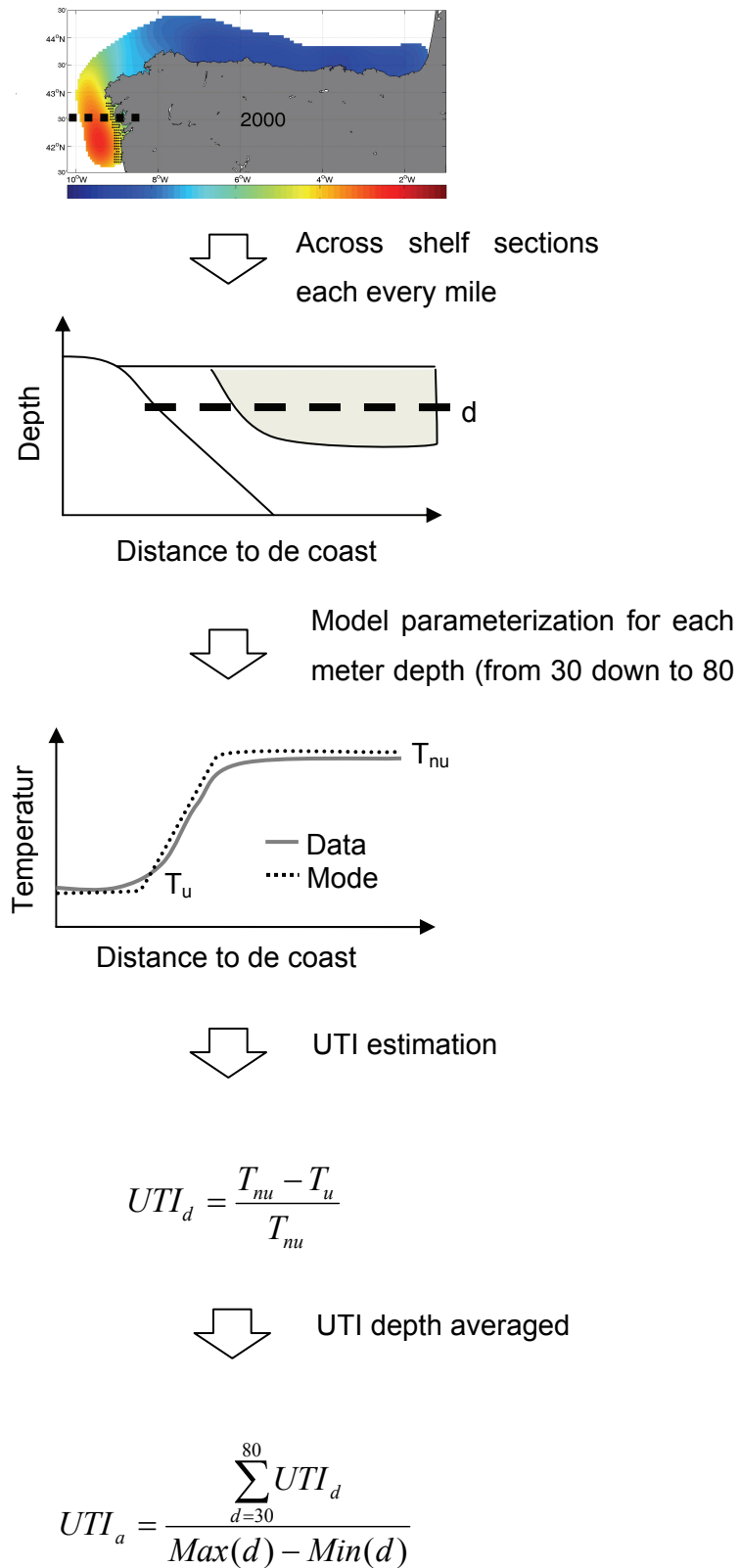


Figure 5: Scheme of the different steps of the upwelling detection method.

Results

Wind patterns

The study of the time series of UFWC showed clear differences in the patterns of variations for the two coastal orientations along the NIS, i.e. western/northwestern (NW) and northern (N) Iberian shelves. The raw time series for the two areas are plotted in Figure 6a-d and the values of the parameters of the time series decomposition model are shown in Table 2. The seasonal component of the UFWC is more intense in the NW than in the N coast (8.8 and 1.6% of explained variance respectively, Table 2). During autumn and winter, southerly winds predominate, exhibiting moderate average velocities ($0-2 \text{ m}\cdot\text{s}^{-1}$) (Figure 6b). In contrast, the rest of the year, the northerly wind component predominates, especially during the summer, when upwelling favorable winds are more frequent and intense ($< -3\text{m}\cdot\text{s}^{-1}$). These patterns were supported by the results of the time series analysis (Table 2).

The mean value of the Atlantic coast series was $-1.35 \text{ m}\cdot\text{s}^{-1}$, remarking the dominance of northerly winds in this area in an annual basis. We measured an increasing linear trend of UFWC along the western coast of $0.01 \text{ m}\cdot\text{s}^{-1}\cdot\text{year}^{-1}$, explaining 0.1% of total variance, $p\text{value} < 0.001$), which reflects a reduction of the dominance of northerly winds during the studied period. The seasonality was captured by the first harmonic of the annual period ($T= 365$ days), which explained 8.7 % of total variance of the daily time series. The rest of significant harmonic oscillate from $T = 46$ to $T = 194$ days, but explained percentages of total variance below 0.4 %. The significance of these harmonics reflects the intrinsic temporal compartment of winds at monthly and sub-seasonal scales. The high values of autocorrelation ($\phi = 0.70$) and the amount of explained variance by the autoregressive component (44.39 %) showed the strong persistence, or serial dependence, of coastal upwelling at the daily scale.

The Cantabrian Coast presented different variability pattern of UFWC. Most of the year was dominated by westerlies with moderate velocities (around $2 \text{ m}\cdot\text{s}^{-1}$). Only during summer we can find a weak predominance of the easterly wind component (lower than $-1 \text{ m}\cdot\text{s}^{-1}$). The Cantabrian Coast was dominated by westerlies with a mean value of $1.23 \text{ m}\cdot\text{s}^{-1}$. Seasonality is less intense than in the Atlantic Coast; the variances explained by the harmonics close to the annual period, $T = 365$ and 321 days, were of 1.63 % and 0.28 % respectively. The other significant harmonics oscillate between periods of 37 and 145 days which, explained a marginally significant amount of the total variance. The autocorrelation was also high too ($\phi = 0.70$), explaining 50.9 % of total variance.

Table 2: Parameters derived from time series analysis applied to the daily time series of the upwelling favorable wind ($\text{m}\cdot\text{s}^{-1}$) components (meridional at 42°N , 10°W ; zonal at 45°N , 5.5°W) from the NCEP/NCAR database (<http://www.cdc.noaa.gov/>); b and a represent, respectively, the slope and intercept of the long-term linear trend; T , A , F and T_{max} are, respectively, the period, amplitude, phase and time when the (first) maximum occurs for the different significant periodic components; ϕ is the magnitude (dimensionless) of the autoregressive parameter for a given time lag; %EV is the percentage of explained variance associated to each of the extracted temporal components.

Location	Mean	Periodic Trends					Autocorrelation		
		T	A	F	T_{max}	%EV	lag	ϕ	%EV
42.0 N 10.0 W	-1.35	365.22	2.53	6.18	5.88	8.76	1	0.70	44.39
		121.74	0.52	4.71	30.47	0.37			
		194.13	0.49	4.89	43.02	0.33			
		151.75	0.46	4.61	40.35	0.29			
		100.22	0.43	2.83	55.03	0.26			
		92.48	0.42	4.31	29.11	0.24			
		46.34	0.42	0.03	46.10	0.24			
45.0 N 5.5 W	1.23	365.25	1.15	6.13	9.14	1.63	1	0.72	50.89
		52.43	0.56	3.09	26.62	0.39			
		37.48	0.50	3.89	14.28	0.31			
		321.64	0.48	4.70	80.91	0.28			
		110.51	0.46	1.92	76.77	0.26			
		145.61	0.43	3.53	63.88	0.23			

Table 3: Results of the time series analysis applied to the time series of the Upwelling Thermal Index (UTI) calculated for the across-shelf sections of the RADIALES temperature data (<http://www.seriestemporales-ieo.com/>); T , A , F and T_{max} are, respectively, the period, amplitude, phase and time when the (first) maximum occurs for the different significant periodic components; ϕ is the magnitude (dimensionless) of the autoregressive parameter for a given time lag; %EV is the percentage of explained variance associated to each of the extracted temporal components.

Section	Period	Mean	Periodic Trends					Autocorrelation		
			T	A	F	T_{max}	%EV	lag	ϕ	%EV
Vigo	1994-2006	0.10	12	0.10	2.03	8.13	60	1	0.20	2
Coruña	1994-2006	0.06	12	0.10	1.92	8.34	66	1	0.17	1
Cudillero	1994-2006	0.03	12	0.06	2.78	6.69	26			
Gijón	2001-2006	0.05	12	0.05	2.01	8.17	26			
Santander	1994-2006	0.04	12	0.07	2.69	6.87	27			

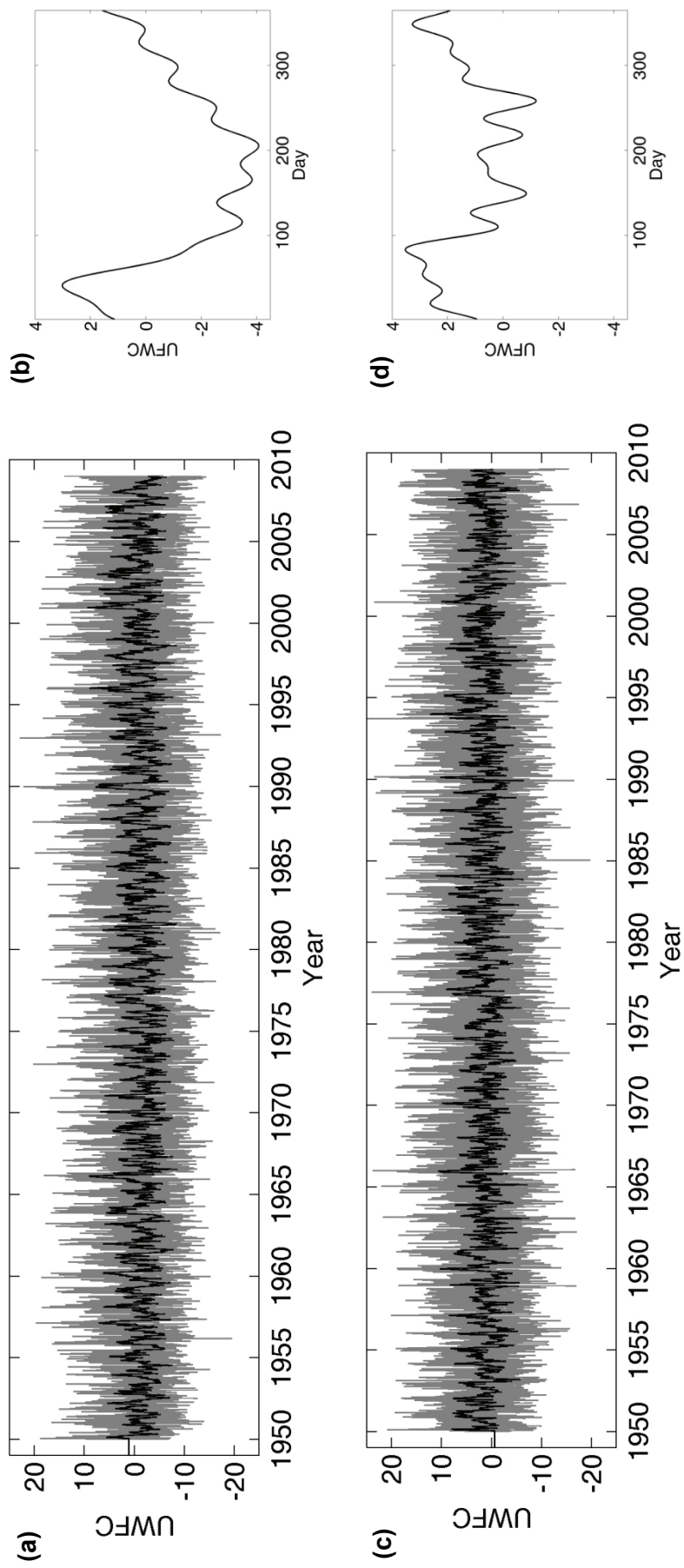


Figure 6: Raw daily time series and seasonal cycles of the upwelling favorable wind (UFW) components (a-b) v-component of the wind ($\text{m}\cdot\text{s}^{-1}$) in the Atlantic coast and (c-d) u-component of the wind ($\text{m}\cdot\text{s}^{-1}$) in the Cantabrian coast.

Across-shelf variability

Upwelling Thermal Index (UTI) time series

The time series and seasonal cycles of the UTI of the five across-shelf sections are showed in figure 7. High values of this index correspond with the presence of relatively cold waters in the coast and warm waters offshore. Low values were measured under the opposite situations. The results of time series analysis showed different patterns of variation in the NW and N Iberian shelves (Table 3). The mean values of the UTI were higher in the Atlantic Coast (0.10 and 0.06 for Vigo and A Coruña across-shelf sections respectively) than in the Cantabrian Coast (0.03, 0.05 and 0.04 for Cudillero, Gijón and Santander sections respectively). The seasonal component was significant for the five sections, although its intensity was higher in the Atlantic than in the Cantabrian sections (60% versus 25% of explained variance of the respective UTI monthly time series). Maximum values of the seasonal cycle occurred around August in the NW shelf (T_{\max} of 8.13 and 8.34 months for Vigo and A Coruña respectively) whereas in the Cantabrian sections occurred earlier, around July (T_{\max} of 6.7, 8.2 and 6.9 months for Cudillero, Gijón and Santander respectively). Long-term linear trends were only found in the section off A Coruña, although the estimated upward trend was weak (0.003 year^{-1}) and marginally significant (3% of explained variance). The autocorrelation of the de-seasonalized time series was only significant for the Atlantic across-shelf sections. Thus, there were clear differences in the temporal pattern of the UTI between the NW and N Iberian shelves. Coastal upwelling, according to the UTI, was more intense and predictable in the former of these spatial domains, showing significant seasonality and persistence (i.e. correlation between contiguous months).

Relationship between the upwelling thermal index (UTI) and wind patterns

The relationship between upwelling, defined by the UTI, and wind intensity was calculated using a threshold of $UTI_c = 0.05$ as a criterion of occurrence versus non-occurrence of upwelling ($UTI \geq UTI_c$ versus $UTI < UTI_c$ respectively) (Figure 8). The fitted logistic model was:

$$U_p = \frac{e^{-0.206w_{15}-0.379}}{1 + e^{-0.206w_{15}-0.379}}$$

where, U_p is the probability of upwelling occurrence and W_{15} is the mean velocity of the upwelling favourable wind component averaged over the 15 days before the sampling day at sea for which the UTI was calculated ($n = 549$, $r = 0.32$ and $p < 0.001$). Wind velocities of the upwelling favourable component lower than $-2 \text{ m}\cdot\text{s}^{-1}$ (i.e. northerly and easterly

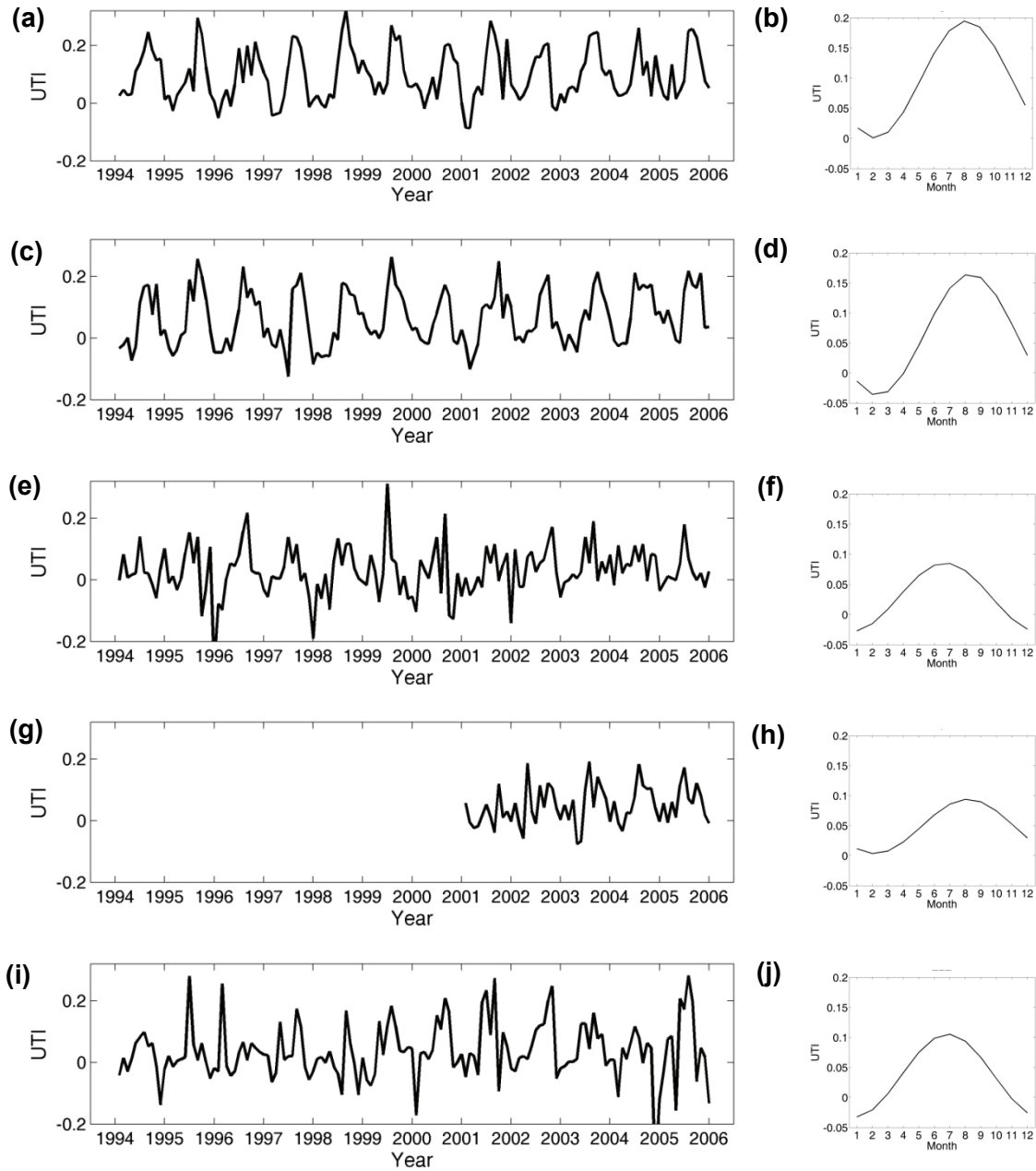


Figure 7: Monthly time series and seasonal cycle of the Upwelling Thermal Index for (a-b) Vigo, (c-d) A Coruña, (e-f) Cudillero, (g-h) Gijón y (i-j) Santander sections.

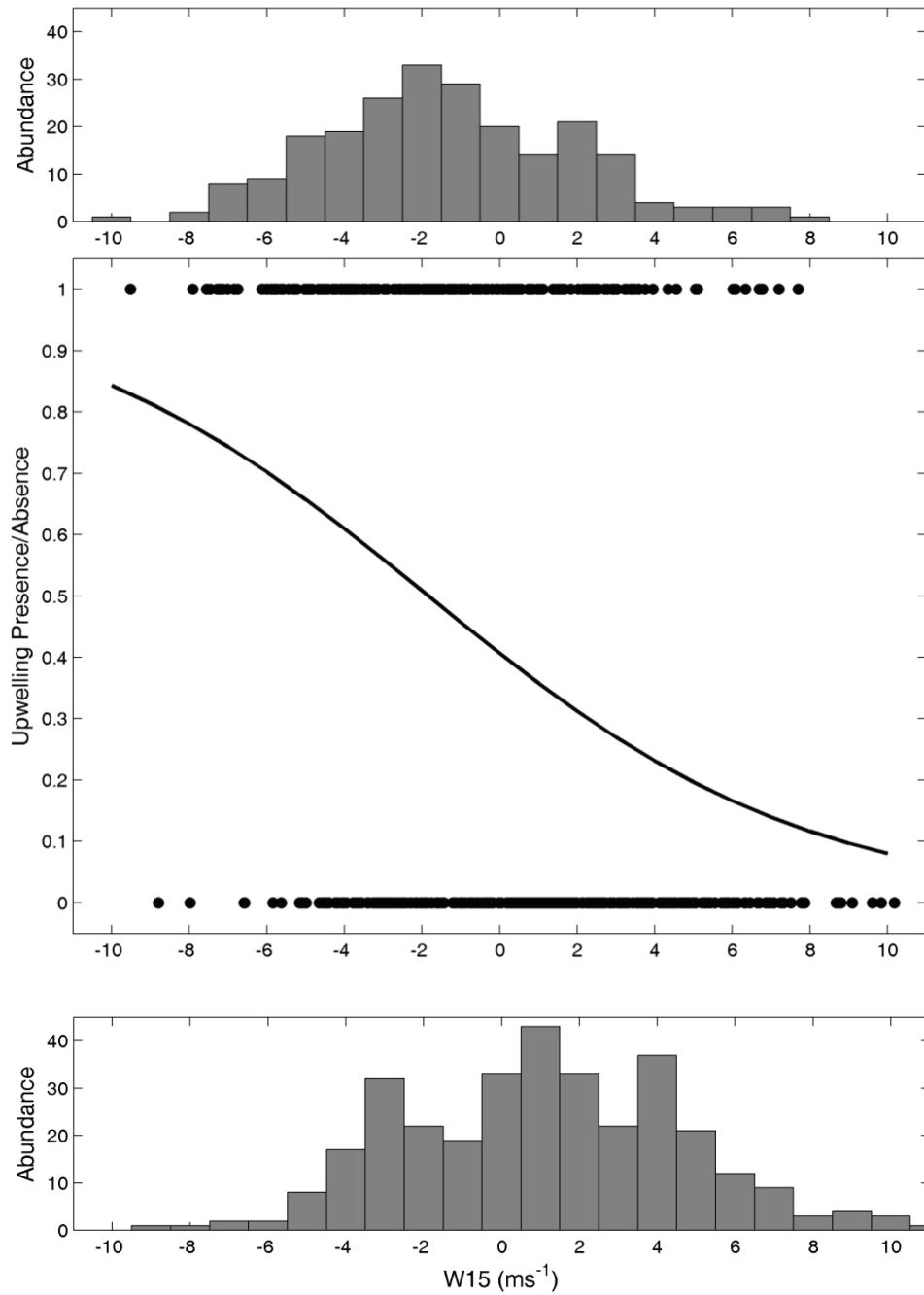


Figure 8: Relation between the Upwelling favorable wind component averaged 15 days before the sampling (W15) and the upwelling presence/absence calculated using temperature data from the across-shelf sections. The black line represents the logistic fit. In the upper (upwelling presence) and lower (upwelling absence) panels are showed the abundance of measurements as a function of W15.

winds for the NW and N Iberian shelves respectively) had a probability of upwelling occurrence higher than 50%.

The probability of upwelling occurrence was calculated for every month in each of the across-shelf sections using the approach based on the UTI_c (Figure 9). For the Galician sections, the patterns of seasonal variation of the probability of upwelling occurrence were similar, with maximum probabilities (>70% of probability of occurrence) during summer months. The difference between the two Galician sections was perceptible in the spring season when the southernmost section (off Vigo) exhibited a secondary maximum.

The probability of upwelling occurrence was lower in the Cantabrian across-shelf sections all year round, being June and July the months when higher probabilities were observed (around 50% of probability of upwelling occurrence). The high values obtained in Gijon in October could be a consequence of the reduced number of sampling events.

The wind intensity measured as $W15$ was directly correlated with the UTI (Figure 10). The fitted linear model for all the data pooled was $UTI = -0.007 W15 + 0.039$, ($n = 549$, $r = 0.332$, $p < 0.001$). This general relationship varies, however, depending of the month of the year. The seasonal variation of the slope is showed in Figure 11 and the parameters of the models estimated for each month are compiled in Table 4. The highest significance (p -value) of the relationship between the UTI as a function of $W15$ was measured between summer and autumn (from June to November).

Table 4: Seasonal variation of the parameters (slope, intercept and correlation coefficient b , a and r respectively) of the linear relationship between the UTI as a function of $W15$ with data from all the across-shelf sections.

Month	Slope (b)	Intercept (a)	r	p -value
1	-0.001	0.001	-0.032	0.839
2	-0.003	0.008	-0.168	0.253
3	-0.004	0.006	-0.375	0.011
4	-0.004	0.008	-0.222	0.174
5	-0.002	0.045	-0.085	0.554
6	-0.012	0.097	-0.451	0.001
7	-0.018	0.099	-0.581	0.000
8	-0.023	0.123	-0.624	0.000
9	-0.019	0.105	-0.656	0.000
10	-0.010	0.080	-0.376	0.008
11	-0.013	0.032	-0.531	0.000
12	-0.002	0.005	-0.073	0.618

Coastal upwelling along the NW and N Iberian shelf in spring

Similarly to what we have done in the analysis of the across-shelf sections, we have explored the relationship between the intensity of the wind and the occurrence of upwelling along the NW and N Iberian shelf during spring on the basis of the temperature fields measured in the studied area during this part of the year (Table 1). This relationship was formalized fitting a logistic model (Figure 12):

$$U_p = \frac{e^{-0.899w_{15}-1.761}}{1 + e^{-0.899w_{15}-1.761}}$$

where, U_p is the probability of upwelling occurrence and W_{15} is the mean of the velocity of the upwelling favourable wind components averaged over the 15 days before the sampling of temperature values at sea ($n = 32$, $r = 0.72$, $pvalue < 0.001$). We have obtained a more robust and less noisy relationship than that obtained for the across-shelf sections. Values of averaged wind velocity lower than $-2.5 \text{ m}\cdot\text{s}^{-1}$ had probabilities of upwelling occurrence higher than 50% and values lower than $-4 \text{ m}\cdot\text{s}^{-1}$ reach probability values of upwelling occurrence close to 100%.

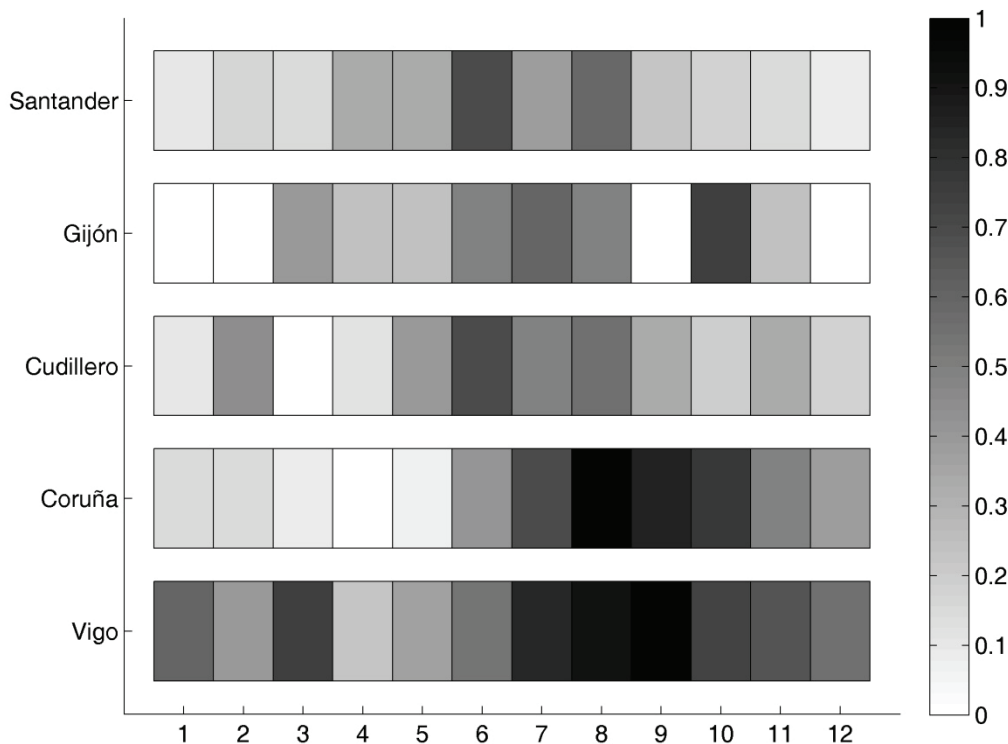


Figure 9: Seasonal cycle of the probability of upwelling occurrence. Dark color (light) represents high (low) probabilities.

The *ad hoc* method developed for the spatial detection of upwelling allowed us to infer the extent of the area influenced by upwelled waters (U_a). The calculated values oscillate between $0.1 \cdot 10^4 \text{ Km}^2$ in 2004 for the Galician Coast to $2.2 \cdot 10^4 \text{ Km}^2$ in 1998 for the Cantabrian Coast. The mean values were $1.1 \cdot 10^4$ and $1.2 \cdot 10^4 \text{ Km}^2$ for the Galician and Cantabrian shelves respectively. This parameter presented a significant linear relationship with the intensity of W15 ($U_a = -1941.5 W15 + 4012$, $n = 14$, $r = -0.74$, $p\text{value} < 0.005$)(Figure 13).

The temporal variation of the areas influenced by upwelled waters was determined using the UTI_c for each spring survey (Figure 14). The pattern of temporal variation differed between the Atlantic and Cantabrian shelves. Thus, the Atlantic shelf was affected by upwelling during the spring of the years 1990, 1991, 1992, 1995, 1998, 1999, 2000, 2004, 2007 and 2008, while the Cantabrian shelf was affected by upwelling in 1990, 1995, 1998 and 2007. It is noticeable that the occurrence of upwelling in the Cantabrian shelf is coincident with the occurrence of this process in the Galician shelf. The probability of upwelling occurrence in spring was 48% and 19 for the Galician and Cantabrian shelves respectively. The differences between the NW and N Iberian parts of the NIS were reflected in the spatial distribution of the probability of upwelling occurrence (Figure 15). The higher values of probability of occurrence were found off the Rías Baixas (45%) and diminish northwards (i.e. Rías Altas), defining two distinguishable domains along the Galician shelf. Other location with relatively high probability of occurrence was found in the vicinity of Cape Peñas, with probability values around 15%.

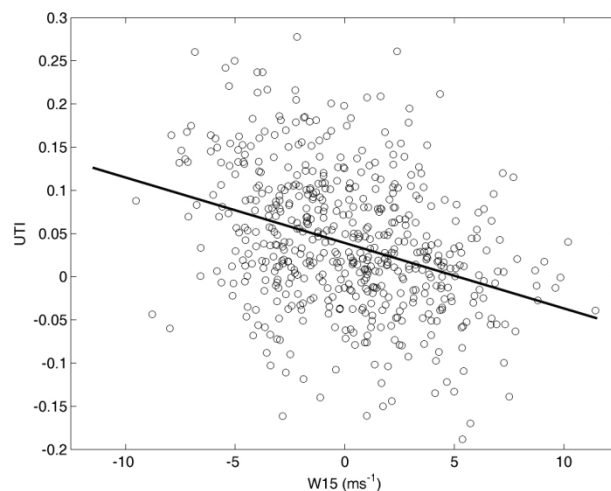


Figure 10: Relationship between W15 and UTI calculated using the across-shelf section data. The Black line represents the linear fit.

Discussion

Methodological considerations

The methods that we have developed to detect the occurrence of coastal upwelling on the basis of *in situ* sea surface temperature (SST) allowed us to determine the temporal and spatial variability of this process along the NIS. Similarly to other upwelling detection methods based on SST data, the method presents, however, some limitations since other hydrographic process than upwelling, such as river runoff and concomitant plumes or the advection of warm waters linked to poleward currents, influence also SST fields. Besides, the detection of upwelling could be blurred when it is not sufficiently strong to promote the outcrop of sub-surface, cooler waters. However, in spite of the changes in SST associated to process other than upwelling, in general terms the upwelling thermal index (UTI) we have developed is sufficiently robust to detect the occurrence of upwelling in most situations.

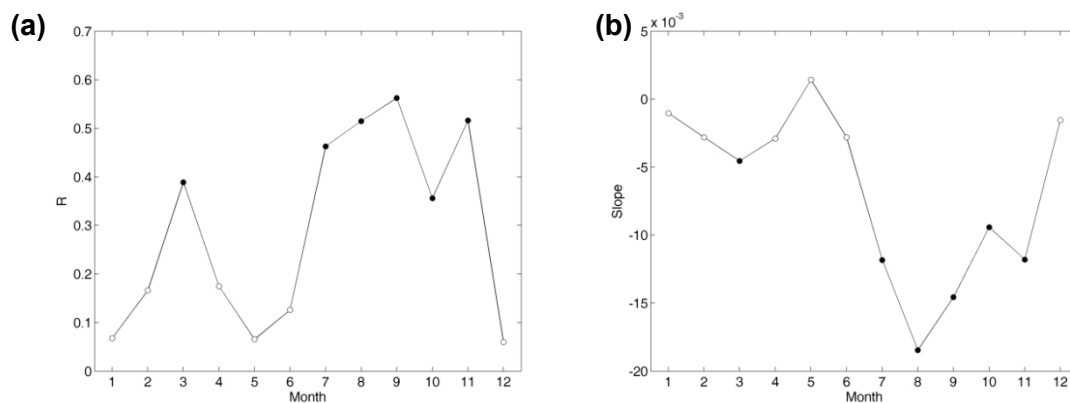


Figure 11: Seasonal cycle of the slope of the linear fit between W15 and UTI derived for across-shelf section data: (a) correlation coefficient and (b) value of the slope. Solid circles represent significant slopes (p-value < 0.05).

Some of the aforesaid caveats are minimized when the method is applied to a 3D temperature field data. In the case of the spring surveys analyzed in the present work, temperature data from the surface layer (between 0 and 30 m depth) were not used in order to reduce the influence of other hydrographic processes that, apart for upwelling, can influence SST. The detection of false positives of upwelling occurrence is reduced because we focused the analysis on the sub-surface temperature field, using data from 30 down to 80 m depth. In spite of the improvement associated to the use of sub-surface temperature data, we have found several situations in which false positives of upwelling occurrence have taken place. For instances, in the years 2001 and 2006, intense river plumes occurred, affecting to whole studied area in the former of these years and the

easternmost part of the Cantabrian Sea in the later. The influence of these river plumes extended down to more than 30 m depth, interfering with an unequivocal detection of coastal upwelling.

The assumption of the existence of three distinguishable domains regard to the across-shelf distribution of temperature associated to coastal upwelling, allowed us to localize the position of the frontal structure associated to the occurrence of this process. In general terms, this conceptual model could be applied to explore the spatial variability of conservative properties, and thus could be adjusted to account for the existence and characterization of other hydrographic processes. For instances, it has been applied to localize the along-shelf frontal structure generated by the intrusion onto the Cantabrian Sea of warm and salty (spicy, Flament, 1986) waters conveyed by the Iberian Poleward Current (See Chapter 3).

The calculations of the threshold value selected to indicate upwelling occurrence (UTI_c) were made independently for the across-shelf (RADIALES sections) and field (spring surveys) temperature databases. The resulting values were comparable, but slightly higher for the across-section data (UTI_c of 0.050 and 0.034). The difference between the threshold values results from the input temperature data used for the calculation of the UTI time series, that is, monthly time series of surface data for the across-shelf sections versus sub-surface temperature (30-80 m depth) fields covering the whole NIS during one month in spring. The UTI time series derived from SST tend to reach higher values than that derived using sub-surface temperature data. The same intensity of upwelling produces different values of UTI depending of the water column structure. For instances but under conditions of strong thermal stratification conditions, weak upwelling generates higher values of UTI than in other cases with mixed water columns.

Temporal patterns of upwelling along the NIS

The analysis of daily time series of the wind components and monthly coastal-offshore temperature gradients in the across-shelf sections distributed along the NIS region showed distinct temporal patterns of variability of upwelling in the Galician and Cantabrian shelves. The observed patterns are mainly a consequence of the change in the orientation of the coast along the NIS, which determines different regimens of the upwelling favourable wind component in each zone, meridional and zonal respectively (Table 2) (Fraga, 1981; Botas *et al.*, 1990).

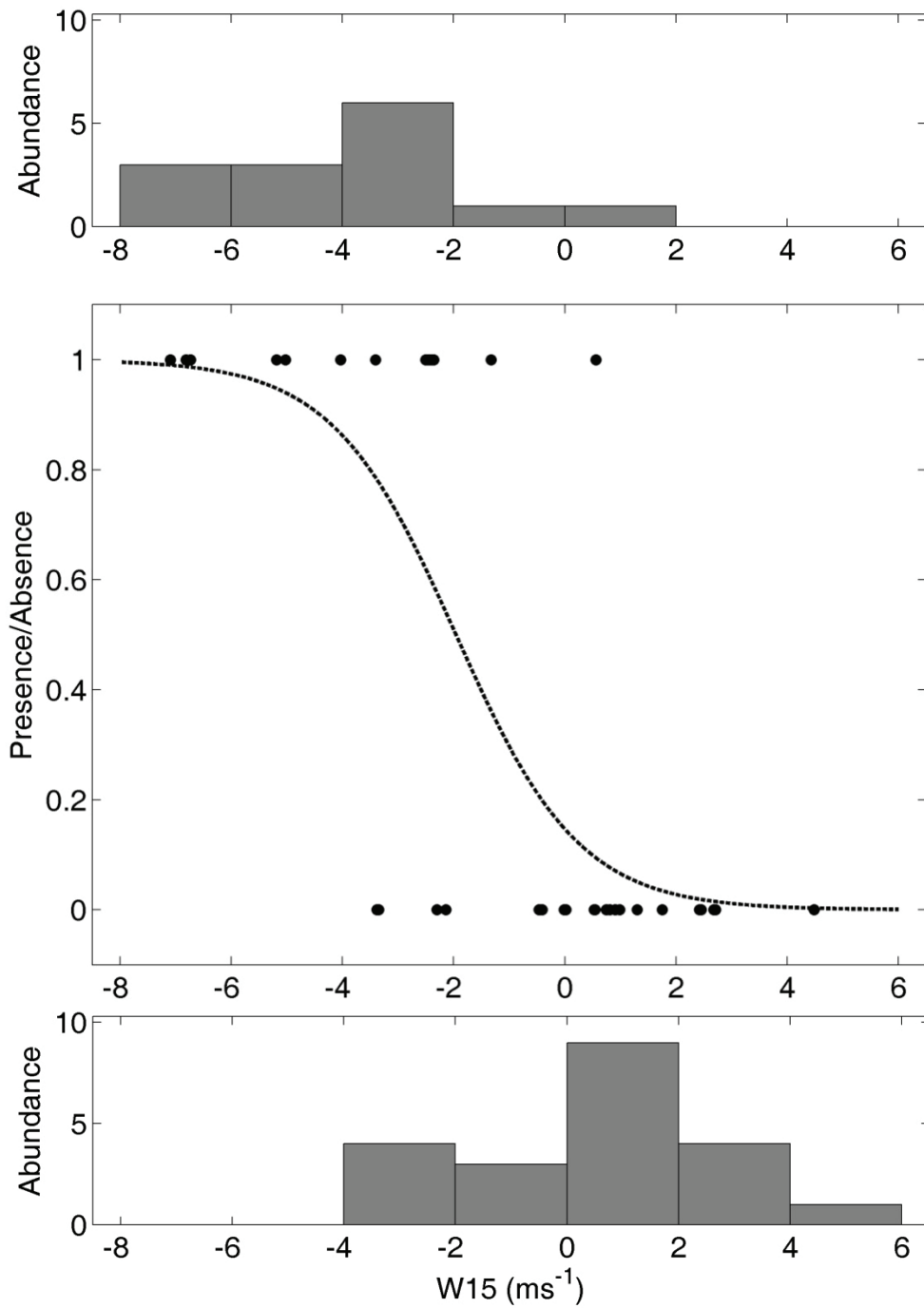


Figure 12: Relationship between the Upwelling favorable wind component averaged 15 days before the sampling at sea (W_{15}) and the upwelling presence/absence calculated using data from the spring surveys. The black line represented the logistic fit. In the upper (upwelling presence) and lower (upwelling absence) panels are showed the abundance of measurements in function of W_{15} .

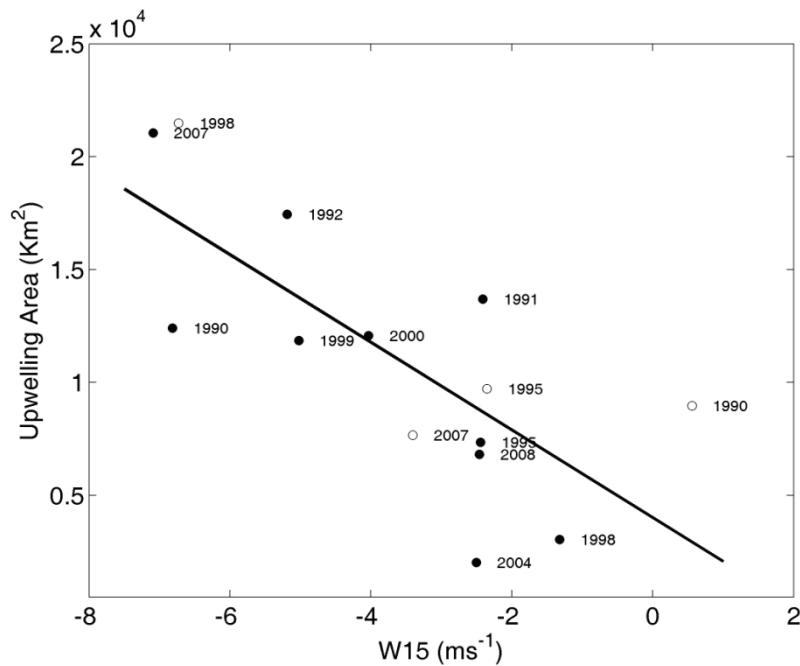


Figure 13: Relationship between W15 and upwelling area (U_a) for the Galician (black dots) and Cantabrian shelves (white dots).

The major differences between wind components are the predominance, on an annual basis, of upwelling favourable winds (northerlies) and marked seasonality in Galicia, contrasting with relative predominance of downwelling favourable winds (westerlies) and weak seasonality of upwelling occurrence in the Cantabrian shelf. Besides, a significant long-term linear trend towards the reduction of upwelling intensity (i.e. positive slope) was detected for the meridional component. This trend was also pointed out by other authors for different periods and based also on the analysis of wind patterns (Álvarez-Salgado *et al.*, 2008; Bode *et al.*, 2009). Both components have in common the timing of the annual cycle, which present minimum values (upwelling favourable wind direction) during the summer.

The time series of upwelling thermal index (UTI) showed more neatly the contrasted characteristics of the upwelling regimes along the NIS. In Galicia, upwelling exhibits a strong seasonality and (monthly) persistence, and the probability of upwelling occurrence during the upwelling favourable (spring-summer) and non-favourable (autumn-winter) season were 80 and 20% respectively.

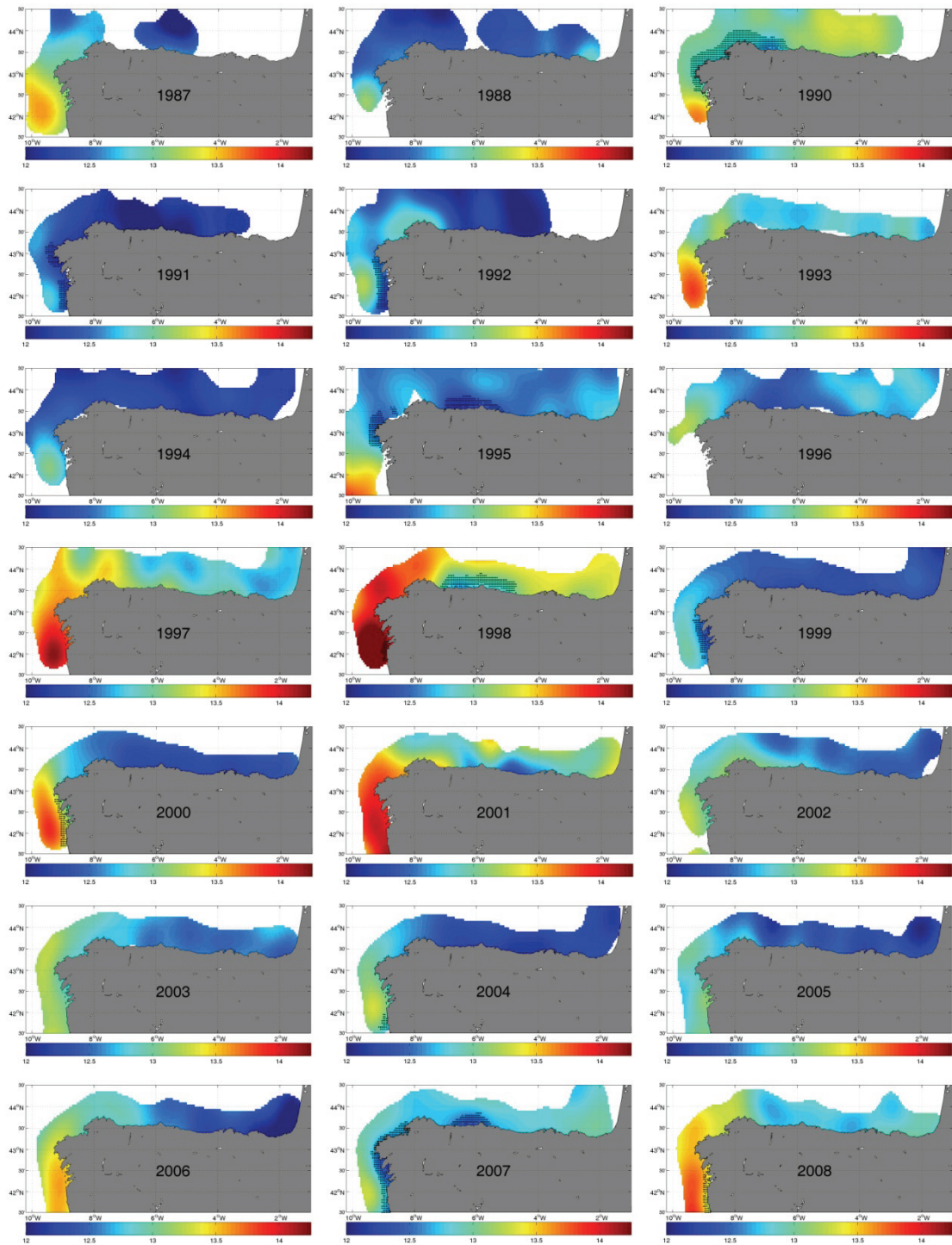


Figure 14: Interannual spatial variability of temperature measured at 50 m. The areas influenced by upwelling are enhanced using black dots.

The patterns of upwelling occurrence were similar to those provided by other authors, although the probability values were slightly higher: 60 and 30 % probability of upwelling occurrence during the upwelling and non-upwelling favorable seasons respectively according to (Alvarez *et al.*, 2008), or 65 and 25 % according to (deCastro *et al.*, 2006). In the Cantabrian shelf, the UTI indicate lower occurrence of upwelling, with relatively weak seasonality and persistence, and probability of upwelling occurrence around 50 and 20 % during spring–summer and autumn–winter respectively, values that oscillated around 25 % all the year round (Álvarez-Salgado *et al.*, 2008).

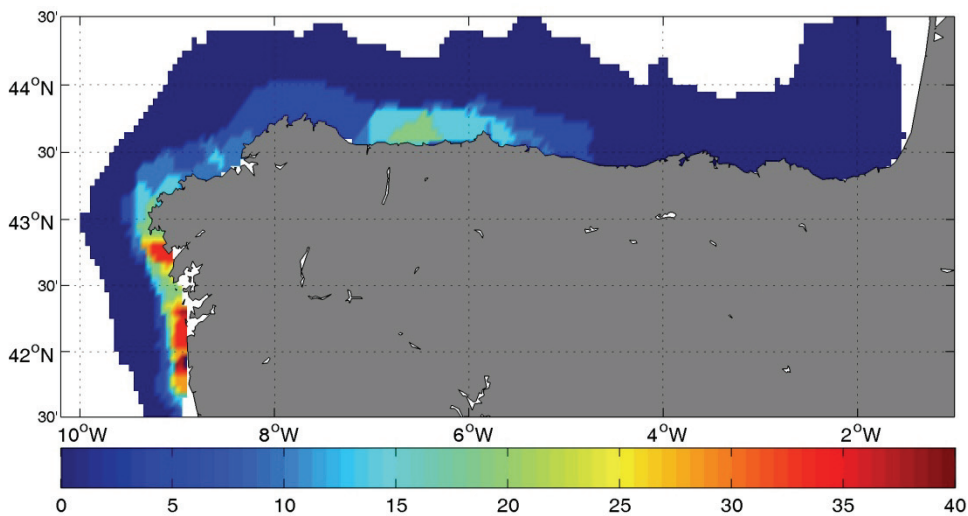


Figure 15: Spatial distribution of the probability of upwelling occurrence calculated using temperature data from the spring surveys.

General overviews about eastern boundary upwelling ecosystems pointed out the intensification of the upwelling favorable winds as a consequence of climate warming produced by greenhouse gasses (Dickson *et al.*, 1988; Bakun, 1990; Demarcq, 2009). The proposed mechanism is that the different thermal behavior of land and ocean produces the intensification of thermal lows over the continent and the concurrent intensification of upwelling favorable winds. This mechanism is probably not operating in the Western Iberian Peninsula according to recent estimations based on time series of wind data, which indicate decreasing trends in upwelling favorable winds (Álvarez-Salgado *et al.*, 2008; Bode *et al.*, 2009). Our analysis of the time series of the meridional component of the wind showed also a significant reduction of upwelling favorable winds from 1950 to 2008. The time series of the UTI did not showed, however, significant trends during the period from 1994 to 2005, apart from a marginally significant increasing trend,

which indicate the intensification of the across-shelf thermal gradient, linked to enhance coastal upwelling, off A Coruña.

Spatial patterns of upwelling along the NIS during spring

The application of the upwelling detection method to *in situ* temperature fields allowed us to discern the characteristic spatial patterns of upwelling occurrence along the NIS, during spring. This part of the year, at the beginning of the upwelling season, upwelling occurred along the Galician shelf in almost half of the analysed surveys (10 out of 22), and upwelled waters covered the whole shelf from the Rías Baixas to Cape Finisterre. In the Cantabrian Sea shelf, upwelling was detected only in 4 surveys, in the vicinity of Cape Peñas and westward. The observed spatial differences, added to the temporal ones, stress the distinct character of both shelves regard to upwelling, and suggest the consideration of each of these areas of the NIS as separate sub-regions. It is worth noting, however, that the positive correlation between the meridional and zonal components of the wind, which translates in the predominance of north-easterlies during the upwelling season along the NIS (Villarreal *et al.*, 2012), promote the intensification of upwelling westward Cape Peñas (McClain *et al.*, 1986; Gil, 2008) and the co-occurrence of upwelling along the Cantabrian and Galician shelves in 1990, 1995, 1998 and 2007.

We have also found a robust relationship between the upwelling favorable wind component and the occurrence of coastal upwelling along the NIS. The empirical model allowed us to estimate the probability of upwelling occurrence, its intensity and the area affected by upwelled waters. Accordingly, using the model it is possible to determine areas of the NIS affected by upwelling and to analyze its influence on the dynamics of pelagic and demersal habitats and communities. That is of utmost relevance for ecosystem management and spatial planning, necessary for instances for the implementation of the Marine Strategy Framework Directive within European waters.

Chapter 6: Mesozooplankton species distribution in the NW and N Iberian shelf during spring 2004: Relationship with frontal structures

Introduction

The physical environment affects the composition and structure of plankton communities, and therefore modulates ecosystem function and dynamics (Paffenhofer, 1980; Landry *et al.*, 2001). The mesozooplankton community, as a key component of the food web plankton ecosystem that channels matter and energy from the lower to the higher trophic levels (Longhurst & Harrison, 1989), is strongly controlled by the physical environment, which influence their growth, reproduction and distribution (Mauchline *et al.*, 1998). This control could propagate up and down different levels of the food web (Kiorboe *et al.*, 1988; Munk *et al.*, 1995), including different life stages of commercially important fishes stocks, such as sardine, anchovy, mackerel and horse mackerel (OSPAR, 2000).

Hydrographic conditions in the NW and N Iberian shelf (between 42 and 45°N) show a marked seasonality. Apart from the water column mixing-stratification cycle characteristic of temperate seas (Longhurst, 1998), the development and decay of a warm and saline poleward current flowing along the slope is another salient hydrographic feature. This poleward flow, named Iberian Poleward Current (IPC) (Peliz *et al.*, 2003), Portugal Coastal Counter Current (PCCC) (Ambar *et al.*, 1994; Álvarez-Salgado *et al.*, 2003) or “Navidad” (Christmas) Current (García-Soto *et al.*, 2002), is a common feature of the winter circulation of eastern ocean margins (Neshyba *et al.*, 1989). In the Iberian shelf, this narrow, upper slope trapped current develops in winter forced by the meridional density gradient, through the ‘Joint Effect of Baroclinicity and Relief’ JEBAR (Huthnance, 1984; Huthnance, 1986; Pingree & Le Cann, 1989), and decays during the spring–summer period (González-Nuevo & Nogueira, 2005; Peliz *et al.*, 2005).

The NW and N Iberian shelf is located in the intergyre zone that separates the subpolar and subtropical gyres of the North-East Atlantic (Pollard *et al.*, 1996). The subpolar gyre is the formation area of the Eastern North Atlantic Central Water Subpolar mode (ENACWsp), while to the south of the inter-gyre zone the formation of the subtropical mode of this water mass (ENACWst) (Perez *et al.*, 2001) takes place. These modes of central waters differ in their thermohaline characteristics being the subtropical, which are warmer and saltier, thus spicier (Flament, 1986), than the subpolar mode waters (Ríos *et al.*, 1992; Perez *et al.*, 1995).

(Fraga, 1981) found a sub-surface front between the subtropical and subpolar modes of ENACW off Cape Finisterre (43°N, 9°W), and were the first to suggest a poleward advection of ENACWst along the Iberian margin. Their results were later confirmed by (Perez *et al.*, 1993) using a biogeochemical approach. The presence of relatively warm and salty waters off NW Iberia has been noted since then by different authors (Pingree &

Le Cann, 1990; Ríos *et al.*, 1992). These spicy waters enter into the Southern Bay of Biscay moving eastward along the Cantabrian continental shelf and slope (Pingree & Le Cann, 1992b; Bode *et al.*, 2002b; Garcia-Soto *et al.*, 2002).

Several studies have focused on the influence of the Poleward current on phytoplankton and mesozooplankton biomass and on metabolic rates, both off NW Spain (Castro *et al.*, 1997; Álvarez-Salgado *et al.*, 2003; Huskin *et al.*, 2003; Isla & Anadon, 2004) and in the central Cantabrian Sea (Fernández & Bode, 1991; Cabal, 1993; Fernandez *et al.*, 1993). However, information on the mesozooplankton community composition and distribution remains limited (Cabal, 1993; Blanco-Bercial *et al.*, 2006). Besides, most of the studies on mesozooplankton composition in the southern Bay of Biscay were restricted to local (e. g. Alvarez-Marqués, 1980; Valdés *et al.*, 1991; Cabal, 1993; Villate *et al.*, 2004) or meso-scales (e. g. Barquero *et al.*, 1998a; Blanco-Bercial *et al.*, 2006).

Here, we present the results on mesozooplankton species distribution and its relationship with the physical environment from the data acquired during the PELACUS-0404 cruise, conducted in the continental shelf of the NW and N Iberian Peninsula between March 30 and April 22 of 2004. As far as we know, this is the first comprehensive study on the distribution of mesozooplankton during spring covering the entire northern Spanish shelf, from Galicia up to the French border.

Materials and methods

A total of 98 CTD (conductivity–temperature– depth–fluorescence) casts were recorded all along the NW and N Iberian shelf in the PELACUS-0404 cruise (30 March–22 April) with a SeaBird 25 CTD probe with a SeaTech fluorometer. Water column density was derived from temperature and salinity records (UNESCO, 1983). The mixed layer depth (MLD) was calculated using a density gradient criterion of 0.01 m^{-1} (Kara *et al.*, 2000). Fluorescence measurements were transformed into chlorophyll a (Chl a) concentration (mg m^{-3}) according to the fluorescence/Chl a relationships obtained during the cruise ($\text{Chl a} = 0.80 \times \text{Fluorescence} - 0.11$; $n = 296$, $r = 0.81$, $p < 0.001$). For mapping the distribution of thermohaline characteristics and Chl a, we have applied an objective interpolation method (Haagenson, 1982) using a Gaussian variogram model (signal to noise ratio = 0.11, and correlation scale coefficient = 40 km).

In order to locate the frontal area that defines the limit of influence of the IPC, which separates bodies of water that are subject to distinct influence of the Subtropical and Subpolar modes of Eastern North Atlantic Central Water (ENACW_{sp} and ENACW_{st} respectively), we analyzed the change in the slope of the along-shelf transect of sub-surface (average values in the 70–80 m depth layer) spiciness (Flament, 1986; Flament,

2002), according to the method proposed by González-Nuevo and Nogueira (2005). Otherwise, to define frontal areas associated with freshwater inputs we have used salinity data at 5 m and 10 m depth to determine the limit of influence of river plumes. These salinity data were interpolated using objective functions for a grid with 0.1 degrees. These frontal areas associated to river plumes were defined by a difference of 0.15 salinity units in 10 nautical miles (nm).

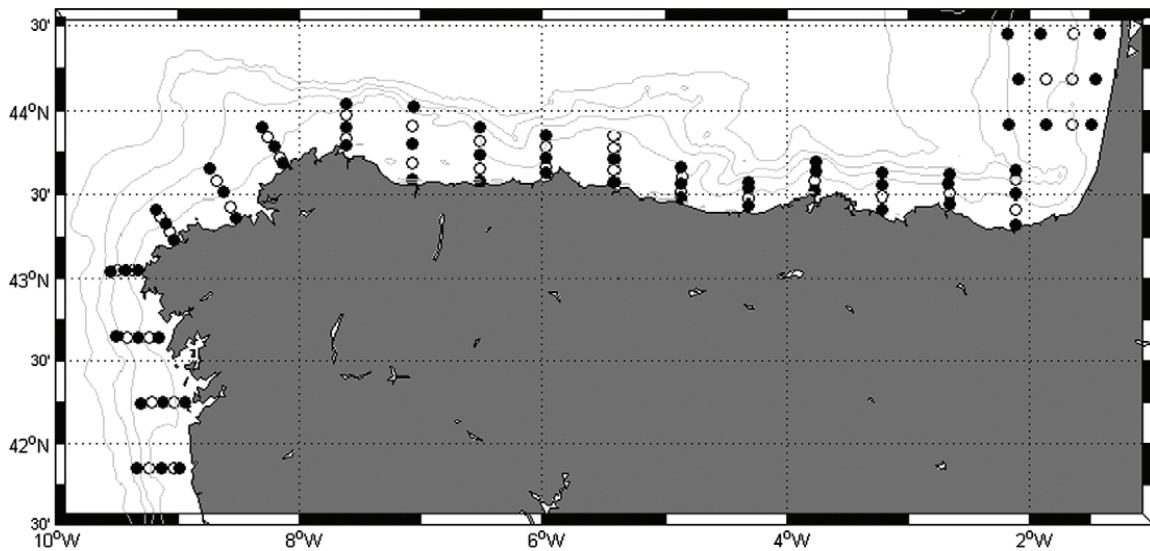


Figure 1. Position of the hydrographical and biological sampling stations during the PELACUS 0404 cruise (black dots are biological and hydrographical stations, white dots are hydrographical stations).

Mesozooplankton samples were taken by means of vertical hauls from 100 m depth, or from 5 m above the bottom in shallower stations, up to the surface in 61 out of the 98 hydrographical stations with a triple WP2 net of 200 μm mesh-size and 0.125 m^2 of mouth area (Figure 1). Samples were collected between sunset and sunrise. Samples for taxonomic analysis from one cod-end were preserved in 4% sodium borate-buffered formalin-seawater solution, and later examined under a stereomicroscope to assess the species composition and abundance. Actinopoda and Phoraminifera were not included in our taxonomic analysis, in spite of their high abundances at some locations, because our sampling method was not adequate for these groups. Similarly, the abundance data of large-sized mesozooplankton (e.g. Euphausiids and Salps) have to be considered with caution because of potential net avoidance or extremely patchy distributions. Other cod-end was used to estimate mesozooplankton fractionated biomass. Cod-end contents were immediately fractionated into three size fractions, 200–500 (small), 500–1000 (medium), and > 1000 μm (large), using sieve cups equipped with Nitex screens. Samples for biomass analysis were rinsed with 0.2 μm filtered seawater, filtered onto

pre-combusted (450 °C, 24 h), pre weighted Whatmann GF/A filters and dried at 60 °C for 24 h. The dry weight was measured with a Sartorius microbalance.

In order to group stations with similar composition of mesozooplankton species, we performed a cluster analysis on the \log_{10} (species abundance + 1) mesozooplankton abundance data, using the Ward's method on the Euclidean distance matrix. Rare species (those present in less than 10% of the samples) were excluded for the analysis. ANOVA and a posteriori Student–Newman–Keuls test (Keuls, 1952) were used to assess the significance of the difference between cluster groups. SPSS + PC and Statistica packages were used for statistical data analysis.

Mantel and partial Mantel correlations among physical, biological and space matrices were calculated to assess the relationship between the biological (response) and physical (explanatory) variables taking into account the common spatial structure (Legendre & Legendre, 1998; Legendre *et al.*, 2005). Both for the physical and the mesozooplankton data, the respective distance matrices were defined assigning 1 when two stations belong to the same physical domain or mesozooplankton cluster, and 0 when two stations belong to different domains or clusters respectively. The spatial matrix was defined as the geographic (i.e. Euclidian) distance among the sampling stations.

Results

Physical characterization

Hydrographic conditions in the southern Bay of Biscay during spring 2004 differed markedly along the shelf, allowing us to differentiate three distinct hydrographic regions. The westernmost part of the shelf (WC region) was characterized by relatively warm (> 13 °C) and salty (> 35.65), thus spicy, waters that denote the presence of ENACW_{st} advected by the Iberian Poleward Current (Figure 2). At the extreme of the sampled area, in the cul-de-sac of the Bay of Biscay (EC region), colder and fresher water was found (< 12.5 °C and < 35.5 respectively) due to the influence of ENACW_{sp} and the continental inputs from the Adour river in the French coast (Figure 2 and 3). In between these two zones, we observed a transitional area in the Central Cantabrian Sea (CC region), where thermohaline conditions were intermediate between these two extremes. In this region it is also noticeable the influence of freshwater discharges from the small Cantabrian rivers. The river plumes associated to these discharges affect only the upper layers (< 10 m depth) of the water column (Figure 3a).

The separation between the WC and CC regions takes place by a neat frontal area, located around Cape Estaca de Bares (7°W), associated with the limit of influence of the

IPC, while the CC and EC regions are separated also by a frontal area located around Cape Machichaco (3°W) that in this case was related with the limit of influence of the Adour river plume (Figure 3b). The mixing regime in these areas was also different according to the criterion used to define the MLD (Figure 4). The WC region was characterized by a mixed water column, whereas in the EC region the river discharges produces stratification of the upper meters of the water column (< 10 m). In the CC region, we found a distinct vertical mixing regime that separated coastal (stratification) from shelf (mixed water column) stations, giving rise to a notorious across-shelf front (Figure 4).

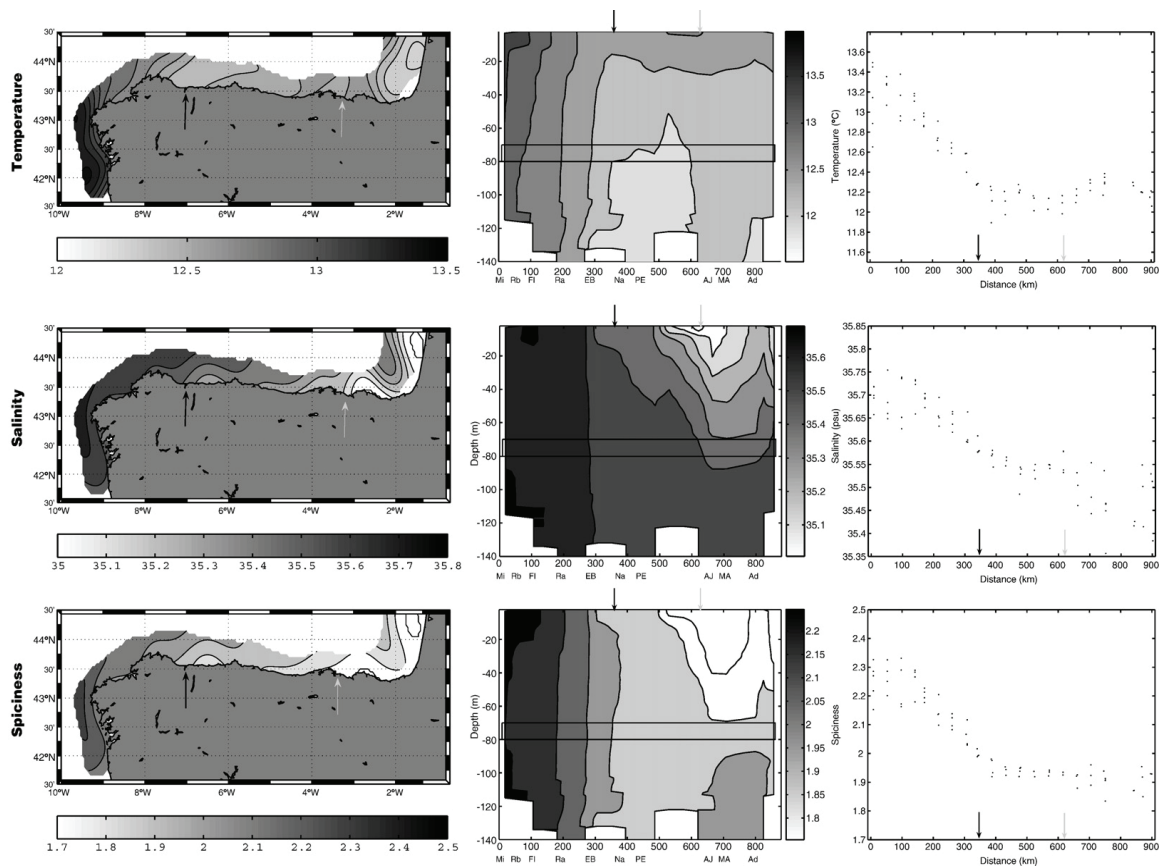


Figure 2. Spatial (left), vertical (centre) and 70–80 m integrated (right) distributions of temperature, salinity and spiciness. The black arrow represents the limit of influence of spicy waters (IPC_i) and the grey arrow the limit of influence of the Adour river plume.

Biological variables: phytoplankton biomass and mesozooplankton biomass and species composition

Spatial distribution of 50 m integrated chlorophyll a (Figure 5) showed maximum values in the shelf-edges located between the WC and the CC regions, and in the northern part of the EC region, associated with the limit of influence of the IPC and the river plume from

the Adour river respectively. A spot of high concentration was also found at the coast in the southernmost part of the sampling area (around 42°N). Phytoplankton biomass at 10 m and 30 m depth was low ($< 1.5 \text{ mg m}^{-3}$) all along the coast, except in the southernmost stations, in the proximity of the frontal area that separates the WC and the CC regions, and in the across-shelf front located in the EC region, where chlorophyll a concentration was $4\text{--}5 \text{ mg m}^{-3}$.

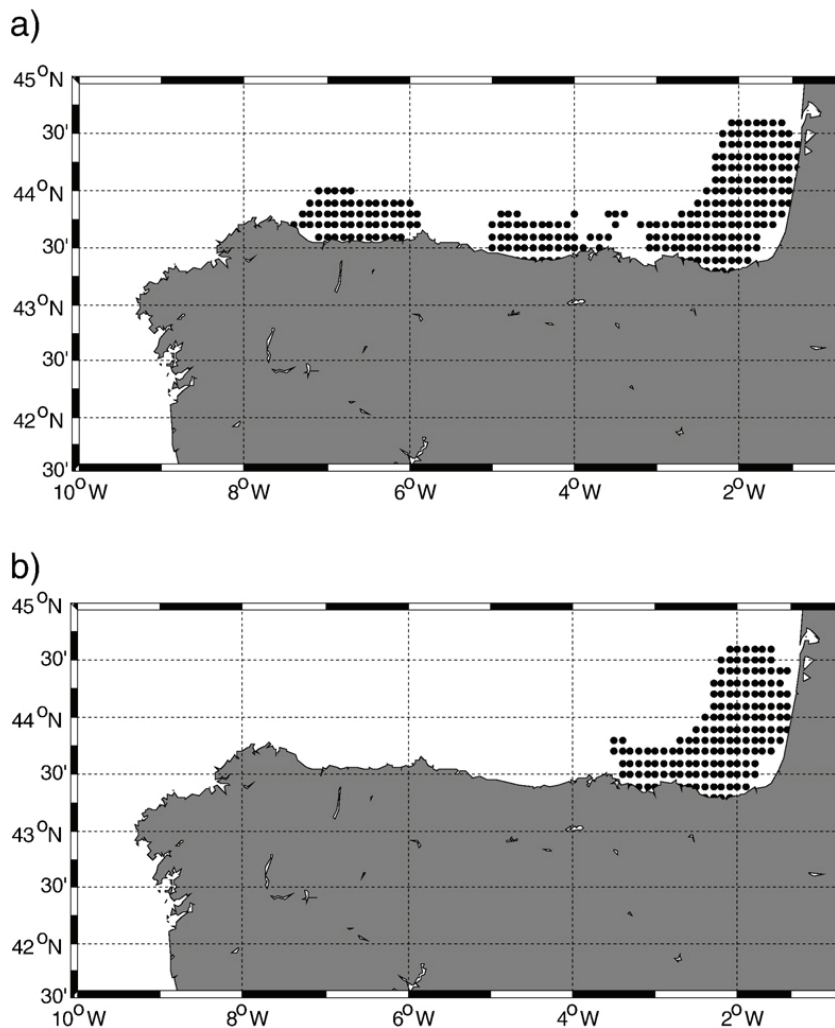


Figure 3. Distribution of the influence of river plumes for a) 5 m and b) 10 m.

Mesozooplankton community was dominated by the small-sized fraction ($200\text{--}500 \mu\text{m}$) (Figure 6a), which all along the shelf attained average values around 15 mg m^{-3} respectively, thus contributing around 50% to total biomass averaged for the whole sampling area (Figure 6d). The maximum values for this fraction (around 40 mg m^{-3}) were found in the proximity of the frontal areas associated with the limit of influence of the IPC and the river plume from the Adour river, and also in the CC region off Cape Peñas (around

6°W) (Figure 6a). The contribution of the medium and large-sized fraction (Figure 6b and c respectively) to total mesozooplankton biomass averaged for the whole area was of the same magnitude (about 25% each), although high biomass values were found in a spot located in the southernmost part of the sampling area (around 42°N), where biomass in the medium and large-sized fraction reached values around 40 mg m⁻³ each. In this spot, where also chlorophyll a concentration was high (150 mg m⁻²), total mesozooplankton biomass attained the highest values of the whole sampled area (around 140 mg m⁻³).

Mesozooplankton abundance varied between $2.4 \cdot 10^4$ and $50 \cdot 10^4$ individuals m⁻². A total of 107 mesozooplankton taxa were found, of which 63 were retained for further analysis (Table 1). Holoplankton organisms are the major constituent of mesozooplankton taxa, despite the high relative abundance of meroplankton organisms (cirripedia, echinodermata and gastropoda larvae) in coastal areas.

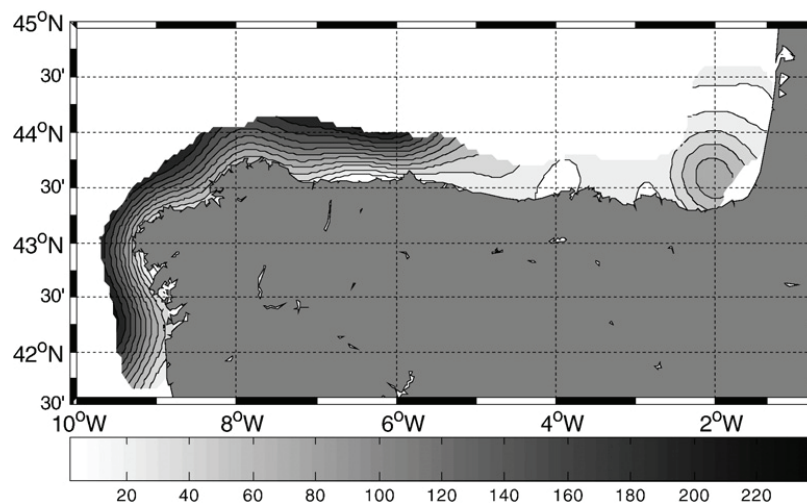


Figure 4. Spatial distribution of mix layer depth (MLD).

Cluster analysis on the mesozooplankton species abundance matrix ($\log(\text{individuals m}^{-2} + 1)$) allowed us to discriminate three major (distance level 50%) groups of stations (Figure 7, insert): cluster groups A, B and C (Table 1). These cluster groups matched the zonation based on hydrographic conditions. Group A corresponded with the WC region, characterized by the presence of the IPC; group B, with the transitional CC region; while group C related to the EC region, where colder and fresher water was found. The Mantel analysis of the relationship among the matrices that define the physical domains, the zooplankton clusters and the spatial structure are shown in Table 2. The simple Mantel correlations were highly significant ($p < 0.001$) for all the possible pairs of

matrices, although the highest correlation corresponded to the pair physical-mesozooplankton ($r = 0.70$, $p < 0.001$, $n = 63$). However, when the effect of the common spatial structure is taken into account (partial Mantel correlations, Table 2), only the physical mesozooplankton relationship remains highly significant ($r = 0.56$, $p < 0.001$, $n = 63$).

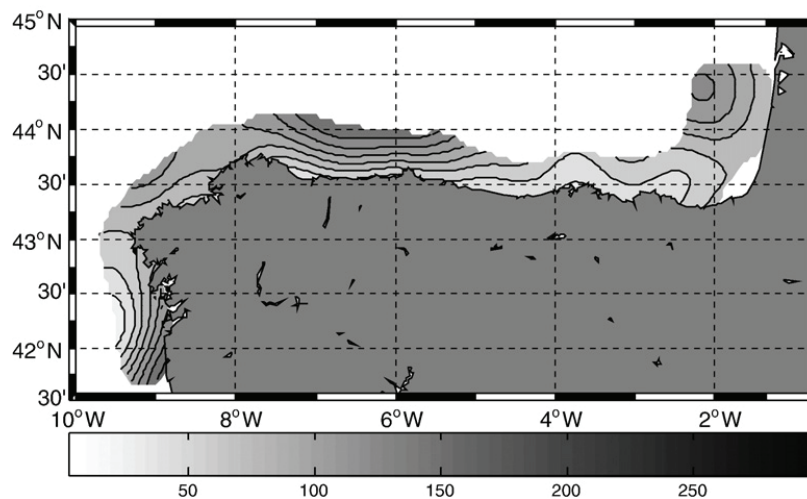


Figure 5. Spatial distribution of chlorophyll a integrated for the first 50 m of the water column (mg m^{-2}).

In group A, *Paracalanus parvus* (24.4%), *Oithona helgolandica* (14.1%), *Acartia clausi* (13.7%), *Clausocalanus pergens* (7.8%), *Pseudocalanus elongatus* (2.3%), *Ctenocalanus vanus* (2.1%), and larva of Cirripedia (2.8%) were the dominant species. Group B share with group A these dominant species, but with different relative abundance (*A. clausi* 20.5%, *O. helgolandica* 18.8%, *P. parvus* 16.9%, *P. elongatus* 4.7%, *C. pergens* 3.6%) and also the distinctive relative high abundance of *Calanus helgolandicus* (2.1%), *C. arcuicornis* (2%), *C. lividus* (2.2%), larvaceans (*O. fusiformis* 2.4%, *O. longicauda* 1.9% and *F. pelucida* 4.5%) and cladocerans (*Evadne nordmanni* 1.4% and *Podon intermedius* 1.9%). Group C was defined by the dominance of *Noctiluca scintillans* (45%) coupled with relative high abundances of *O. helgolandica* (10.2%), *Oncaea media* (6.9%), *Temora longicornis* (3.60%), *Ditrichocorycaeus anglicus* (0.7%), and the presence of species as *P. parvus* (3.9%), *A. clausi* (3.3%) and *F. pelucida* (3.3%) (Table 1).

The distribution of values of the environmental variables (temperature, salinity and spiciness) for each of these groups is shown in Figure 8.

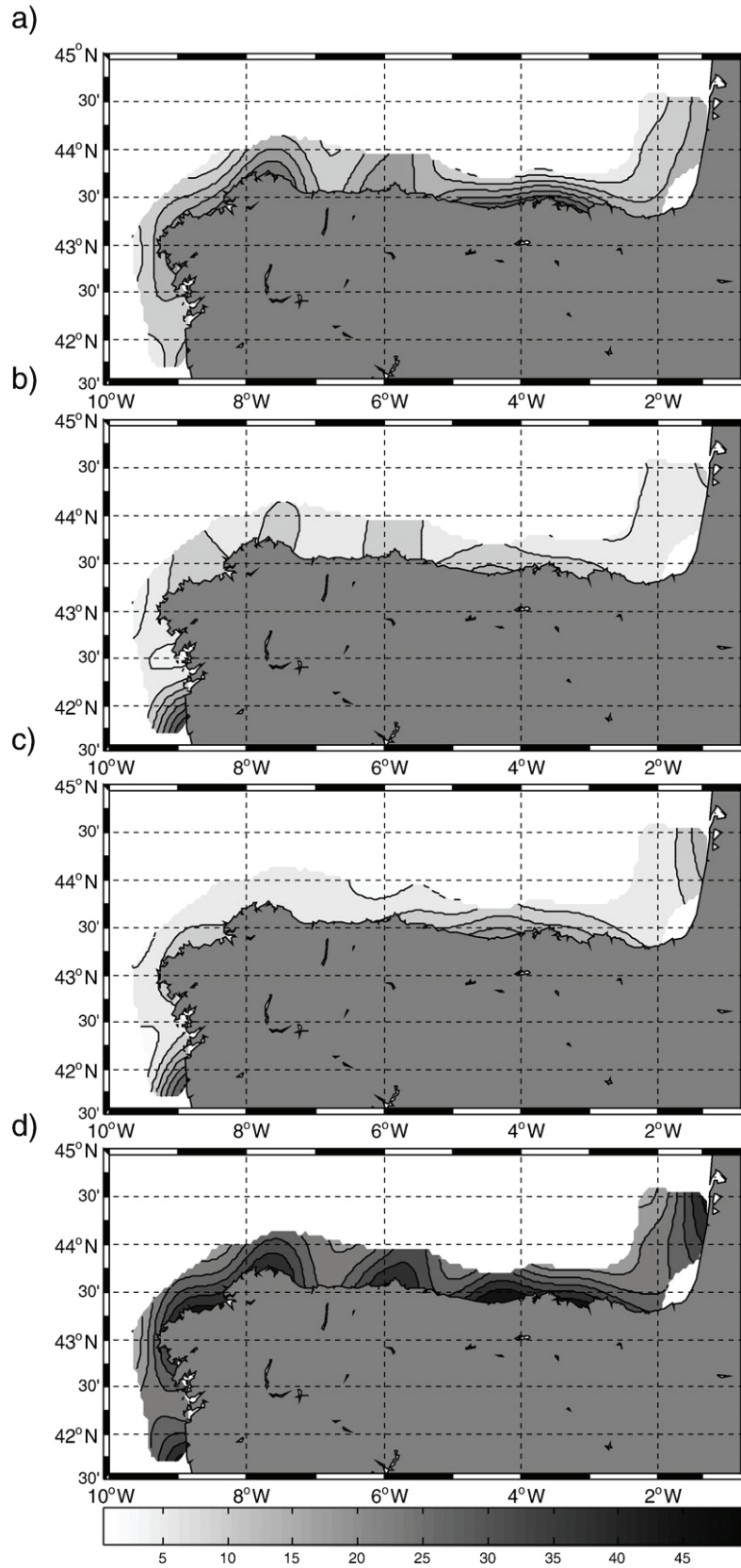


Figure 6. Spatial distribution of mesozooplankton size fractionated biomass (mg m^{-3}): a) 200–500 μm size fraction, b) 500–1000 μm size fraction, c) 1000–2000 μm size fraction and d) total biomass.

Table 1: Mean (number m⁻²) abundance of zooplankton taxa in each group, between brackets percentage of presence in the samples of each group. White spaces indicate species that were not included in the distance matrix. Comparison of variables between cluster groups (A, B, C) according to a multiple range SNK test (Note “>” significance (p>0.05) difference, “=” and “n.s.” non-significance (p>0.05) difference).

Group	Taxon	Cluster A	Cluster B	Cluster C	SNK
Copepods	<i>Rhincalanus nasutus</i>				
	<i>Calanus helgolandicus</i>	1780 (96)	4157 (94)	2848 (100)	n.s.
	<i>Mesocalanus tenuicornis</i>	974 (96)	1640 (94)	1715 (71)	n.s.
	<i>Calanoides carinatus</i>	1108 (96)	1163 (88)	733 (94)	A=B>C
	<i>Neocalanus gracilis</i>	69 (11)	515 (19)	344 (24)	n.s.
	<i>Nannocalanus minor</i>				
	<i>Subeucalanus elongatus</i>				
	<i>Subeucalanus monachus</i>	0 (0)	207 (13)	0 (0)	C>A=B
	<i>Ischnocalanus tenuis</i>				
	<i>Paracalanus parvus</i>	49979 (100)	33775 (100)	8393 (100)	A=B>C
	<i>Calocalanus contractus</i>	1078 (18)	1061 (19)	0 (0)	n.s.
	<i>Calocalanus styliremis</i>	2371 (89)	3694 (88)	1507 (71)	n.s.
	<i>Pseudocalanus elongatus</i>	4746 (93)	9425 (100)	1506 (88)	B>A>C
	<i>Clausocalanus arcuicornis</i>	2650 (93)	4095 (100)	2057 (82)	B>C
	<i>Clausocalanus farrani</i>	646 (25)	3820 (6)	0 (0)	n.s.
	<i>Clausocalanus jobei</i>	1106 (7)	359 (13)	669 (29)	n.s.
	<i>Clausocalanus lividus</i>	1416 (93)	4333 (81)	1181 (88)	n.s.
	<i>Clausocalanus paululus</i>	700 (14)	668 (6)	1592 (6)	n.s.
	<i>Clausocalanus pergens</i>	16082 (96)	7272 (100)	1872 (76)	A>B>C
	<i>Ctenocalanus vanus</i>	4245 (100)	4628 (100)	3958 (88)	A=B>C
	<i>Aetideus armatus</i>	62 (14)	272 (44)	66 (35)	B>A=C
	<i>Euchirella rostrata</i>				
	<i>Euchirella curticauda</i>				
	<i>Euchaeta hebes</i>	1082 (96)	799 (81)	645 (65)	A>B=C
	<i>Paraeuchaeta norvegica</i>				
	<i>Paraeuchaeta tonsa</i>				
	<i>Phaenna spinifera</i>	914 (18)	1124 (25)	0 (0)	n.s.
	<i>Scolecithrix ovata</i>	7 (4)	318 (6)	301 (24)	n.s.
	<i>Scolecithricella bradyi</i>				
	<i>Diaxis pigmea</i>				
	<i>Diaxis hibernica</i>	674 (11)	292 (19)	465 (18)	n.s.
	<i>Temora longicornis</i>	1098 (36)	621 (25)	7842 (100)	C>A=B
	<i>Temora stylifera</i>	0 (0)	191 (13)	205 (24)	n.s.
	<i>Heterorhabdus robustus</i>				
	<i>Heterorhabdus papilliger</i>				
	<i>Heterostylites longicornis</i>				
	<i>Metridia lucens</i>	595 (86)	1317 (88)	938 (76)	n.s.
	<i>Pleuromamma gracilis</i>	366 (36)	284 (56)	308 (35)	n.s.
	<i>Pleuromamma robusta</i>				
	<i>Pleuromamma abdominalis</i>				
	<i>Centropages chierchiae</i>	2311 (96)	1241 (75)	249 (65)	A>B=C
	<i>Centropages typicus</i>	711 (43)	799 (81)	214 (35)	B>A=C
	<i>Isias clavipes</i>				
	<i>Candacia armata</i>	293 (21)	540 (69)	321 (71)	B>A=C
	<i>Anomalocera pãtersoni</i>				
	<i>Acartia clausi</i>	28041 (100)	41074 (88)	7224 (94)	A=B>C
	<i>Oithona helgolandica</i>	28886 (100)	37646 (94)	22277 (100)	A=B>C
	<i>Oithona plumifera</i>	1042 (25)	1924 (75)	914 (29)	B>A=C
	<i>Oithona nana</i>				
	<i>Microsetella rosea</i>	840 (29)	1716 (50)	419 (71)	n.s.
	<i>Microsetella novergica</i>				
	<i>Euterpina acutifrons</i>	921 (25)	359 (6)	852 (47)	n.s.
	<i>Clitemnestra rostrata</i>				
<i>Oncaea media</i>	1491 (43)	2368 (88)	14995 (94)	C>A=B	

	<i>Oncaea subtilis</i>				
	<i>Ditrichocorycaeus anglicus</i>	668 (4)	509 (19)	1510 (94)	C>A=B
	<i>Ditrichocorycaeus brehmi</i>				
	<i>Sapphirina angusta</i>				
	Copepod nauplii	2306 (64)	1114 (69)	1340 (76)	n.s.
Other holoplankton	<i>Noctiluca scillitans</i>	0 (0)	398 (6)	97998 (100)	C>A=B
	Flatworms				
	<i>Hydromedusae</i>	682 (11)	749 (56)	344 (29)	B>A=C
	<i>Podocoryne spp.</i>				
	<i>Solmundella bitentaculata</i>				
	<i>Obelia spp.</i>				
	<i>Liriope spp.</i>				
	<i>Siiphonophora Calicophora</i>	336 (25)	1430 (100)	3229 (100)	C>B>A
	<i>Beroe cucumis</i>				
	<i>Ctenophora larvae</i>	68 (7)	979 (19)	368 (35)	n.s.
	<i>Pteropoda</i>	103 (14)	64 (6)	0 (0)	n.s.
	<i>Tomopteris helgolandica</i>	72 (4)	356 (19)	849 (18)	n.s.
	<i>Podon intermedius</i>	1617 (36)	3919 (94)	1896 (59)	B>A=C
	<i>Evadne nordmanni</i>	1094 (25)	2783 (94)	2049 (88)	C>A=B
	<i>Evadne spinifera</i>	0 (0)	438 (19)	716 (6)	n.s.
	<i>Ostracoda</i>	0 (0)	519 (31)	52 (12)	B>A=C
	<i>Nauplius of Euphausiacea</i>				
	<i>Calyptopis larvae</i>	772 (54)	544 (44)	493 (88)	n.s.
	<i>Furcilia Larvae</i>				
	<i>Meganyctiphanes norvegica</i>	503 (68)	550 (81)	597 (76)	n.s.
	<i>Stylocheiron</i>				
	<i>Tessarabrachion oculatum</i>				
	<i>Thysanoessa viana</i>				
	<i>Mysidacea</i>	322 (25)	46 (13)	426 (41)	C>A=B
	<i>Amphipoda</i>				
	<i>Isopoda (Microniscus)</i>				
	<i>Sagitta spp.</i>	72 (7)	299 (25)	292 (88)	C>A=B
	<i>Salpa fusiformis</i>	143 (21)	0 (0)	0 (0)	n.s.
	<i>Pegea coeferata</i>				
	<i>Doliolida</i>	0 (0)	189 (13)	141 (18)	n.s.
	<i>Oikopleura fusiformis</i>	1632 (68)	4750 (81)	2231 (76)	B>C
	<i>Oikopleura longicauda</i>	3641 (50)	3913 (56)	2766 (47)	n.s.
	<i>Fritilaria borealis</i>	0 (0)	0 (0)	609 (18)	n.s.
	<i>Fritilaria pelucida</i>	1695 (7)	8903 (94)	7206 (71)	B=C>A
	<i>Brachiostoma lanceolatum</i>	0 (0)	0 (0)	427 (71)	n.s.
Meroplankton	Gastropoda larvae	733 (39)	740 (69)	682 (88)	n.s.
	Bivalvia larvae	716 (4)	597 (31)	477 (41)	n.s.
	Nemertea larvae				
	Polychaeta larvae	586 (21)	372 (31)	465 (35)	n.s.
	Ceriantharia larvae				
	Ectoprocta larvae				
	Cirripedia larvae	5788 (71)	1081 (56)	558 (65)	n.s.
	Decapoda larvae	265 (86)	503 (88)	434 (76)	n.s.
	Echinodermata larvae	843 (43)	568 (56)	1092 (94)	C>A=B
	Anchovise eggs				
	Sardine eggs				
	Fish eggs				
	Fish larvae				

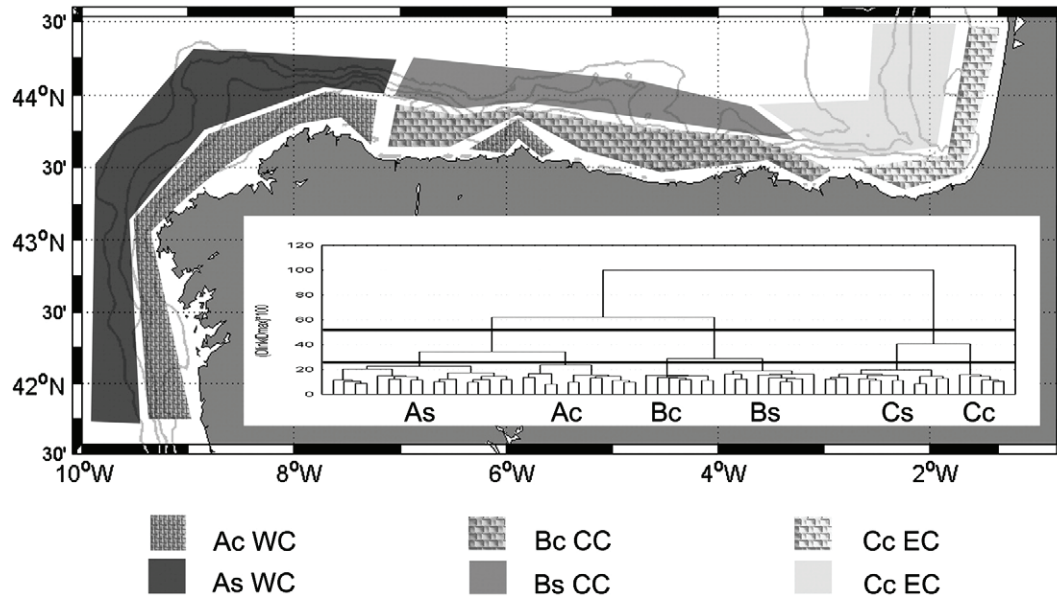


Figure 7. Geographical distribution of station groups (A, B, and C, 'c' and 's' subscript refer to coastal or shelf station) defined by cluster analysis (insert graph) on mesozooplankton species composition. WC, CC and EC refer to the zonation based on hydrography.

Groups differed significantly in temperature a 10 m ($F_{2,60} = 25.089$; $p < 0.001$), 30 m ($F_{2,59} = 28.259$; $p < 0.001$) and 70 m ($F_{2,40} = 38.675$; $p < 0.001$), which were ranked A N B=C by the post hoc SNK test. Salinities were significantly different a 10 m ($F_{2,60} = 43.214$; $p < 0.001$), 30 m ($F_{2,59} = 47.637$; $p < 0.001$) and 70 m ($F_{2,40} = 73.229$; $p < 0.001$), resulting in the rank A > B > C. Spiciness were also significantly different ($p < 0.001$) among these three groups at 10 m, 30 m and 70 m ($F_{2,60} = 54.292$; $F_{2,59} = 55.246$; $F_{2,40} = 72.043$), resulting in a rank at 10 m and 30 m A > B > C and at 70 m, A > B = C. In summary, the group A presented the highest values of temperature, salinity and spiciness at all the depths; group C presented the lowest values of salinity; while group B was characterized by temperature and spiciness equals to C (lower than A) and salinity with intermediate values between A and C.

Table 2: Mantel analysis of the relationship between matrices representing physical variables, zooplankton distribution and space.

	Space	Physical	Mesozooplankto
Space	—	0.57*	0.58*
Physical	0.27	—	0.70*
Mesozooplankto	0.31	0.56*	—

Above the diagonal: simple Mantel test statistics; below diagonal: partial Mantel statistics controlling for the effect of the third matrix.

Each of the cluster groups could be further sub-divided (distance level 25%, Figure 7 insert) in two sub-groups that separate coastal and shelf stations. The sub-division of each of

the major groups in a coastal and shelf sub-groups ('c' and 's' respectively) reflects the higher species densities found in the shelf that environment in the coastal. Thus, the coastal sub-groups showed higher relative abundance of neritic species such as *A. clausi*, *Evadne nordmanni*, *P. intermedius* and meroplankton larvae (e.g. Cirripedia), while the shelf sub-groups showed the presence of oceanic or mesopelagic indicator species, such as *Mesocalanus tenuicornis*, *Metridia lucens*, *Pleuromamma gracilis* and *Diaxis hibernica*. The sub-groups presented significantly differences between the mean values of temperature, salinity and spiciness for the different depths (Table 3). Thus, subgroup Ac had low values of surface (10 m) temperature and salinity than sub-group As, but presented the same values at 30 m. Sub-group Bc did not present significantly differences of temperature with Bs at any of the analyzed depths. Salinity at the surface was always lower in the 'coastal' (Ac, Bc, Cc) than in the 'shelf' sub-groups (As, Bs, Cs. In the case of the Cc, the values of temperature were equal to those of Cs, while salinity in the coast was lower than in the shelf at 10 and 30 m depth.

Discussion

The study showed the spatial coherence between the main hydrographic features off the N-NW Iberian shelf and the composition of the mesozooplankton community in spring. The main hydrographic features that modulate the regional scale distribution of thermohaline properties in this area during the spring of 2004 were the progression of the seasonal thermocline, the intrusion of ENACW_{st} into the Cantabrian Sea advected by the IPC, and the presence of river plumes generated by enhanced river flows due to spring precipitations and melting of the winter snow. The areas of distribution of the 3 groups obtained by the cluster on the mesozooplankton species composition matched the physical zonation. The group A was found in the area of influence of the IPC (WC), the group C was related to the Adour River plume (EC). Between these two distinctive areas, group B corresponded with the Central Cantabrian (CC) Sea region, which is a transition area influenced by both the IPC and the plume from the Adour but also by local river discharges from small Cantabrian rivers. The Mantel analysis supported a causal model according to which the distribution of zooplankton is controlled by the hydrographic environment, and not by the common spatial structure of these two variables (Legendre, 1993).

Biomass of mesozooplankton was relatively high in relation to previous studies (Valdés *et al.*, 1991; Cabal & Alvarez-Marqués, 1995; Villate *et al.*, 2004), and was dominated by small-sized organism. These high values of biomass of mesozooplankton in the small size fraction, the low values of phytoplankton biomass and the mix of the water column (MLD), show a situation of post-bloom in the study area during the cruise PELACUS

0404, except in the areas where chlorophyll a concentration was high (around 5 mg m⁻³) localized in the southernmost stations, in the across-shelf front located in the EC region and in the proximity of the frontal area that separates the WC and the CC regions. These maximum were related to continental freshwater inputs, which in turn influence local currents and salinity patterns allowing a stratification of the water columns that produces a bloom of phytoplankton, and to frontal systems linked to intrusions of saline waters. These types of processes were described in previous works in this area (Fernández & Bode, 1991; Fernandez et al., 1993; Fernández & Bode, 1994) Small sized copepods (200–500 µm) were very abundant in the area of study, (Figure 6A and Table 1). This size fraction was constituted in the WC and CC region mainly by widespread copepod species such as *O. helgolandica*, *P. parvus* and *A. clausi*, while in the EC region were more abundant *O. media* and *O. helgolandica*. Species such as *A. clausi*, *O. helgolandica* and *O. media* are linked to coastal spring bloom (Turner & Graneli, 1992; Atkinson & Shreeve, 1995), but could also feed on small phytoplankton and they were present in great number. Head *et al.* (2002) also found that communities dominated by *Oithona spp.* and *Oncaea spp.* wherever flagellates and picoplankton accounted for 86% of phytoplankton biomass. *A. clausi* showed higher values of abundance in coastal areas than in the shelf areas, and could be a characteristic species of the environment with a wide range of variation in salinity (Rodríguez *et al.*, 1985; Paffenhofer & Stearns, 1988). Opportunistic species (such as *T. stylifera*, *O. media* and *D. anglicus*) have advantage if the environment changes towards stratification conditions whereas other species characteristic of cold waters and blooms of phytoplankton formed by largesized cells are in clear disadvantage if this type of change occurs.

Large-sized copepod Calanidae (*C. helgolandicus* and *C. carinatus*) linked to high phytoplankton concentrations were more abundant in the CC region. These species are considered residents in the northern Iberian shelf with two types of overwintering strategies (diapause at deep waters and reside in the coast waters during the winter) (Cabal, 1993) and that can take advantage of spring blooms in temperate latitudes (Laabir *et al.*, 1998; Weikert *et al.*, 2001; Bonnet *et al.*, 2005), responding with high reproductive activity. Mesozooplankton composition are also affected by topography, the shelf of the N-NW Iberian Peninsula is very narrow, so shelf edge or even oceanic species may penetrates into coastal area and mix with neritic species. In fact the near shore presence of species with deep and oceanic affinity has been reported in several studies (Valdés *et al.*, 1991; Cabal, 1993; Villate *et al.*, 2004). Thus the penetration of such water masses might account for the occasional occurrence of species as other copepod *M. lucens*, *P. gracilis* and *D. hibernica* in the coastal area

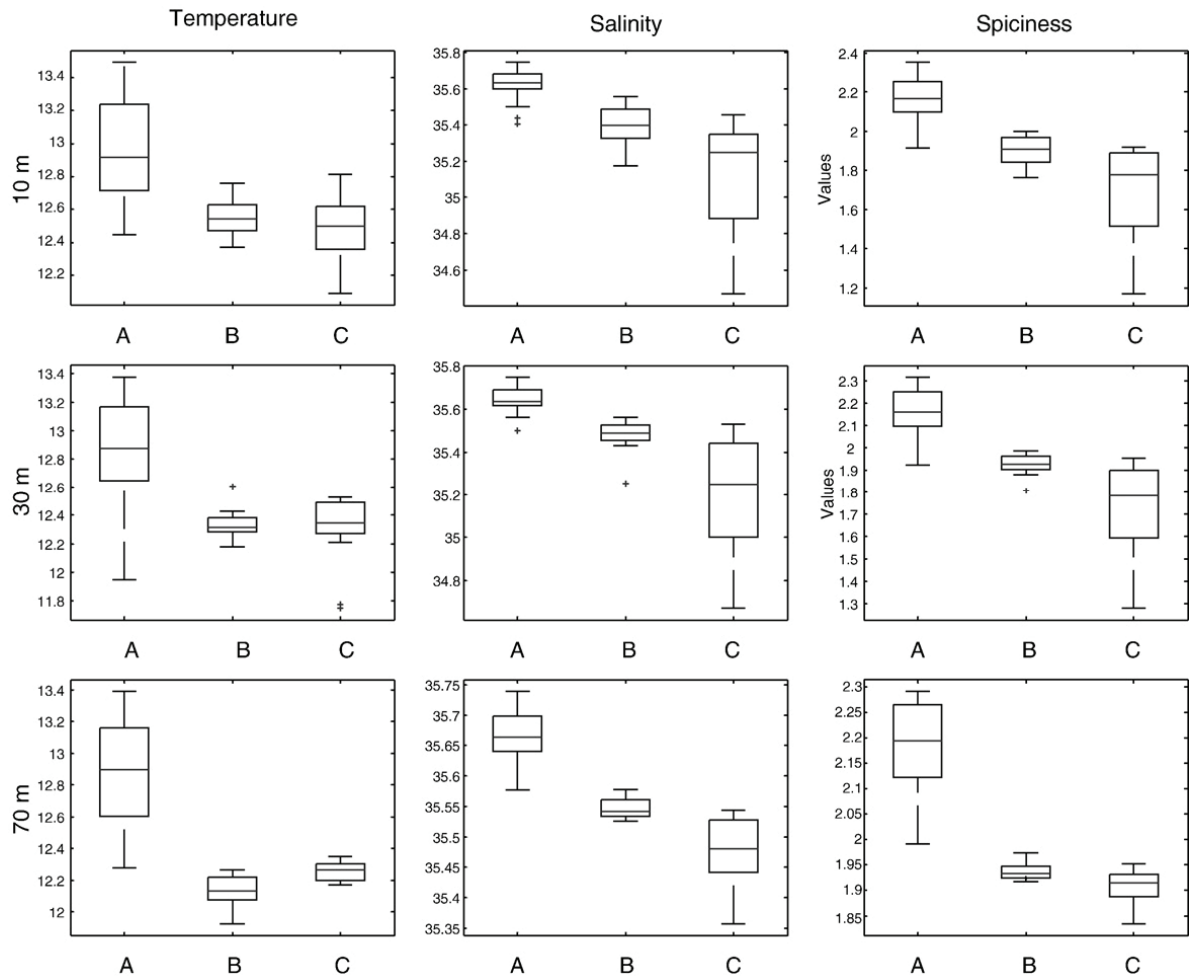


Figure 8. Box and whiskers representation of temperature, salinity and spiciness at 10 m, 30 m and 70 for the groups of stations (A, B and C) obtained from the cluster analysis on mesozooplankton data. The box has lines at the lower quartile, median and upper quartile values and the whiskers represent 1.5* inter-quartile range.

Table 3: Mean and standard error, F of the ANOVA test and SNK post hoc analysis. Note: ">" significance ($p < 0.05$) difference, "=" non-significance ($p > 0.05$) difference for the different clusters using temperature, salinity and chlorophyll a variables.

Variable	Depth	As	Ac	Bs	Bc	Cs	Cc	Total	F	SNK
Temperature	10	13,06 ± 0,07	12,79 ± 0,08	12,51 ± 0,03	12,57 ± 0,04	12,53 ± 0,05	12,41 ± 0,09	12,72 ± 0,04	25,09	$A_s > A_c > B_s = B_c = C_s = C_c$
	30	12,99 ± 0,08	12,68 ± 0,11	12,33 ± 0,03	12,34 ± 0,04	12,37 ± 0,03	12,14 ± 0,16	12,57 ± 0,05	28,26	$A_s > A_c > B_s = B_c = C_s = C_c$
Salinity	10	35,67 ± 0,01	35,55 ± 0,02	35,46 ± 0,03	35,33 ± 0,04	35,28 ± 0,05	34,73 ± 0,09	35,42 ± 0,04	43,21	$A_s > A_c = B_s > B_c > C_s > C_c$
	30	35,68 ± 0,01	35,59 ± 0,01	35,50 ± 0,01	35,46 ± 0,03	35,34 ± 0,04	34,87 ± 0,07	35,48 ± 0,03	47,64	$A_s = A_c > B_s = B_c > C_s > C_c$
Chl-a	Integrated	103 ± 8	93 ± 13	109 ± 14	49 ± 5	91 ± 10	82 ± 9	90 ± 5	13,37	-

Table 4: Comparison of variables between cluster groups according to a multiple range SNK test (Note ">" significance ($p > 0.05$) difference, "=" non-significance ($p > 0.05$) difference).

Taxon	SNK test
<i>Paracalanus parvus</i>	As=Bs >Ac =Bc>Cs=Cc
<i>Acartia clausi</i>	Ac=Bc=Bs >As=Cs=Cc
<i>Centropages chierchiae</i>	Ac=As>Bs=Bc>Cs=Cc
<i>Pseudocalanus elongatus</i>	Ac=Bs=Bc>As=Cs=Cc
<i>Oithona helgolandica</i>	Bs>As>Ac=Cs>Bc=Cc
<i>Temora longicornis</i>	Cc>Cs>Ac>As=Bc=Bs
<i>Noctiluca scintillans</i>	Cc=Cs>As=Ac=Bs=Bc
<i>Oncaea media</i>	Cc=Cs>As=Ac=Bs=Bc
<i>Ditrichocorycaeus anglicus</i>	Cc>Cs=As=Ac=Bs=Bc
<i>Euterpina acutifrons</i>	Cc>Cs=Bs=Bc=As=Ac

The influence of the Poleward current in the NW Iberian shelf has been investigated in relation to the plankton communities distribution (Botas *et al.*, 1988; Fernandez *et al.*, 1993; Fernández & Bode, 1994; Poulet *et al.*, 1996; Bode *et al.*, 2002b), or fish populations (Sanchez & Gil, 2000). Besides, related to intrusions of IPC waters have been described the presence of subtropical species of phytoplankton (Fernández & Bode, 1994) and copepods (Cabal, 1993) in the central Cantabrian sea. In the present study, several species that were not very abundant in the samples, but its relative distribution concerns them an indicator character. *Clausocalanus farrani*, *Phaenna spinifera* and *Calocalanus contractus*, only were collected in the WC region related to IPC current and in the transition region CC, and not in the EC domain. These copepods are considered tropical/subtropical species (Frost & Flemiger, 1968; Bradford-Grieve *et al.*, 1999), which would likely prefer the warm, saline poleward current that was found here. *Salpa fusiformis* only was collected in the samples belonging to the WC region, and the relatively high temperature and salinity observed in the IPC would also favour this species because it seems to have an affinity for warm saline water (Lavaniegos *et al.*, 2002). On the contrary, *N. scintillans*, *Scolecithrix ovata*, and *Temora stylifera* was restricted to EC domain and in the coastal area of CC region related saline stratification in the upper meters of the water column, derived from the input of freshwater from Adour River and Cantabrian rivers respectively. In this study *N. scintillans* average abundance ranged from $89 \cdot 10^3$ to $323 \cdot 10^3$ cell m^{-3} , with maximum abundances in the EC region.

These dense swarms of *N. scintillans* are comparable to others that reported in the literature (Le Fèvre & Grall, 1970; Sekiguchi & Kato, 1976; Daan, 1987; Quevedo *et al.*, 1999), related to water column stability and under calm conditions (Le Fèvre, 1986; Gaines & Elbrachter, 1987; Huang & Qi, 1997). The predation of *N. scintillans* on eggs of broadcast spawning copepods, such as, *Acartia* and *Temora* suggesting that this mechanism could be highly relevant to population dynamics of neritic mesozooplankton. (Kimor, 1979; Daan, 1987; Quevedo *et al.*, 1999), and could be one of the cause of the lower abundance of species linked to lower salinity in the EC domain, such as *A. clausi*.

T. stylifera is considered in the northern Iberian shelf as a summer–autumn species related to water column stratification (Valdés *et al.*, 2007) and it is a copepod species typical of subtropical and Mediterranean areas (Razouls, 1995), however *T. stylifera* was not collected in the WC region related to intrusions of ENACst, and it was present in the EC region related to the saline stratification produced from the discharges of the river plume

Chapter 7: Conclusions

Chapter 2: Temporal and spatial variability of thermohaline properties in the North Iberian Shelf: 1987-2008

The SST values of the area of study suffered strong oscillations in the last 150 years. Nowadays we are in a warm period that began in 1970. High amount of the total variability of the SST is coherent with changes of the sunspot activity cycles.

The time-series of temperature showed a strong seasonality that is characteristic of the latitude of the sampling area, with low temperatures in winter that contrast with high temperatures in summer. Over this general pattern, the seasonality of temperature in Galician Sections was less intense than the measured in the Cantabrian Sections as a consequence of the reduction of temperature produced by summer upwelling. The seasonal signal of salinity distribution was strongly related with the presence of fresh water sources.

The mean values of temperature and salinity of the sections diminish alongshelf in the sampling area. This general pattern is probably related with differences in the latitude of the sections and with the gradient of the influence of the IPC.

We only found significant linear trends of temperature in the section off Cudillero and of salinity in the section off Santander. Long-term periodic trends of salinity with periods of 2, 4, 6 and 16 years were measured at different depths. These salinity variations were probably related with interannual variability of precipitation in the sampling area.

The spring survey showed the same pattern of along-shelf descent of temperature and salinity derived from the monthly time series of the sections. This general pattern of variation was modified in those zones influenced by river plumes in the Atlantic Coast associated with Miño River and in the easternmost part of the Cantabrian Sea associated with Adour River. Other important process that affect to the distribution of thermohaline properties in spring was the occurrence of upwelling in the Galician coast.

We only found significant linear trend of temperature and salinity in spring off Santander. Temperature increased in the whole studied area in the last two decades but this change was less intense eastward. This pattern is probably related with the differential influence of the IPC. The same pattern was found with salinity. In this last case the interannual variability could be associated with the IPC and with a descent of precipitations.

Chapter 3: Seasonal and interannual variation of the incursion of the Iberian Poleward Current (IPC) along the Northern Iberian Shelf derived from *in situ* thermohaline data

The methods we have applied for the characterization of the Iberian Poleward Current (IPC), based on the analysis of fields and time series of spiciness, allowed us to define the seasonal and interannual (spring, 1987-2008) variability of the incursion of the current along the North Iberian Shelf (NIS), the spatial distribution (in spring) of frontal structures associated with the dynamics of the IPC (and of other hydrographic process in the area –runoff and coastal upwelling), and the role of meteo-hydrographic (wind patterns and MTG) and climatic (EA pattern) drivers on the observed patterns. We argue that the methods based on *in situ* thermohaline data are more robust for the characterization of the IPC than those based on satellite-derived SST data.

The spatial-temporal distribution of spiciness derived from the analysis of the five across-shelf sections distributed along the NIS illustrated the seasonal pattern of the dynamics of the IPC, which is in general terms similar to the one proposed by Peliz *et al.* (2005). The seasonal pattern is characterized by: a development phase in winter, when ENACW_{sp} conveyed by the IPC is present all along the NIS, and a decaying phase the rest of the year, when the IPC shrunk westward. Short transitional periods occur between this two phases.

The IPC is an important hydrographic process which affects multiple ecosystem components in the NW and N Iberian shelf. Its dynamics influence, directly or indirectly, the variability of the pelagic ecosystem. In this work it was measured an increase in the influence of subtropical waters (ENACW_{sp}) in the Cantabrian sea during the last 20 years. We must be cautious interpreting these results because in terms of long-term variability the time series analyzed are short. The trend that we found could be a consequence of sampling in the increasing part of a system oscillation that in forthcoming years could become a decreasing trend. Whether linear or periodic, the study of the long-term dynamics of the IPC is relevant due to its effects on ecosystem functioning along the NIS.

The influence of the IPC on the Cantabrian Sea during spring is related with the changes in the Meridional Thermal Gradient (MTG) in the North Atlantic, in coherence with the hypothesis proposed by the JEBAR forcing mechanism (Huthnance, 1984). The influence of the IPC in the Cantabrian Sea during spring is positively related with the pattern of upwelling favorable winds (northerlies and easterlies) during winter. This result agree with those derived from modeling approaches but contradict other

observational studies based on satellite SST that correlate the strength of the IPC (in winter) with southerly and westerly winds.

Chapter 4: Temporal and spatial variability of river plumes in the NW and N Iberian Shelf (1987-2007)

The method proposed here to characterize river plumes is conceptually simple and easy to implement. It permits to determine the probability of occurrence of low-density buoyancy structures and to characterize them objectively both in space and time. The descriptors of river plumes, such as the area of influence of the plume or mean depth, are useful variables to explore the characteristics of the plume in relation to its forcing factors of plume development and to explore the relationship of the plume with different ecosystem components.

The seasonal cycle of the probability of occurrence of the plumes, derived from the analysis of the salinity gradient in the across-shelf sections of Vigo, A Coruña, Cudillero, Gijón and Santander, showed a clear relationship with the precipitations and river runoffs of each zone. The differences among sections could be associated with a local characteristic, such as the regime of the rivers or the continental relief.

The spatial distribution and temporal variability of the influence of river plumes along the North Iberian Shelf during spring exhibited different regional patterns. The zones which are more influenced by such structures were the western part of the studied area influenced by Miño River and the rest of Galician Rivers and the easternmost part mainly influenced by Adour River. These zones contrast with the moderate occurrence measured in the Central Cantabrian Sea. The main factors that conditioned this distribution are the precipitation regimen and the continental relief that modulate the intensity and seasonality of river discharge rates.

The interannual variability of the influence of river plumes during spring was different in the three regions. The GWC zone showed two clear periods with low and high influence that contrasted with the higher variability of the CC and the more intense and constant presence of plumes in EC.

The descriptors of the spring river plumes were correlated with precipitation and river runoffs of previous months. In Galicia and West Cantabrian (GWC) and in East Cantabrian (EC) zones we found a statistically significant relationship with winter precipitations.

Chapter 5: Temporal and spatial variability of wind-driven coastal upwelling in the NW and N Iberian shelf from 1987 to 2008

The methods developed for the detection of upwelling using both across-shelf sections and field survey data are useful tools to characterize, both in terms of occurrence and intensity, the temporal and spatial variability of coastal upwelling along the North Iberian Shelf.

We have found empirical relationships between the parameters that characterize the occurrence of upwelling and the upwelling favorable wind component.

The intensity of the upwelling favorable winds (UFW) presented a weakening trend from 1950 to 2007. This trend was not found using the time series of the Upwelling Thermal Index (UTI) from 1994 to 2005.

Distinct temporal and spatial patterns were found in the Galician and Cantabrian Sea shelves, suggesting the definition of distinct sub-regions of the NIS. The seasonality of the upwelling was clearly different between the Atlantic and Cantabrian coasts both for the Upwelling Thermal Index (UTI) series and for the probability of occurrence data. The Atlantic upwelling was strongly seasonal in contrast with the Cantabrian upwelling that appeared as a more stochastic process. The spatial distribution of the upwelling probability calculated for the spring surveys presented similar patterns than those obtained with the across-shelf section data. The Atlantic upwelling during spring was more frequent (50 % of the cruises) than the Cantabrian upwelling (20 %).

Chapter 6: Mesozooplankton species distribution in the NW and N Iberian shelf during spring 2004: Relationship with frontal structures.

Three different hydrographic zones along the shelf were obtained according to the distribution of thermohaline properties. These zones are separated by neat frontal areas and presented significantly different thermohaline characteristics.

Three major groups of stations were obtained according to the composition of mesozooplankton species. This major zonation could be further subdivided to take into account the difference between coastal and shelf stations.

There was a highly significant spatial correlation (Mantel test) between the hydrographic zones and the distribution of mesozooplankton species assemblages. The resulting causal model is indicative of the hydrographic control exerted on the distribution of mesozooplankton.

Chapter 8: Conclusiones (Castellano)

Chapter 2: Variabilidad espacio temporal de la propiedades termohalinas de la plataforma norte de la Península Ibérica: 1987-2008

Los valores de SST del área de estudio han sufrido fuertes oscilaciones en los últimos 150 años. En la actualidad nos encontramos en un periodo cálido que comenzó en 1970. Una cantidad importante de la variabilidad total de la SST es coherente con los cambios en los ciclos de actividad de las manchas solares.

Las series temporales de temperatura mostraron una fuerte estacionalidad que es característica de la latitud en la que se encuentra el área de estudio, con bajas temperaturas en invierno que se contraponen con valores altos en verano. Sobre este patrón general, la estacionalidad de la temperatura en las secciones de Galicia fue menos intensa que la medida en las secciones del Cantábrico como consecuencia de la reducción de temperatura producida por el afloramiento de verano. La señal estacional de la distribución de salinidad estuvo fuertemente relacionada con la presencia fuentes de agua dulce.

Los valores medios de temperatura y salinidad de las secciones disminuyen a lo largo de la costa en el área de estudio. Este patrón, está probablemente relacionado con diferencias en la latitud de las secciones así como en la influencia diferencial de la IPC.

Solo se encontraron tendencias lineales significativas de temperatura en la sección frente a Cudillero y en la salinidad en la sección de Santander. Se determinaron tendencias periódicas de larga escala con periodos de 2, 4, 6 y 16 años a distintas profundidades. Estas variaciones de salinidad están probablemente relacionadas con la variabilidad de las precipitaciones en el área de estudio.

Las campañas de primavera mostraron el mismo patrón descendente de la temperatura y salinidad derivado utilizando las series temporales mensuales de las secciones. Este patrón general de variación fue modificado en aquellas zonas influenciadas por plumas de ríos, en la costa Atlántica asociadas con el río Miño y en la parte más al este de la península Ibérica asociadas con el río Adour. Otro proceso importante que afecta a la distribución de las condiciones termohalinas en primavera fue el afloramiento en la costa de Galicia.

Solo se encontraron tendencias lineales significativas de temperatura en primavera en las secciones de Santander. La temperatura se incrementó en todo el área de estudio en las últimas dos décadas pero este cambio fue menos intenso hacia el este. Estos cambios, en esta época del año podrían estar relacionados con la variabilidad de la influencia de la IPC en la zona. Los mismos resultados se encontraron con la salinidad. En este caso los cambios de larga escala en esta variable podrían estar relacionados con la variabilidad de la IPC y con el descenso en las precipitaciones.

Chapter 3: Variación estacional e interannual de la incursión de la Corriente Ibérica hacia el Polo a lo largo de la plataforma norte de la Península Ibérica derivada utilizando datos termohalinos in situ

Los métodos que hemos aplicado para la caracterización de la Corriente Ibérica hacia el Polo (IPC), basados en los campos y las series temporales de spiciness, nos permiten definir la variación estacional e interannual (primavera, 1987-2008) de la incursión de la corriente a lo largo de la plataforma norte de la Península Ibérica (NIS), la distribución espacial (en primavera) de las estructuras frontales asociadas con la dinámica de la IPC y el papel de los forzadores méteo-hidrográficos (vientos y MTG) y climáticos (EA) sobre los patrones observados.

La distribución espacio temporal de spiciness derivada del análisis de las cinco secciones distribuidos a lo largo de NIS ilustraron el patrón estacional de la dinámica de la IPC, el cual en términos generales es similar al propuesto por Peliz *et al.* (2005). El patrón estacional se caracteriza por: una fase de desarrollo en invierno, el agua ENACW_{sp} advectada por la IPC está presente en todo la NIS, y una fase de decaimiento durante el resto del año, donde la IPC se retrae hacia el este. Entre las dos fases, los periodos de transición son cortos.

La IPC es un proceso importante hidrográfico que afecta al múltiples componentes del ecosistema en el Noroeste y Norte de la plataforma de la Península Ibérica. Su dinámica influye, directa o indirectamente, sobre la variabilidad del ecosistema pelágico. En este trabajo se ha medido un incremento de la influencia de aguas subtropicales (ENCW_{st}) en el mar Cantábrico en los últimos 20 años. Debemos ser cautelosos a la hora de interpretar esto resultados porque en términos de variabilidad de larga escala la serie temporal analizada se puede considerar como corta. La tendencia encontrada podría ser el resultado de haber muestreado en un periodo de incremento de una oscilación del sistema que en los siguientes años podría convertirse en una tendencia de decrecimiento, ya sea una tendencia lineal o periódica.

La influencia de la IPC sobre el mar Cantábrico durante la primavera está relacionada con los cambios en el gradiente térmico meridional (MTG) en el Atlántico Norte, en coherencia con la hipótesis propuesta por el mecanismo de forzamiento JEBAR (Huthnance, 1984). La influencia de la IPC presenta una relación positiva con vientos forzadores del afloramiento (nortes y estes) durante la primavera. Este resultado concuerda con los derivados de modelos pero contradice otros estudios observacionales basados en datos de satélite, los cuales relacionan la intensidad de la IPC (en invierno) con vientos de sur y el oeste.

Chapter 4: Variabilidad temporal y especial de las plumas de ríos en el NO y N de la plataforma Ibérica (1987-2007).

El método propuesto para la caracterización de plumas de ríos es conceptualmente simple y de fácil aplicación. Permite determinar la probabilidad de ocurrencia estructuras de baja densidad y caracterizarlas de forma objetiva tanto en el espacio como en el tiempo. Los descriptores de las plumas de ríos, como el área de influencia o la profundidad media, son variables muy útiles para explorar las características de las plumas en relación con sus principales forzadores así como estudiar su relación con los diferentes componentes del ecosistema.

El ciclo estacional de la probabilidad de ocurrencia de las plumas, derivada del análisis del gradiente de salinidad en las secciones de Vigo, A Coruña, Cudillero, Gijón y Santander, mostró una clara relación con las precipitaciones y las descargas de los ríos en cada zona. Las diferencias que se encontraron entre las distintas secciones podrían estar asociadas con las características locales como son el régimen de los ríos o el relieve del continente.

La distribución espacial y la variabilidad temporal de la influencia de las plumas de ríos a lo largo de la NIS en primavera exhibieron diferentes patrones regionales. Las zonas más influenciadas por estas estructuras se localizaron en la parte más al oeste del área estudiada en relación con el río Miño y el resto de ríos de Galicia, y la parte más al este que estuvo principalmente influenciada por el río Adour. Estas dos zonas contrastan con la ocurrencia moderada medida en el Cantábrico central. Los principales factores que condicionan esta distribución son el régimen de precipitación y el relieve continental, los cuales modulan la intensidad y estacionalidad de las descargas de los ríos.

La variabilidad interanual de la influencia de las plumas de ríos en primavera fue distinta en las tres regiones. La zona GWC mostró dos periodos claros con baja y alta

influencia que contrasta con la mayor variabilidad del CC y la mayor intensidad y constancia que caracterizó a EC.

Los descriptores de las plumas de ríos de primavera se correlacionaron con la precipitación y con las descargas de ríos de los meses previos al muestreo. En Galicia y en el Cantábrico Oeste (GWC) y en el Cantábrico Este (EC), encontramos una relación significativa con las precipitaciones producidas durante el invierno.

Chapter 5: Variación temporal y espacial del afloramiento forzado por vientos en el Noroeste y Norte de la plataforma Ibérica desde 1987 hasta 2008

Los métodos desarrollados para la detección del afloramiento usando las secciones y los datos de las campañas son herramientas útiles para caracterizar, tanto en términos de ocurrencia como de intensidad, la variabilidad temporal y espacial del afloramiento costero a lo largo de la NIS.

Se encontró una relación empírica entre los parámetros que caracterizan la ocurrencia del afloramiento y las componentes del viento forzadores del mismo.

La intensidad de los vientos forzadores del afloramiento (UFW) presentó un debilitamiento desde 1950 y 2007. Esta tendencia no se encontró cuando se analizó la serie temporal del índice térmico de afloramiento (UTI) entre 1994 y 2005

Se encontraron distintos patrones de variación temporal y espacial en las plataformas Gallega y Cantábrica, lo que sugiere la definición de distintas sub-regiones de la NIS. La estacionalidad del Afloramiento fue claramente diferente entre la Costa Atlántica y Cantábrica tanto para las series temporales del UTI como para la probabilidad de ocurrencia. El afloramiento Atlántico presentó una estacionalidad marcada en contraste con el afloramiento Cantábrico que se presentó como un proceso más estocástico. La distribución espacial de la probabilidad de ocurrencia de afloramiento calculada usando las campañas de primavera presentó unos patrones de variación similares a los obtenidos con los datos de las secciones. El afloramiento atlántico fue más frecuente (50% de las campañas) que el Cantábrico (20%)

Chapter 6: Distribución de las especies de mesozooplancton en el NO y N de la plataforma Ibérica en la primavera del 2004: Relación con estructuras frontales.

Se obtuvieron tres zonas hidrográficas a lo largo de la plataforma en teniendo en cuenta la distribución de condiciones termohalinas. Estas zonas están separadas por

áreas frontales y presentaron diferencias significativas en sus características termohalinas.

Basándose en la composición de las especies de mesozooplankton las estaciones de muestreo se clasificaron en tres grupos. Esta clasificación principal se subdividió para tener en cuenta las diferencias entre las estaciones costeras y las estaciones de plataforma propiamente dichas.

Se encontró una correlación espacial significativa (test de Mantel) entre las zonas basadas en la hidrografía y la distribución de las agrupaciones de especies de mesozooplankton. El modelo causal resultante es indicativo del control que ejerce la hidrografía sobre la distribución de las especies del mesozooplankton

Chapter 9: Bibliography

- Acuna, J.L., & Anadon, R. (1992) Appendicularian assemblages in a shelf area and their relationship with temperature. *Journal of Plankton Research*, 14, 1233-1250.
- Akaike, H. (1974) A new look at the statistical model identification. *Automatic Control, IEEE Transactions on*, 19, 716-723.
- Albaina, A., & Irigoien, X. (2007a) Fine scale zooplankton distribution in the Bay of Biscay in spring 2004. *Journal of Plankton Research*, 29, 851-870.
- Albaina, A., & Irigoien, X. (2007b) Zooplankton communities and oceanographic structures in a high-resolution grid in the south-eastern corner of the Bay of Biscay. *Estuarine Coastal and Shelf Science*, 75, 433-446.
- Albaina, A., Villate, F., & Uriarte, I. (2009) Zooplankton communities in two contrasting Basque estuaries (1999-2001): reporting changes associated with ecosystem health. *Journal of Plankton Research*, 31, 739-752.
- Alvarez-Marqués, F. (1980) Copépodos pelágicos de la costa asturiana: Contribución al conocimiento de las especies de la zona de Gijón. *Boletín de Ciencias de la Naturaleza. I.D.E.A.*, 25, 215-223.
- Álvarez-Salgado, X.A., Doval, M.D., & Pérez, F.F. (1999) Dissolved organic matter in shelf waters off the Ría de Vigo (NW Iberian upwelling system). *Journal of Marine Systems*, 18, 383-394.
- Álvarez-Salgado, X.A., Figueiras, F.G., Pérez, F.F., Groom, S., Nogueira, E., Borges, A.V., Chou, L., Castro, C.G., Moncoiffé, G., Ríos, A.F., Miller, A.E.J., Frankignoulle, M., Savidge, G., & Wollast, R. (2003) The Portugal coastal counter current off NW Spain: new insights on its biogeochemical variability. *Progress In Oceanography*, 56, 281-321.
- Álvarez-Salgado, X.A., Labarta, U., Fernández-Reiriz, M.J., Figueiras, F.G., Rosón, G., Piedracoba, S., Filgueira, R., & Cabanas, J.M. (2008) Renewal time and the impact of harmful algal blooms on the extensive mussel raft culture of the Iberian coastal upwelling system (SW Europe). *Harmful Algae*, 7, 849-855.
- Alvarez, I., Gomez-Gesteira, M., deCastro, M., Lorenzo, M.N., Crespo, A.J.C., & Dias, J.M. (2011) Comparative analysis of upwelling influence between the western and northern coast of the Iberian Peninsula. *Continental Shelf Research*, 31, 388-399.
- Alvarez, I., Gomez-Gesteira, M., deCastro, M., & Novoa, E.M. (2008) Ekman transport along the Galician Coast (NW, Spain) calculated from QuikSCAT winds. *Journal of Marine Systems*, 72, 101-115.
- Alvarez, I., Ospina-Alvarez, N., deCastro, M., Varela, M., Gomez-Gesteira, M., & Prego, R. (2010) Poleward intrusion in the northern Galician shelf. *Estuarine, Coastal and Shelf Science*, 87, 545-552.
- Alvarez, I., Ospina-Alvarez, N., Pazos, Y., deCastro, M., Bernardez, P., Campos, M.J., Gomez-Gesteira, J.L., Alvarez-Ossorio, M.T., Varela, M., Gomez-Gesteira, M., & Prego, R. (2009) A winter upwelling event in the Northern Galician Rias: Frequency and oceanographic implications. *Estuarine, Coastal and Shelf Science*, 82, 573-582.
- Allain, G., Petitgas, P., & Lazure, P. (2001) The influence of mesoscale ocean processes on anchovy *Engraulis encrasicolus* recruitment in the Bay of Biscay estimated with a three-dimensional hydrodynamic mode. *Fisheries Oceanography*, 10, 151-163.
- Ambar, I., Fiuza, A., & Amer Meteorol, S.O.C. (1994) Some features of the Portugal Current System: A poleward slope undercurrent, an upwelling-related summer southward flow and an autumn-winter poleward coastal surface current. *Second International Conference on Air-Sea Interaction and on Meteorology and Oceanography of the Coastal Zone*, 286-287.
- Ambar, I., Fiuza, A.F.G., Boyd, T., & Frouin, R. (1986) Observations of warm oceanic current following northward along the coast of Portugal and Spain during Nov-Dec 1983. *Eos*, 67, 1054.
- Atkinson, A., & Shreeve, R.S. (1995) Response of the copepod community to a spring bloom in the Bellingshausen Sea. *Deep-Sea Research Part II-Topical Studies in Oceanography*, 42, 1291-1311.

- Bakun, A. (1990) Global Climate Change and Intensification of Coastal Ocean Upwelling. *Science*, 247, 198-201.
- Banas, N.S., MacCready, P., & Hickey, B.M. (2009) The Columbia River plume as cross-shelf exporter and along-coast barrier. *Continental Shelf Research*, 29, 292-301.
- Barbosa, A.B., Galvão, H.M., Mendes, P.A., Álvarez-Salgado, X.A., Figueiras, F.G., & Joint, I. (2001) Short-term variability of heterotrophic bacterioplankton during upwelling off the NW Iberian margin. *Progress In Oceanography*, 51, 339-359.
- Barquero, S., Botas, J.A., & Bode, A. (1998a) Abundance and production of pelagic bacteria in the southern Bay of Biscay during summer. *Scientia Marina*, 62, 83-90.
- Barquero, S., Cabal, J.A., Anadon, R., Fernandez, E., Varela, M., & Bode, A. (1998b) Ingestion rates of phytoplankton by copepod size fractions on a bloom associated with an off-shelf front off NW Spain. *Journal of Plankton Research*, 20, 957-972.
- Barton, E.D. (1989). The Poleward Undercurrent on the Eastern Boundary of the Subtropical North Atlantic. In S.J. Neshyba, C.N.K. Mooers, R.L. Smith, & R.T. Barber, *Poleward Flows Along Eastern Ocean Boundaries*, Vol. 34 (pp. 82-95): Springer New York.
- Beaugrand, G., Ibanez, F., & Reid, P.C. (2000) Spatial, seasonal and long-term fluctuations of plankton in relation to hydroclimatic features in the English Channel, Celtic Sea and Bay of Biscay. *Marine Ecology Progress Series*, 200, 93-102.
- Begon, M., Harper, J.L., & Townsend, C.R. (2006). *Ecology: Individuals, Populations and Communities*. Oxford. Blackwell Science, 1068 pp.
- Blanco-Bercial, L., Alvarez-Marques, F., & Cabal, J.A. (2006) Changes in the mesozooplankton community associated with the hydrography off the northwestern Iberian Peninsula. *ICES J. Mar. Sci.*, 63, 799-810.
- Blanton, J.O., Tenore, K.R., Castillejo, F., Atkinson, L.P., Schwing, F.B., & Lavin, A. (1987) The relationship of upwelling to mussel production in the rias on the western coast of Spain. *Journal of Marine Research*, 45, 497-511.
- Bode, A., Alvarez-Ossorio, M.T., Cabanas, J.M., Miranda, A., & Varela, M. (2009) Recent trends in plankton and upwelling intensity off Galicia (NW Spain). *Progress In Oceanography*, 83, 342-350.
- Bode, A., Alvarez-Ossorio, M.T., Miranda, A., Lopez-Urrutia, A., & Valdes, L. (2012) Comparing copepod time-series in the north of Spain: Spatial autocorrelation of community composition. *Progress In Oceanography*, 97, 108-119.
- Bode, A., & Fernandez, E. (1992) Influence of water-column stability on phytoplankton size and biomass succession patterns in the central cantabrian sea (Bay of Biscay). *Journal of Plankton Research*, 14, 885-902.
- Bode, A., Fernández, E., Botas, A., & Anadón, R. (1990) Distribution and composition of suspended particulate matter related to a shelf-break saline intrusion in the Cantabrian Sea (Bay of Biscay). *Oceanologica Acta*, 3, 219 – 228.
- Bode, A., González, N., Rodríguez, C., Varela, M., & Varela, M.M. (2005) Seasonal variability of plankton blooms in the Ria de Ferrol (NW Spain): I. Nutrient concentrations and nitrogen uptake rates. *Estuarine, Coastal and Shelf Science*, 63, 269-284.
- Bode, A., Varela, M., Casas, B., & Gonzalez, N. (2002a) Intrusions of eastern North Atlantic central waters and phytoplankton in the north and northwestern Iberian shelf during spring. *Journal of Marine Systems*, 36, 197-218.
- Bode, A., Varela, M., Casas, B., & González, N. (2002b) Intrusions of eastern North Atlantic central waters and phytoplankton in the north and northwestern Iberian shelf during spring. *Journal of Marine Systems*, 36, 197-218.
- Bonnet, D., Richardson, A., Harris, R., Hirst, A., Beaugrand, G., Edwards, M., Ceballos, S., Diekman, R., Lopez-Urrutia, A., Valdes, L., Carlotti, F., Molinero, J.C., Weikert, H., Greve, W., Lucic, D., Albaina, A., Yahia, N.D., Umani, S.F., Miranda, A., dos Santos, A., Cook, K., Robinson, S., & de Puellas, M.L.F. (2005) An overview of *Calanus helgolandicus* ecology in European waters. *Progress In Oceanography*, 65, 1-53.

- Borges, A.V., & Frankignoulle, M. (2002) Aspects of dissolved inorganic carbon dynamics in the upwelling system off the Galician coast. *Journal of Marine Systems*, 32, 181-198.
- Botas, A., Fernández, E., Bode, A., & Anadón, R. (1989) Water masses off the Central Cantabrian Coast. *Scientia Marina*, 53, 755-761.
- Botas, J.A., Bode, A., Fernández, E., & Anadón, R. (1988) Descripción de una intrusión de agua de elevada salinidad en el Cantábrico central: distribución de los nutrientes inorgánicos y su relación con el fitoplancton. *Investigacion Pesquera*, 52, 561-574.
- Botas, J.A., Fernandez, E., Bode, A., & Anadon, R. (1990) A persistent upwelling off the Central Cantabrian Coast (Bay of Biscay). *Estuarine, Coastal and Shelf Science*, 30, 185-199.
- Box, G.E.P., & Jenkins, G.M. (1976). *Time Series Analysis Forecasting and Control*. San Francisco-USA. Holden-Day, 575 pp.
- Bradford-Grieve, J.M., Markhaseva, E.L., Rocha, C.E.F., & Abiahy, B. (1999). Copepoda. In D. Boltovskoy, *South Atlantic Mesozooplankton* (pp. 869–1098). Leiden: Backhuys Publishers.
- Cabal, J. (1993). Estructura y Dinámica de las poblaciones de Copépodos plantónicos en la Costa Central de Asturias Vol. Ph.D. Thesis (p. 349 pp): Universidad de Oviedo.
- Cabal, J., & Alvarez-Marqués, F. (1995). Biomasa zooplanctónica en el cantabrico Central. Distribución espacial. Composición y estructura de tamaños de los Copépodos en el Mar Cantabrico. *Actas del IV Colloquio Internacional Oceanographia del Golfo de Vizcaya* (pp. 249–254.).
- Cabal, J., González-Nuevo, G., & Nogueira, E. (2008) Mesozooplankton species distribution in the NW and N Iberian shelf during spring 2004: Relationship with frontal structures. *Journal of Marine Systems*, 72, 282-297.
- Cabanas, J.M., Lavin, A., García, M.J., Gonzalez-Pola, C., & Tel, E. (2003) Oceanographic variability in the northern shelf of the Iberian Peninsula 1990–1999. *ICES Marine Science Symposia*, 219, 71–79.
- Calvo-Díaz, A., Moran, X.A.G., Nogueira, E., Bode, A., & Varela, M. (2004) Picoplankton community structure along the northern Iberian continental margin in late winter-early spring. *J. Plankton Res.*, 26, 1069-1081.
- Calvo-Díaz, A., Morán, X.A.G., & Suárez, L.Á. (2008) Seasonality of picophytoplankton chlorophyll a and biomass in the central Cantabrian Sea, southern Bay of Biscay. *Journal of Marine Systems*, 72, 271-281.
- Castro, C.G., AlvarezSalgado, X.A., Figueiras, F.G., Perez, F.F., & Fraga, F. (1997) Transient hydrographic and chemical conditions affecting microplankton populations in the coastal transition zone of the Iberian upwelling system (NW Spain) in September 1986. *Journal of Marine Research*, 55, 321-352.
- Ceballos, S., Viesca, L., & Alvarez-Marques, F. (2006) Copepod egg production during highly productive late spring conditions: importance of freshly ingested food and lipid storage. *Marine Ecology Progress Series*, 317, 171-186.
- Coelho, H.S., Neves, R.J.J., White, M., Leitão, P.C., & Santos, A.J. (2002) A model for ocean circulation on the Iberian coast. *Journal of Marine Systems*, 32, 153-179.
- Coelho, H.S., Neves, R.R., Leitão, P.C., Martins, H., & Santos, A.P. (1999) The slope current along the western European margin: A numerical investigation. *Bol. Inst. Esp. Oceanogr.*, 15, 67-72.
- Crespo, B.G., Teixeira, I.G., Figueiras, F.G., & Castro, C.G. (2008) Microplankton composition off NW Iberia at the end of the upwelling season: source areas of harmful dinoflagellate blooms. *Marine Ecology Progress Series*, 355, 31-43.
- Chassot, E., Bonhommeau, S., Reygondeau, G., Nieto, K., Polovina, J.J., Huret, M., Dulvy, N.K., & Demarcq, H. (2011) Satellite remote sensing for an ecosystem approach to fisheries management. *Ices Journal of Marine Science*, 68, 651-666.
- Chatfield, C. (1996). *The Analysis of Time Series: An Introduction*. Chapman & Hall, 303 pp.

- Chaudhuri, A., Gangopadhyay, A., Balasubramanian, R., & Ray, S. (2004). Automated oceanographic feature detection from high resolution satellite images. In M.H. Hamza, *7th IASTED International Conference on Computer Graphics and Imaging* (pp. 217-223). Kauai, HI: Acta Press.
- Cheng, Y.H., Ho, C.R., Zheng, Z.W., Lee, Y.H., & Kuo, N.J. (2009) An Algorithm for Cold Patch Detection in the Sea off Northeast Taiwan Using Multi-Sensor Data. *Sensors*, 9, 5521-5533.
- Chust, G., Allen, J.I., Bopp, L., Schrum, C., Holt, J., Tsiaras, K., Zavatarelli, M., Chifflet, M., Cannaby, H., Dadou, I., Daewel, U., Wakelin, S.L., Machu, E., Pushpadas, D., Butenschon, M., Artioli, Y., Petihakis, G., Smith, C., Garcon, V., Goubanova, K., Le Vu, B., Fach, B.A., Salihoglu, B., Clementi, E., & Irigoien, X. (2014) Biomass changes and trophic amplification of plankton in a warmer ocean. *Global Change Biology*, 20, 2124-2139.
- d'Elbee, J., Castege, I., Hemery, G., Lalanne, Y., Mouches, C., Pautrizel, F., & D'Amico, F. (2009) Variation and temporal patterns in the composition of the surface ichthyoplankton in the southern Bay of Biscay (W. Atlantic). *Continental Shelf Research*, 29, 1136-1144.
- Daan, R. (1987) Impact of egg predation by *Noctiluca miliaris* on the summer development of copepod populations in the southern North Sea. *Marine Ecology Progress Series*, 37, 9-17.
- Davis, J.C. (1986). *Statistics and data analysis in geology* Singapur Ed. Wiley and Sons. , 646 pp.
- deCastro, M., Dale, A.W., Gómez-Gesteira, M., Prego, R., & Alvarez, I. (2006) Hydrographic and atmospheric analysis of an autumnal upwelling event in the Ria of Vigo (NW Iberian Peninsula). *Estuarine, Coastal and Shelf Science*, 68, 529-537.
- deCastro, M., Gómez-Gesteira, M., Álvarez, I., & Crespo, A.J.C. (2011) Atmospheric modes influence on Iberian Poleward Current variability. *Continental Shelf Research*, 31, 425-432.
- deCastro, M., Gómez-Gesteira, M., Alvarez, I., & Gesteira, J.L.G. (2009) Present warming within the context of cooling-warming cycles observed since 1854 in the Bay of Biscay. *Continental Shelf Research*, 29, 1053-1059.
- Delbee, J., & Castel, J. (1991) Zooplankton from the continental-shelf of the southern Bay of Biscay exchange with arcachon basin, France. *Annales De L Institut Oceanographique*, 67, 35-48.
- Demarcq, H. (2009) Trends in primary production, sea surface temperature and wind in upwelling systems (1998-2007). *Progress In Oceanography*, 83, 376-385.
- Di Lorenzo, E. (2003) Seasonal dynamics of the surface circulation in the Southern California Current System. *Deep Sea Research Part II: Topical Studies in Oceanography*, 50, 2371-2388.
- Dickson, R.R., Kelly, P.M., Colebrook, J.M., Wooster, W.S., & Cushing, D.H. (1988) North winds and production in the eastern North Atlantic. *J. Plankton Res.*, 10, 151-169.
- Diz, P., Francés, G., & Rosón, G. (2006) Effects of contrasting upwelling-downwelling on benthic foraminiferal distribution in the Ría de Vigo (NW Spain). *Journal of Marine Systems*, 60, 1-18.
- Doval, M.D., Álvarez-Salgado, X.A., & Pérez, F.F. (1997) Dissolved organic matter in a temperate embayment affected by coastal upwelling. *Marine Ecology Progress Series*, 157, 21-37.
- Esnaola, G., Sáenz, J., Zorita, E., Fontán, A., Valencia, V., & Lazure, P. (2012) Daily scale winter-time sea surface temperature variability and the Iberian Poleward Current in the southern Bay of Biscay from 1981 to 2010. *Ocean Sci. Discuss.*, 9, 3795-3850.
- Esnaola, G., Sáenz, J., Zorita, E., Fontán, A., Valencia, V., & Lazure, P. (2013) Daily scale wintertime sea surface temperature and IPC-Navidad variability in the southern Bay of Biscay from 1981 to 2010. *Ocean Sci.*, 9, 655-679.
- Fennel, W. (1999) Theory of the Benguela Upwelling System. *Journal of Physical Oceanography*, 29, 177-190.

- Fernandez, E., Alvarez, F., Anadon, R., Barquero, S., Bode, A., Garcia, A., Garcia-Soto, C., Gil, J., Gonzalez, N., Iriarte, A., Mourino, B., Rodriguez, F., Sanchez, R., Teira, E., Torres, S., Valdes, L., Varela, M., Varela, R., & Zapata, M. (2004) The spatial distribution of plankton communities in a Slope Water anticyclonic Oceanic eDDY (SWODDY) in the southern Bay of Biscay. *Journal of the Marine Biological Association of the United Kingdom*, 84, 501-517.
- Fernández, E., & Bode, A. (1991) Seasonal patterns of primary production in the Central Cantábric Sea (Bay of Biscay). *Scientia Marina*, 55, 629-636.
- Fernández, E., & Bode, A. (1994) Succession of phytoplankton assemblages in relation to the hydrography in the southern Bay of Biscay: A multivariate approach. *Scientia Marina*, 58, 1991-1205.
- Fernandez, E., Cabal, J., Acuna, J.L., Bode, A., Botas, A., & Garcia-Soto, C. (1993) Plankton distribution across a slope current-induced front in the southern Bay of Biscay. *J. Plankton Res.*, 15, 619-641.
- Fernández, E., Madariaga, I., & Serret, P. (1991) Photosynthate partitioning by natural phytoplankton populations in a shallow coastal front. *Scientia Marina*, 55, 599-604.
- Fernandez, E., Maranon, E., Cabal, J., Alvarez, F., & Anadon, R. (1995) Vertical particle-flux in outer shelf waters of the southern Bay-of-Biscay in summer 1993. *Oceanologica Acta*, 18, 379-384.
- Ferrer, L., Fontan, A., Mader, J., Chust, G., Gonzalez, M., Valencia, V., Uriarte, A., & Collins, M.B. (2009) Low-salinity plumes in the oceanic region of the Basque Country. *Continental Shelf Research*, 29, 970-984.
- Figueiras, F.G., Jones, K.J., Mosquera, A.M., Alvarez-Salgado, X.A., Edwards, A., & MacDougall, N. (1994) Red tide assemblage formation in an estuarine upwelling ecosystem: Ria de Vigo. *Journal of Plankton Research*, 16, 857-878.
- Figueiras, F.G., Labarta, U., & Reiriz, M.J.F. (2002) Coastal upwelling, primary production and mussel growth in the Rias Baixas of Galicia. *Hydrobiologia*, 484, 121-131.
- Fiuza, A., de Macedo, M.E., & Guerreiro, M.R. (1982) Climatological space and time variation of the Portuguese Coastal Upwelling. *Oceanologica Acta*, 5, 31-40.
- Fiuza, A., Hamann, M., Ambar, I., Diaz del Rio, G., Gonzalez, N., & Cabanas, J.M. (1998) Water masses and their circulation in the Western Iberian coastal ocean during May 1993. *Deep-Sea Research I*, 45, 1127-1160.
- Fiuza, A.F.G. (1983). Upwelling patterns of Portugal. In J. Thiade, *Coastal Upwelling* (pp. pp 85-98).
- Fiuza, A.F.G. (1984). Dinamica e Hidrologia das Aguas Costeiras Portuguesas. Vol. Doctoral Dissertation (p. 294). Lisbon: Universidade de Lisboa.
- Flament, P. (1986). Fine structure and subduction associated with upwelling filaments. Vol. Ph. D. Dissertation: University of California at San Diego.
- Flament, P. (2002) A state variable for characterizing water masses and their diffusive stability: spiciness. *Progress In Oceanography*, 54, 493-501.
- Foltz, G.R., Grodsky, S.A., Carton, J.A., & McPhaden, M.J. (2003) Seasonal mixed layer heat budget of the tropical Atlantic Ocean. *Journal of Geophysical Research: Oceans*, 108, 3146.
- Fontán, A., Valencia, V., Borja, Á., & Goikoetxea, N. (2008) Oceano-meteorological conditions and coupling in the southeastern Bay of Biscay, for the period 2001-2005: A comparison with the past two decades. *Journal of Marine Systems*, 72, 167-177.
- Fraga, F. (1981). Upwelling of the Galician coast. Northwest Spain. In F.A. Richards, *Coastal Upwelling* (pp. 176-182). Washington DC: AGU.
- Fraga, F., Mouriño, C., & Manriquez, M. (1982) Las masas de agua de las costas de Galicia: Junio-Octubre. *Res. Exp. Cient.*, 10, 51-57.
- Fréon, P., Barange, M., & Arístegui, J. (2009) Eastern Boundary Upwelling Ecosystems: Integrative and comparative approaches. *Progress In Oceanography*, 83, 1-14.

- Frost, B., & Flemiger, A. (1968) A revision of the Genus *Clausocalanus* (Copepoda: Calanoida) with remarks on distributional patterns in diagnostic characters. *Bulletin Scripps Institution of Oceanography*, 12, 1–235.
- Frouin, R., Fiúza, A.F.G., Ambar, I., & Boyd, T.J. (1990) Observations of a poleward surface current off the coasts of Portugal and Spain during winter. *Journal of Geophysical Research: Oceans*, 95, 679-691.
- Gago, J., Gilcoto, M., Pérez, F.F., & Ríos, A.F. (2003) Short-term variability of fCO₂ in seawater and air-sea CO₂ fluxes in a coastal upwelling system (Ría de Vigo, NW Spain). *Marine Chemistry*, 80, 247-264.
- Gaines, G., & Elbrachter, M. (1987). Heterotrophic nutrition. In F.J.R.E. Taylor, *The Biology of Dinoflagellates* (pp. 225–268.). Oxford: Blackwell Scientific publications.
- Gámiz-Fortis, S.R., Pozo, D., Castro, Y., & Esteban, M.J. (2004) Influencia de la SST atlántica sobre las precipitaciones de la Península Ibérica. *Física de la Tierra*, 71, 149-160.
- Gan, J.P., Li, L., Wang, D.X., & Guo, X.G. (2009) Interaction of a river plume with coastal upwelling in the northeastern South China Sea. *Continental Shelf Research*, 29, 728-740.
- Garcia-Soto, C., & Pingree, R.D. (2009) Spring and summer blooms of phytoplankton (SeaWiFS/MODIS) along a ferry line in the Bay of Biscay and western English Channel. *Continental Shelf Research*, 29, 1111-1122.
- Garcia-Soto, C., Pingree, R.D., & Valdes, L. (2002) Navidad development in the southern Bay of Biscay: Climate change and swoddy structure from remote sensing and in situ measurements. *Journal of Geophysical Research-Oceans*, 107.
- García, J.A., Serrano, A., & de la Cruz Gallego, M. (2002) A spectral analysis of Iberian Peninsula monthly rainfall. *Theoretical and Applied Climatology*, 71, 77-95.
- Gil, J. (2003) Changes in the pattern of water masses resulting from a poleward slope current in the Cantabrian Sea (Bay of Biscay). *Estuarine, Coastal and Shelf Science*, 57, 1139-1149.
- Gil, J. (2008) Macro and mesoscale physical patterns in the Bay of Biscay. *Journal of the Marine Biological Association of the UK*, 88, 217-225.
- Gil, J., & Gomis, D. (2008) The secondary ageostrophic circulation in the Iberian Poleward Current along the Cantabrian Sea (Bay of Biscay). *Journal of Marine Systems*, 74, 60-73.
- Gil, J., Valdes, L., Moral, M., Sanchez, R., & Garcia-Soto, C. (2002) Mesoscale variability in a high-resolution grid in the Cantabrian Sea (southern Bay of Biscay), May 1995. *Deep-Sea Research Part I-Oceanographic Research Papers*, 49, 1591-1607.
- Goikoetxea, N., Borja, Á., Fontán, A., González, M., & Valencia, V. (2009) Trends and anomalies in sea-surface temperature, observed over the last 60 years, within the southeastern Bay of Biscay. *Continental Shelf Research*, 29, 1060-1069.
- Gómez-Gesteira, M., deCastro, M., Alvarez, I., & Gómez-Gesteira, J.L. (2008) Coastal sea surface temperature warming trend along the continental part of the Atlantic Arc (1985-2005). *J. Geophys. Res.*, 113.
- Gomez-Gesteira, M., Moreira, C., Alvarez, I., & deCastro, M. (2006) Ekman transport along the Galician coast (northwest Spain) calculated from forecasted winds. *Journal Geophysical Research*, 111, 1-12.
- González-Nuevo, G., & Nogueira, E. (2005) Intrusions of warm and salty waters onto the NW and N Iberian shelf in early spring and its relationship to climate variability. *Journal of Atmospheric & Ocean Science*, 10, 361 - 375.
- González-Nuevo, G., & Nogueira, E. (2014a) Seasonal And interannual variability of the Iberian Poleward Current in the southern Bay of Biscay. *Journal of Geophysical Research*, Submitted.
- González-Nuevo, G., & Nogueira, E. (2014b) Temporal and spatial variability of river plumes in the NW and N Iberian shelf (1987–2007). *Continental Shelf Research*, 91, 95-108.
- González-Nuevo, G., & Nogueira, E. (2014c) Temporal and spatial variability of upwelling in the NW and N Iberian shelf: 1987-2008. *Continental Shelf Research*, Submitted.

- González-Pola, C., Fernández-Díaz, J.M., & Lavín, A. (2007) Vertical structure of the upper ocean from profiles fitted to physically consistent functional forms. *Deep Sea Research Part I: Oceanographic Research Papers*, 54, 1985-2004.
- Gonzalez-Pola, C., Lavin, A., & Vargas-Yanez, M. (2005) Intense warming and salinity modification of intermediate water masses in the southeastern corner of the Bay of Biscay for the period 1992-2003. *Journal of Geophysical Research-Oceans*, 110, 14.
- Grimes, C., & Kingsford, M. (1996) How do Riverine Plumes of Different Sizes Influence Fish Larvae: do they Enhance Recruitment? *Marine and Freshwater Research*, 47, 191-208.
- Grimes, C.B., & Finucane, J.H. (1991) Spatial distribution and abundance of larval and juvenile fish, chlorophyll and macrozooplankton around the Mississippi River discharge plume, and the role of the plume in fish recruitment. *Marine Ecology Progress Series*, 75, 109-119.
- Haagenson, P.L. (1982) Review and evaluation of methods for objective analysis of meteorological variables. *Meteorological Research Bulletin*, 5, 113-132.
- Harvey, J.G. (1982). *Atmosphere and ocean: Our fluid environments*. . Vision Press pp.
- Haynes, R., & Barton, E.D. (1990) A poleward flow along the Atlantic Coast of the Iberian Peninsula. *Journal of Geophysical Research-Oceans*, 95, 11425-11441.
- Haynes, R., & Barton, E.D. (1991) Lagrangian observations in the Iberian coastal transition zone. *Journal of Geophysical Research: Oceans*, 96, 14731-14741.
- Head, R.N., Medina, G., Huskin, I., Anadon, R., & Harris, R.P. (2002) Phytoplankton and mesozooplankton distribution and composition during transects of the Azores Subtropical Front. *Deep-Sea Research Part II-Topical Studies in Oceanography*, 49, 4023-4034.
- Hermant, M., Lobry, J., Bonhommeau, S., Poulard, J.-C., & Le Pape, O. (2010) Impact of warming on abundance and occurrence of flatfish populations in the Bay of Biscay (France). *Journal of Sea Research*, 64, 45-53.
- Herrera, J.L., Rosón, G., Varela, R.A., & Piedracoba, S. (2008) Variability of the western Galician upwelling system (NW Spain) during an intensively sampled annual cycle. An EOF analysis approach. *Journal of Marine Systems*, 72, 200-217.
- Hickey, B.M., & Banas, N.S. (2003) Oceanography of the US Pacific Northwest Coastal Ocean and estuaries with application to coastal ecology. *Estuaries*, 26, 1010-1031.
- Hickey, B.M., Kudela, R.M., Nash, J.D., Bruland, K.W., Peterson, W.T., MacCready, P., Lessard, E.J., Jay, D.A., Banas, N.S., Baptista, A.M., Dever, E.P., Kosro, P.M., Kilcher, L.K., Horner-Devine, A.R., Zaron, E.D., McCabe, R.M., Peterson, J.O., Orton, P.M., Pan, J., & Lohan, M.C. (2010) River Influences on Shelf Ecosystems: Introduction and synthesis. *Journal of Geophysical Research-Oceans*, 115.
- Huang, C., & Qi, Y. (1997) The abundance cycle and influence factors on red tide phenomena of *Noctiluca scintillans* (Dinophyceae) in Dapeng Bay, the South China Sea. *Journal of Plankton Research*, 19, 303-318.
- Hurlburt, H.E., & Thompson, J.D. (1973) Coastal Upwelling on a β -Plane. *Journal of Physical Oceanography*, 3, 16-32.
- Huskin, I., Elices, M.J., & Anadon, R. (2003) Salp distribution and grazing in a saline intrusion off NW Spain. *Journal of Marine Systems*, 42, 1-11.
- Huskin, I., Lopez, E., Viesca, L., & Anadon, R. (2006) Seasonal variation of mesozooplankton biomass, abundance and copepod grazing in the central Cantabrian Sea (southern Bay of Biscay). *Scientia Marina*, 70, 119-130.
- Huthnance, J.M. (1984) Slope currents and JEBAR. *Journal of Physical Oceanography*, 14, 795-810.
- Huthnance, J.M. (1986) The Rockall slope current and shelf-edge processes. *Proceedings of the Royal Society of Edinburgh Section B-Biological Sciences*, 88, 83-101.

- Intxausti, L., Villate, F., Uriarte, I., Iriarte, A., & Amezttoy, I. (2012) Size-related response of zooplankton to hydroclimatic variability and water-quality in an organically polluted estuary of the Basque coast (Bay of Biscay). *Journal of Marine Systems*, 94, 87-96.
- Irigoiien, X., Antonio Fernandes, J., Grosjean, P., Denis, K., Albaina, A., & Santos, M. (2009) Spring zooplankton distribution in the Bay of Biscay from 1998 to 2006 in relation with anchovy recruitment. *Journal of Plankton Research*, 31, 1-17.
- Irigoiien, X., Chust, G., Antonio Fernandes, J., Albaina, A., & Zarauz, L. (2011) Factors determining the distribution and beta diversity of mesozooplankton species in shelf and coastal waters of the Bay of Biscay. *Journal of Plankton Research*, 33, 1182-1192.
- Irigoiien, X., Fiksen, Ø., Cotano, U., Uriarte, A., Alvarez, P., Arrizabalaga, H., Boyra, G., Santos, M., Sagarminaga, Y., Otheguy, P., Etxebeste, E., Zarauz, L., Artetxe, I., & Motos, L. (2007) Could Biscay Bay Anchovy recruit through a spatial loophole? *Progress In Oceanography*, 74, 132-148.
- Isla, J.A., & Anadon, R. (2004) Mesozooplankton size-fractionated metabolism and feeding off NW Spain during autumn: effects of a poleward current. *ICES J. Mar. Sci.*, 61, 526-534.
- Isla, J.A., Ceballos, S., Huskin, I., Anadon, R., & Alvarez-Marques, F. (2004) Mesozooplankton distribution, metabolism and grazing in an anticyclonic slope water oceanic eddy (SWODDY) in the Bay of Biscay. *Marine Biology*, 145, 1201-1212.
- Jackett, D.R., & McDougall, T.J. (1985) An oceanographic variable for the characterization of intrusions and water masses. *Deep Sea Research Part A. Oceanographic Research Papers*, 32, 1195-1207.
- Jiang, L., Yan, X.H., & Klemas, V. (2009) Remote sensing for the identification of coastal plumes: case studies of Delaware Bay. *International Journal of Remote Sensing*, 30, 2033-2048.
- Kara, A.B., Rochford, P.A., & Hurlburt, H.E. (2000) An optimal definition for ocean mixed layer depth. *Journal of Geophysical Research-Oceans*, 105, 16803-16821.
- Keuls, M. (1952) The use of studentized range in connection with an analysis of variance. *Euphytica*, 1, 112-122.
- Kimor, B. (1979) Predation by *Noctiluca miliaris* Souriray on *Acartia tonsa* Dana eggs in the in-shore waters of southern California. *Limnology and Oceanography*, 24, 568-572.
- Kindle, J.C., & O'Brien, J.J. (1974) On Upwelling Along a Zonally-Orientated Coastline. *Journal of Physical Oceanography*, 4, 125-130.
- Kiorboe, T., Munk, P., Richardson, K., Christensen, V., & Paulsen, H. (1988) Plankton dynamics and larval herring growth, drift and survival in a frontal area. *Marine Ecology Progress Series*, 44, 205-219.
- Koutsikopoulos, C., Beillois, P., Leroy, C., & Taillefer, F. (1998) Temporal trends and spatial structures of the sea surface temperature in the Bay of Biscay. *Oceanologica Acta*, 21, 335-344.
- Krauss, W. (1986) The North-Atlantic current. *Journal of Geophysical Research-Oceans*, 91, 5061-5074.
- Krebs, C.J. (1972). *Ecology* New York. Harper & Row, 694 pp.
- Laabir, M., Poulet, S.A., Harris, R.P., Pond, D.W., Cuff, A., Head, R.N., & Ianora, A. (1998) Comparative study of the reproduction of *Calanus helgolandicus* in well-mixed and seasonally stratified coastal waters of the western English Channel. *Journal of Plankton Research*, 20, 407-421.
- Landry, M.R., Al-Mutairi, H., Selph, K.E., Christensen, S., & Nunnery, S. (2001) Seasonal patterns of mesozooplankton abundance and biomass at Station ALOHA. *Deep-Sea Research Part II-Topical Studies in Oceanography*, 48, 2037-2061.
- Lavaniegos, B.E., Jimenez-Perez, L.C., & Gaxiola-Castro, G. (2002) Plankton response to El Niño 1997-1998 and La Niña 1999 in the southern region of the California Current. *Progress In Oceanography*, 54, 33-58.

- Lavin, A., Moreno-Ventas, X., Ortiz de Zarate, V., Abaunza, P., & Cabanas, J.M. (2007) Environmental variability in the North Atlantic and Iberian waters and its influence on horse mackerel (*Trachurus trachurus*) and albacore (*Thunnus alalunga*) dynamics. *ICES J. Mar. Sci.*, 64, 425-438.
- Lavin, A., Valdes, L., Gil, J., & Moral, M. (1998) Seasonal and inter-annual variability in properties of surface water off Santander, Bay of Biscay, 1991-1995. *Oceanologica Acta*, 21, 179-190.
- Lavín, A., Valdés, L., Gil, J., & Moral, M. (1998) Seasonal and inter-annual variability in properties of surface water off Santander, Bay of Biscay, 1991-1995. *Oceanologica Acta*, 21, 179-190.
- Lazure, P., Garnier, V., Dumas, F., Herry, C., & Chifflet, M. (2009) Development of a hydrodynamic model of the Bay of Biscay. Validation of hydrology. *Continental Shelf Research*, 29, 985-997.
- Le Cann, B., & Serpette, A. (2009) Intense warm and saline upper ocean inflow in the southern Bay of Biscay in autumn-winter 2006-2007. *Continental Shelf Research*, 29, 1014-1025.
- Le Fèvre, J., & Frontier, S. (1988). Influence of temporal characteristics of physical phenomena on plankton dynamics, as shown by North-West European marine ecosystem. *Toward a Theory on Biological-Physical Interactions in the World Ocean* (pp. 245-272): B. J. Rothchild.
- Le Fèvre, M.J. (1986). Variations spatio-temporelles du peuplement zooplanctonique du lagon de l'île de Moorea (Archipel de la Société, Polynésie française). *Océanographie biologique*, Vol. Thèse Doctorat (pp. 1-127). Paris: Université Paris VI.
- Le Fèvre, M.J., & Grall, J.R. (1970) On the relationships of Noctiluca swarming off the western coast of Brittany with hydrological features and plankton characteristics of the environment. *Journal of Experimental Marine Biology and Ecology*, 4, 287-306. .
- Lechuga, A. (1973) Periodicidad de las precipitaciones atmosféricas caídas sobre España Peninsular. *Revista de Obras Públicas*, 126, 673-678.
- Legendre, P. (1993) Spatial autocorrelation - trouble or new paradigm. *Ecology*, 74, 1659-1673.
- Legendre, P., Borcard, D., & Peres-Neto, P.R. (2005) Analyzing beta diversity: Partitioning the spatial variation of community composition data. *Ecological Monographs*, 75, 435-450.
- Legendre, P., & Legendre, L. (1998). *Numerical Ecology*. Amsterdam. Elsevier, 870 pp.
- Lezama-Ochoa, A., Ballon, M., Woillez, M., Grados, D., Irigoien, X., & Bertrand, A. (2011) Spatial patterns and scale-dependent relationships between macrozooplankton and fish in the Bay of Biscay: an acoustic study. *Marine Ecology Progress Series*, 439, 151-168.
- Lezama-Ochoa, A., Irigoien, X., Chaigneau, A., Quiroz, Z., Lebourges-Dhaussy, A., & Bertrand, A. (2014) Acoustics Reveals the Presence of a Macrozooplankton Biocline in the Bay of Biscay in Response to Hydrological Conditions and Predator-Prey Relationships. *Plos One*, 9.
- Longhurst, A. (1998). *Ecological Geography of the Sea*. Academic Press, 398 pp.
- Longhurst, A.R., & Harrison, G.W. (1989) The biological pump: Profiles of plankton production and consumption in the upper ocean. *Progress In Oceanography*, 22, 47-123.
- Lopez, E., Viesca, L., & Anadon, R. (2007) Seasonal variation in abundance and feeding rates of the first stages of copepods in a temperate sea. *Marine Ecology Progress Series*, 352, 161-175.
- Lynn, R.J., & Simpson, J.J. (1990) The flow of the undercurrent over the continental borderland off southern California. *Journal of Geophysical Research-Oceans*, 95, 12995-13008.
- Llope, M., Anadón, R., Viesca, L., Quevedo, M., González-Quirós, R., & Stenseth, N.C. (2006) Hydrography of the southern Bay of Biscay shelf-break region: Integrating the multiscale physical variability over the period 1993-2003. *J. Geophys. Res.*, 111, 1-14.
- Maillard, C. (1986). *Atlas hydrologique de l'Atlantique nord-est: H. Lacombe*. IFREMER [Institut français de recherche pour l'exploitation de la mer] pp.

- Marcello, J., Marques, F., & Eugenio, F. (2005) Automatic tool for the precise detection of upwelling and filaments in remote sensing imagery. *Ieee Transactions on Geoscience and Remote Sensing*, 43, 1605-1616.
- Marta-Almeida, M., Dubert, J.s., Peliz, Ã.I., & Queiroga, H. (2006) Influence of vertical migration pattern on retention of crab larvae in a seasonal upwelling system. *Marine Ecology Progress Series*, 307, 1-19.
- Mauchline, J., Blaxter, J.H.S., Southward, A.J., & Tyler, P.A. (1998). Advances in marine biology - The biology of calanoid copepods - Introduction. *Advances in Marine Biology, Vol 33: The Biology of Calanoid Copepods*, Vol. 33 (pp. 1-+). London: Academic Press Ltd-Elsevier Science Ltd.
- McClain, C.R., Chao, S.Y., Atkinson, L.P., Blanton, J.O., & Decastillejo, F. (1986) Wind-driven upwelling in the vicinity of Cape Finisterre, Spain. *Journal of Geophysical Research-Oceans*, 91, 8470-8486.
- Meehl, G.A., Arblaster, J.M., Matthes, K., Sassi, F., & van Loon, H. (2009) Amplifying the Pacific Climate System Response to a Small 11-Year Solar Cycle Forcing. *Science*, 325, 1114-1118.
- Mesias, J.M., Matano, R.P., & Strub, P.T. (2003) Dynamical analysis of the upwelling circulation off central Chile. *J. Geophys. Res.*, 108, 30-31 - 30-18.
- Michel, S., Treguier, A.M., & Vandermeirsch, F. (2009) Temperature variability in the Bay of Biscay during the past 40 years, from an in situ analysis and a 3D global simulation. *Continental Shelf Research*, 29, 1070-1087.
- Monteiro, P.M.S., & Largier, J.L. (1999) Thermal Stratification in Saldanha Bay (South Africa) and Subtidal, Density-driven Exchange with the Coastal Waters of the Benguela Upwelling System. *Estuarine, Coastal and Shelf Science*, 49, 877-890.
- Moran, X.A.G., Bode, A., Angel Suarez, L., & Nogueira, E. (2007) Assessing the relevance of nucleic acid content as an indicator of marine bacterial activity. *Aquatic Microbial Ecology*, 46, 141-152.
- Munk, P., Larsson, P.O., Danielsen, D., & Moksness, E. (1995) Larval and small juvenile cod (*Gadus morhua*) concentrated in the highly productive areas of a shelf break front. *Marine Ecology Progress Series*, 125, 21-30.
- Neshyba, S.J., Mooers, C.N.K., Smith, R.L., & Barber, R.T. (1989). *Poleward flows along eastern ocean boundaries*. Springer-Verlag pp.
- Nixon, S., & Thomas, A. (2001) On the size of the Peru upwelling ecosystem. *Deep Sea Research Part I: Oceanographic Research Papers*, 48, 2521-2528.
- Oliveira, P.B., Moita, T., Silva, A., Monteiro, I.T., & Palma, A.S. (2009) Summer diatom and dinoflagellate blooms in Lisbon Bay from 2002 to 2005: pre-conditions inferred from wind and satellite data. *Progress In Oceanography*, In Press, Accepted Manuscript.
- OSPAR (2000) Quality Status Reprot 2000. *Ospar Commission*, 108+ vii.
- Ostrander, C.E., McManus, M.A., DeCarlo, E.H., & Mackenzie, F.T. (2008) Temporal and spatial variability of freshwater plumes in a semienclosed estuarine-bay system. *Estuaries and Coasts*, 31, 192-203.
- Otero, J., Alvarez-Salgado, X.A., Gonzalez, A.F., Gilcoto, M., & Guerra, A. (2009a) High-frequency coastal upwelling events influence *Octopus vulgaris* larval dynamics on the NW Iberian shelf. *Marine Ecology-Progress Series*, 386, 123-132.
- Otero, P., & Ruiz-Villarreal, M. (2008) Wind forcing of the coastal circulation off north and northwest Iberia: Comparison of atmospheric models. *Journal of Geophysical Research-Oceans*, 113.
- Otero, P., Ruiz-Villarreal, M., Conde, P., Cobas, M., Varela, M., González-Nuevo, G., & Bernal, M. (2008a). Observed and modeled spring circulation of the northern limit of the Canary upwelling system during 2007. *Easter Boundary Upwelling Ecosystems symposium*. Las Palmas. Spain.

- Otero, P., Ruiz-Villarreal, M., García-García, L., González-Nuevo, G., & Cabanas, J. (2013) Coastal dynamics off Northwest Iberia during a stormy winter period. *Ocean Dynamics*, 63, 115-129.
- Otero, P., Ruiz-Villarreal, M., & Peliz, A. (2008b) Variability of river plumes off Northwest Iberia in response to wind events. *Journal of Marine Systems*, 72, 238-255.
- Otero, P., Ruiz-Villarreal, M., & Peliz, A. (2009b) River plume fronts off NW Iberia from satellite observations and model data. *ICES J. Mar. Sci.*, 66, 1853-1864.
- Ou, S.Y., Zhang, H., & Wang, D.X. (2009) Dynamics of the buoyant plume off the Pearl River Estuary in summer. *Environmental Fluid Mechanics*, 9, 471-492.
- Paffenhofer, G.A. (1980) Zooplankton distribution as related to summer hydrographic conditions in Onslow Bay, North-Carolina. *Bulletin of Marine Science*, 30, 819-832.
- Paffenhofer, G.A., & Stearns, D.E. (1988) Why is *Acartia tonsa* (copepoda, calanoida) restricted to nearshore environments. *Marine Ecology Progress Series*, 42, 33-38.
- Pascual, M., Borja, A., Eede, S.V., Deneudt, K., Vincx, M., Galparsoro, I., & Legorburu, I. (2011) Marine biological valuation mapping of the Basque continental shelf (Bay of Biscay), within the context of marine spatial planning. *Estuarine Coastal and Shelf Science*, 95, 186-198.
- Pelegrí, J.L., Arístegui, J., Cana, L., González-Dávila, M., Hernández-Guerra, A., Hernández-León, S., Marrero-Díaz, A., Montero, M.F., Sangrà, P., & Santana-Casiano, M. (2005) Coupling between the open ocean and the coastal upwelling region off northwest Africa: water recirculation and offshore pumping of organic matter. *Journal of Marine Systems*, 54, 3-37.
- Peliz, A., Dubert, J., Haidvogel, D.B., & Le Cann, B. (2003) Generation and unstable evolution of a density-driven Eastern Poleward Current: The Iberian Poleward Current. *Journal of Geophysical Research-Oceans*, 108.
- Peliz, Á., Dubert, J., Santos, A.M.P., Oliveira, P.B., & Le Cann, B. (2005) Winter upper ocean circulation in the Western Iberian Basin--Fronts, Eddies and Poleward Flows: an overview. *Deep Sea Research Part I: Oceanographic Research Papers*, 52, 621-646.
- Peliz, A., & Fiúza, A.F.G. (1999) Spatial and Temporal Variability of CZCS-Derived Phytoplankton Pigment Concentrations Off the Western Iberian Peninsula *International Journal of Remote Sensing*, 20, 1363-1403.
- Peliz, Á., Rosa, T.L., Santos, A.M.P., & Pissarra, J.L. (2002) Fronts, jets, and counter-flows in the Western Iberian upwelling system. *Journal of Marine Systems*, 35, 61-77.
- Perez, F.F., Castro, C.G., Alvarez-Salgado, X.A., & Rios, A.F. (2001) Coupling between the Iberian basin - scale circulation and the Portugal boundary current system: a chemical study. *Deep-Sea Research Part I-Oceanographic Research Papers*, 48, 1519-1533.
- Perez, F.F., Mourino, C., Fraga, F., & Rios, A.F. (1993) Displacement of water masses and remineralization rates off the iberian peninsula by nutrient anomalies. *Journal of Marine Research*, 51, 869-892.
- Perez, F.F., Rios, A.F., King, B.A., & Pollard, R.T. (1995) Decadal changes of the 0-8 relationship of the eastern North Atlantic central water. *Deep-Sea Research Part I-Oceanographic Research Papers*, 42, 1849-1864.
- Pimenta, F.M., Kirwan, A.D., & Huq, P. (2011) On the Transport of Buoyant Coastal Plumes. *Journal of Physical Oceanography*, 41, 620-640.
- Pingree, R. (1994) Winter warming in the southern Bay of Biscay and Lagrangian eddy kinematics from a Deep Drogued Argos Buoy. *Journal of Marine Biology Association of UK*, 74, 107-128.
- Pingree, R.D. (1993) Flow of surface waters to the west of the British Isles and in the Bay of Biscay. *Deep Sea Research Part II: Topical Studies in Oceanography*, 40, 369-388.
- Pingree, R.D., & Le Cann, B. (1989) Celtic and armorican slope and shelf residual currents. *Progress In Oceanography*, 23, 303-338.

- Pingree, R.D., & Le Cann, B. (1990) Structure, strength and seasonality of the slope currents in the bay of biscay region. *Journal of the Marine Biological Association of the United Kingdom*, 70, 857-885.
- Pingree, R.D., & Le Cann, B. (1992a) Anticyclonic eddy x91 in the southern Bay of Biscay, may 1991 to February 1992. *Journal of Geophysical Research-Oceans*, 97, 14353-14367.
- Pingree, R.D., & Le Cann, B. (1992b) Three anticyclonic slope water oceanic eDDIES (SWODDIES) in the Southern Bay of Biscay in 1990. *Deep Sea Research Part A. Oceanographic Research Papers*, 39, 1147-1175.
- Piola, A.R., Romero, S.I., & Zajaczkovski, U. (2008) Space-time variability of the Plata plume inferred from ocean color. *Continental Shelf Research*, 28, 1556-1567.
- Planque, B., Beillois, P., Jégou, A.M., Lazure, P., Petitgas, P., & Puillat, I. (2003) Large scale hydroclimatic variability in the Bay of Biscay. The 1990s in the context of interdecadal changes *ICES Marine Science Symposia*, 219, 61-70.
- Platt, T., & Denman, K.L. (1975) Spectral analysis in ecology. *Annual Review of Ecology and Systematics*, 6, 189-210.
- Pollard, R.T., Griffiths, M.J., Cunningham, S.A., Read, J.F., Pérez, F.F., & Ríos, A.F. (1996) Vivaldi 1991 - A study of the formation, circulation and ventilation of Eastern North Atlantic Central Water. *Progress In Oceanography*, 37, 167-172.
- Poularikas, A.D., & Seely, S. (1991). *Signals and Systems, 2nd Edition*. Boston. PWS-Kent Publishing, 1015 pp.
- Poulet, S.A., Laabir, M., & Chaudron, Y. (1996) Characteristic features of zooplankton in the Bay of Biscay. *Scientia Marina*, 60, 79-95.
- Prego, R., & Bao, R. (1997) Upwelling influence on the Galician coast: silicate in shelf water and underlying surface sediments. *Continental Shelf Research*, 17, 307-318.
- Prego, R., Guzmán-Zuñiga, D., Varela, M., deCastro, M., & Gómez-Gesteira, M. (2007) Consequences of winter upwelling events on biogeochemical and phytoplankton patterns in a western Galician ria (NW Iberian peninsula). *Estuarine, Coastal and Shelf Science*, 73, 409-422.
- Puillat, I., Lazure, P., Jégou, A.M., Lampert, L., & Miller, P.I. (2004) Hydrographical variability on the French continental shelf in the Bay of Biscay, during the 1990s. *Continental Shelf Research*, 24, 1143-1163.
- Quevedo, M., & Anadon, R. (2000) Spring microzooplankton composition, biomass and potential grazing in the central Cantabrian coast (southern Bay of Biscay). *Oceanologica Acta*, 23, 297-309.
- Quevedo, M., Gonzalez-Quiros, R., & Anadon, R. (1999) Evidence of heavy predation by *Noctiluca scintillans* on *Acartia clausi* (Copepoda) eggs of the central Cantabrian coast. *Oceanologica Acta*, 22, 127-131.
- Rayner, N.A., Brohan, P., Parker, D.E., Folland, C.K., Kennedy, J.J., Vanicek, M., Ansell, T.J., & Tett, S.F.B. (2006) Improved Analyses of Changes and Uncertainties in Sea Surface Temperature Measured In Situ since the Mid-Nineteenth Century: The HadSST2 Dataset. *Journal of Climate*, 19, 446-469.
- Rayner, N.A., Parker, D.E., Horton, E.B., Folland, C.K., Alexander, L.V., Rowell, D.P., Kent, E.C., & Kaplan, A. (2003) Global analyses of sea surface temperature, sea ice, and night marine air temperature since the late nineteenth century. *J. Geophys. Res.*, 108, ACL 2-1 - ACL 2-29.
- Razouls, C. (1995) Diversity and geographical distribution of pelagic copepods .1. Calanoida. *Annales De L Institut Oceanographique*, 71, 81-&.
- Ríos, A.F., Pérez, F.F., & Fraga, F. (1992) Water masses in the upper and middle North Atlantic Ocean east of the Azores. *Deep Sea Research Part A. Oceanographic Research Papers*, 39, 645-658.

- Rodríguez, F., Varela, M., Fernández, E., & Zapata, M. (2003) Phytoplankton and pigment distributions in an anticyclonic slope water oceanic eddy (SWODDY) in the southern Bay of Biscay. *Marine Biology*, 143, 995-1011.
- Rodríguez, J.M., González-Nuevo, G., González-Pola, C., & Cabal, J. (2009) The ichthyoplankton assemblage and the environmental variables off the NW and N Iberian Peninsula coasts, in early spring. *Continental Shelf Research*, 29, 1145-1156.
- Rodríguez, J.M., González-Nuevo, G., González-Pola, C., & Cabal, J. (2008) Environmental forcing and ichthyoplankton composition and distribution off the NW and N Iberian Peninsula coast, in spring. *Ciencia marina*, 3, 228-229.
- Rodríguez, V., Rodríguez, J., & Niell, F.X. (1985) Coexistencia de especies congénicas de *Acartia* (Copepoda) en sistemas alterados: una aproximación empleando la teoría del nicho. *Investigaciones Pesqueras*, 49, 25-34.
- Ruiz-Villarreal, M., Coelho, H., del Río, G.D., & Nogueira, J. (2004) Slope current in the Cantabrian: Observation and modeling of seasonal variability and interaction with Aviles Canyon. *ICES C. M.*, N, 12.
- Ruiz-Villarreal, M., González-Pola, C., Díaz del Río, G., Lavin, A., Otero, P., Piedracoba, S., & Cabanas, J.M. (2006) Oceanographic conditions in North and Northwest Iberia and their influence on the Prestige oil spill. *Marine Pollution Bulletin*, 53, 220-238.
- Ruiz, A., Franco, J., & Villate, F. (1998) Microzooplankton grazing in the estuary of Mundaka, Spain, and its impact on phytoplankton distribution along the salinity gradient. *Aquatic Microbial Ecology*, 14, 281-288.
- Ruiz, J., & Navarro, G. (2006) Upwelling spots and vertical velocities in the Gulf of Cadiz: An approach for their diagnose by combining temperature and ocean colour remote sensing. *Deep-Sea Research Part II-Topical Studies in Oceanography*, 53, 1282-1293.
- Sanchez, F., & Gil, J. (2000) Hydrographic mesoscale structures and Poleward Current as a determinant of hake (*Merluccius merluccius*) recruitment in southern Bay of Biscay. *Ices Journal of Marine Science*, 57, 152-170.
- Sánchez, F., González-Pola, C., Druet, M., García-Alegre, A., Acosta, J., Cristobo, J., Parra, S., Ríos, P., Altuna, Á., Gómez-Ballesteros, M., Muñoz-Recio, A., Rivera, J., & del Río, G.D. (2014) Habitat characterization of deep-water coral reefs in La Gavieta Canyon (Avilés Canyon System, Cantabrian Sea). *Deep Sea Research Part II: Topical Studies in Oceanography*, 106, 118-140.
- Santos, A.M.P., de Fatima Borges, M., & Groom, S. (2001) Sardine and horse mackerel recruitment and upwelling off Portugal. *ICES J. Mar. Sci.*, 58, 589-596.
- Santos, A.M.P., Peliz, A., Dubert, J., Oliveira, P.B., Angélico, M.M., & Ré, P. (2004) Impact of a winter upwelling event on the distribution and transport of sardine (*Sardina pilchardus*) eggs and larvae off western Iberia: a retention mechanism. *Continental Shelf Research*, 24, 149-165.
- Santos, A.M.P., Ré, P., dos Santos, A., & Peliz, Á. (2006) Vertical distribution of the European sardine (*Sardina pilchardus*) larvae and its implications for their survival. *Journal of Plankton Research*, 28, 523-532.
- Schiller, R.V., & Kourafalou, V.H. (2010) Modeling river plume dynamics with the HYbrid Coordinate Ocean Model. *Ocean Modelling*, 33, 101-117.
- Sekiguchi, H., & Kato, T. (1976) Influence of Noctiluca's predation on the *Acartia* population in Ise Bay, Central Japan. *Journal of the Oceanographical Society of Japan*, 32, 195-198.
- Serrano, A., García, J.A., Mateos, V.L., Cancillo, M.L., & Garrido, J. (1999) Monthly Modes of Variation of Precipitation over the Iberian Peninsula. *Journal of Climate*, 12, 2894-2919.
- Serrano, A., Sanchez, F., Punzon, A., Velasco, F., & Olaso, I. (2011) Deep sea megafaunal assemblages off the northern Iberian slope related to environmental factors. *Scientia Marina*, 75, 425-437.

- Smith, T.M., Miller, J.R., & Russell, G.L. (1989) Seasonal oceanic heat transports computed from an atmospheric model and ocean temperature climatology. *Dynamics of Atmospheres and Oceans*, 14, 77-92.
- Stenseth, N.C., Llope, M., Anadon, R., Ciannelli, L., Chan, K.-S., Hjermann, D.O., Bagoien, E., & Ottersen, G. (2006) Seasonal plankton dynamics along a cross-shelf gradient. *Proceedings of the Royal Society B-Biological Sciences*, 273, 2831-2838.
- Swallow, J.C., Gould, W.J., & Saunders P.M. (1977) Evidence for a poleward eastern boundary current in the North Atlantic Ocean. *ICES C.M.*, 1977/C:32, 20 pp.
- Tapia, F.J., Navarrete, S.A., Castillo, M., Menge, B.A., Castilla, J.C., Largier, J., Wieters, E.A., Broitman, B.L., & Barth, J.A. (2009) Thermal indices of upwelling effects on inner-shelf habitats. *Progress In Oceanography*, 83, 278-287.
- Teodoro, A.C., Goncalves, H., Veloso-Gomes, F., & Goncalves, J.A. (2009) Modeling of the Douro River Plume Size, Obtained Through Image Segmentation of MERIS Data. *Ieee Geoscience and Remote Sensing Letters*, 6, 87-91.
- Tomczak, M., & Godfrey, J.S. (1994). *Regional Oceanography: an Introduction*. Oxford. Pergamon, 442 pp.
- Torres, R., & Barton, E.D. (2006) Onset and development of the Iberian poleward flow along the Galician coast. *Continental Shelf Research*, 26, 1134-1153.
- Tortajada, S., Niquil, N., Blanchet, H., Grami, B., Montanie, H., David, V., Gle, C., Saint-Beat, B., Johnson, G.A., Marquis, E., Del Amo, Y., Dubois, S., Vincent, D., Dupuy, C., Jude, F., Hartmann, H.J., & Sautour, B. (2012) Network analysis of the planktonic food web during the spring bloom in a semi enclosed lagoon (Arcachon, SW France). *Acta Oecologica-International Journal of Ecology*, 40, 40-50.
- Turner, J.T., & Graneli, E. (1992) Zooplankton feeding ecology - grazing during enclosure studies of phytoplankton blooms from the west-coast of Sweden. *Journal of Experimental Marine Biology and Ecology*, 157, 19-31.
- UNESCO (1983) Algorithms for computation of fundamental properties of seawater. *Unesco Technical Papers in Marine Science*, 44, 53.
- Uriarte, I., & Villate, F. (2006) Spatial variations in size, weight and condition factor of the females of *Acartia clausi* (Copepoda : Calanoida) along a salinity gradient in two contrasting estuaries of the Basque coast (Bay of Biscay). *Hydrobiologia*, 571, 329-339.
- Uriarte, L., & Villate, F. (2004) Effects of pollution on zooplankton abundance and distribution in two estuaries of the Basque coast (Bay of Biscay). *Marine Pollution Bulletin*, 49, 220-228.
- Valdes, J.L., Roman, M.R., Alvarez-Ossorio, M.T., Gauzens, A.L., & Miranda, A. (1990) Zooplankton composition and distribution off the coast of Galicia, Spain. *J. Plankton Res.*, 12, 629-643.
- Valdés, L., Alvarez-Ossorio, M., Lavín, A., Varela, M., & Carballo, R. (1991) Ciclo anual de parámetros hidrográficos, nutrientes y plancton en la plataforma continental de La Coruña (NO, España). *Boletín del Instituto Español de Oceanografía*, 7, 91-138.
- Valdés, L., López-Urrutia, A., Cabal, J., Alvarez-Ossorio, M., Bode, A., Miranda, A., Cabanas, M., Huskin, I., Anadón, R., Alvarez-Marqués, F., Llope, M., & Rodríguez, N. (2007) A decade of sampling in the Bay of Biscay: What are the zooplankton time series telling us? *Progress In Oceanography*, 74, 98-114.
- Valdes, L., & Moral, M. (1998) Time-series analysis of copepod diversity and species richness in the southern Bay of Biscay off Santander, Spain, in relation to environmental conditions. *ICES J. Mar. Sci.*, 55, 783-792.
- van Aken, H.M. (2002) Surface currents in the Bay of Biscay as observed with drifters between 1995 and 1999 *Deep-Sea Research II*, 49, 1071-1086.
- Varela, M.M., Barquero, S., Bode, A., Fernandez, E., Gonzalez, N., Teira, E., & Varela, M. (2003) Microplanktonic regeneration of ammonium and dissolved organic nitrogen in the upwelling area of the NW of Spain: relationships with dissolved organic carbon production and phytoplankton size-structure. *J. Plankton Res.*, 25, 719-736.

- Villarreal, M.R., Cabanas, J.M., González-Nuevo, G., Bode, A., Nogueira, E., González-Pola, C., & Lavín, A. (2012). Clima y meteorología. *Instituto Español de Oceanografía. Cambio climático y oceanográfico en el Atlántico del norte de España* (pp. 37 – 68): Instituto Español de Oceanografía.
- Villate, F. (1991a) Annual cycle of zooplankton community in the Abra Harbor (Bay of Biscay) - abundance, composition and size spectra. *Journal of Plankton Research*, 13, 691-706.
- Villate, F. (1991b) Zooplankton assemblages in the shallow tidal estuary of Mundaka (Bay of Biscay). *Cahiers De Biologie Marine*, 32, 105-119.
- Villate, F. (1997) Tidal influence on zonation and occurrence of resident and temporary zooplankton in a shallow system (estuary of Mundaka, Bay of Biscay). *Scientia Marina*, 61, 173-188.
- Villate, F., Aravena, G., Iriarte, A., & Uriarte, I. (2008) Axial variability in the relationship of chlorophyll a with climatic factors and the North Atlantic Oscillation in a Basque coast estuary, Bay of Biscay (1997-2006). *J. Plankton Res.*, 30, 1041-1049.
- Villate, F., Moral, M., & Valencia, V. (1997) Mesozooplankton community indicates climate changes in a shelf area of the inner Bay of Biscay throughout 1988 to 1990. *Journal of Plankton Research*, 19, 1617-1636.
- Villate, F., Uriarte, I., Irigoien, X., Beaugrand, G., & Cotano, U. (2004). *Mesozooplankton communities in Oceanography and Marine Environment of the Basque Country*. Borja, A., Collins, M. (Eds.), 640 pp.
- Wei, W.W.S. (1989). Time series analysis. (p. 478): Addison-Wesley Publishing Company.
- Weikert, H., Koppelman, R., & Wiegatz, S. (2001) Evidence of episodic changes in deep-sea mesozooplankton abundance and composition in the Levantine Sea (Eastern Mediterranean). *Journal of Marine Systems*, 30, 221-239.
- Woillez, M., Petitgas, P., Huret, M., Struski, C., & Leger, F. (2010) Statistical monitoring of spatial patterns of environmental indices for integrated ecosystem assessment: Application to the Bay of Biscay pelagic zone. *Progress In Oceanography*, 87, 83-93.
- Wooster, W.S., Bakun, A., & McLain, D.R. (1976) Seasonal upwelling cycle along eastern boundary of North-Atlantic. *Journal of Marine Research*, 34, 131-141.
- Zarauz, L., Irigoien, X., & Fernandes, J.A. (2008) Modelling the influence of abiotic and biotic factors on plankton distribution in the Bay of Biscay, during three consecutive years (2004-06). *Journal of Plankton Research*, 30, 857-872.
- Zarauz, L., Irigoien, X., & Fernandes, J.A. (2009) Changes in plankton size structure and composition, during the generation of a phytoplankton bloom, in the central Cantabrian sea. *Journal of Plankton Research*, 31, 193-207.
- Zarauz, L., Irigoien, X., Urtizberea, A., & Gonzalez, M. (2007) Mapping plankton distribution in the Bay of Biscay during three consecutive spring surveys. *Marine Ecology Progress Series*, 345, 27-39.